RARE-EARTH DOPED (α'/β')-SIALON CERAMICS

Naima Ramadan Gajum (M.Sc)

Thesis Submitted For the Award of
Doctor of Philosophy

Department of Physics
Centre for Advanced Materials
January 2001

Contents

List of Figures

List of Tables

ACKNOWLEDGMENTS

I would like to acknowledge the financial support of my home country Libya who supported me during my study.

I am especially grateful to my supervisor professor M. H. Lewis for his guidance, advice and encouragement throughout the period of this research. I would like to thank Dr. R.J. Lumby for collaboration with the experimental programme and his advice and helpful discussions.

I would like also to thank my colleagues and the departmental technical staff, especially Steve York for his tuition and assistance in electron microscopy, Steve Carpenter, Dan Lee and Keith Briggs for their help.

I am also very grateful to all my family and in particular my parents for support and encouragement throughout my whole academic career, my husband Hakem and finally my special thanks and acknowledgements go to my children, Taha, Rehab Al Huda and Mohammed Yasser to whom I wish to dedicate this work. Without their love, patience and understanding this work would have not been completed.

DECLARATION

This thesis contains the result of my independent research work unless specifically referenced. No part of this work has been submitted for the award of a degree at any other university.

Parts of this work have appeared in the following Proceeding;

- Nordmann, M.H.H. Jumali, M.H. Lewis, R. J. Lumby and N. R. Gajum, Microstructure and stability of Nd, Gd and Yb-doped α'/β' sialons, Proceedings of the IOM Annual Ceramics Convention, Cirencester, April 21th- 23 rd 1998

- Nordmann, M.H.H. Jumali, M.H. Lewis, R. J. Lumby and N. R. Gajum, Microstructural development of Nd, Gd and Yb doped α'/β' sialons, Proceedings of the international Symposium on Nitrides II. Limerick, Ireland, June 9-11, 1998

ABSTRACT

The objectives of this research were to investigate the possibility of controlling the α'/β' phase ratio and morphology in Sialon ceramics. These objectives have been sought by the control of the starting composition, and by post sintering heat treatment. The main emphasis has been on the production of a series of α' and (α'+β') Sialon ceramics with a minimum amount of the glass phase by the pressureless sintering technique and using ytterbium (Yb) as an α' stabilising element. The Yb additions were made via the oxide or the alumino- silicate presynthesised glass; the latter was found to improve the density. The XRD analysis of the as sintered materials revealed α' to be the dominant phase with minor contributions from β' sialon and/ or 12H AlN polytype.

Additions of SiO_2 or β-Si_3N_4 were made to various materials to assess potential mechanisms for obtaining control over the microstructural development of α'/β' sialon materials. The addition of silica (SiO_2) to sialon with high α' content in Yb system significantly improves the densification and increased the amount of β' phase. The incorporation of β-Si_3N_4 as a seeding agent had a very small effect on the α'/β' phase ratio and the phase morphology.

Further experiments were aimed at optimizing sinterability and sialon microstructure through the introduction of two α' stabilizing cations. Compositions were prepared that contained a combination of light and heavy rare-earth (Yb-Nd and Gd-Nd), and then pressurless sintered and compared with the single cation materials. Materials in the as sintered state were composed of a high α' sialon content with a minor amount of β' sialon and 12H AlN polytype indicating that the heavy rare-earth (which is the principal α' stabilizer) has a dominant effect although EDAX analysis confirmed the presence of both cations (light and heavy) within the α' structure.

The research also compared, and developed an understanding of, the thermal stability of α'-sialon using single Yb or mixed cations. The Yb single cation α'/β' materials exhibited excellent stability over a range of temperature (1200 - 1600°C) and for different periods of time up to 168 hrs. The heat treatments result in the crystallisation of the residual phase as a Yb garnet phase which formed at ~1300°C. The mixed cation α'/β' materials showed some α'-β' transformation. The transformation was accompanied by dissolution of $RAlO_3$ (normally crystallized with R=Nd,Gd) and crystallization of melilite.

The hardness values were found to depend on the α' content, amount of residual glassy phase and the porosity level. A high average of 18 GPa has been obtained with Yb single cation materials. The fracture toughness was found to depend mainly on the amount of β' and its morphology; the highest $K_{IC} \sim 5.2$ MPa.$m^{1/2}$ was measured for materials containing a combined SiO_2 and β-Si_3N_4 addition. In the heat-treated materials the hardness was found to increase slightly whereas the fracture toughness decreased consistent with more complete crystallization and the absence of grain or phase boundary crack deflection. The Yb single cation materials exhibited good resistance to oxidation at 1350^0C and 1450^0C compared with the mixed cation materials.

CHAPTER 1

INTRODUCTION

1.1- Introduction

Ceramics can be defined as inorganic materials consisting of metallic and non-metallic elements bonded together, to give a product that exhibits excellent mechanical and chemical properties which are often retained at high temperatures.

1.2- Engineering Ceramic Materials

In the last 20-30 years the use of ceramics in engineering or structural application has become more widespread. This is because ceramics provide strong, hard, stiff, light-weight components capable of withstanding high temperatures and operating in corrosive environments. The combination of these properties offers performance improvement and makes engineering ceramics the ideal candidates for many applications. Examples of engineering ceramics (also known as 'structural' ceramics) includes carbides, nitrides and oxides of silicon, aluminium, boron and beryllium, with silicon carbide and silicon nitride based ceramics showing the greatest promise for high temperature applications. Some of the properties are shown in table 1.1. Most of the engineering materials have a high degree of covalent bonding which results in good intrinsic thermo-mechanical properties, but the best mechanical properties are obtained only when the materials are fully dense.

Ceramics	Meltin or decomposition temperature (^{0}C)	Specific modulus (GPa)	Thermal expansion coefficient x10^{-6} $^0C^{-1}$ (20-1000^{0}C)
Al_2O_3	2050	90	8.5
AlN	2450	103	4.9
BeO	2530	124	9.0
SiC	2600	172	4.3
BN	2700	48	0.8 (normal to C-axis) 7.5 (parallel to c-axis)
Si_3N_4	1830	117	3.0
TiN	2930	43	9.3
ZrO_2	2700	212	10.0

Table 1.1 Properties of selected high temperature ceramics

1.3- Silicon Nitride Based Ceramics

Silicon nitride (Si_3N_4) is one of the most promising materials as a high temperature structural material. Interest in Si_3N_4 ceramics intensified with the realisation that they may be suitable substitutes for high temperature metal alloys in a range of gas turbine engines, due to the good combination of excellent high temperature mechanical properties. In particular, Si_3N_4, has a high strength at a high temperature, a good thermal stress resistance due to the low coefficient of thermal expansion, and a relatively good resistance to oxidation compared to other high temperature structural materials. This combination of properties can be used to increase operating temperatures. Moreover, the low density of Si_3N_4 of 3.2 gcm^{-3} (40% of the density of high temperature superalloys) may offer components of a lower weight which can operate at a faster rotational speed which can lead to a significant increase in engine efficiency.

Silicon nitride is a strongly covalent material. Thus, pure silicon nitride cannot be densified by conventional sintering processes. Hence the focus of much of the research on silicon nitride during the past 50 years has been on developing processing techniques to yield fully dense, high strength and tough materials. Much of this effort has been driven by the goal of exploiting the low density, high temperature strength, and excellent thermal shock resistance of silicon nitride.

Silicon nitride based ceramics are a family of materials produced by four major processing routes; Reaction bonded silicon nitride (RBSN), hot pressed silicon nitride (HP), sintered silicon nitride (SSN), and hot isostatically pressed silicon nitride (HIP). With the exception of RBSN each processing route requires substantial amounts of oxide additives to promote sintering. These additives react with the silicon nitride starting powder and its native silica layer to create a grain boundary oxynitride liquid phase whose composition generally controls the high temperature behaviour of the resultant product, although the addition of sintering aids is a necessary requirement in order to improve the densification of sialon materials. After sintering these additives usually result in the formation of a residual grain boundary glass phase which has a negative effective on the high temperature properties.

Derivatives of silicon nitride based ceramics are the 'Sialons', originally believed to be solid solutions of Si_3N_4 and Al_2O_3 (Oyama et al. 1971; Jack and Wilson 1972). This offers several advantages because the sintering temperature can be reduced considerably and the overall composition can be balanced so that all of the sintering aids are taken up in the crystalline grains in a solid solution, hence reducing any remaining amorphous phase and thereby maintaining the high temperature properties. The Sialon phases which have attracted most attention are β sialon (which is isostructural with β Si_3N_4 and is formed by the substitution of Si by Al and N by O and has a linear compositional range (not on the Si_3N_4-Al_2O_3 join) with a general formula $Si_{6-z}\,Al_z\,O_z\,N_{8-z}$ where $0<z>4.2$), and α Sialon which is isostructural with α Si_3N_4 with a limited two dimensional extension in the plane defined by the formula $M_{m/v}\,Si_{12-(m+n)}\,Al_{(m+n)}\,O_n\,N_{16-n}$.The

substitution in α' is similar to the β Sialon but its stability requires the addition of different metal oxides, such as Li, Na, Mg, Ca, Y, Sr or many of the rare-earth elements.

Sialon ceramics offer the advantages of the easier fabrication of complex shapes using pressureless sintering, the flexibility in selection of residual intergranular phase constitution, and the possibility of producing single phase ceramics via transient liquid sintering. The compatibility between the α' and β' enables the formation of composite microstructures, and the possibility of varying the α'/β' sialon phase ratio by slightly changing the overall composition, opening many possibilities of preparing sialon ceramics with varying properties. High proportions of β phase normally give good levels of toughness, whereas a high α phase content yields a high level of hardness.

1.4- Properties of Si_3N_4 Ceramics

The use of silicon nitride ceramic materials in many application has been limited by their mechanical properties.

1.4.1- Fracture Toughness

At low temperatures, due to their strong bonding and lack of plastic flow, ceramics are inherently brittle and frequently undergo sub-critical growth resulting in failure. Their resistance to crack propagation is termed the fracture toughness (K_{IC}) which also partially controls mechanical strength. An increase in fracture toughness is an important goal for many structural ceramics and can be achieved by modifying the microstructural features in order to reduce the stress concentration near the crack tip. The stress reduction can be achieved by different toughening mechanisms, such as crack deflection, which requires a weak interface and grain anisotropy, microcracking and dilatational phase transformation and crack bridging/ grain pullout. Figure (1.1) illustrates the

established toughening mechanisms which can offer resistance to this crack growth within the ceramic (Lewis 1993).

1.4.2- Hardness

Ceramic materials are known to have high hardness when compared to metals. The hardness is determined by the volume of plastic deformation caused by the indenter. Plastic deformation in crystalline ceramics is normally determined by the resistance to dislocation motion in the direction of the resolved stress, thus the greater the resistance to plastic deformation the higher the hardness value. The microstructure of polycrystalline ceramic materials will determine its hardness by means of grain size, residual stress, properties of intergranular phase and the amount of porosity present in addition to the intrinsic lattice friction stress for dislocation motion in major phases.

1.4.3- Oxidation Behaviour

Oxidation resistance is one of the most important properties for ceramic materials to be used at high temperature. In Si_3N_4 based ceramics oxidation occurs by forming a thin protective layer of silica (SiO_2) according to

$$Si_3N_4 + 3O_2 \Rightarrow 3SiO_2 + 2N_2$$

This describes low temperature oxidation of dense Si_3N_4 but at higher temperatures in materials containing sintering aids the oxidation is controlled by the rate of counter diffusion of oxygen and metal ion through the SiO_2. Some densification aids or their oxidation product can have high diffusion rates, allowing the Si_3N_4 to oxidise more quickly. In materials where the intergranular phase is a crystalline oxynitride the oxidation products can undergo large volumeteric changes causing cracking of the surface, exposing fresh surface for oxidation.

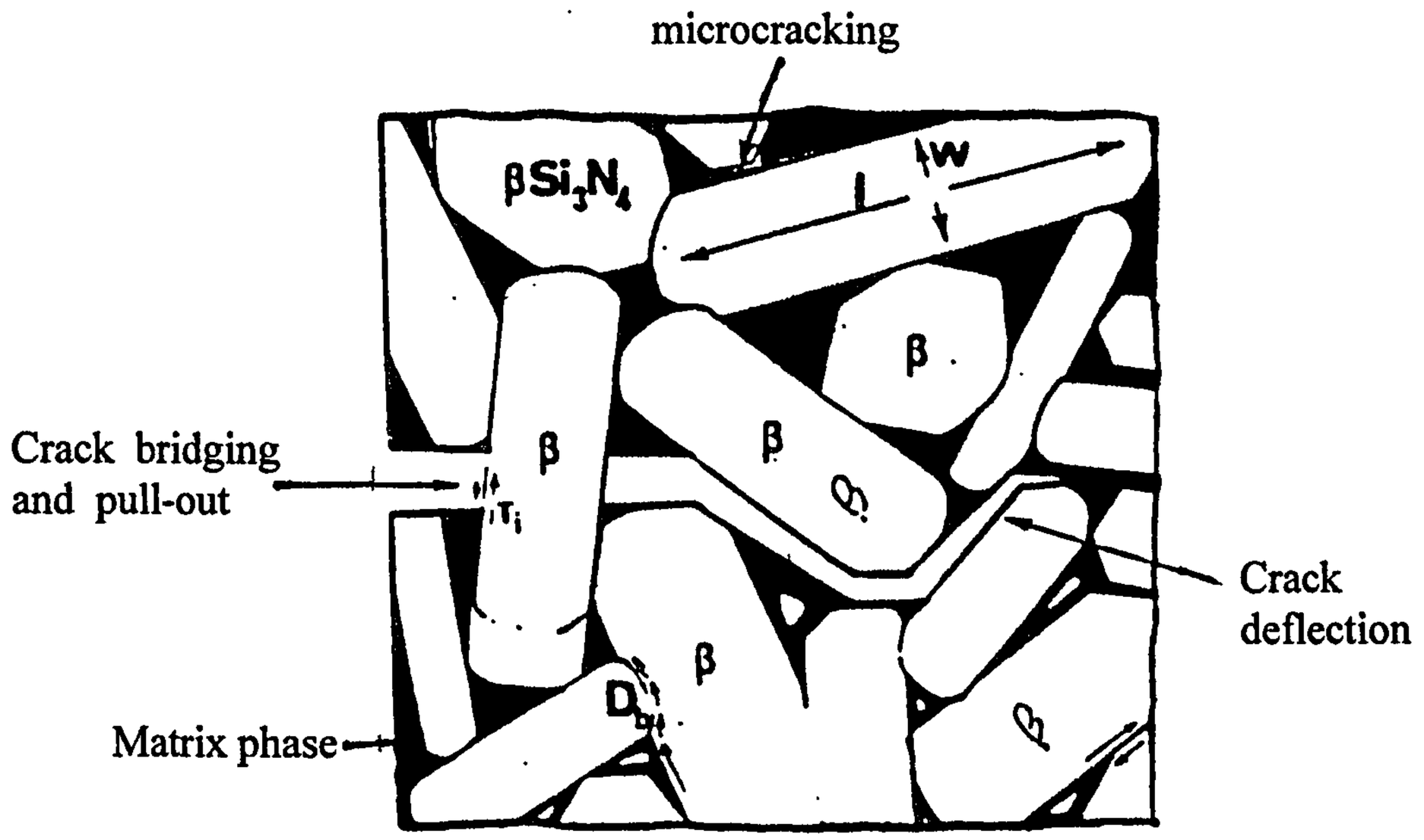

Figure 1.1 A schematic diagram illustrating the toughening mechanisms conferred by elongated grains

1.5- Thesis Structure

This thesis is composed of 8 chapters including this introduction.

Chapter 2 contains a review of the literature relevant to the present work. This includes a review of silicon nitride-based ceramics, particularly β-Sialon and α-Sialon , general information on Sialon and Me-Sialon systems, representation diagrams, densification and heat treatment products as well as thermal stability and phase transformations in the rare-earth sialon systems. It concludes with a brief review of the mechanical properties of sialon ceramics.

Chapter 3 outlines the experimental techniques used in the present investigation.

Chapter 4 is based on the study of Yb α/β-sialon ceramics and the possibility of controlling the α'/β' phase content and other microstructural features with variations in the starting composition, mainly within the sialon plane.

Chapter 5 presents the results obtained from the study of the effect of silica additions as well as that of β-Si_3N_4 'seeding' on the phase content and phase morphology in Yb-sialons. This chapter also contains the results from the study of thermal stability of Yb α'/β' sialons over a range of temperature.

Chapter 6 is based on experiments carried out to determine the effect of the addition of mixed cations on the phase content and the stability of α' in Yb/Nd and Gd/Nd-sialon systems.

Chapter 7 summarises the results from mechanical property measurements (hardness, fracture toughness) and the high temperature oxidation resistance.

Chapter 8 presents the conclusions obtained from this investigation.

CHAPTER 2

STRUCTURE AND PROPERTIES OF Si_3N_4 BASED CERAMICS

2.1- Introduction

This chapter presents a review of the literature with respect to silicon nitride and related materials. It explores the history of sialons through to current research, and emphasis is placed on α-sialon. General information relating to Si-Al-O-N and M-Si-Al-O-N systems is also included, such as graphical representation, densification and thermal stability of these system. The mechanical properties of such materials are also reviewed.

2.2- Silicon Nitride Structure

Silicon nitride exists in two common polymorphic structures known as α and β- Si_3N_4 (Hardie and Jack 1957; Marchand et al 1969 and Kato et al 1975) and is a strongly covalent material which forms tetrahedra, joined in a three-dimensional network by sharing corners, with silicon (Si) at the centre and nitrogen (N) atoms at the corners. Each nitrogen corner atom is a member of another 3 tetrahedra to form a continuous network with a hexagonal crystal structure (Figure 2.1). In β-Si_3N_4 (Figure 2.1a) the unit cell contains 6 silicon and 8 nitrogen atoms, forming tetrahedra layered in the sequence ABAB....(Hampshire 1978). The resultant lattice contains continuous channels parallel to the c-direction of the unit cell.

In α-Si_3N_4 Figure (2.1b) the unit cell contains 12 silicon and 16 nitrogen atoms forming layers of Si and N atoms stacked in the sequence ABCD ABCD (Hampshire 1978). The different stacking causes the long channel in

a

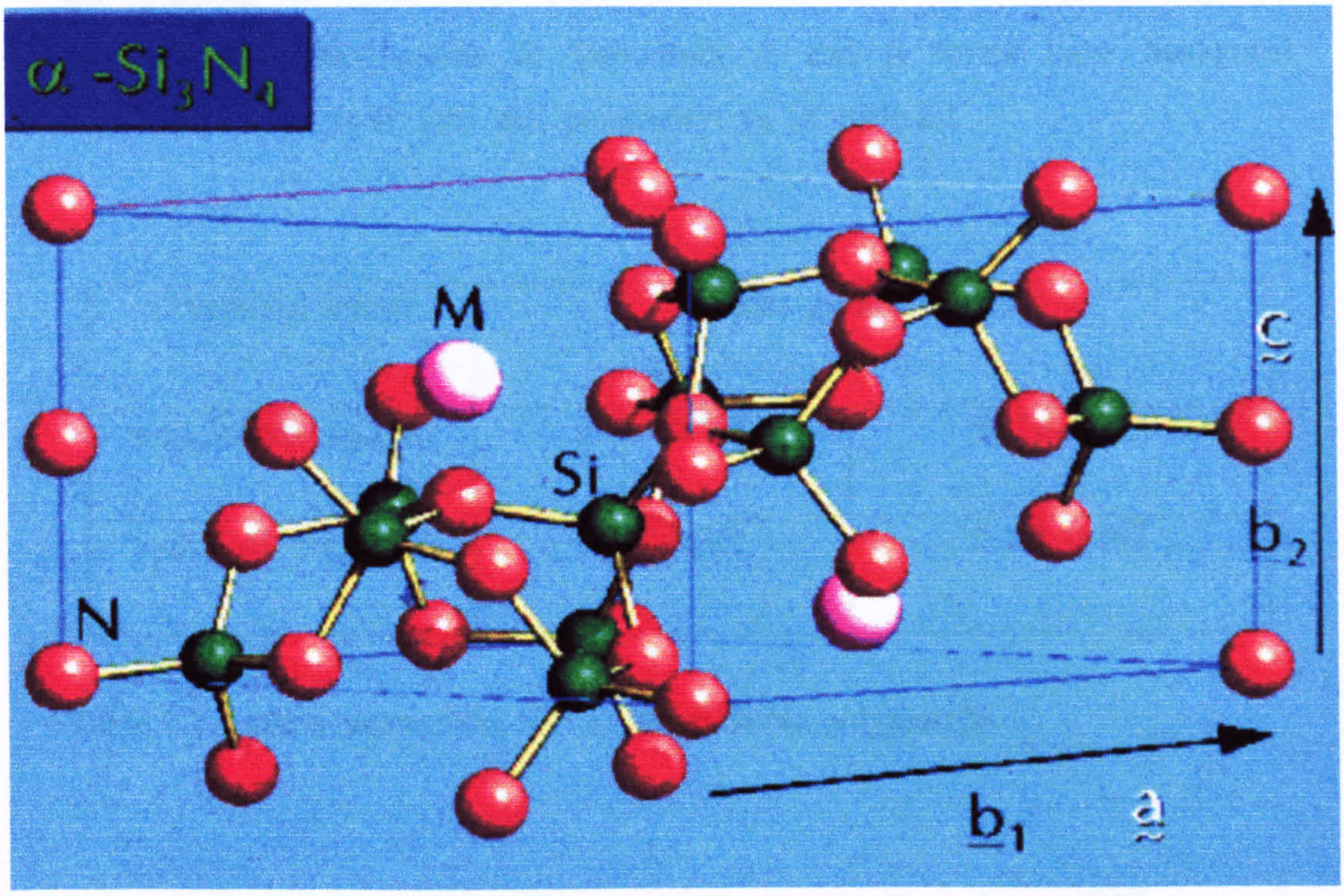

b

Figure 2.1. The crystal structure of silicon nitride (a) α-Si_3N_4 and (b) β-Si_3N_4

the β-phase to break and forms two interstitial sites large enough to accommodate other atoms or ions. Both α and β forms have hexagonal crystal structures with unit cell parameters as in table 2.1

Crystalline phase	Lattice parameters (nm)	
	a_o	c_o
α-Si_3N_4 (Hexagonal)	0.775-0.777	0.516-0.569
β-Si_3N_4(Hexagonal)	0.759-0.761	0.271-0.292

Table 2.1 Lattice parameters for α and β-Si_3N_4 polymorphs

The α structure is slightly distorted from the idealised form, which suggests that it is an oxynitride with a range of composition (Hardie and Jack 1957). More recent work revealed that α-Si_3N_4 may occur as a pure silicon nitride (Priest et al 1973, Edwards et al 1974 and Kato et al 1975). The presence of oxygen has been suggested as a thin layer of silica on the Si_3N_4 particles. Peuckert and Greil (1987) show that the oxygen impurities in the α-Si_3N_4 exist not only as a thin layer, but also in the bulk of the particles.

The phase transformation from α to β-Si_3N_4 is reconstructive and takes place at high temperatures (1600-1800^{0}C), usually via a solution-precipitation process in the liquid phase.

The good mechanical properties of silicon nitride ceramics are achieved only in fully dense materials. But as a highly covalent compound, Si_3N_4 exhibits a very low diffusivity and can only be densified by means of liquid phase sintering and using a sintering additive. Upon cooling this liquid phase forms a glassy phase at the grain boundaries, and is found to degrade the chemical and mechanical properties of the densified products at a high temperature.

2.3- Structure of Sialon Ceramics

Sialon ceramics are materials that have been derived from the α- and β-Si_3N_4 crystalline polymorphs and the word sialon is the acronym given to the phases in the Si-Al-O-N and related systems which were discovered independently in the early 1970s in both Japan, by (Oyama & Kamagaito 1971, Oyama 1972), and in England, by (Jack and Wilson 1972). Both investigations reported that it is possible to substitute the Al^{3+} ions for Si^{4+} ions in silicon nitride provided that the charge balance is then maintained simultaneously by the substitution of O^{2-} for N^{3-} in the structure. The X-ray diffraction pattern of the Si_3N_4 solid solution was found to be very similar to the Si_3N_4, with a slight peak shift to a lower 2θ angle, thus the (hkl) Bragg planes which give rise to the X-ray reflection remain the same, indicating the retention of a parent structure. The β-sialon is a solid solution based on β-Si_3N_4 and is formed by the simultaneous equivalent substitution of Al-O bonds for Si-N bonds. Since the difference between the (Si-N) and (Al-O) bond lengths (0.174 nm and 0.175 nm respectively) is small, the structural strain is also small and the crystal structure remains unchanged. The cation/anion balance remains at 3:4 and no constitutional vacancies are formed, hence for β-sialon the aluminium substitution leads to the formula:

$$Si_{6-z}Al_zO_zN_{8-z}$$

in which the z-value can vary continuously from zero to about 4.2. The β-sialon was originally described as a solid solution based on a simple mixture of stoichiometeric compounds Al_2O_3/ Si_3N_4 which implies a defect structure with Si vacancies, but this is not applicable with the modified formula.

α-Sialon (α') is a solid solution based on α-Si_3N_4 in which m(Al-N) and n(Al-O) bonds replace (m+n) (Si-N) bonds in each unit cell thus giving rise to the general formula for α' sialon as

$$M_x Si_{12-(m+n)} Al_{(m+n)} O_n N_{16-n} \qquad 2.2$$

The replacement is largely by (Al-N) bonds, and as the trivalent Al^{3+} replaces Si^{4+}, a negative charge imbalance results. The stabilisation of the α' sialon structure is achieved by the incorporation of modifying cations into the interstitial sites of the unit cell. The modifying cation has a solubility range $x \leq 2$ and is related to the valency, v, of the stabilising cation, M, according to the relationship $x=m/v$ (Hampshire et al 1978). The elements M, that are usually used as a modifying cation include Ca, Y, Mg Li and the rare earth elements except La, Eu, Pr.

2.4- Representation of the Sialon System.

2.4.1- The Si-Al-O-N System

As a four-component system, it is represented by a square diagram whose corners correspond to components Si_3N_4, AlN, SiO_2 and Al_2O_3. The behaviour diagram of the SiAlON system at different temperatures is best illustrated as a reciprocal salt system where the concentrations are expressed in equivalents rather than as atoms or percentages of atoms present (Jack 1976, Ekstrom and Nygren 1992). Figure (2.2) is the simplest representation of the Si_3N_4-AlN-Al_2O_3-SiO_2 system (Jack 1976). Although the bonding in Si-Al-O-N materials is predominantly covalent, all compounds are expressed in ionic terms. Hence any point on the diagram represents 12 positive and 12 negative valences. This behaviour diagram does not represent thermodynamic equilibrium phase relationships. The β sialon phase is represented by a single line extended from the Si_3N_4 corner toward the Al_2O_3-AlN line.

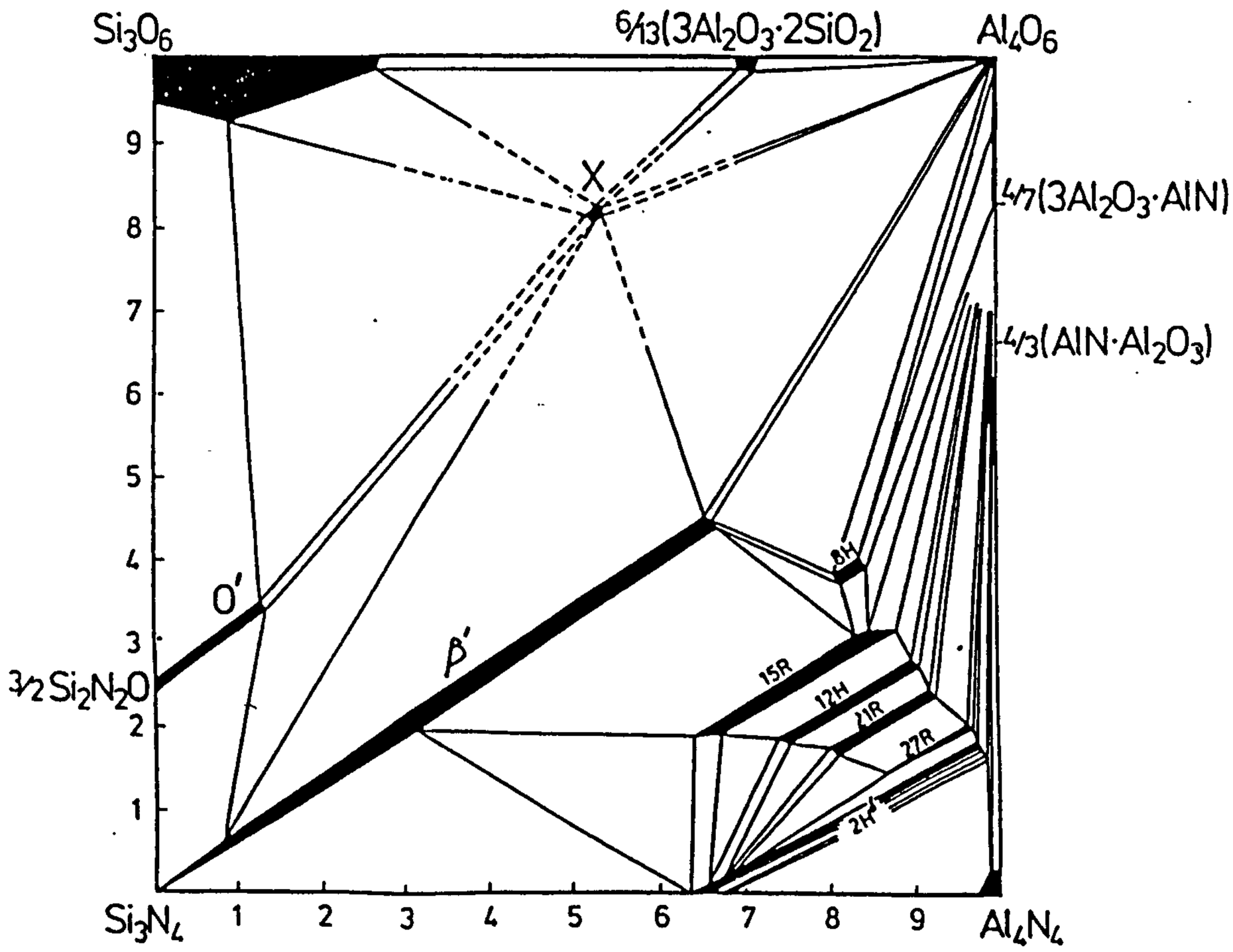

Figure 2.2. The square equivalence diagram of Si_3N_4-AlN-Al_2O_3-SiO_2 system.

In addition to the β-sialon phase, other phases have also been reported. O-sialon (O') (Jack 1976) is a solid solution of silicon oxynitride Si_2N_2O, and formed by the same mechanism as β-sialon with a limited range of compositions extending from Si_2N_2O towards the Al_2O_3 corner along the 2M:3X line. The minor X-phase is found close to the liquid phase region at high temperatures. This phase is formed by reactions between the α-Si_3N_4 and Al_2O_3 and exists in two modifications, high and low X-phase (Drew and Lewis 1974).

The sialon polytypoid phases are formed near the AlN rich corner of the SiO_2-Al_2O_3-AlN-Si_3N_4 diagram (Figure 2.2) with a limited range of compositions along the M_m:X_{m+1} ($4 \leq m \leq 10$) lines (Gauckler et al 1975). The phases observed in the AlN based system are 8H, 27R, 21R, 15R, 12H and 2H. The phases are structurally similar and based on the Wurtzite type structure of unmodified AlN, with stacking sequences related to their composition. The R and H indicate rhombohedral and hexagonal unit cells and the numerals denote the number of layers within the structure along the c-axis (Thompson 1977, Van Tendeloo et al 1983). Each polytypoid has a constant metal / non-metal ratio (M/X) which can be related to the number of layers present in the unit cell. For example 12H has a structure composed of 2 layers repeated 6 times and the M:X ratio observed is 6/7.

2.4.2- Me-Si-Al-O-N System

The use of an additional metal cation, M, results in expansion of the sialon system into a five-component system (Me-Si-Al-O-N). A simple representation of compositions in this system may be expressed using Janecke's triangular prism in which all edges, expressed in equivalent units, are equal. The base of the prism is the standard square diagram of the Si_3N_4-SiO_2-AlN-Al_2O_3 system discussed above in section 2.4.1, with the fifth Me-component being represented along the third dimension, thus forming two

more squares of AlN-Al_2O_3-MeN-Me_2O_3 and Si_3N_4-SiO_2-MeN-Me_2O_3 Figure (2.3). The triangular faces at both sides are the nitride and the ternary oxide systems. The concentration of all components is expressed in equivalent units as mentioned above, so that any point in the prism represents a combination of 12 positive and 12 negative valences. This representation of the M-Si-Al-O-N system in equivalents is a behavioural diagram and, as such, does not represent thermodynamical equilibrium phase relationships.

The α' sialon has a two-dimensional solid solution range in the Si_3N_4 - 4/3(Al_2O_3-AlN) - MeN.3AlN plane in the Janecke prism (Figure 2.3). This plane intersects the basal plane of the prism along the β-sialon solid solution line (following the Si_3N_4-Al_2O_3.AlN join) and the α-sialon is separated from the β-sialon by an α- β two phase area.

2.5- β'-Sialon

The β-sialon ceramics formed by the substitution of Al-O bonds for Si-N bonds have a homogeneity range as defined in equation 2.1. Hence increasing the z-value increases the number of Al-O bonds within the structure and also increases the unit cell size. Thus the changes in the z-value, are directly related to the aluminium content, which may affect the properties of the materials. The range of solid solutions for the β-sialon materials is demonstrated on the square equivalence diagram shown in Figure (2.2) with Si_3N_4 , Al_2O_3. AlN and SiO_2 as the terminal compounds. The first description of a β-solid solution was based on a simple mixture of stoichiometric compounds Al_2O_3/Si_3N_4 which implies a defect structure with Si vacancies. It was demonstrated later from the creep and microscopy measurements that the Al_2O_3/Si_3N_4 mixtures were in fact diphasic (i.e containing glass or X-phase) (Drew and Lewis 1974). Lumby et al. (1974)

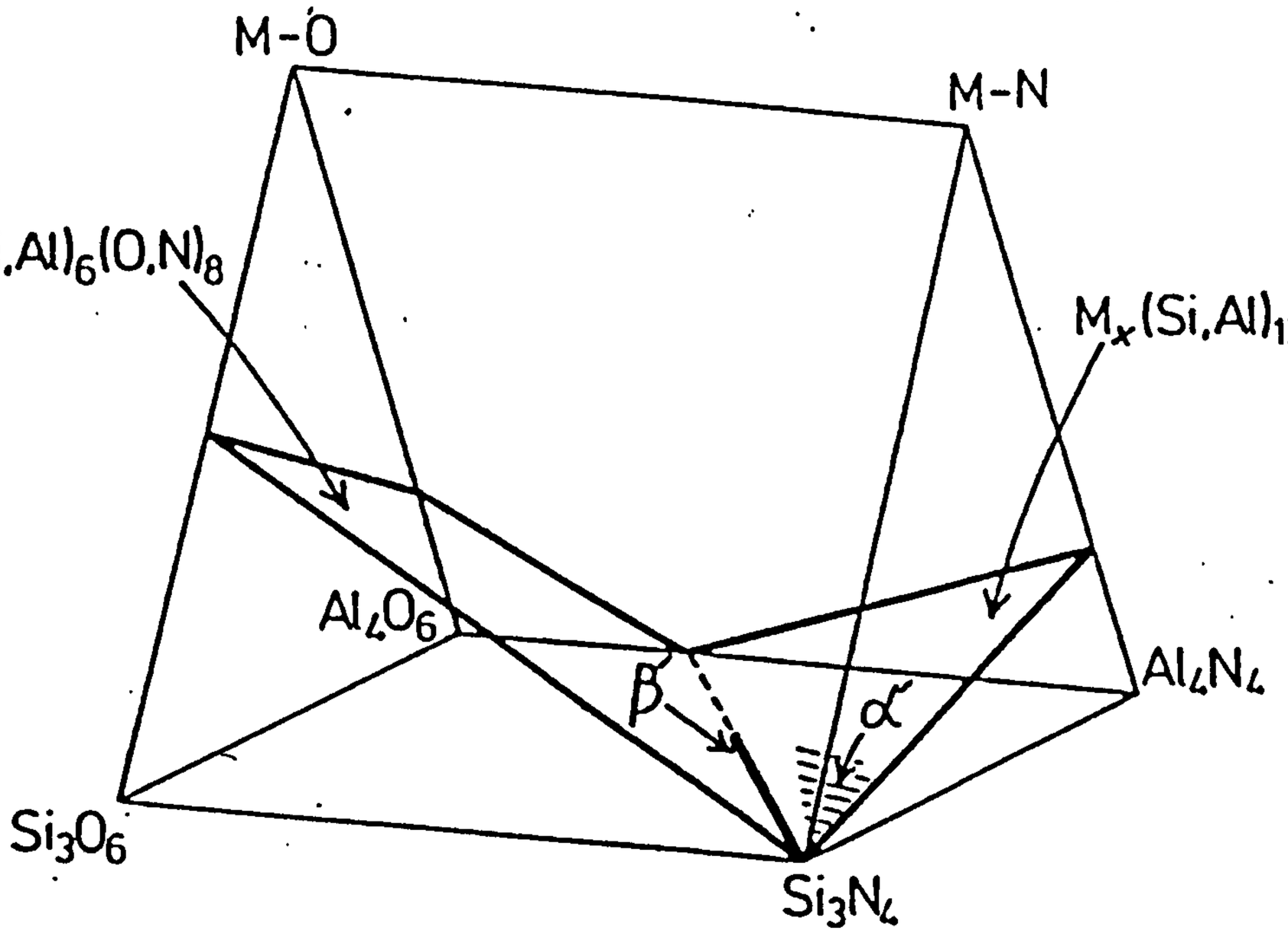

Figure 2.3. The Janecke prism for the M-Si-Al-O-N system.

revealed that an addition of AlN is required to balance the presence of SiO_2 layer on Si_3N_4 powder.

The β-sialon composition lies along the Si_3N_4 /Al_3O_3N line. From the liquid phase region shown in Figure (2.2), it should be possible to use this liquid phase to densify sialon material without the addition of sintering aids (Drew and Lewis 1974, Bandyopadhyay and Mukerji 1987). The addition of equimolar Al_2O_3 and AlN and sintering at high temperatures will result in β-sialon with a very little or no grain boundary glass phase (Lewis et al 1977, Ekstrom et al 1989). In practice this is however difficult to achieve and the addition of a metal oxide such as MgO, Y_2O_3 and selected rare earth are necessary to produce dense materials. With the addition of these sintering additives more liquid is formed at lower temperatures, and this can have the advantage of improving sinterability, especially by pressureless sintering. However, because the β' structure cannot accommodate the other cations the sintering additives remain as a residual glassy phase at the grain boundaries.

Many of the β-sialon materials which have been successfully developed in engineering ceramics applications contain a low level of solid solution ($z=<0.5$). At these levels of substitution, the β-sialon retains the excellent properties of β-Si_3N_4, while allowing control of the liquid phase sinterability and the composition of the remaining intergranular phase. β-sialons sintered with a larger amount of sintering aids have a microstructure consisting of elongated grains. Sialons with higher z-values exhibit a deterioration in properties such as hardness. Materials with a significant amount of glassy phase have poor high temperature properties which are limited to use below 1000^0C. At low temperatures the presence of an intergranular glassy phase allows a preferred crack path along grain boundaries and fracture toughness is enhanced

To improve the high temperature properties the residual glass in these materials may be crystallised during slow cooling from sintering temperatures or by post-sintering heat treatments to form a refractory product which may

be an oxide. For example in the Y-Sialon system the post-sintering heat treatment crystallises the residual glassy phase into a yttrium aluminum garnet, (YAG, $Y_3Al_5O_{12}$) with small Si and N substitution (Lewis et al, 1980). For β'+YAG the strength degradation temperature improved to around 1320^{0}C over β'+ glass (Lewis et al 1988). A perfect β' and YAG two phase structure can be approached if, simultaneously with the formation of the YAG, the residual Si + N is incorporated into the β-structure. The YAG phase is located on the Y_2O_3-Al_2O_3 line (see Figure 2.5). YAG is not the only devitrification product in this system. Other phases such as $Y_2Si_2O_7$, Melilite ($Y_2Si_3O_3N_4$), Wollastonite ($YSiO_2N$) may also be formed.

2.6- α'-Sialon

As mentioned in section (2.3), the α -sialon phase is defined by equation 2.1. This formula implies that m(Al-N) and n(Al-O) bonds replace (m+n)(Si-N) bonds but the major substitution is by the replacement of Si^{4+} by Al^{3+}, where the electron balance is retained by the introduction of metal cations into the interstices of the α–phase structure (see Figure 2.1). Similar to the formation of the β'-sialon phase, the formation of α' is not a simple reaction between silicon nitride, alumina and the stabilising cations, but also requires the addition of AlN. In the β-sialon system the metal oxide which is added to form the liquid sintering phase, cannot be accommodated in the β structure and remains as a residual glass phase after sintering. The ability of α-sialon to accommodate the metal cation into its structure opens up the possibility of producing a single phase with a minimum amount of residual intergranular glass. In the α-sialon system the choice of a suitable sintering additive is compounded by the fact that in addition to sinterability the metal cation must also be able to stabilise the α' structure. Cheng and Thompson (1994a, 1994b) have suggested the following criteria as requirements for the selection of metal oxides as sintering additives. These criteria are-:

1) The cation must stabilise the α'- structure.
2) The liquid formation temperature of the oxide containing liquid should be lower than the formation temperature of the α' phase, but high enough to give good creep behaviour.
3) Densification must not be slowed down by the formation of any intermediate phase produced by the oxide additive during sintering and the intermediate phase must not remain in the final product.
4) It is desirable but not essential to have a large liquid phase region in the R-Si-Al-O-N system in equilibrium with the α' phase.
5) The cation- containing residual glass phase must crystallise and produce high temperature and oxidation resistant phases.

In addition other factors, such as the thermal stability of the resultant materials and the cost of the raw materials, may also be considered. The elements usually used in the sintering process compensate interstitially in the α' structure for the replacement of m(Si-N) by m(Al-N). The univalent cation Li^+ forms a single phase α-sialon with a maximum solubility of 1.5 cation per unit cell (Kuang et al. 1990).

The divalent elements Mg^{2+} and Ca^{2+} both form a single phase α-sialon, where Ca^{2+} has the largest reported solubility in the α structure 1.83 Ca^{2+} atom per unit cell. Hwang et al. (1995) reported that Sr^{2+} cannot form an α' sialon but it could be accommodated into α' structure only in conjunction with other cations such as Y^{3+} or Ca^{3+}.

The most extensive studies of the various α-sialon systems have been carried out using a trivalent Y^{3+} and lanthanide elements, except La, Ce, Pr and Eu the ionic radii of which, being > 0.1 nm were presumed to be too large to be accommodated in the α' structure. The largest rare-earth cation which has been reported to enter the α-sialon alone is Nd^{3+}, with an ionic radius around 0.099 nm (Ekstrom and Shen 1995; Kall and Ekstrom 1990, Mandal and Thompson 1996, Shen et al 1996a). The slightly larger cation Ce^{3+}, with a radius of 0.103 nm, has not been observed to enter the α sialon structure alone, but

together with a smaller stabilising cation like Y^{3+} (radius 0.089 nm) (Soderlund and Ekstrom and Persson 1990; Ekstrom et al. 1991). Moreover, a recent study by Thompson and Mandal (1997) revealed that the Ce stabilised α-sialon does form and is stable at the sintering temperature. No evidence, however, been found for the incorporation of La^{3+} with an ionic radius of 0.106 nm into a structure even if added together with Yttrium.. The smaller ionic radii of the rare-earth cations, such as Dy^{3+} and Yb^{3+} can be easily incorporated into the α' lattice, and a single phase α' is possible.

2.6.1. The Yttrium α-Sialon System

The Yttrium α-sialon is one of the sialon systems studied in most detail so far (Cao 1991; Chatfield et al 1986; Huang et al 1983; Slasor and Thompson 1987). The phase compatibility regions in the two-dimensional Yttrium α-sialon formation plane have been widely investigated and reported as shown in Figure (2.4) (Slasor and Thompson 1987). Y^{3+} as a stabiliser cation for α sialon phase can be easily accommodated in the structure because of its small ionic radius of 0.0892 nm and it has a maximum solubility limit within the α'-sialon structure of 0.67 cation per unit cell (Huang 1983). This value is comparable to the solubility limit of the majority of the rare earth elements but lower than the values quoted for the single and double valent cations.

Yttrium, as an oxide additive for sintering α-sialon, can satisfactorily meet all the demands mentioned above. In addition to the ability to stabilise the α'-structure, the eutectic temperature in this system, at 1350^0C, is below the 1500^0C for α' formation. The study of the reaction sequence of the formation of Y α' and Y α'/β'-sialon in the Y-Sialon system revealed that intermediate phases, such as Y-Melilite or YAG, were formed as transitory phases which hinder the densification and α' formation at the early stages. These phases were redissolved into the liquid as the temperature increased above 1600^0C (Cao and Metselaar 1991 and Sun et al 1987).

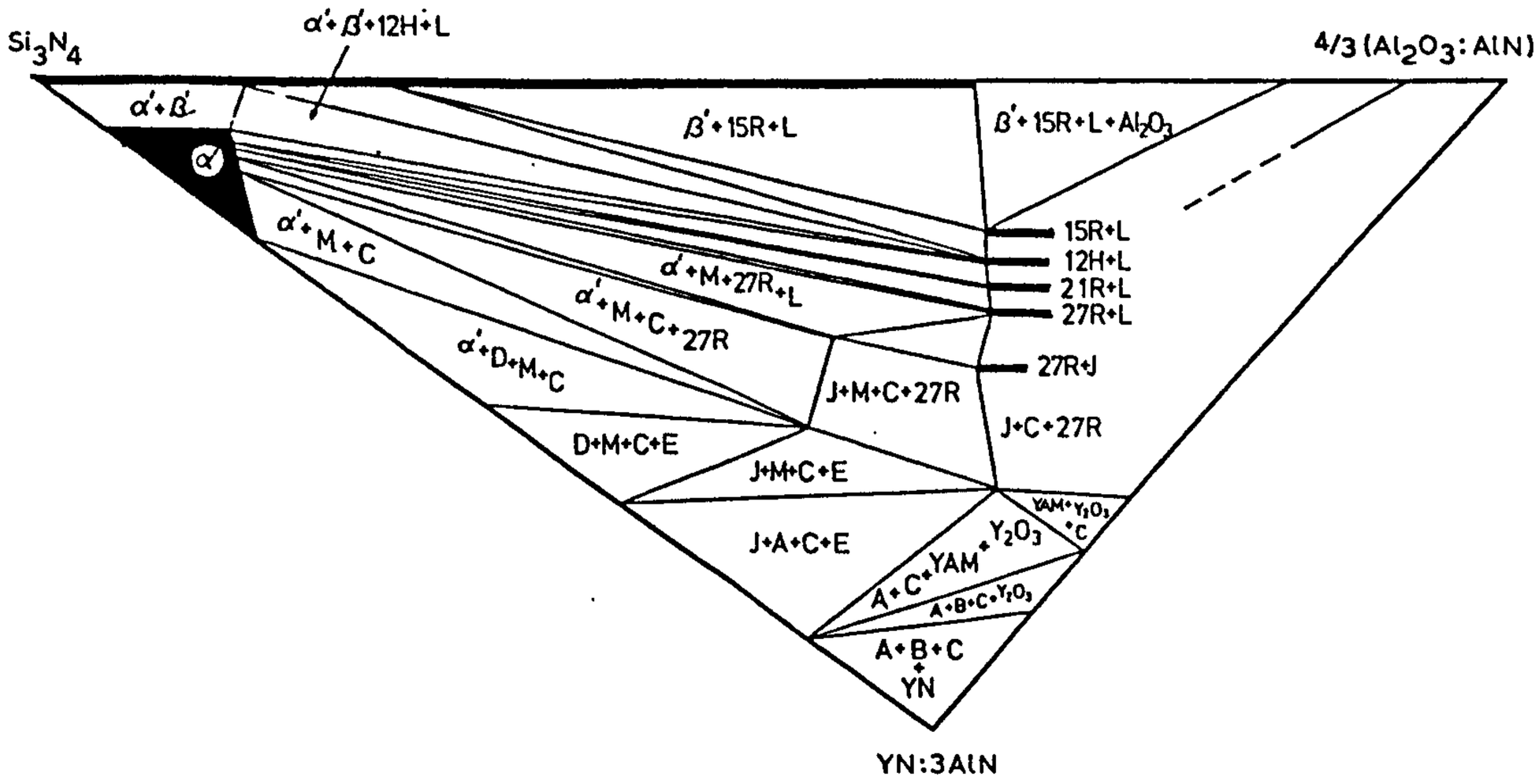

Figure.2.4. The behavior phase relationships in Y-Sialon plane at 1750^{0}C.

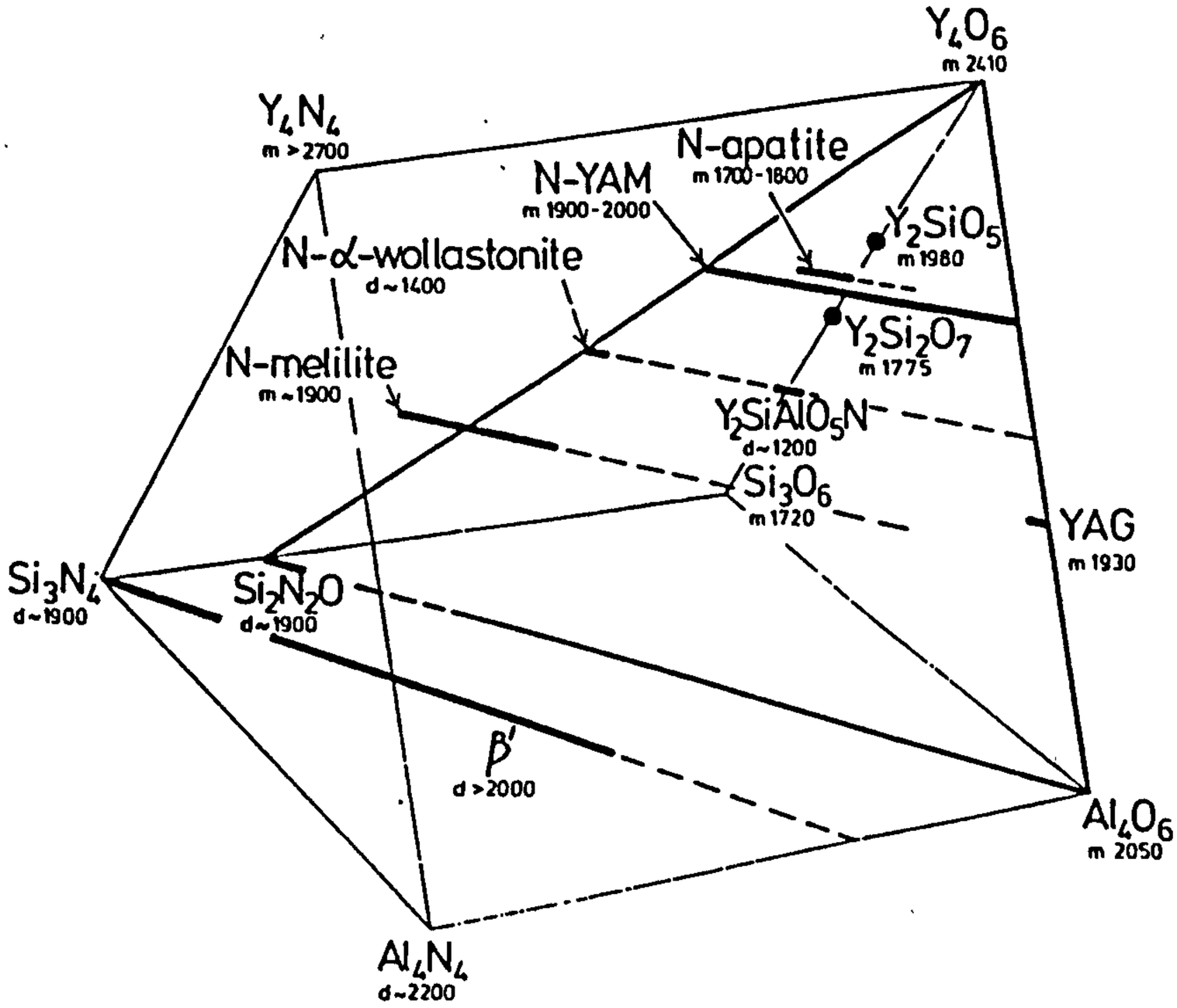

Figure 2.5. The Y-SiAlON Janecke prism showing the crystallisation phases within the system

Yttrium, as a sintering aid, can only be partly consumed by the α' sialon structure, and the excess will form a residual glassy phase, which will determine the high temperature properties. Crystallisation of this residual intergranular glass phase into various phases has been reported as in Figure 2.5 (Jack 1986). The refractory YAG ($Y_3Al_5O_{12}$) phase is one of the most desirable phases for improving the materials overall properties (Lewis et al 1980, Drew et al 1983 and Jasper and Lewis 1992)

2.6.2. The Rare-earth (R) α-SiAlON System

The use of rare earth elements as sintering aids and as stabiliser cations for α-sialon has received a special interest in the past few years. This is because these elements form a refractory glass upon cooling from the sintering temperature and during the crystallisation process form crystalline products similar to those observed in the Y-sialon system. The solubility of rare earth cations within the α-structure in these systems is dependent on the ionic radius of the elements. The lower limits are the same as for yttrium, which is approximately ~0.3.

The maximum solubility limits generally decreases as the cation radius increases i.e as the atomic number increases (Cao and Metselaar 1991 and Huang et al 1986). The Yb^{3+} with the smallest ionic radius (~0.08 nm) exhibits the highest solubility of ~ 1.0 cation per unit cell. This value decreased as the ionic radius increases and Nd^{3+} (~0.099 nm) and Sm^{3+} (~0.09 nm) have been reported to have a maximum solubility limit of ~ 0.6, as shown in figure 2.6 (Huang et al 1986; Huang and Yan 1992). The studies of subsolidus phase relationships in Si_3N_4-AlN-rare earth oxide systems at a temperature of 1700^0C, indicated that these α sialons have a composition field quite similar to that of yttrium α'-sialon, but the limits of these solid solutions widen with the decreasing size of the cations. Figure 2.7 shows that the α' phase area is dependent on the stabilising cation and that the larger the rare earth cation used the smaller the single α'-sialon phase region (Ekstrom et al 1997).

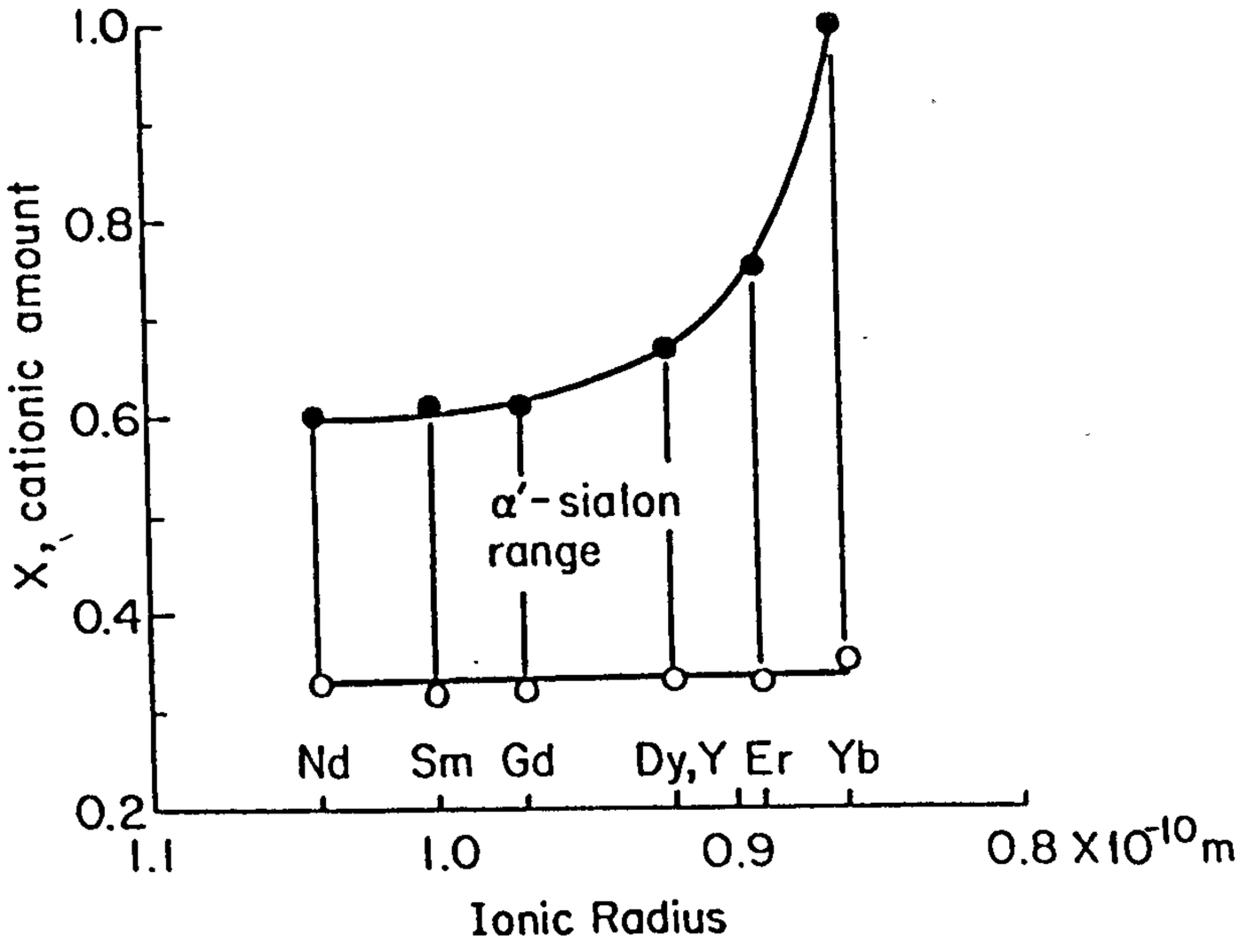

Figure.2.6. The relationship between the α' solid soluibility limit and the rare-earth cation ionic radius.

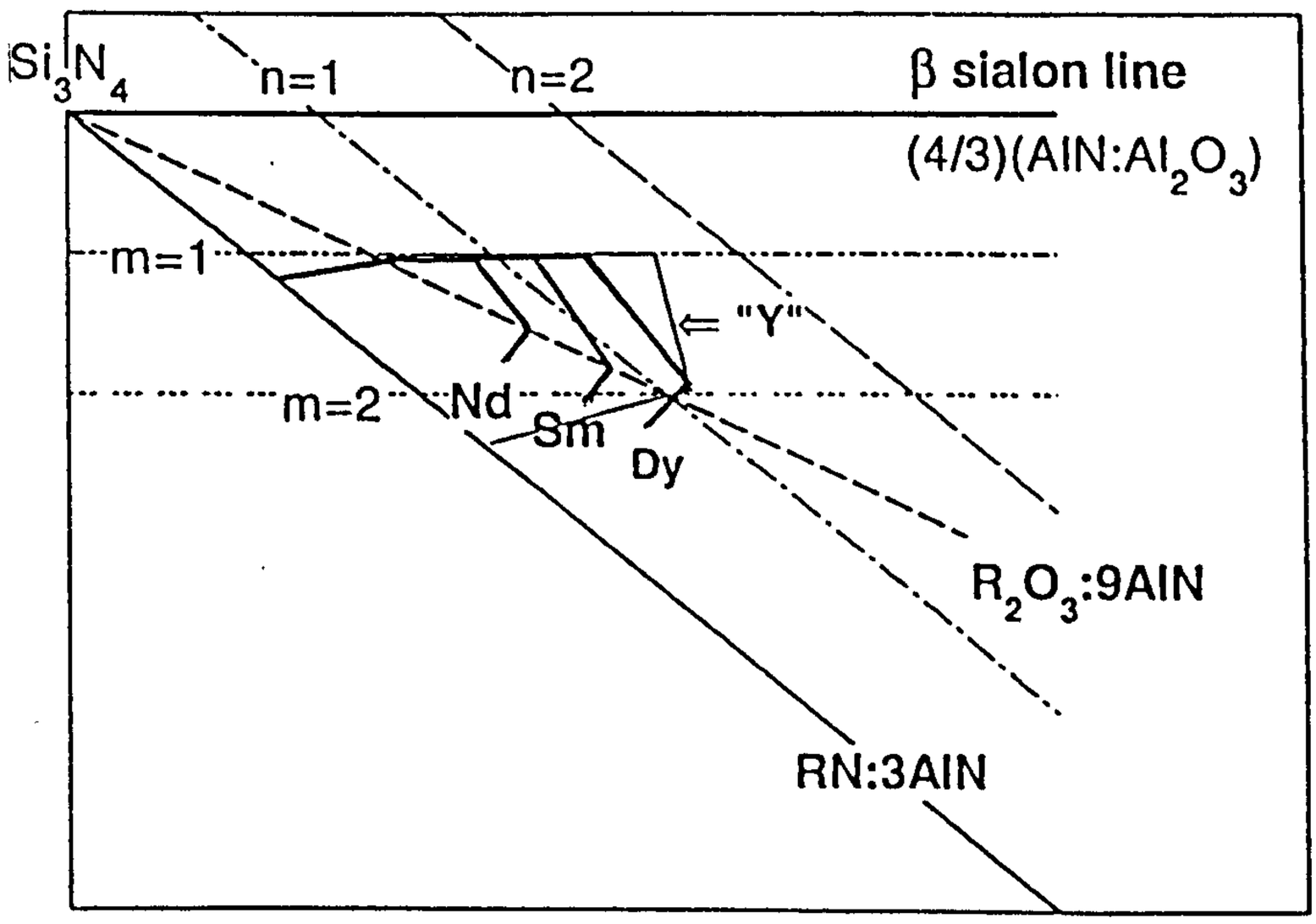

Figure 2.7. The schematic representation of the α-SiAlON forming region for different rare-earth elements.

The rare earth elements especially those with a higher z-value (such as Dy, Er, Yb) are similar to Yttrium in chemical behaviour. The rare earth elements with a low atomic number (z-value) are, however, quite different, especially in regard to compound formation in the LnSiAlON systems. The subsolidus phase relationships in R_2O_3-Si_3N_4-AlN-Al_2O_3 (R= Nd, Sm) systems showed that α-sialon is compatible with the melilite phase M (or the aluminium-substituted melilite phase M') ($Ln_2 Si_{3-x}Al_xO_{x+3} N_{4-x}$; where $0<x<1$). In addition, the $LnAlO_3$ phase was also connected via a tie line to β' and the AlN polytypoids (Sun et al 1995).

The sintering behaviour of rare-earth element-containing α'-sialon ceramics have been investigated by several researchers. The densification of Re α'-sialon materials follow the same order of the maximum solubility limits. Wang et al (1993) reported that the temperatures required for full densification decrease and the content of α'-sialon phase increases with increasing z-value of the stabiliser cation. The reaction sequence in the rare-earth sialon systems is similar to yttrium α-sialon. The sintering behaviour and formation of Re α'-sialon in light rare-earth systems indicated that a M melilite phase (or its solid solution) occurs as a transitional phase during the formation of α' and α'/β' sialons and this phase persists to high temperature which retards the formation of α' sialon.

In the heavier rare earth systems (Dy, Yb), although the cation rich intermediate phases may be formed during sintering, dense single phase α-sialons have been reported (Shen et al 1996c; Ekstrom et. al, 1997). The intermediate phases in these systems become unstable at higher temperatures (above 1600^0C) and remelt in the sintering liquid thus releasing the cations required for the α' precipitation.

Wang et. al. (1993) and Menon and Chen (1995) have reported that the difference in the reaction of the eutectic liquid phase with the nitride starting powders affects the intermediate phases formed during the reaction sequence to form α'.

The crystalline product which may occur after heat treatment is dependent on the atomic number of the stabilising α sialons, heat treatment temperature and the intergranular composition. The potential grain boundary phases determined from the devitrification of the rare-earth-Sialon glasses are shown in Figure (2.8) within the Ln-Sialon prism (Mandal et al 1992).

2.7. Densification of Sialon Ceramics

Sialons ceramics, similar to Si_3N_4 materials, are densified using liquid forming additives that allow densification and transformation to progress via a transient liquid phase sintering where diffusion rates are much greater. These additives are most commonly those which form silicate-related eutectic liquids when they react with the SiO_2 and Al_2O_3 layers inevitably formed on the surface of Si_3N_4 and AlN powders respectively. Intensive studies have been made on the reaction liquid phase sintering of Sialons in the M_xO_y -Si_3N_4-AlN-SiO_2-Al_2O_3 system (Drew and Lewis 1974, Lewis et. al, 1977, 1980, 1993). In these studies the densification mechanisms were identified to be solution-reprecipitation.

There are three general requirements for liquid phase sintering (Kingery 1959)

- A liquid must be present at sintering temperatures
- There should be a good wetting of the solid by the liquid
- The solid must be reasonably soluble in the liquid.

According to Kingery (1959) the process of liquid phase sintering consists of three distinct stages:

I- particle rearrangement

II- solution-precipitation

III- final pore removal (or coalescence of the grains).

In stage I a number of simultaneous processes occur with primary rearrangement immediately following the formation of the liquid. Both the solid particles and the liquid are rearranged by capillary forces in the liquid

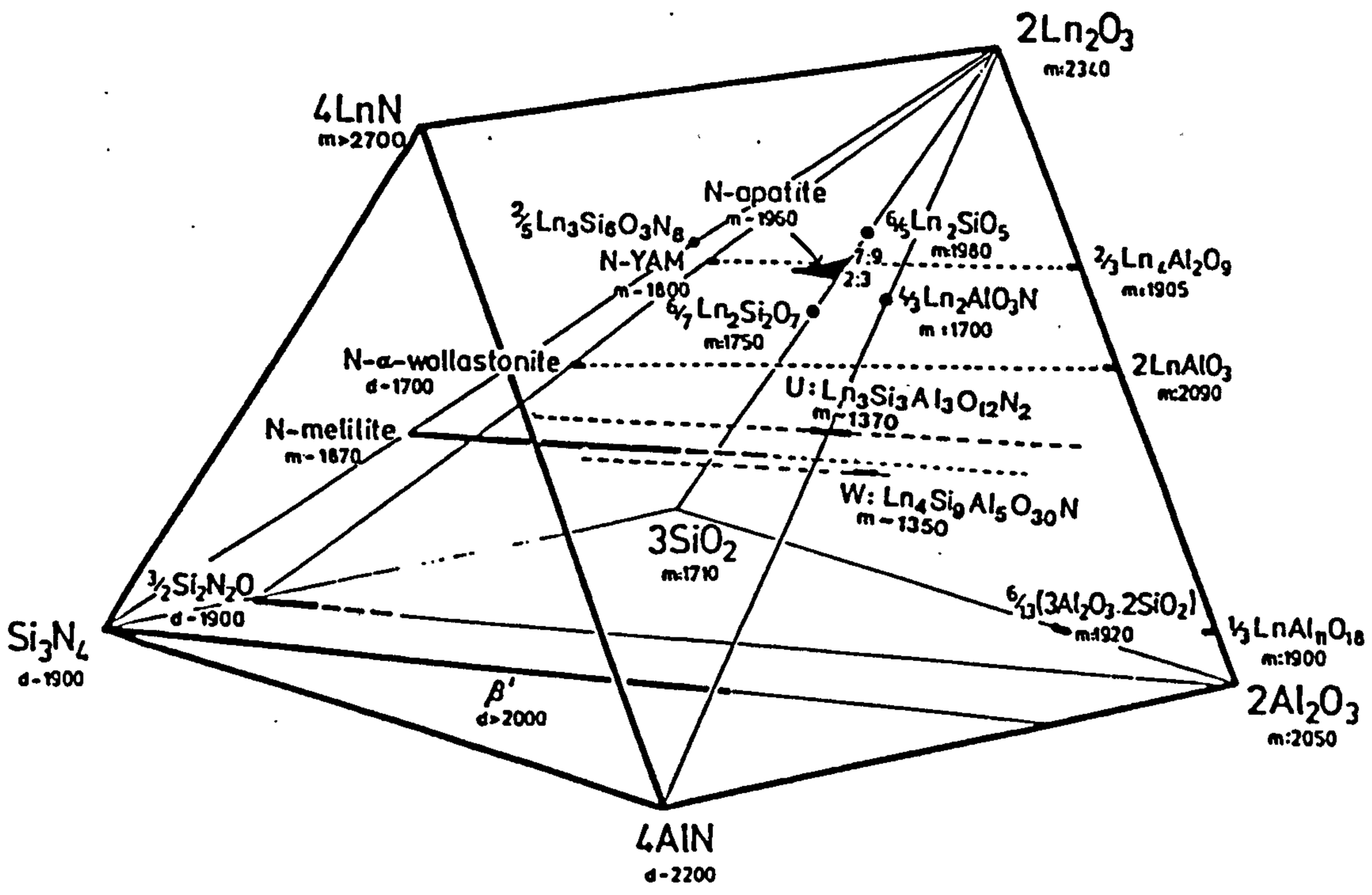

Figure 2.8. The Ln-SiAlON Jancke prism showing the phases determined in the rare-earth system.

situated between the particles. The liquid present between the particles also acts as a lubricant allowing the easy movement of particles. The viscosity of the liquid phase present has a significant effect upon the rate of densification due to rearrangement.

In stage II, solution-precipitation, the reaction proceeds at this stage via the dissolution of the solid material into the liquid phase and then precipitates out onto existing sites. This process is often accompanied by a phase change such as in Si_3N_4 where α-Si_3N_4 dissolves into the liquid and precipitates out as β-Si_3N_4. Differential dissolution takes place according to grain shape and size. Small particles dissolve into the liquid more readily and reprecipitate out onto coarser grains. This process occurs concurrently with a further rearrangement of grains due to capillary forces that are still present.

The final stage III involves grain growth within the structure and the densification rate at this stage is low due to the limited amount of available liquid.

In the densification of α'-sialon materials the liquid flow becomes a limiting factor in the completion of the reaction. The incorporation of the liquid constituents into the α' structures as the precipitation of α' proceeds, increases the viscosity and decreases the amount of the remaining liquid, thus slowing shrinkage as well as densification. The formation of any intermediate phase with α' precipitation has been found to retard both densification and reaction completion as a result of a decrease in the amount of the liquid (Watari 1994). The rate of α'-sialon precipitation will be reduced until the intermediate phases remelt at higher temperatures.

Hwang and Chen (1994) found that the hot pressing reaction of α' and α'/β' Y-sialon took place in three stages. Further, these authors found that the wetting properties of the Y_2O_3-Al_2O_3-SiO_2 eutectic melt controlled the densification behaviour of powder compact. These authors found that the chemical characteristics of the liquid in particular its wetting behaviour will

determine the reaction pathways during α' densification. Menon and Chen (1995a) reported that in the M-Sialon system, (M= Li, Ca, Mg, and rare-earth elements), the wetting behaviour of the ternary oxides on the two nitride powders present (Si_3N_4 and AlN) was different depending on the metal oxide used. Such preference in reaction sequence was explained in terms of acid-base chemistry. Generally the more basic oxides wet Si_3N_4, whereas the more acidic oxides wet AlN. Therefore oxide melts of Li, Ca, Mg and light rare earth elements, such as (Nd, Sm and Gd), react first with silicon nitride powder to form the Al substituted melilite (M') as an intermediate phase. As this phase consumes a large amount of the cations and nitrogen, the reaction to form α-sialon is retarded until M' redissolves into the liquid at a higher temperature (1700^{0}C). The oxide melt in the heavier rare-earth (Dy, Yb) reacts first with the AlN starting powder and forms β' as an intermediate phase.

The reactions sequences which lead towards α' densification have been shown by (Menon 1995a) to proceed in five stages:

- formation of a ternary oxide eutectic liquid
- initial wetting of nitride powder and transient phase precipitation
- secondary wetting of the other nitride powder
- dissolution of the intermediate phase
- precipitation of the final phase, α'

The rare-earth densification additives used for sintering of sialon ceramics are generally insoluble in the β'-sialon structure and even though most of them are α'-sialon formers, some amount of these additives remains as a residual Msialon intergranular glass phase, which consequently degrades the mechanical properties of the materials above the glass-softening temperature which is normally about 900-1100^{0}C. Post sintering heat treatment is one of the accepted methods to eliminate or minimise the glass grain boundary phase by converting it into refractory crystalline phases, thus improving the materials performance at high temperatures.

There has been much work carried out in understanding grain boundary crystallisation, but very little attention has been paid to the effect of the post sintering heat treatments on the stability of the sialon phases.

2.8. Transformation of α'–> β' Sialon

The α-Si_3N_4 to β-Si_3N_4 phase transformation is a reconstructive transformation and requires considerable activation energy for the breaking of Si-N bonds (Messier et al 1978, Jennings 1983 and Sarin 1988). This transformation starts at temperatures exceeding 1400^0C, and requires the presence of a liquid phase (Cao and Metselaar 1991, Hampshire and Jack 1981). From transmission electron microscopy observation Drew and Lewis (1974) concluded that the transformation occurred via a solution precipitation mechanism, dissolution of α-Si_3N_4 into a transient liquid phase and a precipitation of β-Si_3N_4 from the liquid. The reverse β-Si_3N_4 to α-Si_3N_4 transformation has not been observed, and β-Si_3N_4 is assumed to be more stable, whereas α-Si_3N_4 is formed only under special conditions.

Although the structure of both the α' and β' phase is basically built up of corner-sharing (Si,Al) $(O,N)_4$ tetrahedra, there is a distinct difference in the atomic arrangement between the two phases (Jack 1976). The transformation between α' and β' phases has a reconstructive nature, which involves the breaking of chemical bonds and substantial atomic diffusion, and hence requires significant amounts of thermal energy. As a result of the strong covalent nature of the bonding associated with both the α' and β' structures, the atomic diffusivity of the species making up the lattices is inherently low. It is, therefore, generally assumed that the α'→ β' phase transformation requires a liquid phase to assist the necessary atomic diffusion, by analogy with the transformation from α-Si_3N_4 to β-Si_3N_4, which does not occur without the presence of a liquid phase in which α grains could dissolve above 1400^0C (Hampshire and Jack 1981)

Heat treatment of different rare-earth sialon materials at various temperature (in the range 1000-1800^{0}C) yielded the $\alpha' \rightarrow \beta'$ transformation which accompanied the crystallisation of various secondary phases (Mandal and Thompson 1993).The extent of the $\alpha' \rightarrow \beta'$ transformation and the resulting secondary phase are dependent on the type of the stabilising cation used, specifically the size of the cation incorporated into its structure. Recent investigations have provided some evidence for the proposal of increasing α' sialon stability with decreasing cation size in the rare-earth series (Mandal et al 1995a, Falk et al 1997). The studies on sialon stability have shown that the α' phase stabilised with larger cations such as Nd and Sm are less stable and transform to β' and grain boundary phase more easily than α' sialon stabilised with smaller cations. Thompson and Mandal (1997) and Shen et al (1996a) further reported that Ce α' (radius 0.103nm) and Nd α' (0.099nm) is stable only at the sintering temperature and they transform to β' and grain boundary phase on slow cooling or during heat treatment at lower temperatures. On the other hand α sialon stabilised with smaller cation size such as Yb and Dy was found to be more stable over a wide range of temperature (Shen et al. 1996c, Ekstrom et al 1997).

Further experiments on the stability of sialon systems showed that the grain boundary liquid phase has a marked effect on the $\alpha' \rightarrow \beta'$ transformation. The introduction of an additional amount of glass into previously stable α' composition could significantly destabilise the α' phase and promote the α' to β' transformation (Mandal and Thompson 1995). This investigation and many others have suggested that the residual grain boundary liquid phase is one of the most important factors influencing the transformation. The rate of $\alpha' \rightarrow \beta'$ transformation is dependent on the volume fraction and the nature of the liquid phase present during heat treatment (Mandal and Thompson 1995; Mandal et al 1995; Zhao and Cheng 1995 and Sun et al 1996).

However, other investigation have revealed that although the presence of liquid phase aids the transformation, it is not the only requirement for the transformation to occur. The heavy rare earth sialon materials, with a small amount of glass, such as Yb-α' and Dy-α' sialons show excellent stability

over a wide range of temperature and time (Falk et al 1997; Shen et al 1996c; Shen et al 1997 and Ekstrom et al 1997). In contrast the light rare earth sialon systems such as Nd and Sm have been reported to show a continuous transformation. Cheng 1997 Zhao and Cheng 1996 and Shen et al 1996b have reported that although the grain boundary glass phase crystallised during the initial 24 hours of heat treatment at 1450^{0}C, the transformation continues during extended the heat treatment. This indicates that while the presence of liquid phase may provide the means for cation diffusion out of α' sialon structure other factors may also influence the α' thermal stability.

The stability of α-sialon is also affected by the extent of the α' single phase region Figure 2.6. The smaller region observed in the light rare-earth sialon systems indicates the relative instability of α' in these systems and that a slight compositional change may move the α' composition toward the α' and α'/β' boundary. Recent investigations by Shen et al. (1996b) and Ekstrom et al. (1997) have proposed two possible transformation routes, one involving a liquid phase, i.e α'_1 + liquid → α'_2 + grain boundary phase and other being a direct decomposition of the α' phase to form β' and grain boundary crystalline phase.

The crystallisation of the intergranular glassy phase in rare earth sialon system, will consume the cation from the glass and thus may compete for the remaining cations within the α'. This results in an α' compositional adjustment. α sialon compositions located at the edge of the α sialon region or close to α'/β' phase boundary may have a smaller fraction of stabilising cation. Thus such compositions are less stable with respect to α' to β' transformation and the transformation proceed more readily with increase of the amount and decrease of the viscosity of liquid phase. For the α' sialon composition within the α sialon region a combination of three factors may influence the ease of transformation: the size of the stabilising cation, the presence of β grains and also the amount and viscosity of the liquid phase present during heat treatment.

2.9. Properties of Sialon Ceramics

In sialon ceramics, the monophase β-sialon ceramics are brittle, with a fracture toughness around 3MPam$^{1/2}$, cracks propagate easily in the equiaxed-grain microstructure with partially transgranular path. The presence of a continuous glassy phase in these materials is obtained by adding metal oxide prior to sintering. This glassy grain boundary phase will became a preferred crack path, and crack deflection, crack bridging and grain pull-out will occur, causing mainly intergranular fracture, and the fracture toughness of β sialon materials will then increase to around 4-6 MPam$^{1/2}$.

The addition of higher content of sintering aids (via pressureless sintering) promotes unconstrained growth of anisotropic β-sialon crystals (Lewis et al 1980). The resultant materials contain elongated grains in the microstructures and they have the highest observed fracture toughness values (8-10 MPam$^{1/2}$) at room temperature. Among the different sialon materials, the sintering aids are only partly consumed by sialon crystals, and the excess will form a residual glassy phase, the presence of glassy phase makes them somewhat soft (Hv10=14-16 GPa). The performance of these materials is limited by the softening temperature of the residual glass (typically about 900-1000^{0}C). Therefore elimination of this residual glass phase is desirable. Crystallisation of the glassy phase is one method to improve the high temperature properties, for example the limited performance of β'+ glass materials at 1000^{0}C is improved by crystallised into YAG. Thus β' + YAG exhibit good mechanical properties up to around 1300^{0}C (Lewis et al 1980)

The composition and amount of grain boundary phase have an effect on the room temperature fracture toughness. It has been reported by (Kishi 1990) that the presence of elongated grains without a weak grain boundary is not sufficient to achieve a high K_{IC}. The fracture toughness increases with increasing amount of intergranular glass phase.

In sialon materials the hardness value increases as the fraction of the α' sialon phase increases. The hardness is determined by the Burgers vector of the dislocations which cause localised plasticity. The c-axis of the α' phase is double that of β' c-axis, thus the dislocations in α' have a higher resistance to motion (lattice friction stress) and hence the material has a higher hardness compared to β' (Lewis 1993). There are several parameters, in addition to lattice friction stress, that influence the materials hardness; grain size and the amount of glass phase have been reported to have a significant effect on the measured hardness of the ceramic materials. The fracture toughness decreases with the amount of α' sialon phase which has been related to the morphology of the α' grains not having such an elongated shape as β'. Other factors such as residual porosity, the properties of the intergranular phase (chemical bonding with the sialon grains) may also have an influence. Recently Chen and Rosenflanz (1997) have successfully fabricated single phase α' sialon with higher fracture toughness (6.3 $MPa.m^{1/2}$) by controlling grain morphology.

The possibility of varying the α'/β' sialon phase ratio by slightly changing the overall composition and/ or by post sintering heat treatment opens many possibilities of preparing sialon ceramics with desired properties, a combination of moderately high fracture toughness of β' and good hardness of α', together with the benefits of minimal intergranular residues.

2.10- Research Objectives.

The overall objective of this work was to investigate the possibility of producing dense α'/β' Sialon materials with a controlled phase content and microstructural features using pressureless sintering techniques (since the majority of earlier research has been done on materials sintered under pressure). The main sintering aid used was Yb_2O_3.

The main objectives of this research were:-

- To investigate the possibility of controlling the microstructure (α'/β' ratio and phase morphology) of Sialon materials by varying the initial starting composition and by the addition of β Si_3N_4 'seed' crystals.

- To study the effect of post sintering heat treatment on the crystallisation product of the intergranular phase and on the stability of the as-sintered α'/β' microstructure.

- To compare sinterability and phase evolution in a composite α'/β' sialon, prepared with a single stabilising cation (Yb) with microstructures resulting from mixed cation, (Yb/Nd) and (Gd/Nd) addition. The aim was to improve the density and α'/β' sialon content and morphology as well as to study the possibility of stabilisation of α' sialon containing the larger cations.

- To survey some of the room temperature mechanical properties (hardness and fracture toughness) in addition to studying the high temperature oxidation resistance of selected compositions, with a view to explanation of the underlying mechanisms relative to varying microstructure.

CHAPTER 3

EXPERIMENTAL TECHNIQUES

The production, characterisation and measurement of a ceramic material's properties requires the use of many techniques; this chapter will describe the techniques used throughout this work.

3.1- Materials Preparation :

The starting powders used to prepare the compositions investigated in this work were α-Si_3N_4 (UBE grade SNE10), β-Si_3N_4 (Denka), AlN (Starck grade C), Al_2O_3 (Alcoa 99.8%) , SiO_2 (BDH-Merck) and rare earth oxides (Yb_2O_3, Nd_2O_3 and Gd_2O_3) (Aldrich 99.99%) as the interstitial cation for the α-SiAlON, which was added either in the form of a presynthesised glass or as an oxide powder.

The glass composition was selected to give a low melting clear glass (table 3.1). Due to the hygroscopic nature of the rare earth oxide, the powders were calcined at 1000^0C for 2 hours to remove any water content absorbed during storage. The weighed powders for the glass synthesis were mixed thoroughly for 24 hours, in order to get a homogeneous mixture, and melted in a platinum crucible at 1675^0C for 2 hours. The melted glass was quenched into deionized water. The dried glass was crushed using a pestle and mortar and then milled in isopropyl alcohol in a rotating polyethylene bottle with SiAlON milling media. The glass powder was then sieved through a 38μm mesh and dried.

Composition	R_2O_3	Al_2O_3	SiO_2
Yb_2O_3	63.97	16.56	19.48
Gd_2O_3	60.25	18.25	21.50
Nd_2O_3	62.02	17.45	20.53

Table 3.1. The rare earth glass compositions (in wt%).

For preparation of the ceramic materials, appropriate quantities of nitride powders and glass powder were weighed to an accuracy of ± 0.01g. Batches of approximately 50g were wet ball-milled for 72 hours in a plastic bottle using 750g of SiAlON media and 250ml isopropyl alcohol as the mixing medium. After milling and mixing the slurry was sieved through a 38μm mesh and then dried at 60^0C in an open oven for 24 hrs. The dried powders were then sieved through a 500μm mesh to break up aggregates and remove any large scale contamination from the milling media before cold iso-statically pressing (150 MPa for 15 sec) into green body billets.

In the case of the mixed cation materials, batch mixtures of 100g were prepared in a 50/50 ratio by wet milling of the powders for 72 hours. Subsequent green body pressing was similar to the single cation materials described above.

3.2- Pressureless Sintering :

The prepared billets were pressureless sintered in a resistance furnace (maximum temperature 1900^0C) which could be evacuated to a level of approximately $1x10^{-6}$ mbar. The element was composed of graphite and the samples were contained in a Sialon-lined graphite crucible. A schematic of the furnace is shown in Figure 3.1. The standard operating procedure was to evacuate the chamber to a good vacuum (10^{-5} mbar) before heating under one atmospheric pressure of pure nitrogen. The furnace was de-gassed at

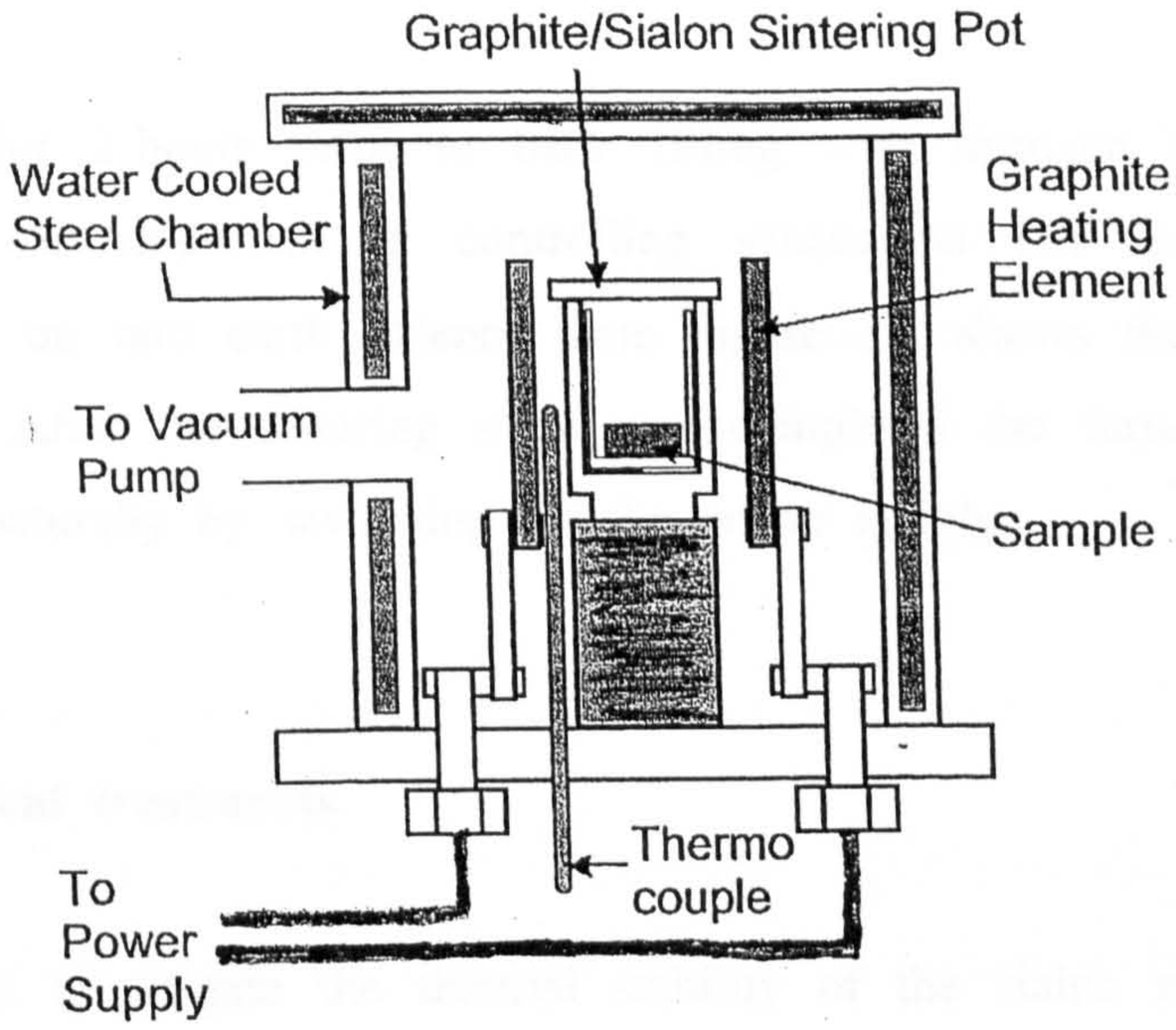

Figure 3.1. The schematic diagram of the furnace used for pressureless sintering

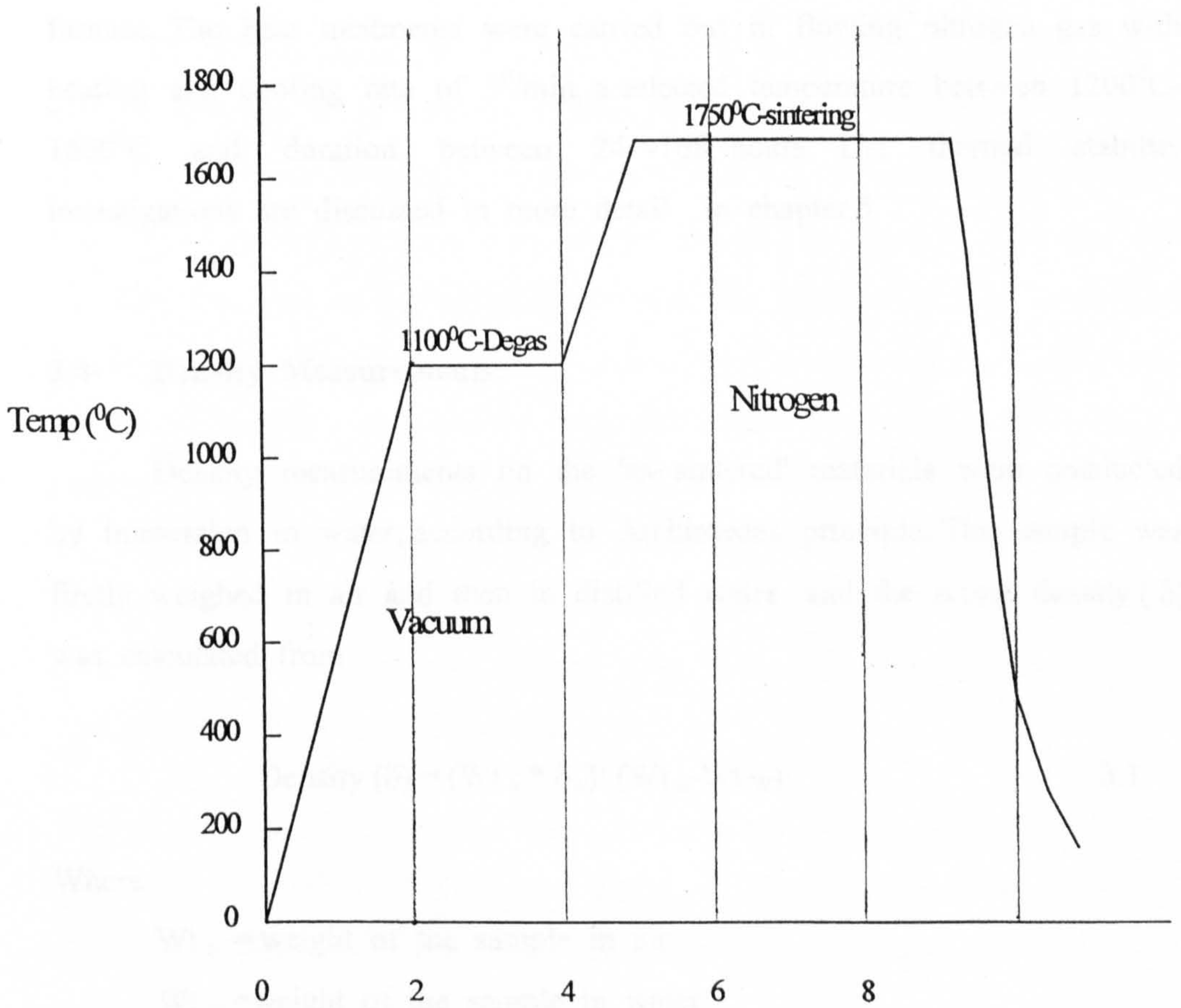

Figure 3.2. The pressureless sintering cycle

1100^{0}C for 2 hours prior to back filling with nitrogen. The vacuum pre treatment is important in controlling subsequent CO formation and its influence on rare earth valence state. Figure 3.2 shows the cycle used for sintering. After the sintering stage was completed the furnace was allowed to cool naturally by switching off the power supply.

3.3- Heat treatments

To investigate the thermal stability of the sialon materials and the crystallisation of glassy phase, selected compositions of pressureless sintered materials were subjected to post sintering heat treatment. The samples were placed in an alumina crucible and then inserted in a vertical alumina tube furnace. The heat treatments were carried out in flowing nitrogen gas with heating and cooling rate of 3^0/min, a selected temperature between 1200^{0}C-1600^{0}C and duration between 24 -168 hours. The thermal stability investigations are discussed in more detail in chapter 5

3.4- Density Measurements:

Density measurements on the 'as- sintered' materials were conducted by immersion in water, according to Archimedes principle. The sample was firstly weighed in air and then in distilled water and the actual density (δ) was calculated from

$$\text{Density } (\delta) = (Wt_a * \delta_w)/ (Wt_a - Wt_w) \qquad 3.1$$

Where

Wt_a = weight of the sample in air

Wt_w =weight of the sample in water

δ_w =density of water =1.0022-0.0002000057T

T =The water temperature

Weighing of the samples in both air and water was carried out using a digital balance (Precisa 125A), with an accuracy of ± 0.002g. Evidence for open porosity in the samples was indicated by a steady rise in weight whilst the samples were immersed in distilled water.

3.5- Materials Characterisation:

The phase content and microstructures of the as-sintered and heat treated ceramics were characterised using the following techniques.

3.5.1- X-Ray Diffraction Techniques:

Crystalline phases were characterised by their X-ray diffraction (XRD) patterns obtained using a Philips (2kW , 60kV) x-ray diffractometer operating at 40kV and 30mA, using monochromatic Cu-Kα_1 radiation of wavelength λ=0.154184 nm. Cut samples were ground flat and polished to 6μm diamond and then mounted on to a glass holder with the polished surface exposed to the X-ray beam. The spectra were recorded at diffraction angles 2θ between 10° and 70°, using a step size of 0.02 and a scan speed of 2°/sec. Silicon (Si) powder was used as an internal standard, which was applied to the face of any sample to be examined. This allowed correction to be made for any error in 2θ. Analysis of the XRD spectra was performed using the 'Origin' peak fitting programme and phases were identified with reference to the standard JCPDS powder diffraction files.

The proportions of α and β-Sialon phases were determined by quantitative estimation from the XRD pattern using the intensities of the (102) and (210) reflections of α-Sialon and (101) and (210) reflections of β-Sialon in the following equation (Lumby 1997)

$$\%\beta=0.01945+49.72086*(I\beta/I\alpha+I\beta)+23.36281*(I\beta/I\alpha+I\beta)^2+27.66654*(I\beta/I\alpha+I\beta)^3 \quad 3.2$$

Where

I(α)= the total intensity from peaks (102) and (201)

I(β)= the total intensity from peaks (101) and (201)

From the a_0 and c_0 lattice parameters the values of m and n (α sialon equation 2.2) were calculated using the following equations (Shen and Nygren 1997)

$$a\ (Å) = 7.752+0.036m+0.02n \quad 3.3$$

$$c\ (Å) = 5.620+0.031m+0.04n \quad 3.4$$

The z values of β sialon phase $Si_{6-z}\,Al_z\,O_z\,N_{8-z}$ were obtained from the mean values of z_a and z_c given by the following equations (Ekstrom 1989)

$$a= 7.603+0.0297z\ Å \quad 3.5$$

$$c= 2.907+0.0255z\ Å \quad 3.6$$

3.5.2- Electron Microscopy

Microstructure features such as the morphology and size of individual grains, the presence of intergranular phases and the level and size of porosity were investigated using both scanning electron and transmission electron microscopy.

3.5.2.1- Scanning Electron Microscopy (SEM):

Cut samples were ground flat and polished by standard diamond polishing techniques, to a 1μm finish. The polished samples were cleaned in acetone and then carbon coated to avoid charging in the electron beam. The

microstructure and the composition of the prepared materials were examined in a JEOL-JSM6100 scanning electron microscope, operating at 10-20kV and using secondary and mainly back-scattered electron imaging modes. Compositional information was obtained with an energy dispersive x-ray analyser (EDAX Oxford / Link ISIS system). Topographical features, such as porosity level and measurement of indent size and crack length, were imaged by the detection of secondary electrons ejected from the sample surface, whilst compositional mapping was obtained from electrons back scattered from the sample, which depend strongly on the atomic number, allowing different ceramic phases to be distinguished by different contrast levels in the resulting image. The back-scattered imaging mode was used extensively to observe the microstructures of the materials and to quantify the amounts of the phases present by using the image in conjunction with image analysis software. Back-scattered contrast was also used to measure crack length when secondary electron contrast was not sufficient.

3.5.2.2- Transmission Electron Microscopy (TEM):

Detailed microstructure was characterised by analytical transmission electron microscopy (JEOL-2000FX, operating at 200kV and equipped with an EDAX analyser).

The samples for TEM study were prepared by cutting a thin slice (a few hundred μm), from the bulk materials, which was mechanically ground to a thickness of about 100 μm and then polished on both side to a much finer surface finish. The ceramic slice was then mounted for dimpling to further reduce the thickness to approximately 50 μm and finally polished with 1/4 μm diamond paste. The thin slice was then affixed to a copper ring and then argon-ion beamed to electron transparency. The thin foil samples were then coated with carbon to prevent charging in the microscope.

High resolution images of the ceramic grains were obtained using the bright field image mode, electron diffraction was used to identify the phases, and some compositional analysis was also performed in TEM, using the EDAX spectrometer and associated Link 'ISIS' software

3.6- Mechanical Properties :

In the following sections, the techniques for measuring the hardness and fracture toughness of the ceramics are described. An indentation technique was used to measure the room temperature hardness and the fracture toughness of the prepared materials. The test samples were prepared by diamond cutting and then mounted into Bakelite for grinding and diamond polishing to 1μm surface finish.

3.6.1- Hardness

Hardness (H_V10) measurements at room temperature were obtained with a Vickers diamond indenter (pyramidal with apex angles of 136^0) mounted on the X-head of an Instron 1122 Universal Testing Instrument (500 kg capacity) with a 0-50 kg load-cell. To perform the indentation, the cross-head was lowered towards the sample at a speed of 0.5mm/min. A load of 50N was held for about 30 second and unloaded at the same speed as for loading, the variation of load over time was monitored using a pen chart recorder. The samples to be indented were positioned on a sliding x-y table and indentations were made at regular intervals. The sample were then coated with gold to prevent charging in the SEM. Indentations were measured using both optical microscopy, for which the scale markers was calibrated against a copper graticule of 10μm spacing, and electron microscopy (SEM). Results were taken as the average size of 10 indents. The hardness values (H_v) were calculated using the relationship

$$H = P / \text{indentation area} \qquad 3.7$$

For the Vickers indenter, the indentation area, is taken as the specimen area in contact with the diamond given by;

$$A = d^2/\sin(136^0/2) \qquad 3.8$$

Hence,

$$H = 1854.4 \times (P/d^2) \qquad 3.9$$

Where

P= the applied load (N)

d= the diagonal length of the indentation(in μm)

3.6.2- Fracture Toughness

There are several methods for determination of the fracture toughness, and the experimental results obtained can be different depending on the testing method. Some of these techniques are

-The single-edge notched beam (SENB) method, in which a bending test sample is used with a sawn notch on the tensile face. The advantages of this technique are that, it can be used for the determination of K_{Ic} at high temperature, test bars are easily prepared and its simplicity. The disadvantages are the care needed when machining the notch and there is some doubt about the resulting microcracking at the tip of the notch.

-The indentation technique in which an indentor is pressed on to the surface of the sample, with a known load to initiate a sharp crack. In this technique the K_{Ic} may be determined using alternative procedures:-

1- Indentation fracture in which a crack is made on the surface of a test bar which is subsequently fractured in four-point bend. This method does

not require measurements of the crack, which is difficult to do accurately.

2- Micro-indentation in which K_{Ic} is determined directly from measurements of the length of the crack without the need for subsequent fracture. This method is very promising because of its simplicity and the small quantity of required materials.

In the present study the fracture toughness measurements of the prepared materials were determined by the indentation method due to the small volume of the material available. Vickers indentations were implanted onto the surface of the samples and median cracks developed around the indentations, of crack size inversely dependent on the toughness of the materials. By measuring the length of the radial (median) cracks emanating from the corner of the Vickers indentations Figure (3.3), the indentation fracture toughness (K_{IC}) in $Mpa.m^{1/2}$ may be estimated using the Anstis relationship (1981)

$$K_{IC} = 0.016(E/H)^{1/2} (P/c)^{-3/2} \qquad 3.10$$

Where E = the elastic Young's Modulus, which is assumed to be 310GPa

H_v = Vickers Microhardness (GPa)

P= applied indenter load

c= the crack radial length (μm)

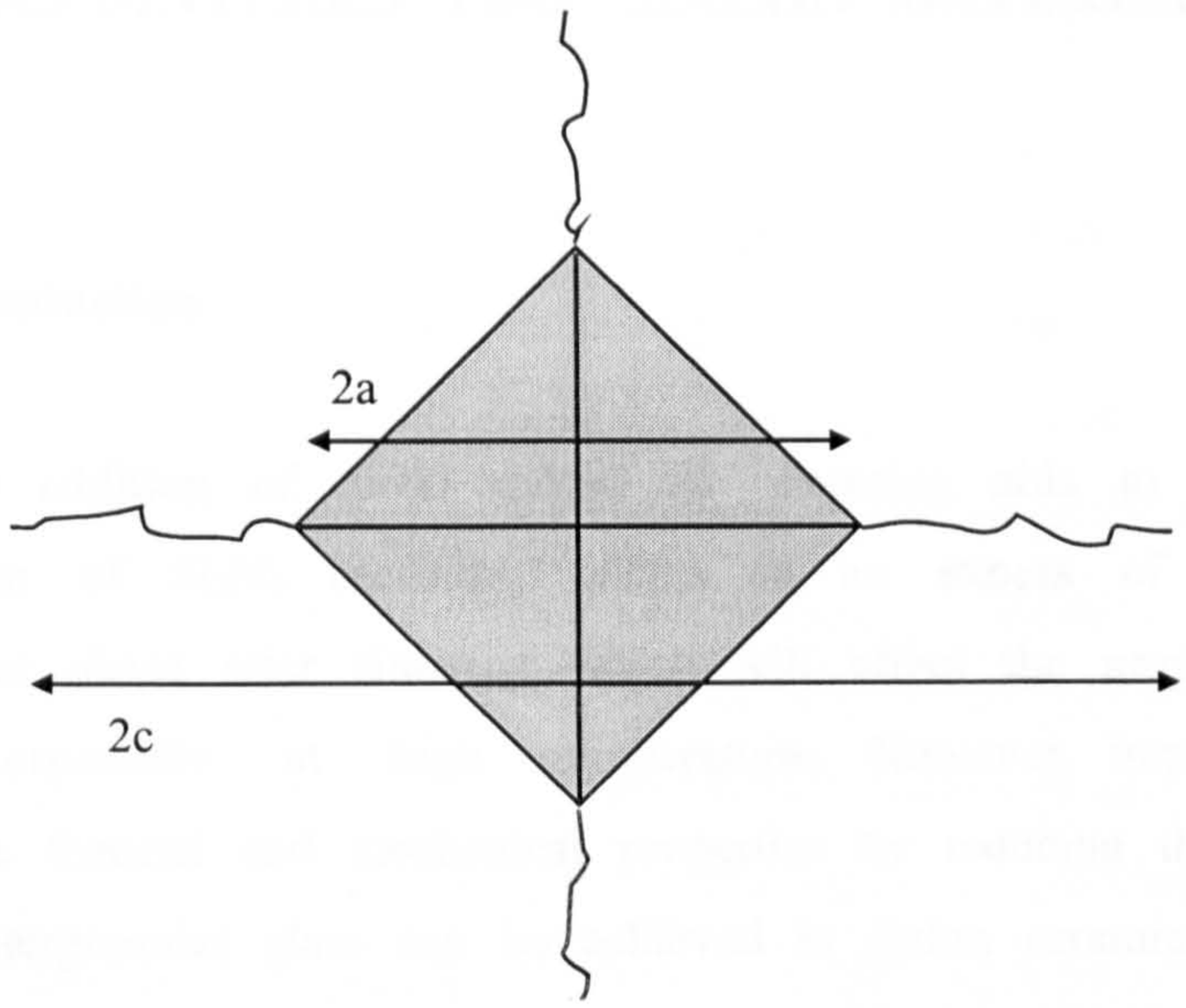

Figure 3.3. Crack formed by the intersection of radial cracks with the surface around a Vickers indent.

3.7- Oxidation behaviour

Oxidation tests were carried out using a horizontal alumina tube furnace. Samples were prepared by cutting from the sintered materials and carefully polished down to 1μm diamond finish. Prior to testing the dimensions of the samples were measured (accuracy of 0.1mm), cleaned in acetone and then weighed to an accuracy of ± 0.002g , and were oxidised for a period of time up to 120 hours at temperatures 1350^0C and 1450^0C in flowing dry air. The samples were arranged in an alumina boat and then inserted into a pre-heated furnace. The weight gain as a function of time was recorded by intermittently removing the samples from the furnace, weighing them at room temperature and then putting them back into the furnace. After oxidation the samples were characterised by XRD and SEM together with EDAX analysis in order to identify crystalline phases present on the surface of oxide materials.

CHAPTER 4

AS SINTERED Yb-α' SIALON MATERIALS

4.1- Introduction

The addition of metal oxides as sintering aids to facilitate the densification of Si_3N_4 ceramics, results in an excess of the residual intergranular phase after sintering which will affect the properties of the material especially at high temperatures. However, improving high temperature thermal and mechanical properties by reducing the amount of residual intergranular glass can be achieved in sialon ceramics. Due to the nature of the α' sialon structure, the metal cation initially present in the liquid can be incorporated within the closed interstices of the α' lattice (Hampshire 1978). Recently special attention has been paid to the rare earth metals as sintering aids for silicon nitride, which form refractory glasses upon cooling from the sintering temperature.

In all R-Si-Al-O-N systems there exists a two phase (α'+β') area between the α'-sialon plane and the linearly extended β'-sialon phase. Therefore ceramics fabricated in this area may have a potential for 'self reinforcement' through development of a microstructure consisting of well- distributed elongated β' grains in an α'-sialon matrix.

The purpose of this work is to develop 'designed' microstructures which optimise mechanical properties. High hardness materials should be attained by producing materials with high α' content, whereas high strength, tough, materials may be produced with materials having high β' content, in the form of large prismatic crystals within a more α' matrix.

Therefore this chapter will investigate the possibility of controlling the α'/β' phase ratio by constitutional change.

4.2- Material Composition

In this study, different α'+β' - sialon starting compositions have been investigated by using Yb_2O_3 as a stabilising cation and added as oxide and/or as presynthesised alumino-silicate glass. The constitution of α' and β'-Sialon phases was predicted by balancing of compositions using a computer programme (developed at Warwick) which assumes that all rare-earth cations are substituted within the α' structure. The programme selects the additive cation (glass level) to form a particular α' content in the final ceramic, with predicted m and n value. The total oxygen content is determined from the glass together with surface contaminants (on Si_3N_4 and AlN powders) at the end of the milling and vacuum degassing cycle. Having subtracted the total Si, Al, O, N and M required to form the α' content, the residue is assumed to form β' and the necessary equivalence of oxygen and aluminium adjusted in the initial mixture (via AlN). The programme output defines β' composition (z value) and component mixture (AlN, Si_3N_4 and glass) necessary to form the chosen α' composition and content.

The compositional programme is over - simplistic firstly because part of the additive cation will remain within the residual glass and, secondly, it assumes that the α' composition will be within the single phase stability region. This latter assumption has been made in the absence of a defined phase limit for Yb-α', whereas the experimental values are expected to occur at the ends of tie-lines from the β' composition through the average (made-up) compositions.

Two series of Yb (α'+β') sialon have been selected with different predicted substitution levels m and n. The first series named as (Series A) was chosen to have a fixed composition with α'-sialon composition set as $Yb_{0.33}Si_9Al_3O_2N_{14}$ (see equation 2.2), where m=1 and n=2. The prepared materials were designed to produce the same α'-sialon composition but with different α'/ β' phase ratio by increasing the glass level in the starting

composition. β' sialon phases were predicted to have variable substitution levels (z-value). Five compositions with predicted α'/β' phase ratio and β'-z value have been prepared as shown in table 4.1. Composition Yb50A was designed to produce material with α'/β' ratio of 50/50, composition Yb75A to give 75/25 and compositions Yb80A, Yb95A, Yb100A to give material with α'/β' ratio of 80/20, 95/5, 100 respectively. The projection of the compositions on the phase diagram is shown in Figure 4.1.

Compositions in series B were also prepared with fixed α' composition set as $Yb_{0.5}Si_{9.75}Al_{2.25}O_{0.75}N_{15.25}$ (m=1.5 and n=0.75). The compositions in this series were designed to produce materials with different α'/β' phase ratios, similar to Series A, by varying the Yb-glass level in the starting composition. Composition Yb50B designed to produce materials with α'/β' ratio of 50/50 and Yb65B, Yb75B and Yb80B were aimed to produce materials with α'/β' ratio of 65/35, 75/25 and 80/20 respectively. The overall compositions of the materials prepared in this series are also given in table (4.1) and their positions in the Si_3N_4 rich corner of the plane Si_3N_4-$YbN.3AlN\text{-}4/3(AlN.Al_2O_3)$ are given in Figure 4.2. The predicted α' composition is indicated by the star shape, whereas β'-sialons with variable compositions (different z-value) are marked β1 , β2,....and so on. Based on the predicted α'/β' phase ratios, the overall compositions thus fall on the lines between the predicted α'-sialon composition and the β'-sialon z value.

All the prepared compositions were pressureless sintered at 1750^0C for 4 hours. Composition Yb75B was also pressureless sintered at a temperature lower than 1750^0C.

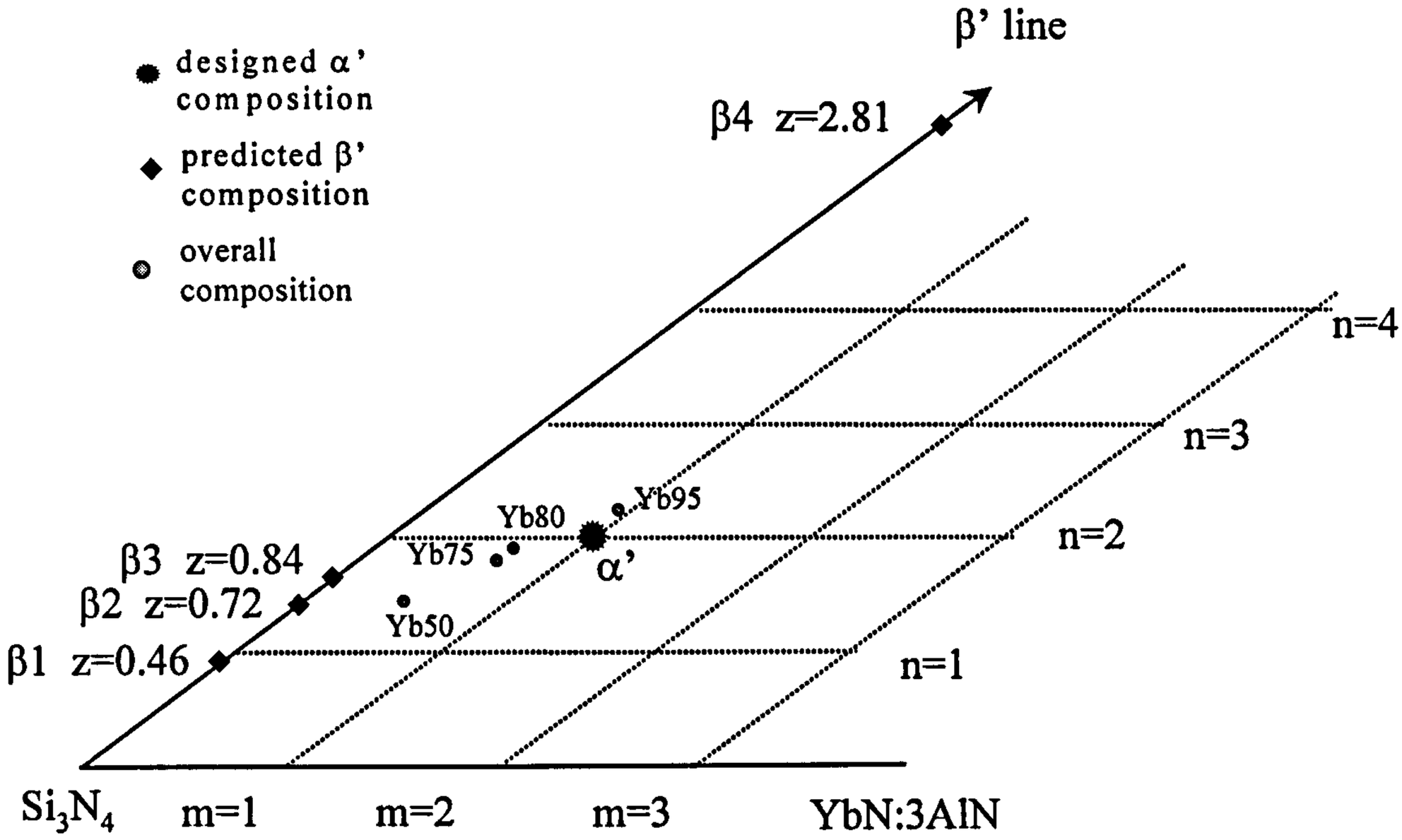

Figure 4.1. The Projection of compositions prepared in series A on the phase diagram.

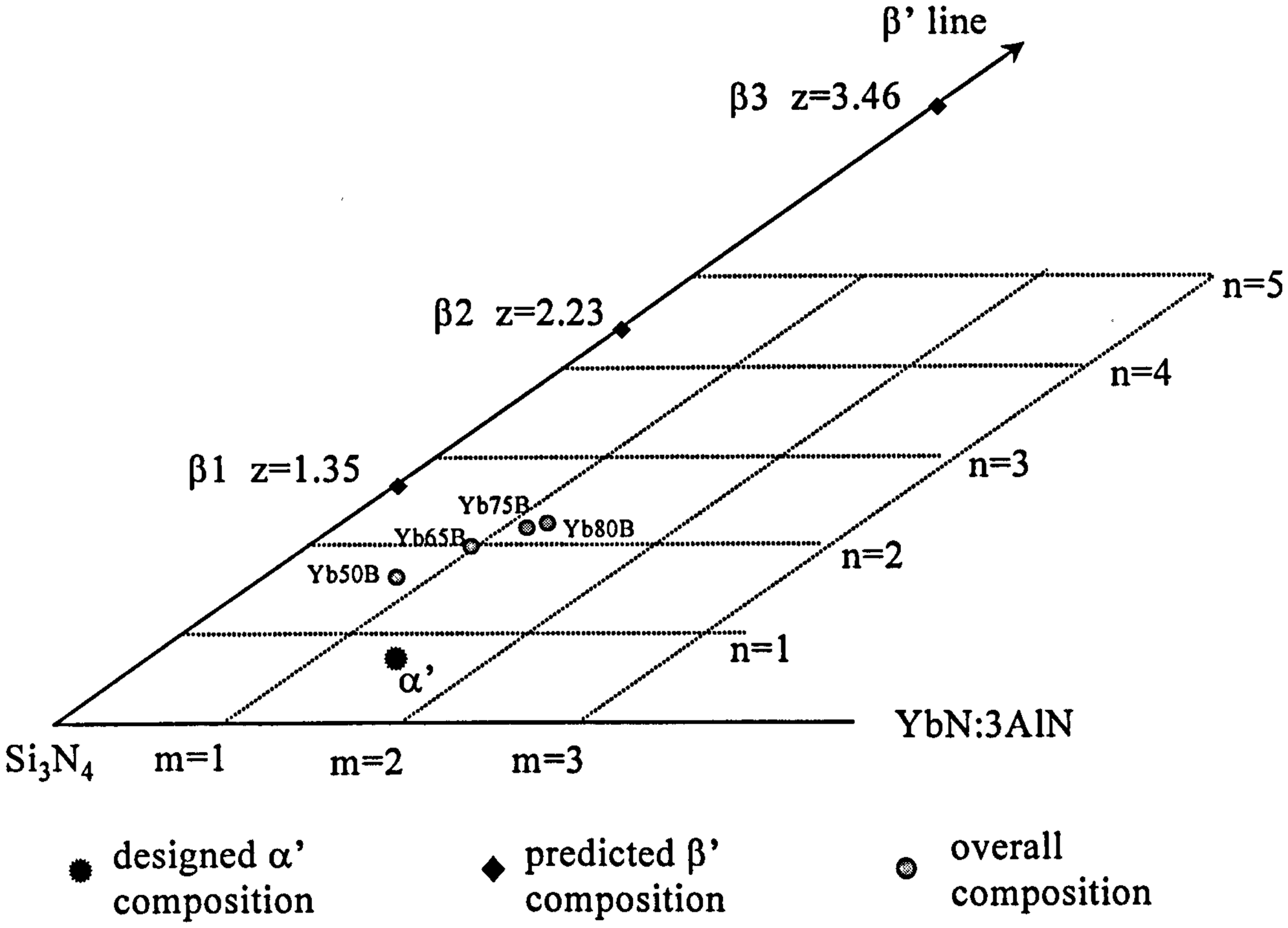

Figure 4.2. The Projection diagram of compositions prepared in series B.

Sample	Compositions	Si_3N_4	AlN	Yb-glass	Yb oxide	Al_2O_3	Z-value before sintering	Density g/cm^3
Series A m=1 and n=2								
A1	50/50	79.4430	12.2700	8.2870			0.458	2.841
A2O	75/25	73.4868	13.7415		7.9517	4.8200	0.72	2.45
A2	75/25	71.5897	15.9800	12.4303			0.715	2.631
A3	80/20	70.0173	16.7227	13.2600			0.844	3.048
A4	95/5	65.3000	18.9500	15.7500			2.81	2.849
A5	100	68.4560	16.1240		10.600	4.800	5.46	2.829
Series B m=1.5 and n=0.75								
B1	50/50	72.577	15.515	11.908			1.35	3.129
B2	65/35	65.8048	18.715	15.4802			2.23	3.025
B3	75/25	61.1212	21.017	17.8618			3.46	3.364
B4O	80/20	71.9853	15.8267		12.188		1.47	2.922
B4	80/20	59.0317	21.9157	19.0526			4.46	3.339

Table 4.1 The starting compositions (in Wt %) and density of the prepared Yb sialon materials

4.3- Density Measurements.

Table (4.1) gives the densities after pressureless sintering at 1750^{0}C for 4 hrs. As it is difficult to calculate the theoretical bulk densities of the materials, because of their multi-phase nature for most of the compositions only the measured bulk densities were used for comparison.

The bulk density results from the as prepared compositions, show however that the materials prepared to give high α' content (~ 100% α') and compositions with m=1 and n=2 lead to poor density. The bulk density of as sintered composition Yb50A was 2.63 g/cm^3. On addition of excess Yb glass to the starting compositions the bulk density was slightly increased and the highest density was measured for composition Yb80A which is 3.01 g/cm^3. This value reduced with compositions designed to give high α' content as in compositions Yb95A and Yb100A, (in Yb100A the Yb cation

was added in the form of oxide since the Yb95A is the designed composition to contain the highest α'/β' ratio that is permissible using presynthesised glass as a processing route).

The densification of Si_3N_4 based ceramics mainly depends on the liquid phase produced by the surface SiO_2 on the Si_3N_4 powder and the oxide additive. Therefore, in series A, the low cation level added to the starting composition leads to poor densification in these compositions, although the reaction to form α' and β' may be complete, and the materials are very porous as shown in Figure 4.5. Increasing (m) in the nominal compositions (i.e m=1.5) results in excess Yb and therefore more glass added to the starting compositions. This, however, results in a greater fraction of liquid phase at the sintering temperature, which consequently increases densification but results in more residual glass after sintering which affects the mechanical properties at high temperature. As can be seen from table 4.1, the bulk density obtained in these materials (i.e compositions with m=1.5) are significantly improved upon the addition of excess Yb and the highest measured bulk density of 3.364 g/cm^3 was obtained with composition Yb75B which aimed to produce material with 75/25 α'/β' phase ratio.

The form in which Yb is added to the starting composition also has an effect on the bulk density measurements. Compositions prepared with Yb added to the starting compositions as an oxide, result in materials with lower density compared with compositions prepared with Yb added in the form of presynthesised glass. A measured bulk density of 3.339 g/cm^3 was obtained with composition Yb80B in which Yb added in the form of glass; this value decreased to 2.922 g/cm^3 for the same composition but with addition of Yb in the form of oxide. This was also clearly observed with compositions prepared in series A; in composition Yb75A the bulk density decreased from 2.631 g/cm^3 to 2.450 g/cm^3.

It is generally accepted that the densification in Si_3N_4 based ceramic proceeds via liquid phase sintering which according to Kingery (1959) consists of three stages, particle rearrangement, solution precipitation and

coalescence of grains (more details in section 2.8). In the α-sialon materials the sintering liquid phase is transient and incorporated into the α' structure, therefore as the precipitation of α' proceeds the liquid volume will be reduced. This increases the viscosity of the remaining liquid thus slowing the densification. The increased amount of the sintering additives enhanced the liquid phase content during sintering, therefore improved the ease of particle rearrangement and solution precipitation kinetics, hence enhancing the sinterability. Furthermore the formation of intermediate phase accompanying the α' precipitation has been found to retard both densification and reaction completion due to a reduction in liquid volume (Watari et al 1994).

The low density measurement in compositions with Yb added in the form of oxide is believed to occur as a result of lower volume liquid phase at sintering temperature. It is possible that inhomogeneous distribution of the oxide additives during the powder mixing results in localised differences in the concentration of Yb_2O_3 oxide. An intermediate phase may form by solid state diffusion reaction at low temperature during the heating up as observed in early work by Jasper (1990). The Yb_2O_3 may react with the Al_2O_3 present on the AlN surface and form ytterbium aluminium garnet phase (YbAG). This garnet phase consumes some of Yb making it no longer available for liquid formation at the Yb_2O_3- SiO_2-Al_2O_3 eutectic temperature, therefore results in lower volume of a transient liquid phase at sintering temperature. In contrast the use of presynthesised alumino-silicate glass has the advantage of improving homogeneity and suppression of additive component reaction prior to liquid formation during the rise time to sintering temperature. Therefore the addition of Yb-alumino silicate glass to the starting materials will provide the system with a larger volume of liquid phase at sintering temperature. This transient liquid phase will facilitate the densification at an early stage of sintering before being removed into sialon phases.

The relationship between densification and sintering time was also investigated and is shown in table 4.2. It is clear that at the same sintering temperature but for longer times higher densities result; Yb75B sintered at 1750^0C for 1hr results in density of 3.07 g/cm^3 which increased to 3.401 g/cm^3 after 10hrs sintering at the same temperature. The further improvement in densification occurs as a result of either continued liquid phase sintering or possibly some solid state diffusion takes place. Examination of micro sections by SEM showed that all the microstructures did contain a retained porosity.

Composition	Yb75S1hr	Yb75S4hr	Yb75S10hr
Density g/cm^3	3.07	3.364	3.401

Table 4.2. Bulk density of composition Yb75B sintered for different times.

The 'as sintered' compositions all exhibited a yellow coloration which is different from most Si_3N_4 based ceramics. The degree of yellow coloration, however, varies from one composition to another. All the compositions prepared in series A were bright yellow throughout, whereas the compositions prepared in series B show yellow / brown colour. However when Yb is added in the form of oxide to either compositions in series A or in series B, the resultant materials all exhibited bright yellow colour.

The previous study by Karunaratne et al (1996) reported that the unusual bright colour of the Yb α -sialons was due to the presence of Yb^{3+} ion in α'-structure rather than Yb^{2+} ions which promoted a black coloration. It was proposed that the yellow material formed as a result of sintering in a neutral environment, thus preserving a higher concentration of Yb in trivalent state and that the black materials formed in a reducing environment due to a CO atmosphere.

In the present study although all the prepared compositions were sintered under similar conditions the resultant materials exhibited different degrees of coloration. However, by comparing the as sintered compositions in table 4.1, it is clear that compositions with lower density all exhibited the brighter yellow colour compared with those with higher density. This suggests that in addition to the valence state of the Yb cation the density may also contribute to the different coloration in the Yb α'-sialons. This indicates that the greater reflectivity (light scattering) in porous materials may be the origin of the graded coloration.

4.4- Phase Analysis and Microstructure Studies

Characterisation of the as sintered Yb-sialon materials was carried out using XRD and electron microscopy (SEM and TEM) for phase identification and microstructural analysis.

4.4.1- Sintered Materials (m1n2 series)

4.4.1.1 Phase analysis

The phase analysis on all 'as-pressureless sintered' materials fabricated at 1750^{0}C for 4 hours, using X-ray diffraction, is summarised in table 4.3. The results show that Yb α'–sialon and β'–sialon are the only crystalline phases detected in most of the compositions. A trace of aluminium-nitride polytypoid phase (identified as 12H) was also observed in compositions designed to give high α'/β' sialon ratio, i.e composition Yb95A and Yb100A. XRD traces from compositions Yb50A, Yb75A and Yb100A are shown in Figure (4.3).

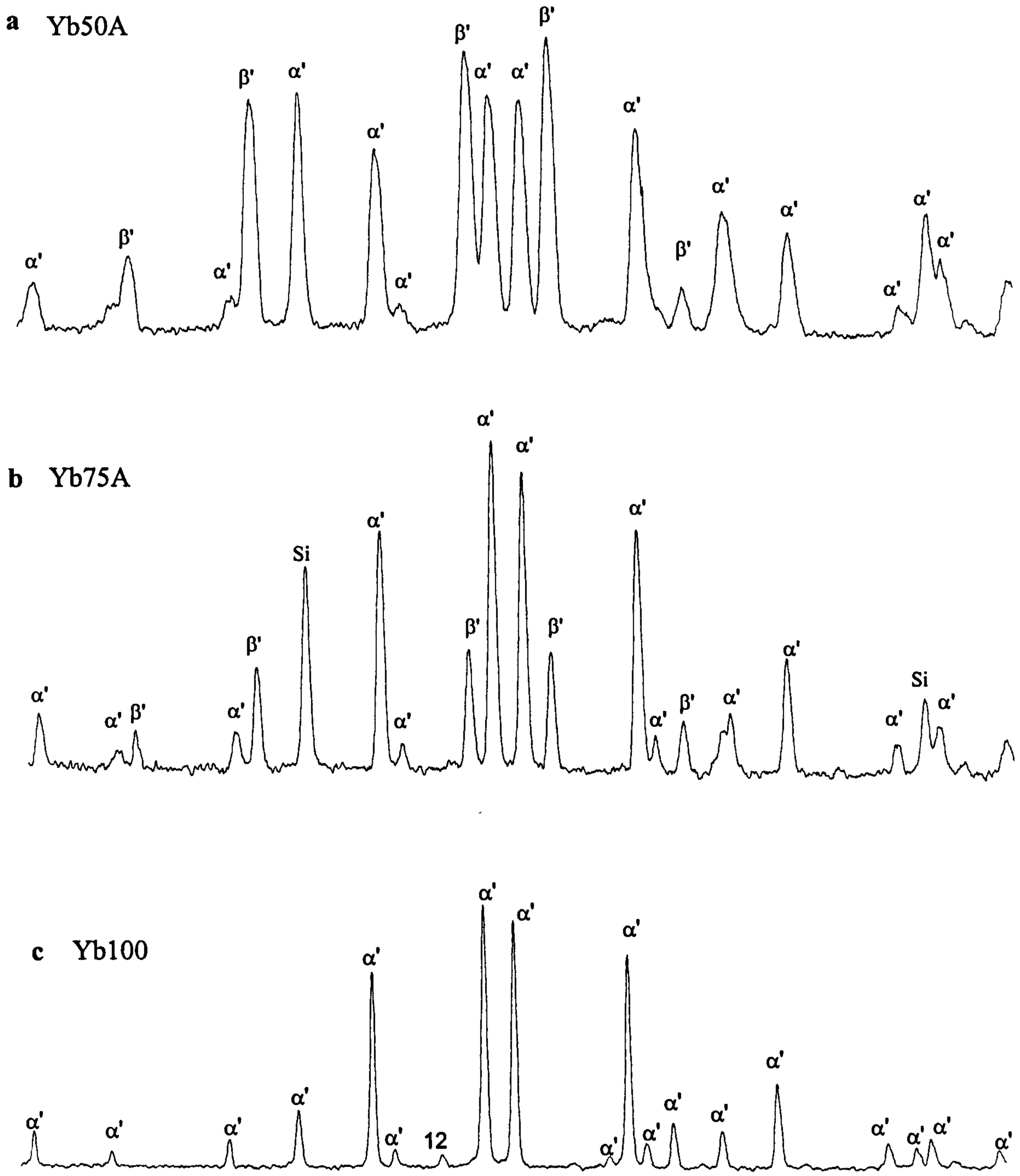

Figure 4.3 The XRD traces of as sintered compositions (a) Yb50A, (b) Yb75A and (c) Yb100

composition	α'/β' sialon	(α')Lattice parameter		SEM		x-value XRD	x-value SEM
		a_0	c_0	m	n		
Yb50A	61/39	7.7956	5.6918	-			-
Yb75A	82/18	7.8112	5.6971	1.08	1.24	0.34	0.36
Yb80A	84/16	_	_	1.18	0.898	-	0.39
Yb95A	93/7	7.8147	5.6972	1.18	1.14	0.39	0.39
Yb100A	100	7.8126	5.6945	1.19	1.28	0.38	0.39

Table 4.3. The α'/β' phase ratios and lattice parameters, x-values of α' phase of compositions in series A after sintering at 1750^{0}C for 4hr.

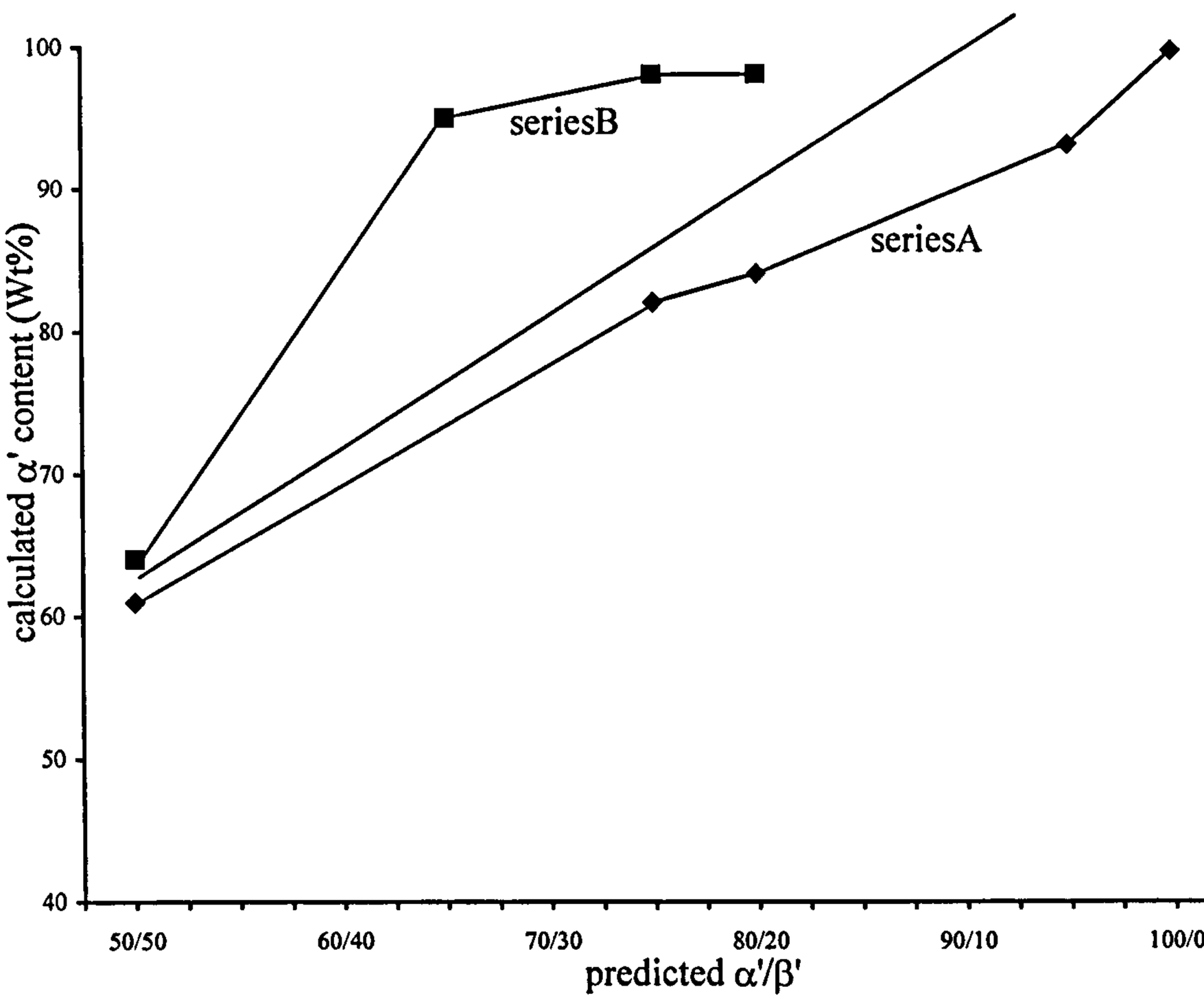

Figure 4.4. The relationship between predicted and calculated α'/β'

The α'/β' Sialon phase ratio after sintering was calculated using equation (3.2) given in chapter 3. The results obtained from all the as-sintered compositions are presented in Figure (4.4) and table (4.3). For example, the spectra shown in Figure 4.3 for compositions Yb50A and Yb75A were calculated to contain α'/β' phase ratios of approximately 61/39 and 82/18 respectively. However as can be seen from Figure 4.4 which illustrates the relationship between the predicted and observed α'/β' sialon phase ratio, although the observed values are slightly shifted (as illustrated by composition Yb50A and Yb75A) the α'/β' ratios formed in these compositions are close to the values predicted from the initial compositions, and compositions Yb80A, Yb95A and Yb100A, gives values very similar to the designed ratios. In general the α' phase content increases with increasing Yb-glass content in the starting materials, the α'/β' ratio increased from 61/39 in composition Yb50A to 93/7 in composition Yb95A and then increased further to approximately 100% in composition Yb100A.

4.4.1.2- Microstructural Observation

The microstructures of as-sintered materials prepared in this series were studied using scanning electron microscopy. Figure (4.5a,b,c) illustrates typical SEM, secondary-electron images corresponding to the sintered compositions Yb50A, Yb75A and Yb100A from which the XRD spectra shown in Figure (4.3) were obtained. The images clearly illustrate the high level of porosity of the compositions prepared in this series, which made the imaging and the analysis of the phases in some compositions somewhat difficult due to charging effects, indicated by the very bright region of the microstructure. Observation of the corresponding back-scattered electron image, Figure (4.5 d,e,f) allowed differentiation between the β'-sialon/or 12H AlN polytype grains (dark grey phase) and the α' grains (light grey) through atomic number contrast arising from the difference in the Yb contents. The

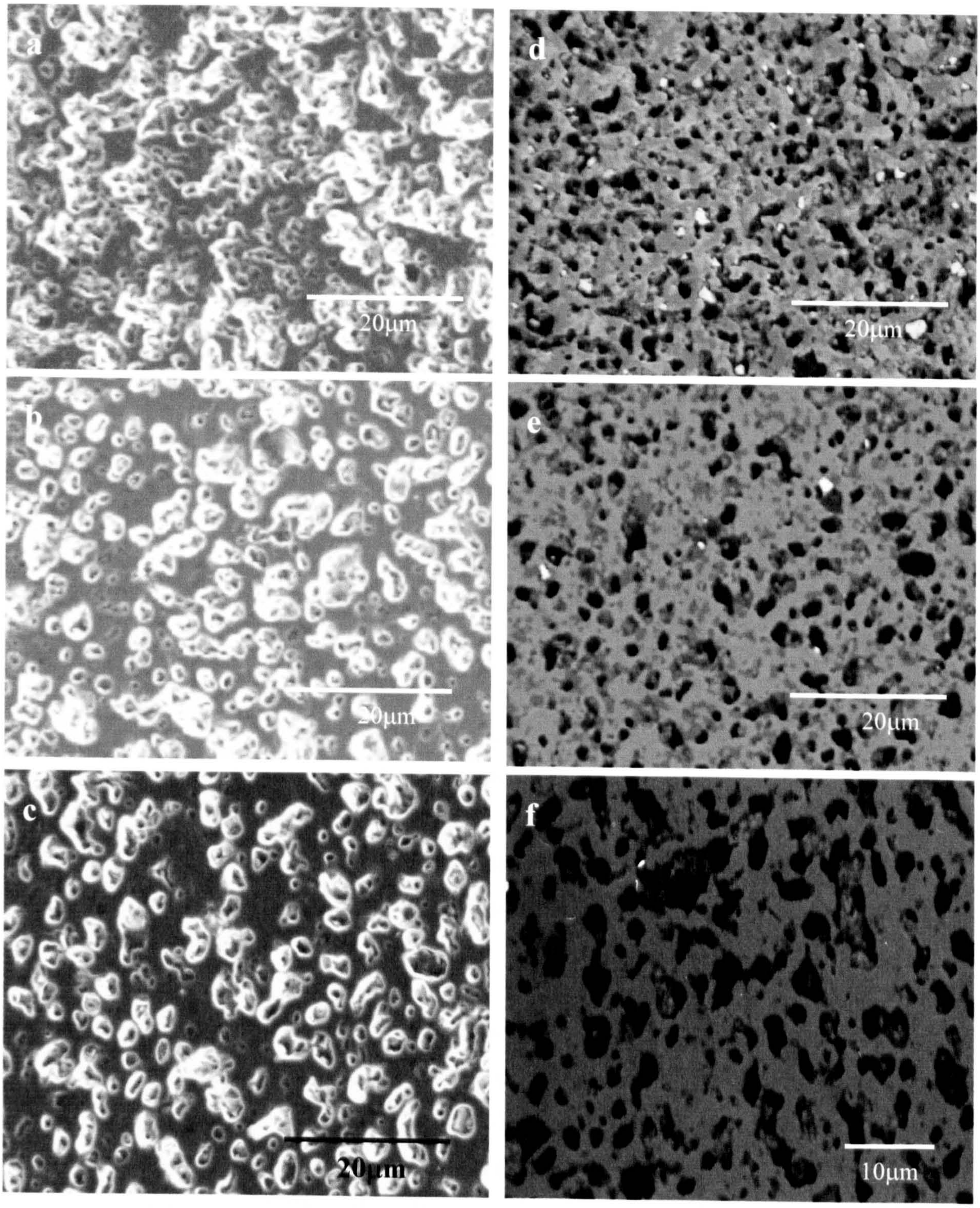

Figure 4.5. The SEM micrographs , secondary electron image (a) Yb50A, (b) Yb75A (c)Yb100 and back-scattered electron image (d) Yb50A, (e) Yb75A and (f) Yb100

microstructures consist of only α'-sialon and β'-sialon, with no intergranular glassy phase detected in these compositions, at the SEM resolution limit.

However despite the higher porosity of these compositions attempts to measure the chemical compositions of individual α' and β' grains were carried out using point analysis via the EDAX facility attached to the SEM. The measurements were carried out only on compositions where it is possible to distinguish between α' and β', and the analysis was made only on relatively large grains to reduce the fluorescence effect from the surrounding neighbouring phases. The Al, Si and Yb contents of α'-sialon grains of each composition were determined and the Al-N substitution level (m value) and the Al-O substitution level (n value) were calculated from the Al/Yb and Si/Yb ratio. Although the m-values were slightly different from the predicted one the n value was however significantly lower which may

be attributed to the formation of 12 H AlN polytype. The results obtained are presented in table 4.3. However for the trivalent element the substitution level (x-value) in α'-sialon can be calculated as m=x/3, therefore the results obtained of the substitution level (x-value) of the Yb^{3+} in all compositions are shown in table 4.3. As can be seen the values are consistent with those obtained from the XRD which suggest that the distribution of the Yb^{3+} cation within the α' is comparable. The x-values are almost similar in most of the compositions which deviate only slightly from the predicted value (x=0.33).

Examination of composition Yb100A in TEM confirmed the observation made in the SEM; the microstructure revealed that the majority of the α' grains were equiaxed Figure (4.6.a). A typical EDAX spectrum from an equiaxed grain of α'-sialon phase, shown in Figure (4.6b), confirms the presence of Yb within the α' grains. For slightly longer grains with high aspect ratio scattered throughout the structure in small volume, the EDAX analysis, shows a relatively high Al content, consistent with the XRD peaks

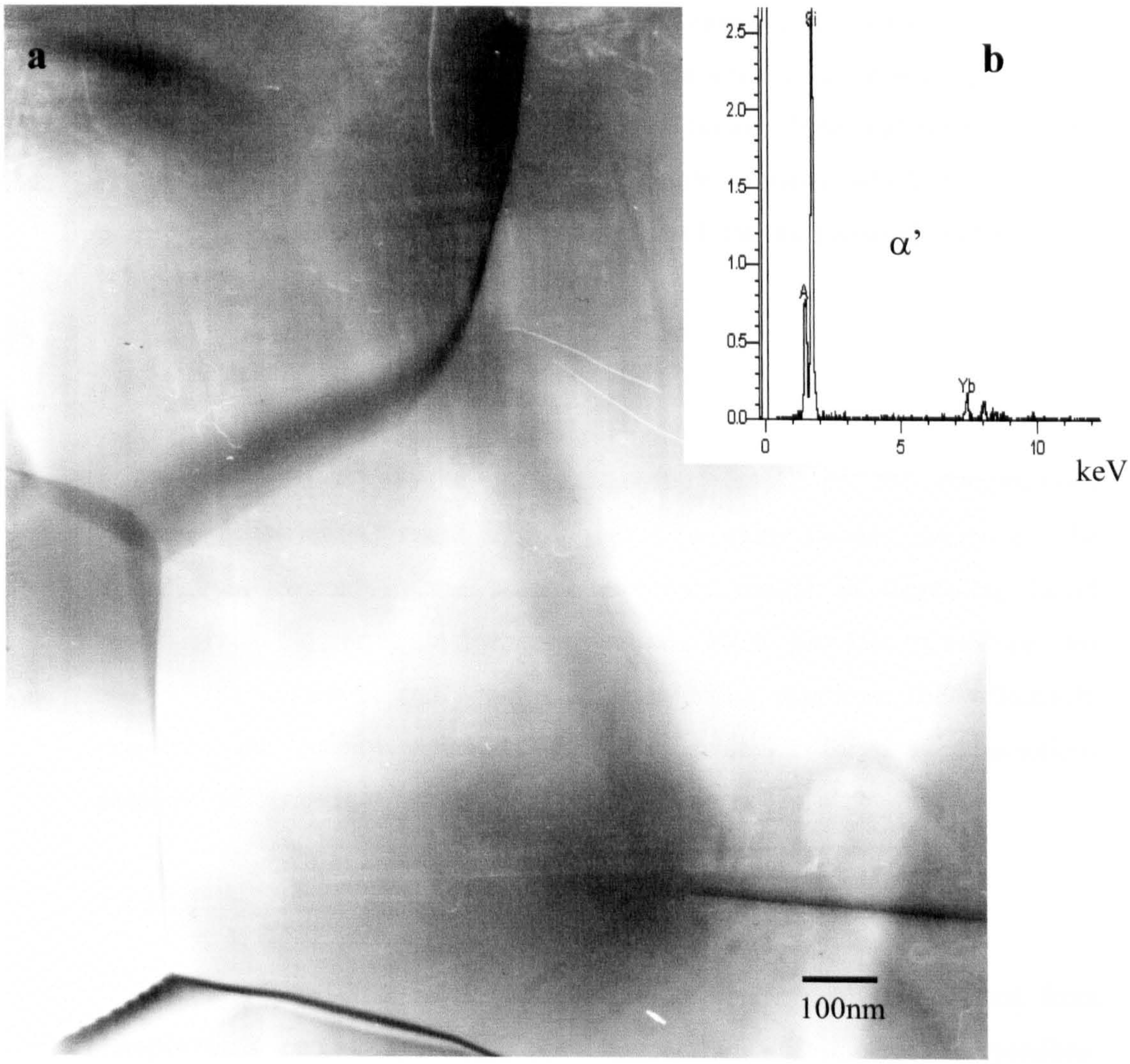

Figure 4.6. TEM micrograph of composition Yb100 sintered at 1750^0C for 4 hrs (a) and the EDAX pattern of equiaxed α' phase (b)

identification as 12H aluminium nitride polytypoid. The micrograph shows the absence of intergranular glass and this would suggest that the Yb must be all dissolved within the α' structure which is in agreement with the observed x-values.

All the prepared compositions in this series, result in materials with α'/β' phase ratio very close to the designed value. However the small level of the Yb glass added to the starting composition, resulted in a limited liquid phase present at the sintering temperature. For this reason these materials exhibited low density with a very high level of visible porosity which will have a negative effect on the mechanical properties of the as prepared materials.

4.4.2- Sintered Materials (m=1.5 n=0.75)

As revealed in the previous section most of the compositions prepared in series (A) result in materials with lower density. Increasing the designed m content in the starting materials results in increasing liquid levels at the sintering temperature and therefore provides a medium for particle rearrangement and solution re-precipitation reactions. This effectively improved the density values, as shown in table 4.1 for the compositions prepared in series B.

4.4.2.1- Phase analysis

From the XRD studies, the results of phase analysis obtained from compositions sintered at 1750^{0}C for 4 hours, show that the major crystalline phase observed in all the as-prepared compositions was Yb α'–sialon, with a very small amount of β'-sialon, and a minor amount of AlN polytypoid, identified as 12H, present in all the compositions. Figure (4.7) represents the XRD traces from as sintered compositions Yb50B, Yb75 and Yb80B.

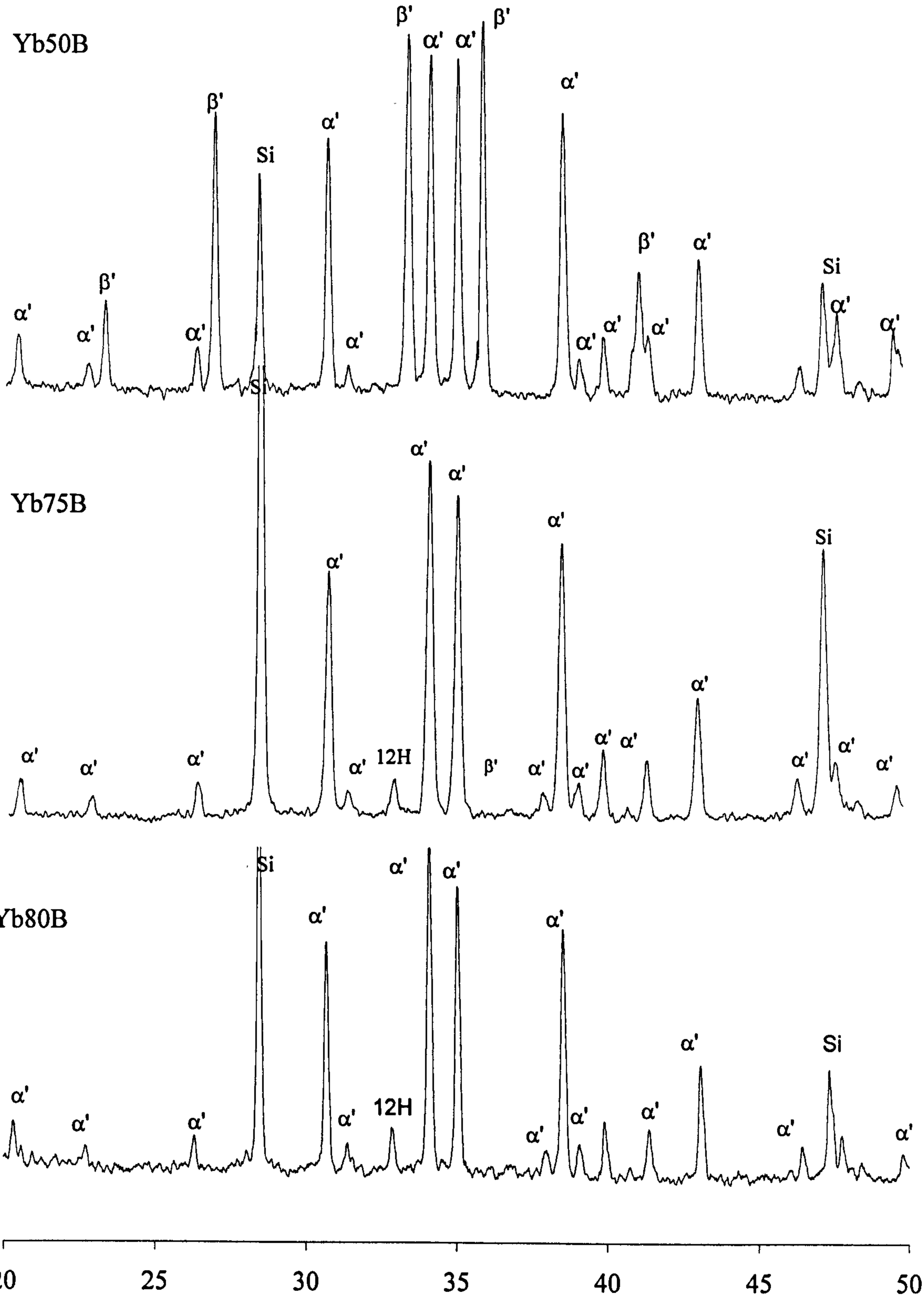

Figure 4.7. The XRD traces of selected as sintered compositions prepared in series B

The relative amounts of α' and β'-Sialon phases after sintering at 1750^{0}C were calculated from XRD data and the results obtained are given in table 4.4 and presented in Figure 4.4. Although all the starting compositions were designed to produce α'/β'-Sialon phase ratios shown in table (4.1), after sintering there was a significant deviation from these ratios (see table 4.4). Composition Yb50B which was designed to produce a composite material with α'/ β' ratio of 50/50 gave results relatively close to this value (the α'/β' ratio after sintering was 64/36) whereas the other prepared compositions Yb65B, Yb75B and Yb80B after sintering resulted in materials with much higher α' content; approximately ~100% α'-sialon. Figure (4.4) shows the α'/ β' phase ratios of all as prepared materials. The α'/β' ratios are slightly increased as the glass level in the starting materials increases.

In the present result the formation of higher α' content than the predicted value indicates that Yb is a good α' former, due to the small ionic radius of Yb cation (~0.086nm) which can easily enter the α' structure. Studies on different sialon systems by Mandal et al (1995) and Wang et al (1993) showed that the heavier rare earth cations with smaller ionic radii can be more easily accommodated in the α'- sialon structure, compared to the lighter rare earth cations with the larger ionic radii. The relative stability of the intermediate phase which forms during sintering has also an effect on the α' formation. For example the stable melilite phase in the light rare-earth sialon materials, which persist up to high temperature, increase the competition with α'-sialon for the stabilising cation and nitrogen thus retarding the α' formation. In contrast, the Yb sialon forms a garnet (YbAG) phase as an intermediate phase.

However a similar result was obtained for materials prepared with identical composition to the materials prepared in this study but using Gd (0.09 nm) as the stabiliser cation for α' (Jumali 1999). In his study Jumali found that the replacement of Gd by Nd with ionic radius (~0.1nm) results in an increase in β' content. The increasing amount of α'-sialon with decreasing

ionic radius is thus indicative of the higher stability of the α'-sialon that contains smaller rare earth cations.

The change in lattice parameters of the α' sialon phase is due to compositional variation in the solid solution. The Al-N bond (0.187nm) is significantly larger than the Si-N bond (0.174nm) and the substitution of Al-N bonds by Si-N bonds within the α' lattice results in an expansion of the cell dimension and requires a higher concentration of cation to stabilise the structure. Because the bond lengths are almost identical the substitution of Al-O bond (0.175nm) by Si-N has a smaller effect on the cell dimensions; which is similar to the substitution in β' sialon. The lattice parameters measurements of α'-sialon via XRD are shown in table 4.4; the values deviate significantly from the lattice parameters of pure α-Si_3N_4, which indicates the formation of a solid solution. As can be seen from the table and Figure 4.8, there is only a slight increase in the unit cell of the α'-sialon as the glass level in the starting materials increases, except composition Yb80B which shows a reduction in the cell parameters. However because the lattice parameters of α'-sialon are more sensitive to the amount of rare earth cation level, the decrease in the lattice parameters implies a decrease in the m-value and therefore indicates the formation of α' sialon with lower concentration of Yb^{3+}.

The α'-sialon lattice parameter (determined from XRD) is known to be a linear function of m and n, thus for the given lattice parameter (table 4.4), according to Shen and Nygren (1997), the m and n values of α'-sialon can be calculated from the relations given in chapter 3, equations 3.5 and 3.6. The results obtained are listed in table 4.4. As can be seen from the table, the calculated m values increase only slightly as the glass content increases in the starting materials and then decreased in composition Yb80B which gives the lowest m value, despite the similar α'/β' phase ratio to composition Yb75B. This however may indicate that the Yb80B has either the larger volume of the residual phase (as this will consume large amounts of the

Yb^{3+}) or that the cation concentration in the intergranular region is higher than the other compositions. However the measured m values of all compositions are slightly shifted and the values were significantly lower than the designed one. The n values are slightly higher and almost double in composition Yb80B, which indicates higher Al-O substitution in α' structure.

composition	α'/β' sialon	Lattice parameter a_0 c_0	m	n	z value (β')
Yb50B	64/36	7.804 - 5.6867	0.929	0.947	0.705
Yb65B	95/5	7.8138 - 5.6986	1.1	1.11	1.158
Yb75B	98/2	7.8142 - 5.6982	1.13	1.08	2.645
Yb80B	98/2	7.8023 - 5.6895	0.759	1.5	0.459

Table 4.4. Phase content and compositional analysis of α sialon / β sialon of as sintered materials

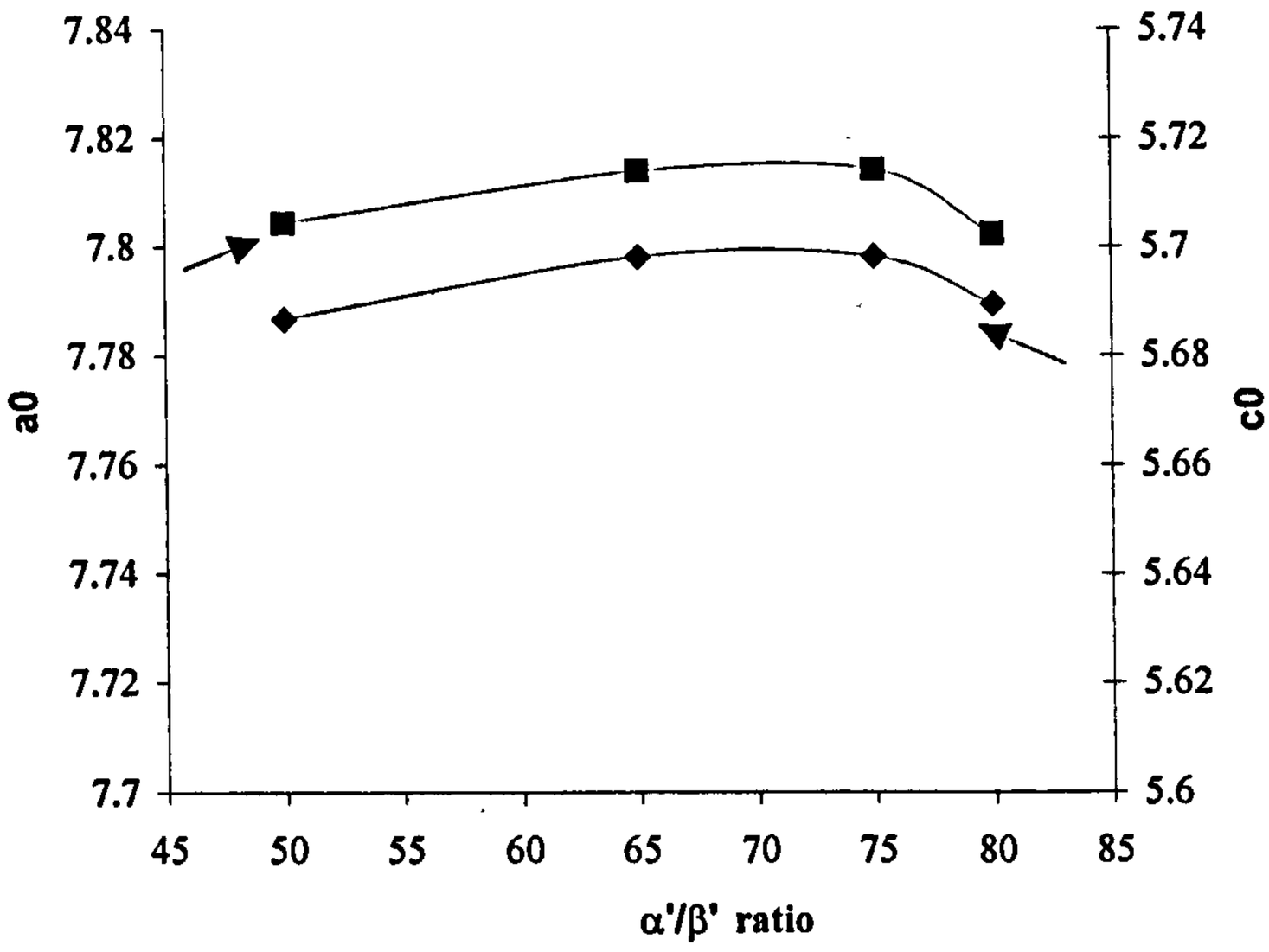

Figure 4.8. The measured α' lattice parameters of as sintered compositions in series B

The phase evaluation of composition Yb75B fabricated at temperatures lower than 1750^{0}C was also investigated (table 4.5). The material was pressureless sintered at two different temperatures: at 1500^{0}C for 1hour and at 1600^{0}C for 4hours. The XRD traces are shown in Figure 4.9. After pressureless sintering at 1500^{0}C for 1hour, the spectra revealed the presence of some unreacted α-Si_3N_4 and small amount of AlN from the starting powders, A significant amount of YbAG garnet phase ($Yb_3Al_5O_{12}$) was present as an intermediate phase together with a small amount of α'-sialon phase. No β'-sialon phase was detected at this temperature, however Menon (1995) reported that the formation of β' phase starts at 1575^{0}C at the expense of YbAG and AlN phases. The formation of garnet (YbAG) as an intermediate phase is in agreement with Hwang and Chen (1994), Menon and Chen (1995a) and more recently Roesenflanz and Chen (1999), who reported that the YbAG phase formed at temperatures as low as 1400^{0}C and completely disappears at 1600^{0}C.

Menon and Chen (1995a) have reported that the differences in wetting behaviour of liquid in compositions containing rare earth cation (R), i.e the reaction of the eutectic liquid with the Si_3N_4 and AlN, cause the formation of the different intermediate phases which may be either Si rich if the eutectic liquid wets Si_3N_4 first or Al rich if the AlN is wetted first. In the heavy rare-earth (Er and Yb) systems the ternary eutectic liquid wets the AlN first, resulting in excess of alumina which is precipitated as a garnet phase RAG, whereas with the lighter rare-earth the eutectic liquid wets the Si_3N_4 first resulting in a Si rich melilite phase, (or its solid solution M' phase).

However, as the sintering temperature increased to 1600^{0}C, more α'-sialon formed, the α-Si_3N_4 and AlN phases completely disappeared and the amount of YbAG phase is significantly decreased. The formation of α'-sialon as a major phase with a small amount of β' phase and 12 H polytype at this temperature suggests that as the temperature increased above 1500^{0}C the

precipitation of more α'-sialon is fed by the dissolution of the remaining α-Si_3N_4 and AlN phases together with the melting of YbAG, which provides the system with a large fraction of liquid phase, which enhances α' formation and results in an improvement in densification. A 6% increase in the bulk density was observed, which was attributed to the solution and reprecipitation mechanism. The XRD data revealed that the α'/β' phase ratio of composition sintered at 1600^0C was about 96/4 which is almost similar to the ratio obtained at 1750^0C.

Temperature	Phases detected (XRD)	Density (g/cm^{-3})
1500^0C	Si_3N_4, AlN, YbAG, α'	2.44
1600^0C	α', β', 12H,YbAG	2.60
1750^0C	α', β',12H	3.36

Table 4.5 Phase analysis and density of composition Yb75B sintered at different temperatures

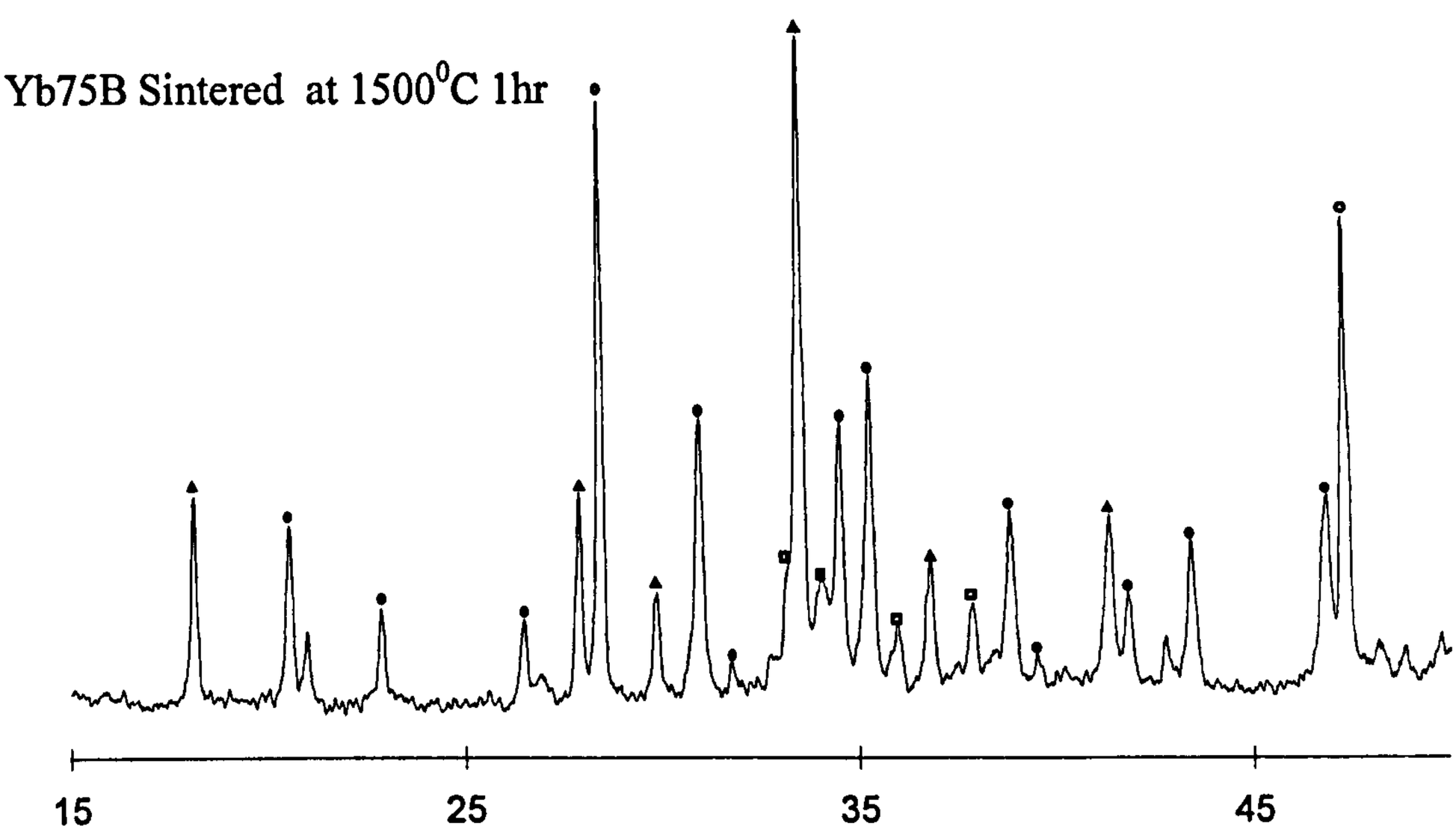

Figure 4.9. The XRD traces of composition Yb75B sintered at 1500^0C for 1 hour ▲ YbAG, • α-Si_3N_4, ■ 12H and ▫ AlN

From the measured lattice parameters of α'-sialon at 1600^{0}C (a_0=7.8114 and c_0=5.693), the substitution level (m-value) was calculated as ~1.12 which is similar to the value calculated at 1750^{0}C (table 4.4). This, together with the formation of nearly similar α'/β' ratio at 1750^{0}C, suggests that the reaction to form α'-sialon was almost completed at 1600^{0}C. This is in contrast to the melilite phase formed in other rare-earth sialon systems such as (Nd and Sm). Although the formation of melilite phase is also transitory, this phase persists to much higher temperature (above 1700^{0}C) before its dissolution (Shen et al 1996 and Ekstrom et al 1997) and competes for the stabilising cation of α' formation and therefore α' formation is retarded.

However above 1600^{0}C the solution of the remaining intermediate phases, YbAG and some of the β'-sialon phase, enhanced the densification and a significant increase in bulk density, (approximately 29%) was observed for the composition sintered at 1750^{0}C (see table 4.5).

4.4.2.2- Microstructural Studies

(a)- SEM Observation:-

The microstructures of compositions pressureless sintered at 1750^{0}C for 4hr were studied using scanning electron microscopy. The scanning electron micrographs of 'as sintered compositions' Yb50B - Yb80B, recorded in back-scattered mode are shown in Figures 4.10(a-d). Because the contrast on back-scattered electron micrographs depends on the mean atomic number, the micrographs very clearly distinguish between various phases; generally the β'-Sialon and the AlN polytypoid phase (which contain no rare-earth element) appear with dark / black contrast (which in turn can be differentiated either by their morphology or more accurately by Al/Si elemental analysis). The α'-Sialon phase (which contains a small amount of Yb cation) appears with medium grey level, and the residual intergranular glassy phase, which is rich in the Yb cation, appears with bright contrast.

Figure 4.10(a) shows the micrograph of as sintered composition Yb50B corresponding to α'/β' ratio of 50/50. The microstructure consists of grey α'-sialon grains which show a small equi-axed grain morphology, the β'-sialon grains which show two different morphologies, namely large prismatic grains with large aspect ratio, (excessively large grains with maximum length approximately 20μm and a diameter of 5μm were also observed), and very small grains with sub-micron size which are present in large amounts. The intergranular glassy phase is finely distributed and concentrated mainly in the small pockets formed between the sialons grains, which made accurate estimation of its volume fraction from SEM uncertain. However quantitative analysis, shows that the volume of α'-sialon phase is approximately 56%. The presence of a large amount of residual porosity was also clearly evident from the microstructure and appears in black contrast, with pore size in the range approximately 0.5μm to 6μm.

The micrograph of Figure 4.10(b), corresponding to composition Yb65B with 65/35 α'/β' phase ratio, shows that this material contained a significantly reduced intergranular volume, and consists mainly of two crystalline phases, a matrix (grey) α'-sialon phase with relatively coarser structure than Yb50B. The small volume of intergranular phase made measuring of the individual grains of the sialon matrix difficult. A second dark phase is present which is mixture of a small amount of β'-sialon phase with finer grains size, and 12H AlN polytype with a plate like morphology. Approximately 5% of residual porosity was also observed in this composition which reflects the relatively low density observed in this material and the pore size is similar to the one observed in composition Yb50B.

In the microstructure shown in Figure 4.10 (c), corresponding to composition Yb75B with α'/β' ratio of 75/25, the α' grains exhibit an equiaxed shape with a grain size varying from sub-micron to an average of 4μm in length. Image analysis indicates that the α'-phase in this composition occupies approximately 86%. A residual intergranular glass phase with volume fraction

of approximately 5% was also observed; the major amount of this glassy phase is located at the multi-grain junctions forming slightly larger pockets than Yb50B; although it sometimes surrounds the small sialon grains. The dark grey phase which is homogeneously distributed also shows different morphology, fine needle like grains with a small grain size and coarse ones with irregular shapes. The chemical analysis (EDAX), showed that most of this dark phase was rich in Al which indicates that it is a 12H aluminium-polytyoid, as identified from the XRD.

The micrograph in Figure 4.10(d) corresponding to composition Yb80B, revealed that the amounts of α' and β' are similar to that of composition Yb75B. However as can be seen from the micrograph, this composition contains a slightly higher volume fraction of residual intergranular glassy phase, estimated from the quantitative analysis to be about ~ 8%. Most of the glassy phase is concentrated around the small sialon grains. The equiaxed α'-sialon grains exhibit a finer grain size than Yb75B which varies from sub-micron to over 4μm. The dark phase, is a mixture of β'-sialon and 12H AlN polytypoid which is present in higher volume fraction than β'.

By comparing all the prepared compositions in series B, the general trend observed is that the α' -sialon phase content increases slightly as the Yb alumino-silicate glass content in the starting powders increases. This mainly occurs as a result of increasing the stabilising Yb cation content within the liquid phase to enhance the precipitation of more α'-sialon, in agreement with that predicted in the simple computer program. As mentioned before Yb is a good α'-sialon former due to the small ionic radius and there is an absence of stable melilite phase which competes with α' phase for the stabilising cation. A similar trend was observed with composition prepared in series A. The volume fraction of residual intergranular glassy phase seems to increase only slightly with increasing the Yb glass content in the starting compositions, except in composition Yb65B which showed the lowest volume fraction of residual glass. The explanation for the reduction of the

residual glassy phase in this composition is probably due to the increased α'/β' phase content as shown from the SEM micrograph and XRD results table 4.4. It is possible that the overall composition of material Yb65B located at the boundary of the α' single phase region thus results in α' rich material. The formation of high α' content during sintering will consume more of Yb cations in its structure and therefore results in a lower volume of the residual phase after sintering.

The microstructural studies revealed that a small amount of a residual glassy phase was present in all compositions. This glassy phase contained appreciable amounts of Yb which implies that the Yb content of α'-sialon must be different from that predicted by the initial compositions. In order to determine the Yb content in α' grains and the Al substitution in β'-sialon, the chemical compositions of individual α' and β' grains were measured by (EDAX) point analysis in the SEM, and the results obtained presented in table 4.6. From the Al-N substitution level (m values) shown in the table, the Yb substitution level (x-values) of α'-sialon in both compositions Yb50B and Yb75B were calculated as approximately ~ 0.33 and 0.38, respectively. These values are in fair agreement with the values determine by XRD (0.32 and 0.38) for Yb50B and Yb75B respectively, which are significantly different from the values predicted by the starting composition (x=0.5).

composition	m^+	n^+	z^+	m*	n*	x-value*
Yb50B	0.92	0.993	0.754	0.97	1.56	0.33
Yb65B	1.1	1.46	1.177	-	-	-
Yb75B	1.2	1.53	1.27	1.15	2.15	0.38
Yb80B	1.19	1.50	2.73	1.21	2.15	0.39

Table 4.6. EDAX compositional analysis of α/β sialon phases in specimens sintered at 1750^0C for 4hrs. * from TEM + from SEM

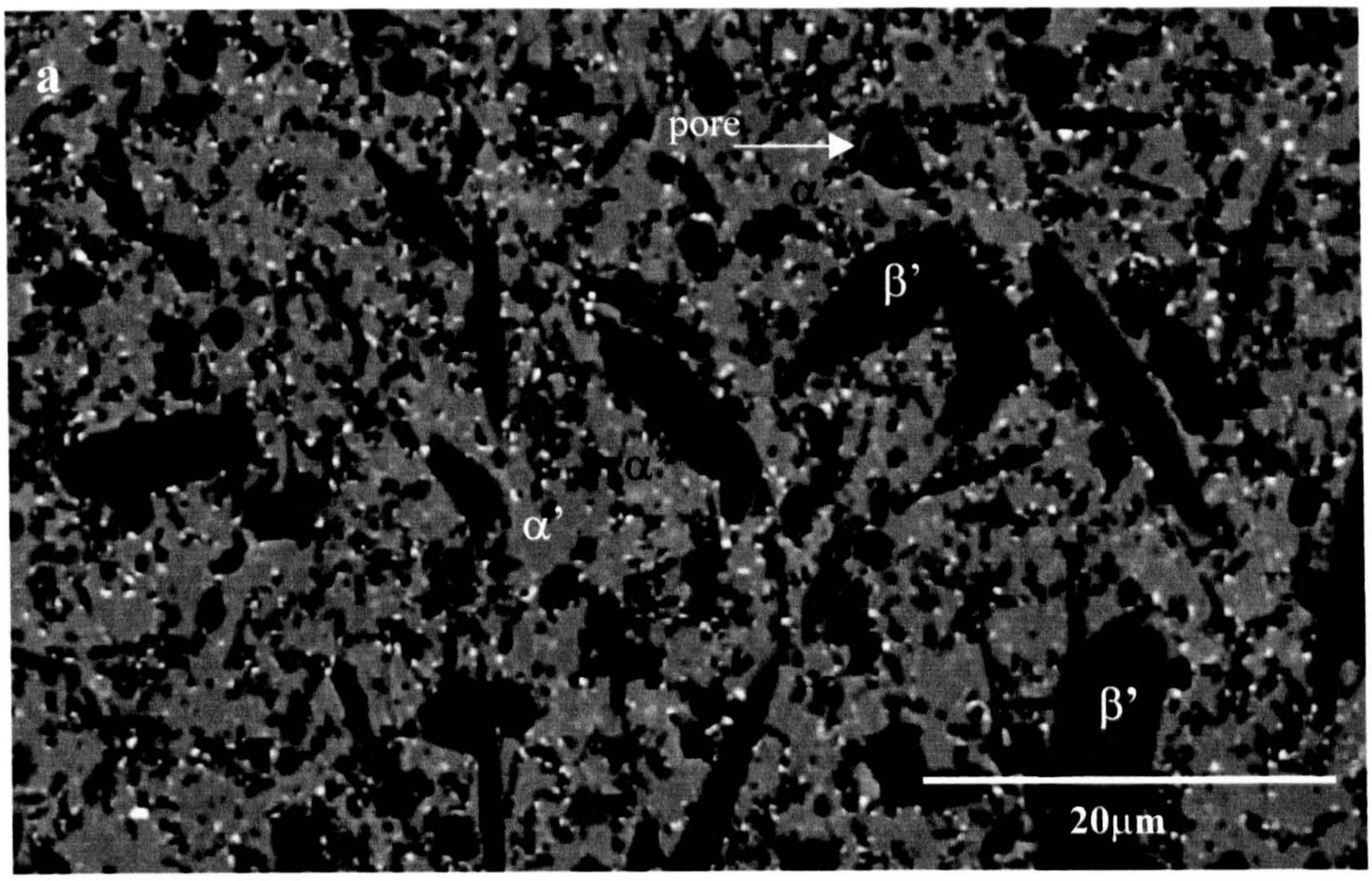

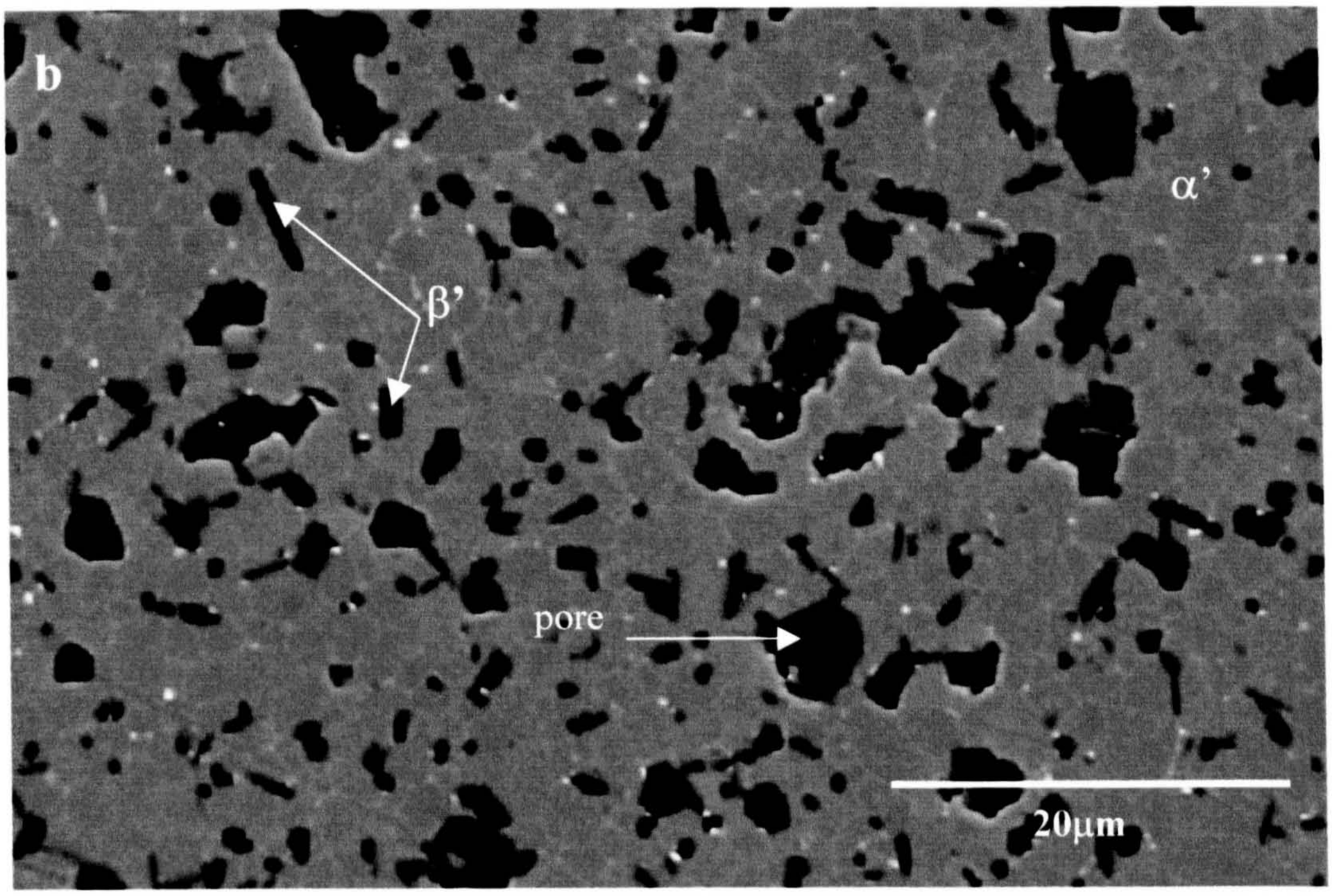

Figure 4.10. The SEM micrographs of compositions; (a)-Yb50B, (b)-Yb65B, (c)-Yb75B and (d)-Yb80B

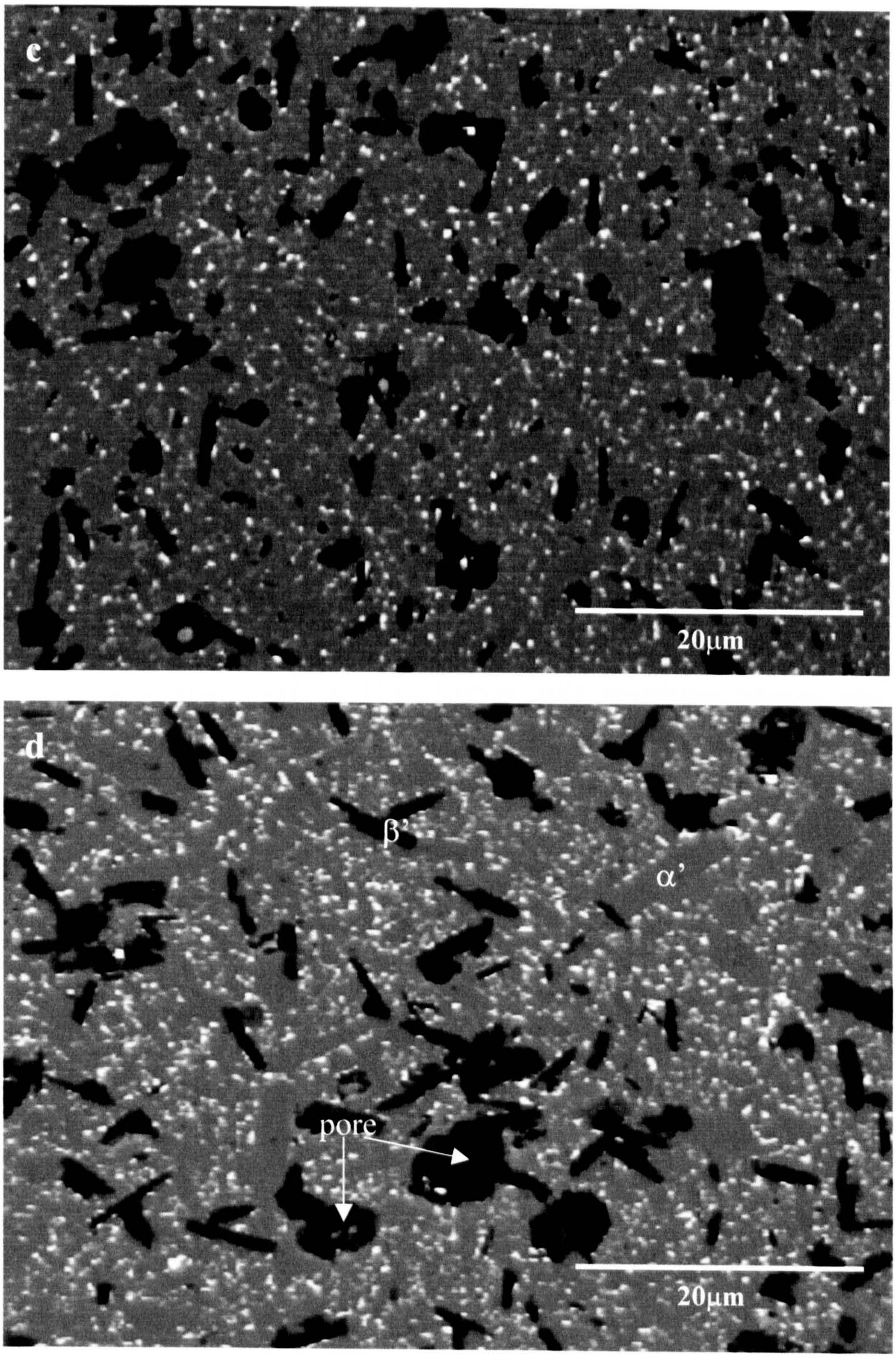
c
20μm
d
β'
α'
pore
20μm

EDAX analysis of individual β' grains gave Al-O substitution levels (z-values) of β'-sialon as in table 4.6. These values are in fair agreement with the overall z-values determined from XRD but are significantly lower than the predicted values.

(b)- TEM Observation

Further detailed study was carried out on thin foils of selected sintered compositions using transmission electron microscopy (TEM). Figure (4.11) shows typical bright field TEM images of as-sintered compositions Yb50B and Yb75B. Although the equiaxed nature of the α'- sialon grains is clearly seen in both compositions, in Yb50B the structure showed a large variation in grain size and shape. This is mostly observed for the β-sialon phase which is a mixture of fine grains with average grain diameter of less than 1 μm and extremely large elongated grains with average grain diameter of 3μm and average length of 15μm. Curved grain boundaries between adjacent grains were frequently observed in these structures. This feature suggests that the large sialon grains are growing by nucleation on β-Si_3N_4 seeds present in the starting powder. These grains grow continuously when the liquid is available. In Yb75B the grain size of α'-sialon, which is the major phase, is generally larger, with average grain diameter of approximately 4μm. A second crystalline phase which is present in a small amount and has longer grains with irregular shape, analysed to contain higher Al content was identified from XRD as 12H polytypoid, the EDAX pattern is shown in Figure (4.11c). The metal elements in relation to α'- sialon grains were detected by EDAX to be Si, Al and the rare earth cation Yb in a decreasing sequence of the peak height.

The TEM microstructure study of compositions Yb50B, Yb75B and Yb80B also confirms that the intergranular glass volume increased slightly with increasing glass addition in the starting composition, in agreement with SEM

observations. In composition Yb50B, the grain boundaries are very sharp and there is very little glassy phase at the triple junctions. In contrast, the grain boundaries in composition Yb75B are slightly larger and the glassy pockets at the triple junctions are bigger.

The EDAX analysis of the glassy phase in compositions Yb75B and Yb80B, (analysis of the glass phase in composition Yb50B was not attempted due to the small pocket size), shows that the intergranular glass phase comprises all the elements in the system. Although its composition may vary slightly from pocket to pocket (Figure 4.11d), an increase in the peak height of Al and Yb relative to Si was observed, the average glass composition in Yb75B was measured as 57:25:17 for Al:Yb:Si respectively which is similar to the glass composition in Yb80B.

In order to know how much the Yb content enters the α' structure more detailed compositional analysis of the α' phase was carried out using EDAX point analysis in the TEM and the results of the average measurements of m, n and x values are also shown in table 4.6. As can be seen from the table, the values are in good agreement with that obtained from XRD and SEM although the n values from TEM are slightly higher. The calculated m-values show a slight increase and this is similar to those obtained with compositions prepared in series A table 4.3, however the results obtained in this work all show very small spread in m value around the value m=1. This in good agreement with the observation made by Lewis et al (1996), who found that in different rare earth stabilised α'-sialon systems, α' composition favours a linear compositional variation along m=1 which is also a characteristic of the β' sialon phase. The solubility of Yb in α' sialon (the x value) is slightly lower than that aimed for by the starting powder composition (x=0.5).

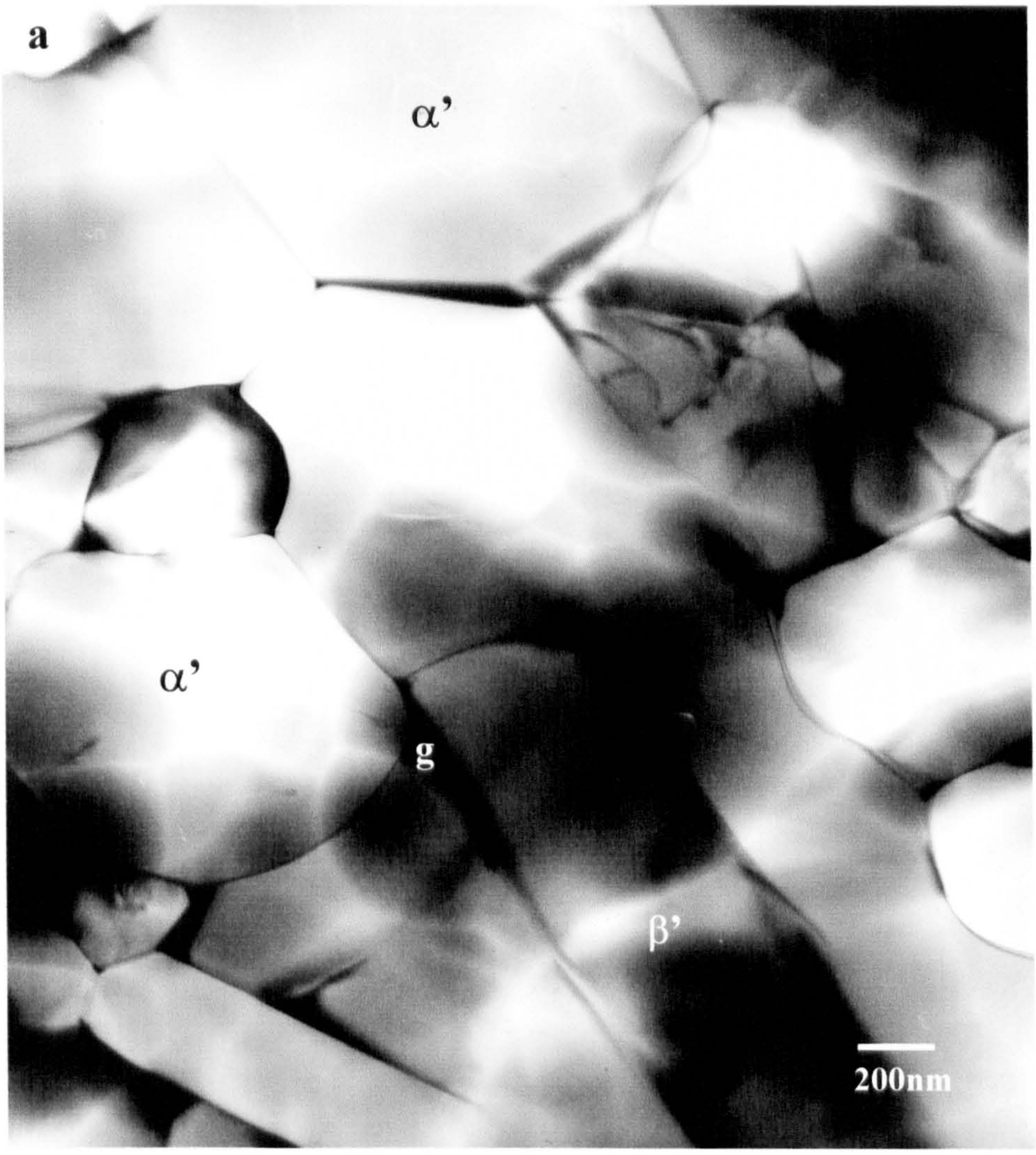

Figure 4.11. The TEM micrographs of as sintered compositions Yb50B and Yb75B, (a) bright field image of Yb50B; (b) bright field image of Yb75B, (c) EDAX of 12H phase and (d & f) EDAX patterns of glass phase of composition Yb75B.

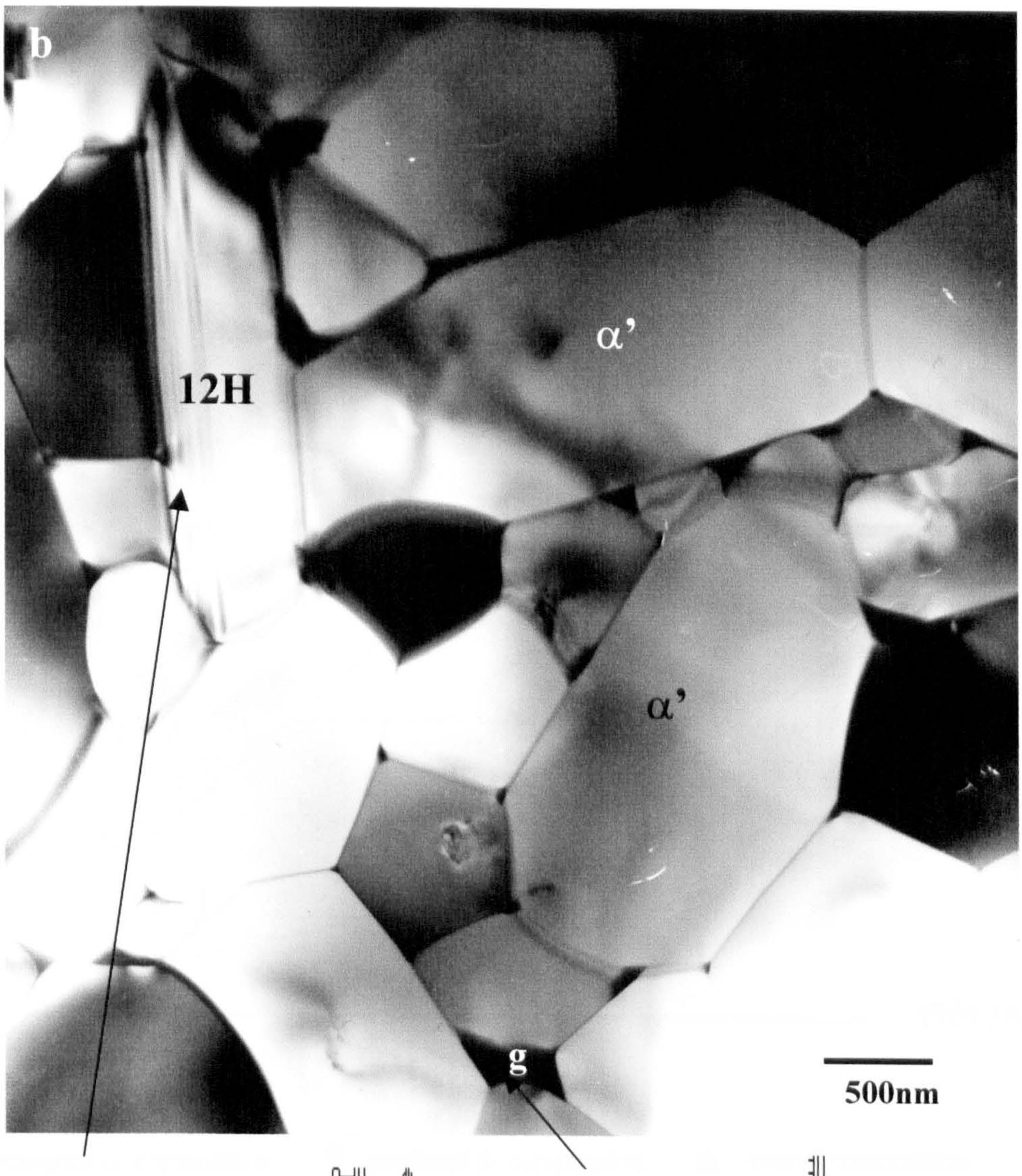
b
α'
12H
α'
g
500nm
c
12H
Al
Si
Cu
0
2
4
6
0
5
keV
d
glass
Al
Si
Yb
0
.5
1.0
1.5
0
5
10
keV
f
glass
Al
Si
Yb
Yb
Cu
0
1
2
3
0
5
10
keV

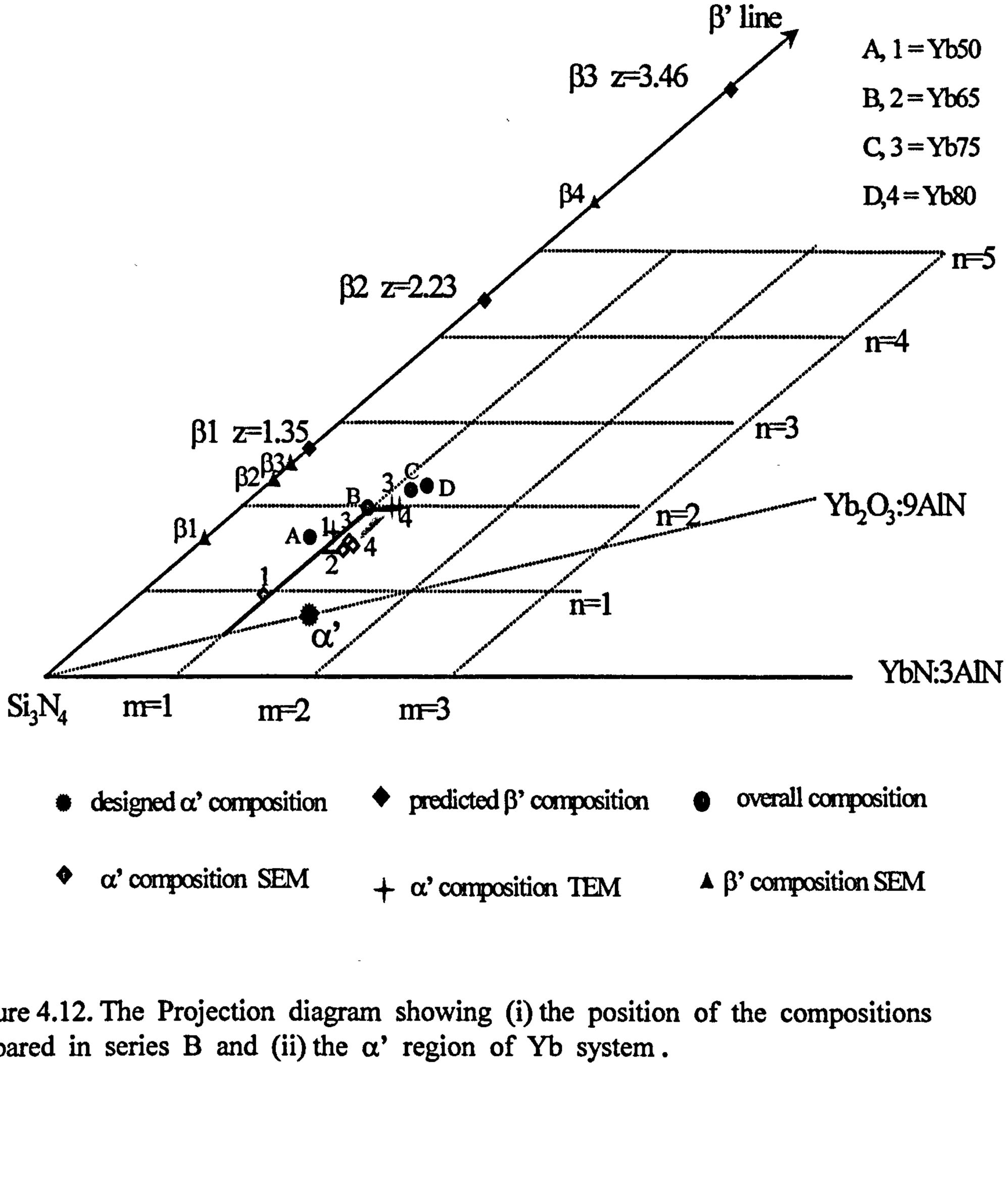

Figure 4.12. The Projection diagram showing (i) the position of the compositions prepared in series B and (ii) the α' region of Yb system.

The experimental α'/β' phase ratios are higher than predicted by the simplistic computer program (described in 4.2). This may be partially explained by the analysed α' compositions which occur at the periphery of the α' phase-field, near to m=1, and which represent the ends of tie-lines from β' compositions drawn through the average initial compositions. Since these average initial compositions are near to the analysed α' compositions the α' content are generally higher than predicted. Figure 4.12, is a projection diagram of compositions prepared in series B showing the actual phase field for the single phase of Yb α' as measured from the EDAX analysis (in both SEM and TEM). The EDAX analysis of α' composition shows the m-value located around m=1 which is common in all the rare earth systems. The maximum oxygen content (n-value) is approximately 2 and was found to depend on the techniques used as shown in Figure 4.12. It is evident from the figure that the compositional area of α'-sialon is larger in the Yb-sialon system than that in the Y-system (see Figure 2.7).

The close positioning of the real (analysed) α' compositions and the average initial composition means that small errors in α' analysis give rise to large variations in tie-line position on the β' linear composition. However, the analysed β' compositions are in much better agreement with these modified tie-lines than the β' compositions predicted on the assumption of a fixed (designed) α'.

The formation of the residual glassy phase with high concentration of Al and the stabilising cation Yb in these compositions would account for the lower x values discussed above. The glass phase competes for the cation and makes the actual content in α' lower than that predicted. In composition Yb50B the actual Yb level in α' is around 65% of the added amount, for composition Yb75B about 77% and for composition Yb80B about 80%. The observed formation of the sialon polytypoid in these compositions will also consume Al-N units resulting in slightly more oxygen rich α'-sialon.

CHAPTER 5

CONSTITUTION MODIFICATION AND HEAT TREATMENT

5.1- Constitution Modification

As shown in chapter 4, the two series prepared in the Yb-sialon system resulted, after sintering, in either materials with α'/β' ratio as expected from the designed composition but with a low density due to the lack of the liquid phase at sintering temperature, or in reasonably dense materials but with a high α' content. In order to investigate the possibility of controlling the microstructure by altering the initial composition, particular emphasis was placed on the effect of adding silica (SiO_2) to the initial composition to control the α'/β' phase ratio. In addition excess β'-Si_3N_4 was introduced into the initial composition to evaluate its effectiveness as a seeding mechanism for enhancing the β'-sialon content and morphology to optimise mechanical properties.

5.1.1- Silica (SiO_2) addition

The silica (SiO_2) was added to the starting composition in order to supplement the oxides present and thus result in more liquid phase being present at the sintering temperature which may facilitate the α'-β' transformation and also move the overall composition further into the α'+β' phase field in the as sintered materials. In order to examine the effect of the addition of SiO_2, six additional compositions were prepared based on compositions Yb75A from series A and composition Yb75B from series B see table (4.1).

The SiO_2 was added in two different ways. Firstly the SiO_2 powder was added to the starting composition and balanced with an extra addition of AlN in

order to keep the composition on the α' plane. This however will keep the composition parallel to the β' phase. The compositions were predicted not to exhibit a change in α'/β' phase ratio. An addition of 2wt% and 5wt% of SiO_2 was made to composition Yb75B to form compositions Yb75B2b and Yb75B5b respectively. In order to study the effect of the SiO_2 addition on the sinterability (by introducing a larger volume fraction of liquid at the sintering temperature), the same additions were also made to composition Yb75A to form composition Yb75A2b and Yb75A5b.

The second addition was unbalanced and the SiO_2 was added directly to the compositions without compensating with AlN. This unbalanced addition, however, will move the composition off the α'- plane but within the prism in the direction of the expanded β' as shown in Figure (5.1). Unbalanced additions of 2wt% and 5wt% of SiO_2 were made only to composition Yb75B to create composition Yb75B2un and Yb75B5un respectively. The overall starting compositions of both balanced and unbalanced materials are shown in table 5.1. All the compositions were pressureless sintered at a temperature of 1750^0C for 4 hours.

Composition	Si_3N_4	AlN	Yb-glass	SiO_2	z-values
Yb75B2b	56.6180	23.5200	17.8620	2.000	4.16
Yb75B5b	49.6114	27.5266	17.8620	5.000	5.28
Yb75B2un	61.1212	21.0170	17.8620	2.000	
Yb75B5un	61.1212	21.0170	17.8620	5.000	
Yb75A	71.5897	15.9800	12.4303	-	0.71
Yb75A2b	66.9187	18.6510	12.4303	2.000	1.44
Yb75A5b	59.9127	22.6570	12.4303	5.000	2.54

Table 5.1. The overall starting compositions (in Wt%) and the predicted z-values of Yb sialon materials with SiO_2 additions.

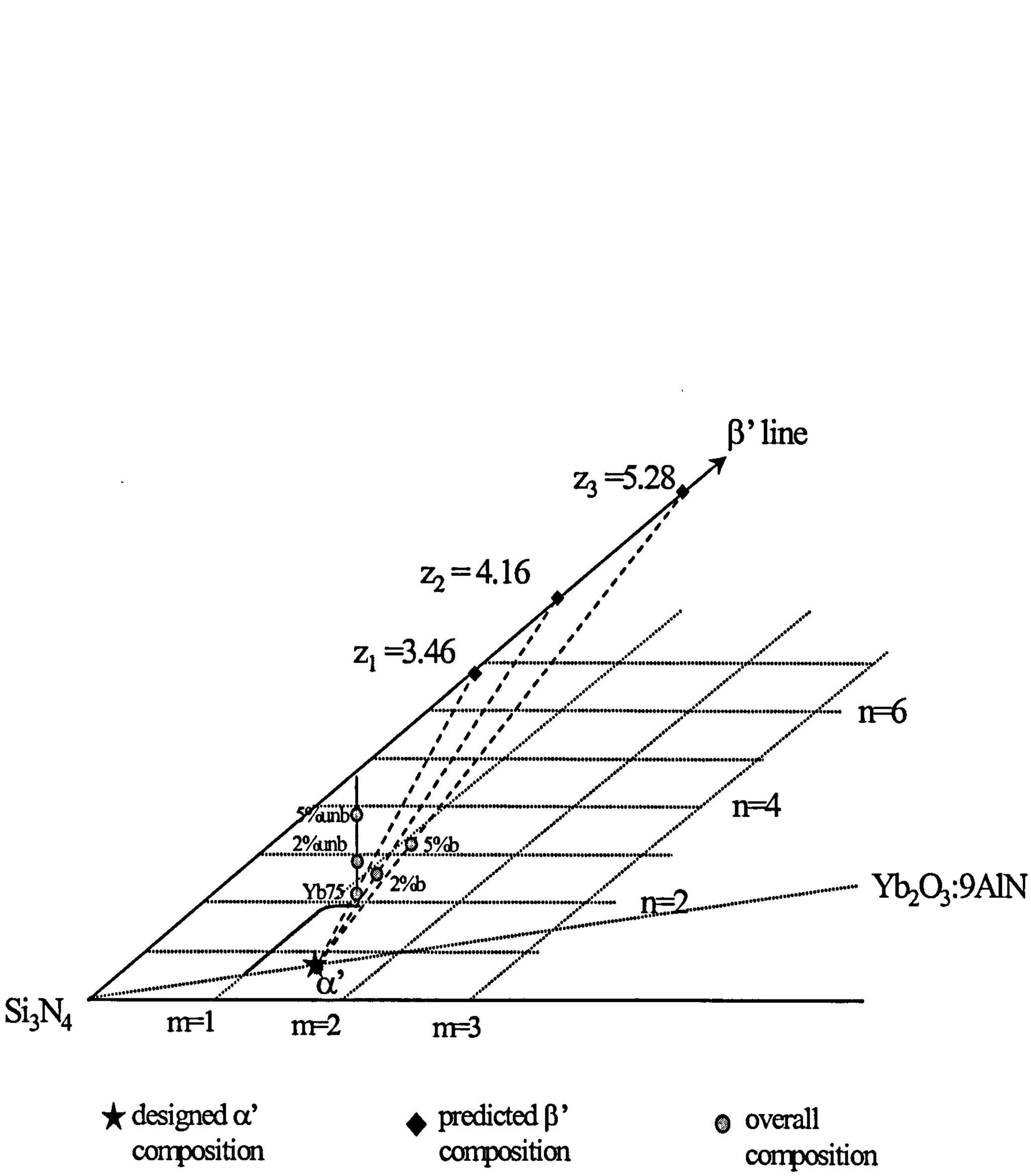

Figure 5.1. The Projection Diagram of composition Yb75B with different level of silica additions

5.1.1.1- Density Measurements

The bulk densities of as sintered materials for both balanced and unbalanced SiO_2 additions are also presented in table 5.2. The general trend observed from the results shown in the table is that the bulk density increased with an increase in the addition of balanced SiO_2 to the starting materials. The improvement in density was also obvious when compared with the density results obtained from the original compositions in chapter 4. For example the densities of compositions Yb75A and Yb75B were 2.631 and 3.362 g/cm^3 respectively. Upon the addition of excess SiO_2 (5wt%) to both compositions an improvement in densification results. The bulk densities recorded after sintering were 3.327 and 3.487 g/cm^3 for the modified compositions Yb75A5b and Yb75B5b respectively. The increase in density indicates that the addition of excess SiO_2 to the original compositions may have provided the system with a larger fraction of liquid phase at the sintering temperature which enhances the particle rearrangement and solution-reprecipitation mechanism and therefore improved the densification.

It was thought however that the addition of unbalanced SiO_2 to composition Yb75B would also significantly improve the density due to the formation of more liquid at the sintering temperature, but as can be seen from table 5.2, the unbalanced additions of silica did not appear to influence it any more than the original composition Yb75B. The possible explanation for the lower density is that the addition of silica without compensating with AlN may result in a change in the composition of the liquid phase at the sintering temperature. The liquid phase may became more viscous with addition of SiO_2 and this is supported by the EDAX analysis in section 5.1.1.3 which shows that the composition of the residual glass in materials with the unbalanced SiO_2 was slightly richer in Si compared with the balanced and the unmodified compositions.

5.1.1.2- Phase Analysis.

The XRD results presented in table 5.2 show that in all as sintered compositions the major crystalline phases were α' and β'-sialons. A small amount of 12H AlN polytypoid was also observed. It was predicted from the starting compositions that the addition of two levels of balanced SiO_2 will increase the β'-sialon content after sintering, but at the same time produce compositions which contain similar α'/β' phase ratio (75/25). The substitution level (z value) was predicted to increase with the level of SiO_2 in the starting compositions (see table 5.1). The XRD data in table 5.2 show that although the balanced silica addition enhances the formation of β'-sialon after sintering the intended α'/β' phase ratio was not obtained. Figure 5.2(a & b) shows the XRD traces of compositions Yb75B2b and Yb75B5b together with the trace of the unmodified composition Yb75B for comparison. It is clear from the figure that the peak height of the β' phase increases as the addition of silica is increased. In comparison with the original composition Yb75B the addition of 2wt% of balanced silica increases the β' sialon content after sintering from approximately 2% to 15% in composition Yb75B2b. This value significantly increased to 34% with the addition of excess 5wt% SiO_2 in composition Yb75B5b.

The unbalanced silica addition was observed to result in materials with almost similar α'/β' phase ratio to the predicted value. The β'-sialon content increased from 2% in the unmodified composition to approximately 22% with the addition of 2wt% of SiO_2, this value increased only slightly to 28% with the addition of 5wt% SiO_2 represented by composition Yb75B5un.

It is clear from the above results that the addition of silica to the starting composition, both balanced and unbalanced, had moved the unmodified composition of Yb75B away from the α'-sialon single phase region to the α'/ β' sialon region. However such a change in the phase content implies a change in the composition of the phases present. From the XRD results the lattice parameters of α'-sialon and the corresponding values of m and the z-value of β'-sialon were

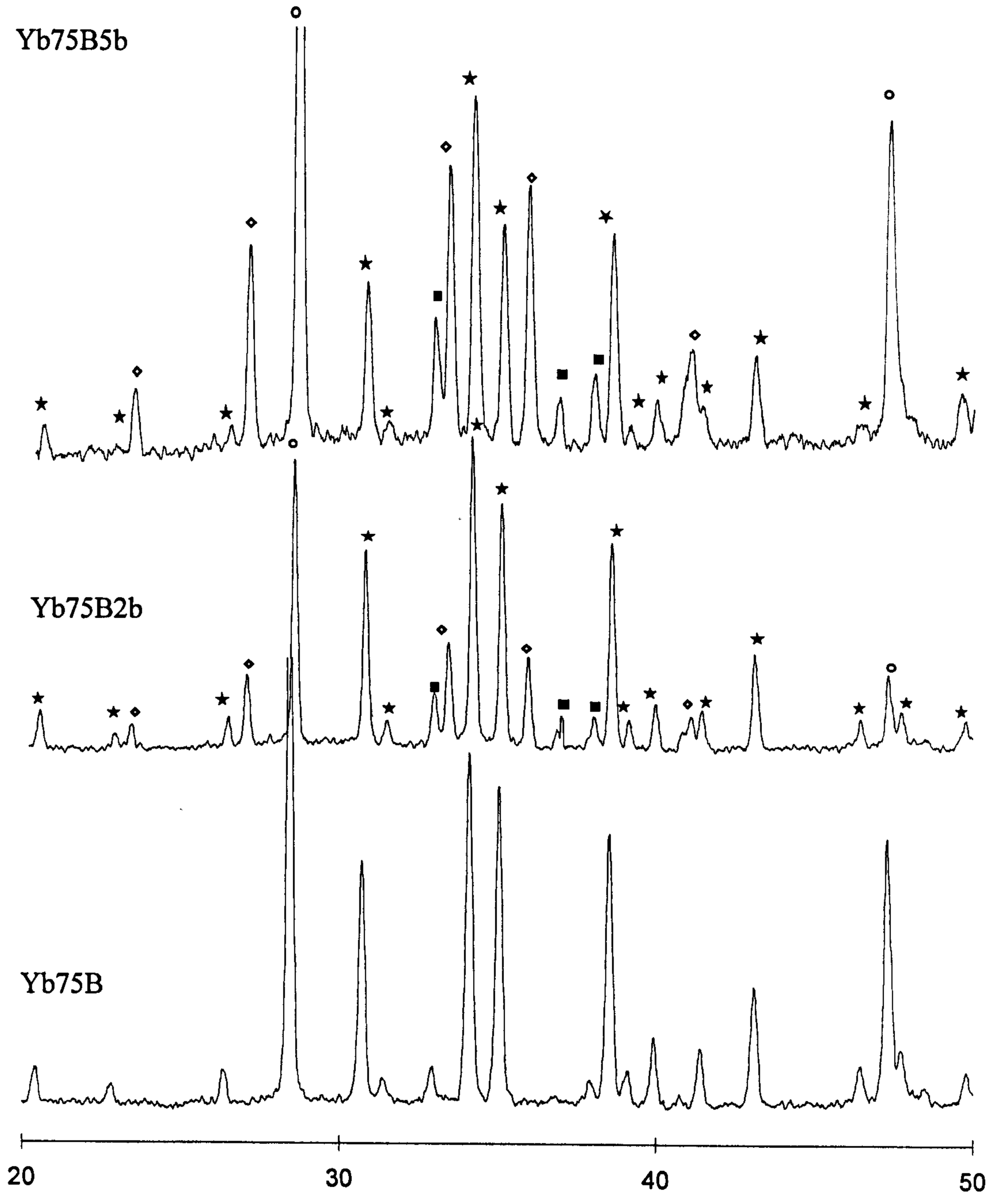

Figure 5.2 The XRD patterns for compositions Yb75B2b and Yb75B5b after pressureless sintering at 1470^{0}C for 4 hr (★) α'-Sialon (◇) β'-Sialon, (■)12H and (○) Si standard

calculated and presented in table 5.2. It is noted that the α' composition in Yb75B2b shows no significant change in the lattice parameters, indicating that the Yb^{3+} content in the α' structure is the same as in the unmodified Yb75B. This implies that composition Yb75B2b possibly contained a larger volume fraction of residual glass than Yb75B which will accommodate the excess of cation resulting from the reduction of the α' phase content. However the α' phase in composition Yb75B5b shows a larger unit cell and therefore a high m value which suggests that the α' structure in this composition incorporates the larger fraction of Yb^{3+} and has the highest substitution of Al-N bond for Si-N bonds. This material contained a lower α'/ β' phase ratio, which suggests that the reduction in the volume fraction of the α'-sialon at sintering temperature will increase the Yb^{3+} concentration in the liquid. Therefore a new partition of Yb^{3+} between the liquid and the remaining α' may take place resulting in higher m values.

The addition of 2wt% of balanced SiO_2 to composition Yb75A results in only a small increase in the β' sialon content of approximately 21% compared to 15% in the unmodified composition and this value increased to 38% as the addition of SiO_2 content increased to 5wt%. The lattice parameters of composition Yb75A2b, and therefore the m-values, are higher than that of the original composition Yb75A. This composition shows no residual phase after sintering (Figure 5.5a). As β'-sialon can not accommodate the stabilising cation in its structure therefore the excess Yb^{3+} which results from the small reduction of α' content must be incorporated in the remaining α' structure. The α' phase in composition Yb75A5b had a slightly higher m-value than the unmodified Yb75A. This implies that composition Yb75A5b contains a larger glass content.

The Al-O substitution level in β' (z-value) was observed to increase by increasing the SiO_2 addition which is in agreement with what was predicted.

composition	Density g/cm^{-3}	α'/β' wt%	m(XRD)	z(XRD)	m(TEM)	z(TEM)	Lattice-parameter
Yb75B	3.364	98/2	1.13	2.645	1.15	2.15	a_0-7.8142 c_0-5.6982
Yb75B2b	3.446	85/15	1.14	0.847	1.13	1.35	a_0-7.8141 c_0-5.6976
Yb75B5b	3.487	67/33	1.5	1.458	1.16	1.44	a_0-7.8249 c_0-5.704
Yb75B2un	3.282	78/22	1.4	1.065	1.12	1.34	-
Yb75B5un	3.350	72/28	-	-	-	-	-
Yb75A2b	3.055	79/21	1.34	1.042	-	-	a_0-7.8202 c_0-5.701
Yb75A5b	3.328	62/38	1.18	1.10	-	-	a_0-7.816 c_0-5.6996

Table 5.2 The bulk density, phase content and phase analysis of compositions prepared with SiO_2 additions

5.1.1.3- Microstructural Observation.

As observed from the XRD results in the previous section, the addition of SiO_2 to composition Yb75B changed the phase content leading to a significant increase in the fraction of β' within the materials. This in turn will affect the resulting microstructure. An examination of the microstructures of as sintered compositions in the scanning electron microscope (SEM), revealed a significant difference in the phase content and morphologies resulting from the addition of SiO_2 to the starting materials. Figure (5.3) presents SEM micrographs of the SiO_2 modified compositions Yb75B2b and Yb75B5b imaged in back scattered electron mode. The micrographs revealed the majority of the

α'-sialon grains to be equiaxed in shape similar to the original composition Yb75B (see Figure 4.10d). In the modified compositions the α'-sialon phase has a finer grained microstructure than that observed for the original composition. For example in composition Yb75B2b the larger grains ranged from approximately~1-2 μm in diameter compared to the range of ~ 3-4 μm observed in composition Yb75B.

The effect of the additions of SiO_2 on the volume fraction and morphology of the β'-sialon phase can also be clearly seen from the micrographs. Generally the addition of more SiO_2 resulted in the formation of more elongated β'-sialon grains. These grains show a broad size distribution ranging from those large, elongated grains with a high aspect ratio, which appeared in excess of 10μm in length, down to smaller sub-micron grains which were present in large amounts especially with higher SiO_2 additions. The increased aspect ratio of the β' grains may be due to the greater volume fraction of the liquid present during sintering. This suggests that the addition of SiO_2 possibly reduces the constraint on grain growth from the liquid during liquid phase sintering, resulting in longer, more acicular β morphology than that which occurred in the original composition Yb75B. However the large grains of β' were thought to form early during sintering when a large amount of liquid phase is present at sintering temperature, whereas the smaller ones form later when the transient liquid reduced (by absorbing in the sialon phases) or during cooling from sintering temperature via transformation of the unstable α' to β'. The image analysis was used to estimate the amount of the β' phase, and for Yb75B2b the result was 22% which increased further to 38% with addition of 5wt% in composition Yb75B5b.

The presence of a fraction of the 12 H AlN polytypoid was also confirmed by EDAX and can be seen as a dispersion of dark, rectangular crystals throughout the matrix, often irregularly shaped. In addition the volume fraction of the residual Yb-rich intergranular glassy phase had also changed. The addition of SiO_2 increased the residual glassy phase, estimated to be around 12% in

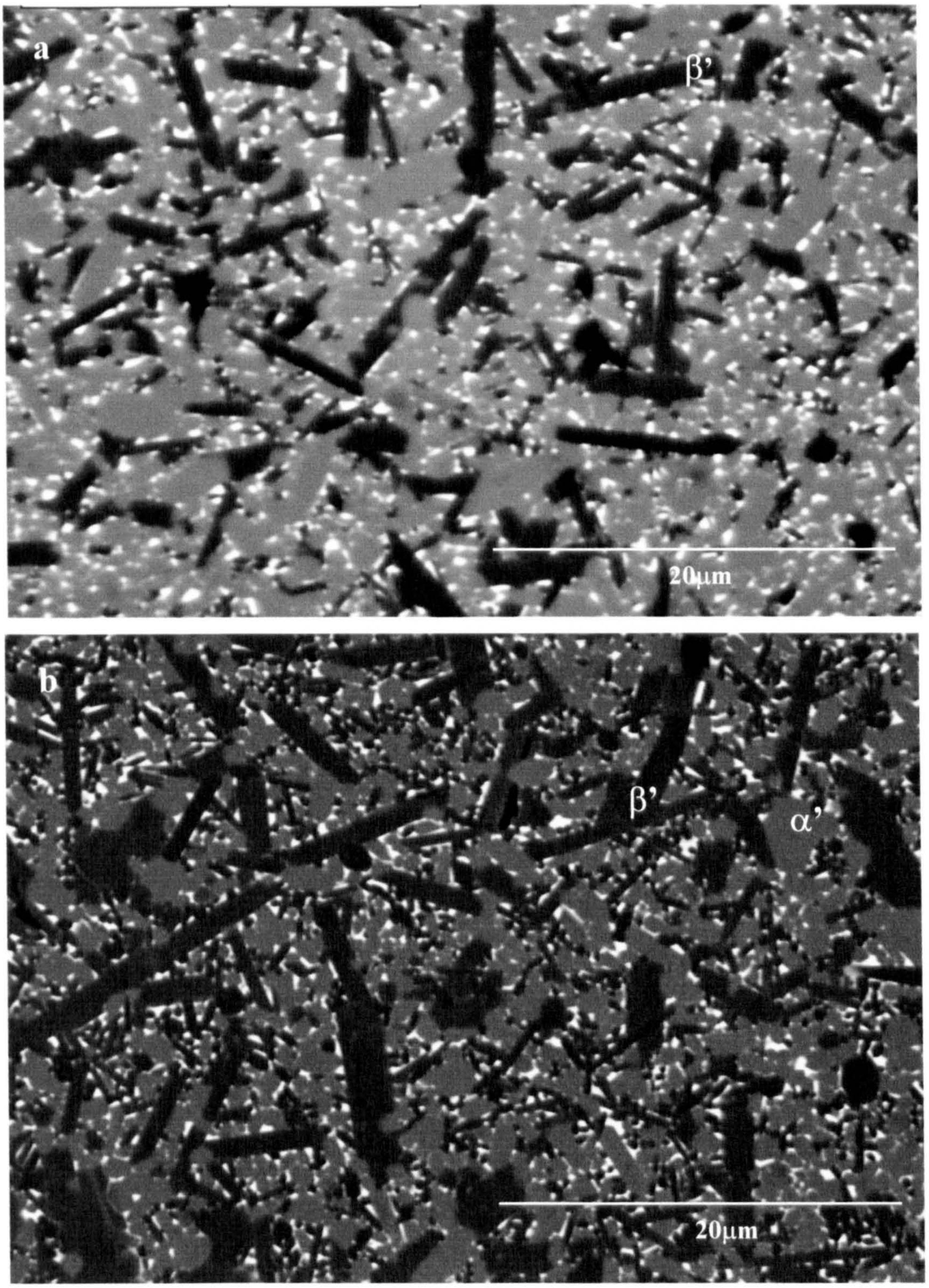

Figure 5.3. The SEM images of compositions (a) Yb75B2b and (b) Yb75B5b after sintering at 1750^0C for 4hrs

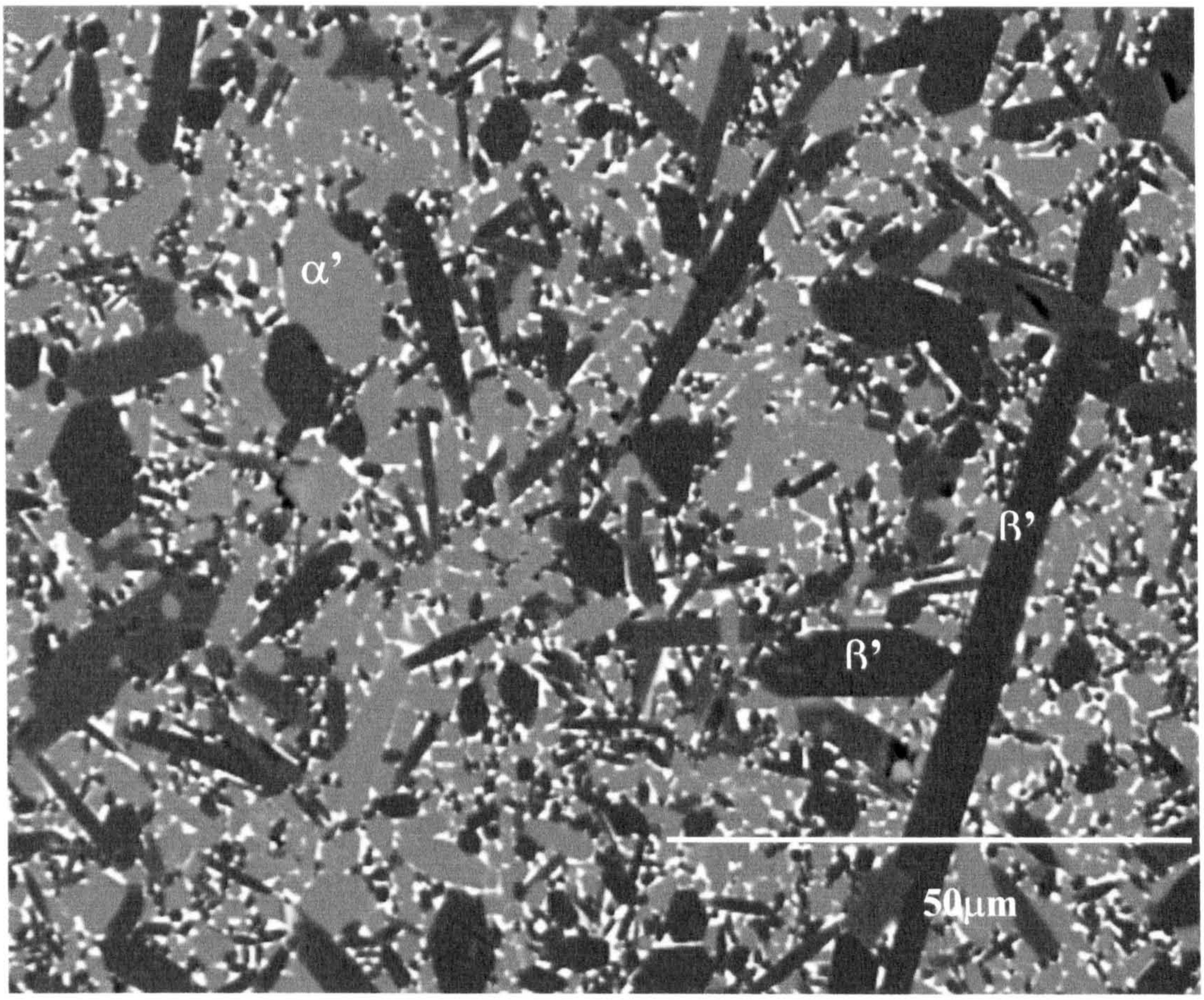

Figure 5.4. Back-scattered electron micrograph of as sintered composition Yb75B5un

composition Yb75B2b, and this value increased with the addition of more silica to 16% in composition Yb75B5b. No retained porosity was observed in this composition, which suggests that the amount of liquid phase at the sintering temperature was sufficient to complete densification.

Similar microstructural results were observed from compositions prepared with an unbalanced addition Figure 5.4. In this case β' grains were again more elongated and this was more pronounced when a higher level of SiO_2 was added. The large β' grains exhibited an average length of approximately 7μm. The decrease in the α' content in these compositions also results in an increase in the amount of the Yb-rich glass phase.

The change in the phase content that resulted from an addition of balanced SiO_2 to composition Yb75A is also reflected in the microstructure of these materials. Figure 5.5 presents SEM micrographs of Yb75A2b and Yb75A5b as can be clearly seen from the figure, the addition of 2wt% SiO_2 had increased the β' content after sintering. Although there was a slight improvement in the density measurement of this composition the material still contained a large amount of porosity. The size of pores varied from <1μm to >5μm. It is possible that the amount of the liquid phase formed at the sintering temperature is too low to allow complete densification. The most dramatic effect of the addition of SiO_2 was observed on the microstructure obtained from composition Yb75A5b (see Figure 5.5b). The structure consists of equiaxed α'-sialon grains with a small grain size and β'-sialon with different grain sizes; large grains with a high aspect ratio and grains about ten times smaller. These small grains possibly form by transforming of the unstable α' in the presence of larger liquid phase on post sinter cooling. The presence of the intergranular residual glass phase can be clearly observed which also reflects the improvement in density in this composition.

An examination of selected compositions on the TEM (table 5.2) confirmed the observations made in the SEM. The presence of a significant fraction of glassy grain boundaries was clearly observed. The EDAX analysis of the residual

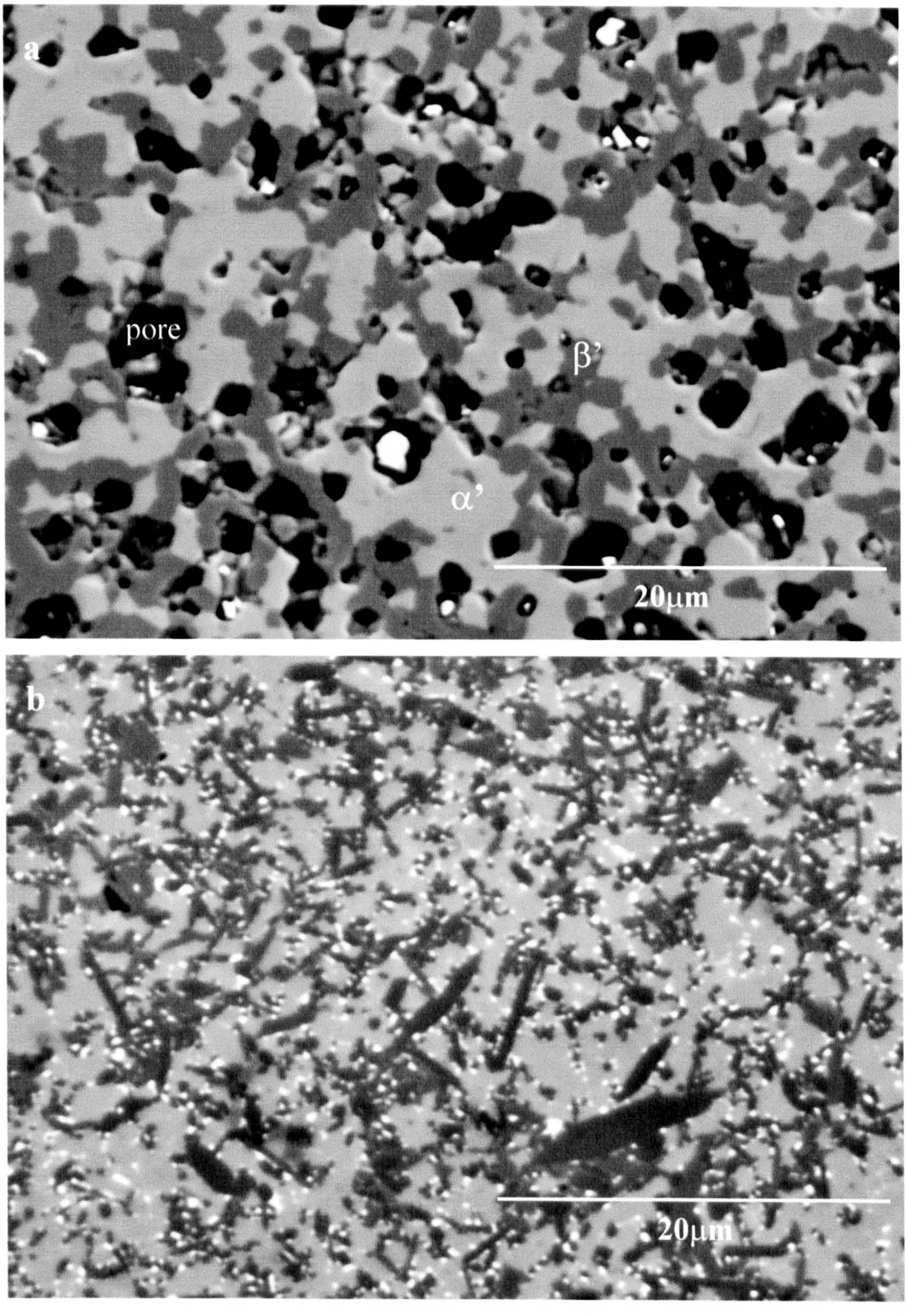

Figure 5.5.The back-scattered electron micrographs of as sintered materials (a) composition Yb75A2b and (b) composition Yb75A5b

glassy phase shows that its composition varied significantly from one pocket to another. However measurements on 10-15 points show no significant differences between the balanced composition and the unmodified one, whereas the unbalanced shows a slightly higher Si content. The compositional analysis on α'-sialon grains shows no appreciable difference and the substitution levels (m values) were almost similar (see table 5.2). Thus the solubility of Yb^{3+} in the α'-sialon structure was approximately x=0.38. This value is similar to the one obtained from the unmodified composition (see table 4.4). The Al-O substitution level (z) in the β'-sialon shows an increase by increasing the SiO_2, which is consistent with the XRD results and that predicted by the computer programme. However the actual values are lower than predicted which is possibly related to the formation of the residual glass phase and the AlN polytype which contained an appreciable Al content in its structure.

The significant variation observed in the microstructure, resulting from the addition of SiO_2 to the same initial composition fabricated under similar conditions implies that the resultant ratio between the α' and β' phase is dependent on the composition of the liquid phase that formed during sintering and prior to sialon precipitation. This opens the possibility of controlling the microstructure and the ratio of α'/β' sialon in order to optimise their mechanical properties.

5.1.2- β -Si_3N_4 Seeding Addition

As shown in the previous section and chapter 4 , the β'-sialon formed after sintering has variable grain size and morphology which will affect the fracture toughness of the prepared materials. Therefore additions of β-Si_3N_4 were made to the Yb α' material with a high α' content in an attempt to encourage β'-sialon formation during sintering and improve their morphology. Since β'-sialon has a similar crystallographic structure to β-Si_3N_4 it was thought

that a dispersion of β-Si_3N_4 seeds throughout the material would provide sites for the nucleation and subsequent growth of β'-sialon.

The addition of seeds was made by substituting the equivalent wt% of β-Si_3N_4 for α -Si_3N_4 in the starting composition so that the chemistry will remain the same. Table 5.3 shows the compositions prepared in this work. Different levels of β-Si_3N_4, such as 2%, 20%, 30% and 50% were added to the starting powders.

Composition	α-Si_3N_4	β-Si_3N_4	AlN	Yb-glass	Density g/cm^3	α'/β' wt%
Yb75B	61.1212	-	21.017	17.8618	3.36	98/2
D2	59.9	1.22	21.02	17.86	3.29	95/5
D20	48.90	12.22	21.02	17.86	3.32	93/7
D30	42.78	18.34	21.02	17.86	3.35	95/5
D50	30.56	30.56	21.02	17.86	3.17	99/1

Table 5.3 The starting compositions, density and the α'/β' ratio of Yb-sialon materials with β-Si_3N_4 seeding.

Density and XRD results from the as sintered seeded materials, are given in table 5.3. As can be seen the density results obtained from the seeded materials were lower than the unseeded one. With the addition of 2% of β Si_3N_4 seeds the measured density decreased slightly to 3.29 g/cm^3 and decreased further to 3.17 g/cm^3 with the addition of 50% of β-Si_3N_4.

From the XRD results it is noted that the addition of β-Si_3N_4 seeds had a small effect on the α'/β' phase ratio relative to the unseeded composition. Figure (5.6) illustrates the XRD traces of the seeded materials. The addition of 2% and 20% of β-Si_3N_4 seeds gave α'/β' phase ratio of about 95/5 and 93/7

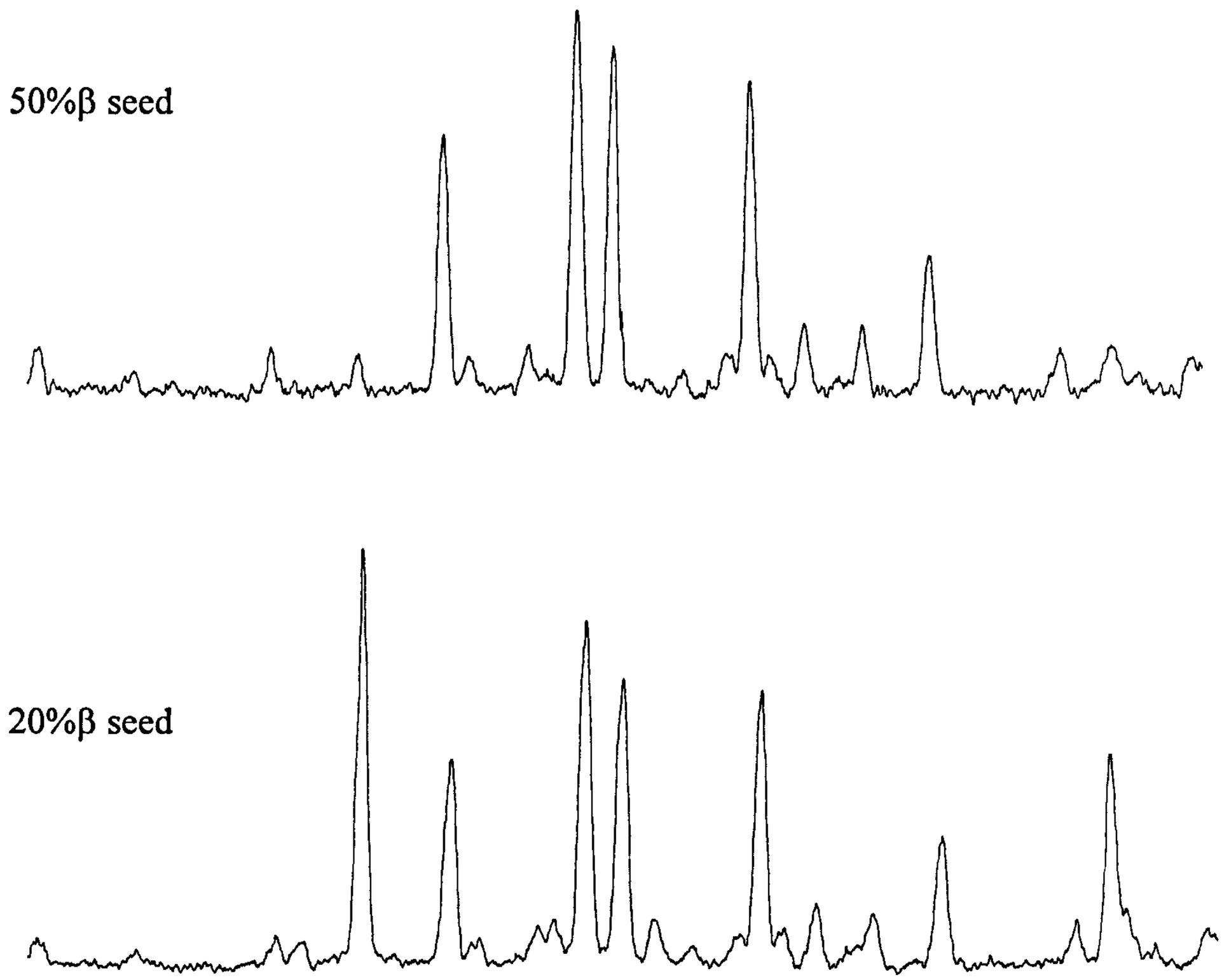

Figure 5.6. The XRD traces of as sintered selected seeded compositions

respectively. However by increasing the addition of β-Si_3N_4 seeds to 30% the α'/β' ratio started to increase again and the estimated α'/β' ratio is 95/5 which increased further to 99/1 with the addition of 50% of β-Si_3N_4. Therefore, from the presented results, it is clear that the addition of β-Si_3N_4 seeds to the Yb α'-sialon system has a small effect on the β'-Sialon content. It has been suggested previously by Cao and Metselaar (1990) that using β-Si_3N_4 powder as a starting material does not affect the formation of α'-sialon. More recently Chen and Rosenflanz (1997) reported that by using a high proportion of β-Si_3N_4 as the starting materials, a single Yb α'-sialon material with an elongated grain can be produced. These authors have suggested that although the α → α' transformation proceeds faster than β → α', in both cases the transformation proceeds at higher rate in Yb system than the other rare earth α'-sialon systems (Rosenflanz and Chen 1999a).

However similar negligible effects on β'-sialon were also observed in the Gd-sialon materials, whereas the addition of a small amount of β–Si_3N_4 seeds (2 wt%) to the Nd sialon materials significantly enhanced the β' content of the as sintered material (Jumali 1999). The different effect of β-Si_3N_4 seeds on the formation of the β'-sialon phase in different rare-earth systems is related to their phase stability which is related to the ionic size of the stabilising cations. The α' stability region of Yb-α'-sialon system is much larger than that of Nd-α' at the same temperature. Thus Yb α'-sialon is more stable and the driving force for α/β → α' transformation is higher in agreement with Rosenflanz and Chen (1999 b) who revealed that the α' formation is the fastest for Yb cation (heavier) and the lowest for Nd cation (lighter).

Figure 5.7 presents the SEM micrographs of composition Yb75B sialon materials to which different levels of β-Si_3N_4 had been added as a seeding agent. As indicated by the micrographs, the addition of 2wt% and 20wt% β-Si_3N_4 seeding to composition Yb75B during processing had no significant effect on the α'/β'

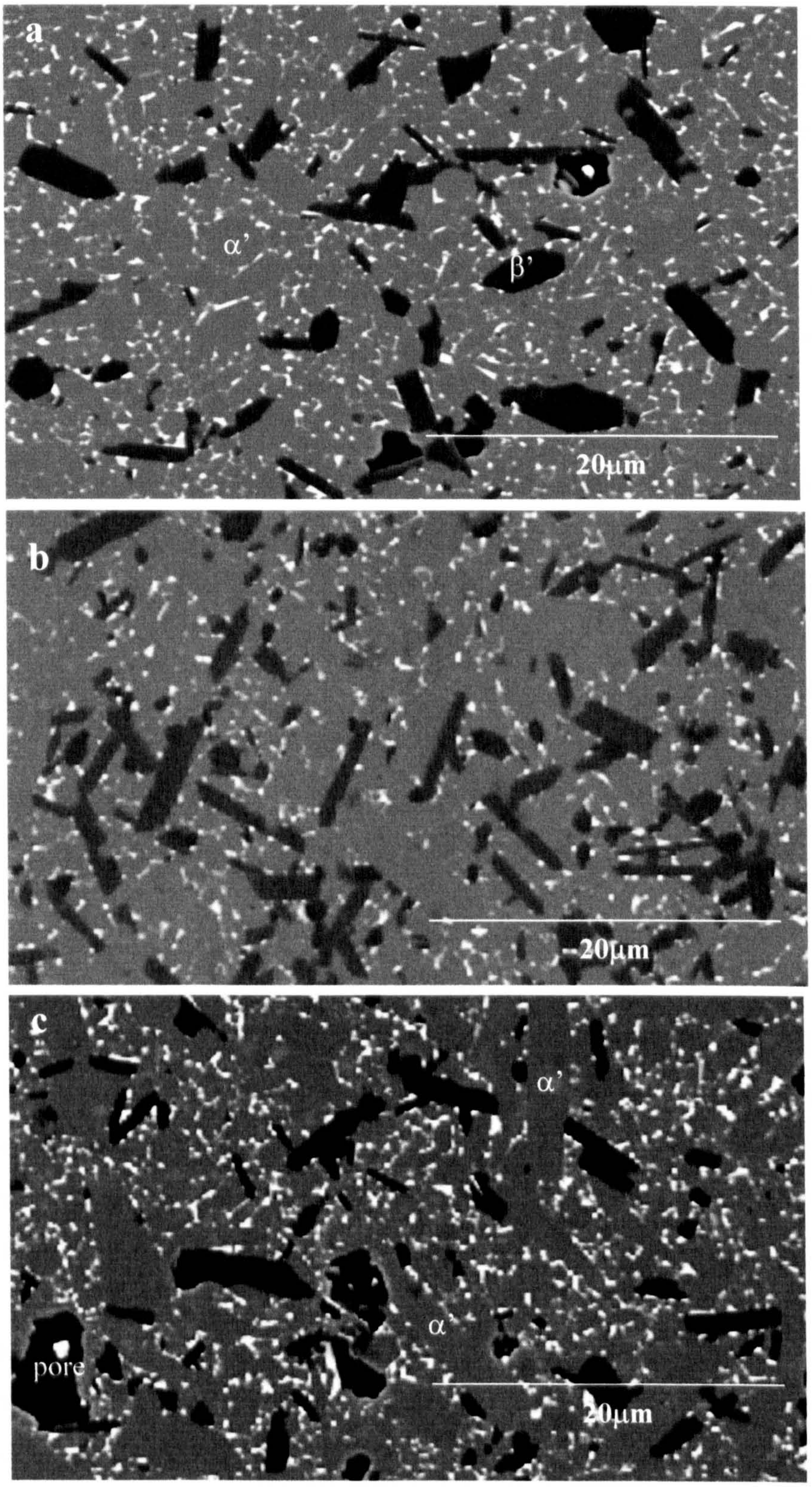

Figure 5.7. The back-scattered electron images of seeded compositions after sintering at 1750^0C for 4h (a) 2% β seed (b) 20% β seed and (c) 50% β seed

phase ratio. The microstructural morphology changed only slightly, unlike Chen data, the grain size and shape of α' remained essentially unchanged, whereas β' grains became more uniform and sometimes have an elongated shape. However with the addition of more seeds (50 wt% β-Si_3N_4 composition D50), no significant increase in the β' content relative to the as sintered unmodified material was observed. The α' grains became more elongated where as the dark phase which is mostly 12H appears more coarser sometimes with an irregular shape and more retained porosity was observed in this composition compared with the other which contributed to the lower measured density.

The image analysis revealed a small increase in the volume fraction of the Yb rich residual phase and this was observed in all compositions. This occurred as a result of the small reduction of the α' content. The volume fraction of the residual glass phase in seeded composition D20 was estimated to be around 7% compared with 5% in the unmodified composition. The increasing of the liquid phases results in the formation of more elongated α' grain as observed in composition D50.

5.1.3- Combined SiO_2 and β-Si_3N_4 Seeding Addition

Additions of SiO_2 and β-Si_3N_4 seeds have been made at the same time to composition of Yb75B to examine their effect on β' formation and morphology. 2wt% of SiO_2 was added to composition Yb75B in which approximately 20wt% of β-Si_3N_4 was substituted for an equivalent of α-Si_3N_4 to form composition S2D20.

After sintering composition S2D20 showed no improvement in density compared to the unmodified composition Yb75B and the measured density was 3.32 g/cm^3. The XRD analysis revealed that the α' and β'-sialons are the major crystalline phases present in this composition, with a trace of 12H AlN polytypoid. The phase content measurement showed a decrease in the α'/ β' ratio

from 98/2 in the unmodified composition to 80/20, similar to the composition with 2wt% SiO_2 alone.

The SEM observation revealed that the microstructure of this composition is not homogenous, giving some regions which are α'-sialon rich or contain small amount of β'-grains, separated by adjacent regions which are β'-sialon rich. This is believed to occur as a result of poor mixing during powder preparation. The SEM micrograph of composition 20D2S (Figure 5.8) shows that the microstructure is coarser than composition Yb75B2un and consists of an equiaxed α'-sialon with some large grains about 9μm in length and approximately 2μm diameter. The β'-sialon shows a coarser grain morphology, a number of large prismatic β' crystals with lower aspect ratio, and small grains with an equiaxed shape were also seen. The large grains possibly nucleate on the β-Si_3N_4 seeds at the early stage of sintering when a large amount of liquid is present; whereas the smaller ones formed later when the transient liquid reduced (consumed by the sialon phase) or from α'–> β' transformation during cooling from sintering temperature. The image analysis of the microstructure revealed that the glass phase in this material occupies approximately 12%. The microstructure also contains some retained porosity.

The present result shows that although the addition of β-Si_3N_4 seeds to the composition containing a SiO_2 addition did not change the α'/β' phase ratio, the presence of these seeds significantly enhanced the grain growth of the β' and α' sialon. However the differences in microstructures between the compositions suggests that there is scope for altering the compositions to produce dense α'/β' sialons in which grain size and morphology and the amount of residual glassy phase, may be tailored to optimise their mechanical properties.

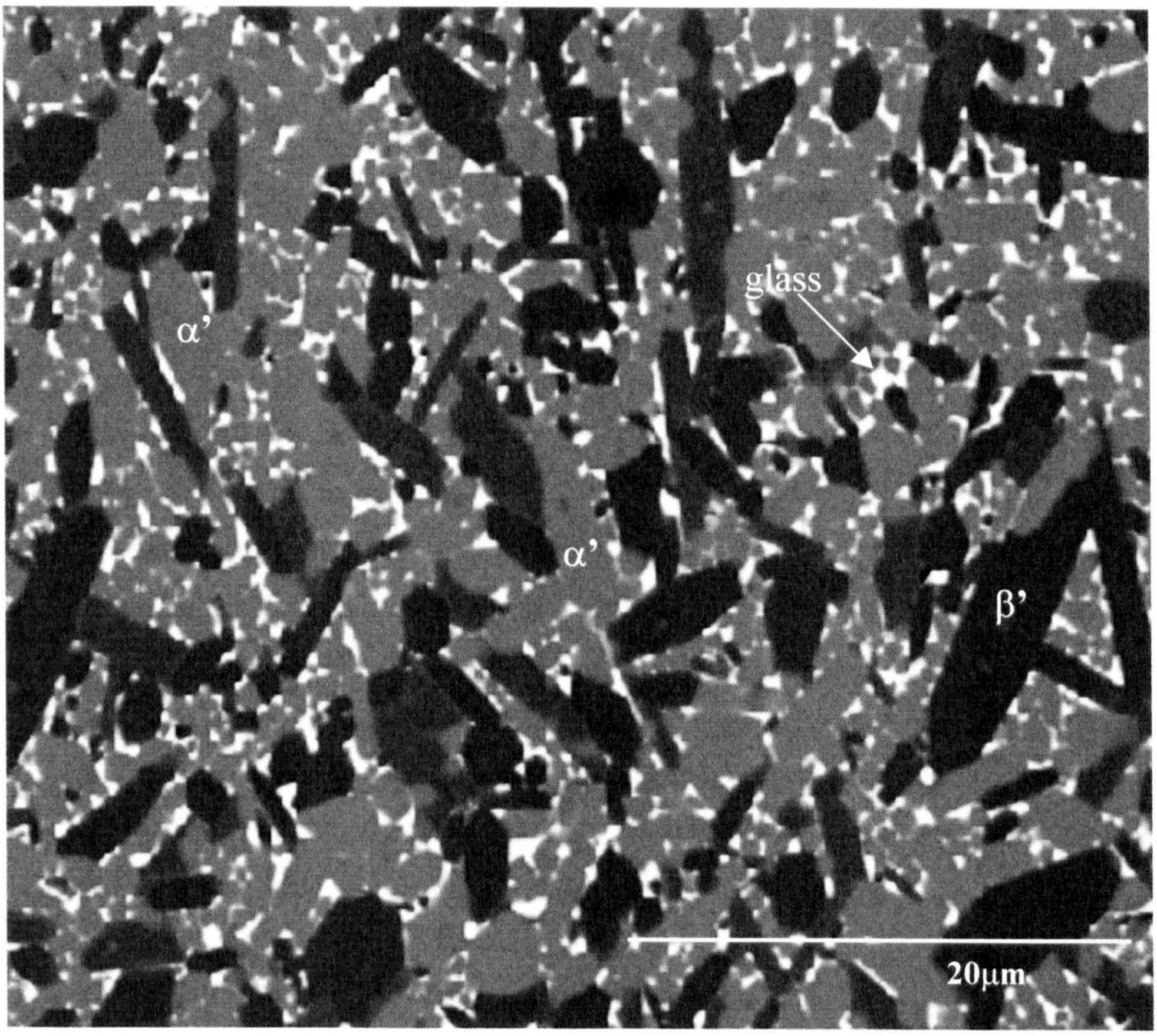

Figure 5.8. Back-scattered electron micrograph of as sintered composition 20D2S

5.2- Post Sintering Heat Treatment and Devitrification Products.

Recent studies have revealed that the composition and microstructure of some rare earth α' and α'/β' sialon ceramics are greatly affected by post sintering heat treatments and that α'-sialon may only be stable at high temperatures and undergoes a transformation to β' and other crystalline phases in temperature ranges of 1100 to 1550^{0}C (Thompson and Mandal 1997). However, although this transformation provides a convenient mechanism for controlling the microstructure and therefore the mechanical properties of the final materials, the occurrence of the α'/β' transformation indicates the instability of the α'-sialon phase and thus casts some doubt on the potential of these materials for high temperature structural applications.

Although it would be desirable to produce a single phase sialon or a mixed α'/β'-sialon material, in practice, however, it is almost inevitable that some secondary glassy phase will remain after liquid phase sintering. The softening of this glass phase above the glass transition temperature (Tg), ranging between 900-1000C, will degrade the high temperature properties. Therefore it is always desirable to devitrify the residual glass into refractory crystalline phases. So far YAG ($Y_3Al_5O_{12}$) has been widely accepted as the best intergranular phase for commercial β'-sialon ceramics. Therefore it is important to understand the factors which may affect the thermal stability of the α'/ β'-sialon materials.

This section will describe the thermal and time-dependent stability of the α'-phase in ytterbium doped α'- sialon ceramics. The eutectic temperature of Yb Si Al O N system is > 1350^{0}C. Therefore heat treatment was carried out above and below this temperature. Selected materials previously sintered at 1750^{0}C have been post-heat treated at different temperatures and for different periods of time in order to investigate both the different phase transformation behaviour and the effect of heat treatment on the devitrification of the grain boundary phase.

5.2.1- Heat Treatment at (1200-1600^{0}C)

The post sintering heat treatments of selected compositions from series B Yb50B and Yb75B, and compositions with the addition of silica Yb75Bb2 and Yb75B5b, were conducted at temperatures ranging from 1200-1600^{0}C for a duration of 24 hours. The α'/β' phase ratio after heat treatment is presented in table 5.4

The general trend observed from the XRD results of the post sintering heat treatment of all compositions was the crystallisation of the residual inter-granular glass phase in the form of Yb-garnet phase ($Yb_3Al_5O_{12}$). This phase (YbAG) was the only product of crystallisation and was observed to be stable in the range of temperatures from 1200^0 to 1600^{0}C. The YbAG phase was also detected in composition Yb75B, sintered at a temperature of 1600^{0}C and cooled in a conventional way (see section 4.4.2.1), which indicates that it is a stable phase at this temperature and was not formed during cooling. The amount of the Yb-garnet phase seems to increase only slightly during low temperature heat treatments of up to 1450^{0}C.

The XRD analysis of composition Yb50B heat treated between 1300-1600^{0}C for 24 hours, shows that crystallisation of the residual glassy phase was accompanied by a slight reduction in the α'/β' phase ratio and the α' content decreased after heat treatment at 1300^{0}C to approximately 60%. Further heat treatment to 1500^{0}C shows no distinct effect on the α'/β' phase ratio.

Composition Yb75B shows a great stability over a range of temperatures from 1200-1600^{0}C. Figure 5.9, shows the XRD traces of the materials after 24hr heat treatment at temperatures of 1300, 1450 and 1600^{0}C. As can be seen no significant changes in the α'/β' phase ratio were detected by XRD analysis. The 24 hours heat treatment at various temperatures showed that the Yb α'-sialon material has a good thermal stability when compared with other α' systems. For example, Mandal et al (1993) reported that the Sm and Nd sialon materials

PAGE NUMBERING AS ORIGINAL

showed a steady α' to β' transformation when heat treated between 1000^{0}C and 1500^{0}C for 24 hours.

H.T temp/time	Composition Yb50B	Composition Yb75B	Composition Yb75B2b	Composition Yb75B5b
Before H.T	64/36	98/2	85/15	66/34
1300^{0}C(24hr)	60/40	98/2		-
1400^{0}C(24hr)	-	98/2		-
1450^{0}C(24hr)	59/41	94/6	72/28	49/51
1450^{0}C(72hr)	57/43	93/7		-
1450^{0}C(168hr)	47/53	93/7		52/48
1500^{0}C(24hr)	58/42	97/3		66/34
1600^{0}C(24hr)	-	97/3		-

Table 5.4 The α'/β' phase ratio for selected Yb α'-sialon compositions after heat treatment at different temperatures and different durations of time.

5.2.2- Heat Treatment at 1450^{0}C for (24-72-168hrs)

In order to study the effect of prolonged heat treatment on the stability of Yb α'-sialon in more detail isothermal heat treatment was carried out at 1450^{0}C, for an extended period of time of up to 168hr (one week). This temperature has been reported in many studies as the most critical temperature for phase transformation in many of the rare-earth α'-sialon systems. The XRD results of the extended heat treatment on the studied compositions are also included in table 5.4. The results show that the extended heat treatment did not change the grain boundary phase and Yb-garnet was observed as the only crystallisation product of the residual glass phase.

The 24 hours heat treatment of composition Yb50B at 1450^{0}C resulted in a slight decrease of the α'/β' phase ratio from 64/36 in the as sintered

composition to 59/41. Further heat treatment of this composition for an extended duration of up to 168hr results in a continued decrease of the α' content and a simultaneous increase in the β' content (see table 5.4). The XRD results of the phase content of composition Yb50B heat treated at various periods of time are shown in Figure 5.10.

The XRD results from the heat treated composition Yb75B which contained an α'-sialon phase (nearly 100% α'), with approximately 5% volume fraction of the intergranular residual phase, revealed that after 24hours heat treatment at 1450^{0}C, only a small decrease in the α' phase was observed. Further heat treatment at 72 hours results in only a minor decrease in the α' content which indicated a limited α' to β' transformation. However by increasing the heat treatment duration to 168hr the XRD analysis results in no change in the α'/β' ratio which indicates that the system may be approaching an equilibrium state. Figure 5.11 shows the XRD patterns of composition Yb75B after heat treatment at 1450^{0}C for various durations.

The extended heat treatment shows the stability of α'-sialon in the Yb system and this behaviour is shown graphically in Figure 5.12. As can be seen from the figure the α' phase in composition Yb75B showed great stability and no significant change in the α'/β' ratio was detected from the XRD analysis. This, however, is in contrast to the light rare earth (Sm and Nd) α'/β'-sialon materials which showed a continuous α'–>β' transformation when heat treated at 1450^{0}C for an extended period of time.

The significant effect of the β' phase as nuclei and the effect of the amount of glass phase on the α' to β' transformation can be clearly seen from compositions Yb75B2b and Yb75B5b. These composition initially contained a

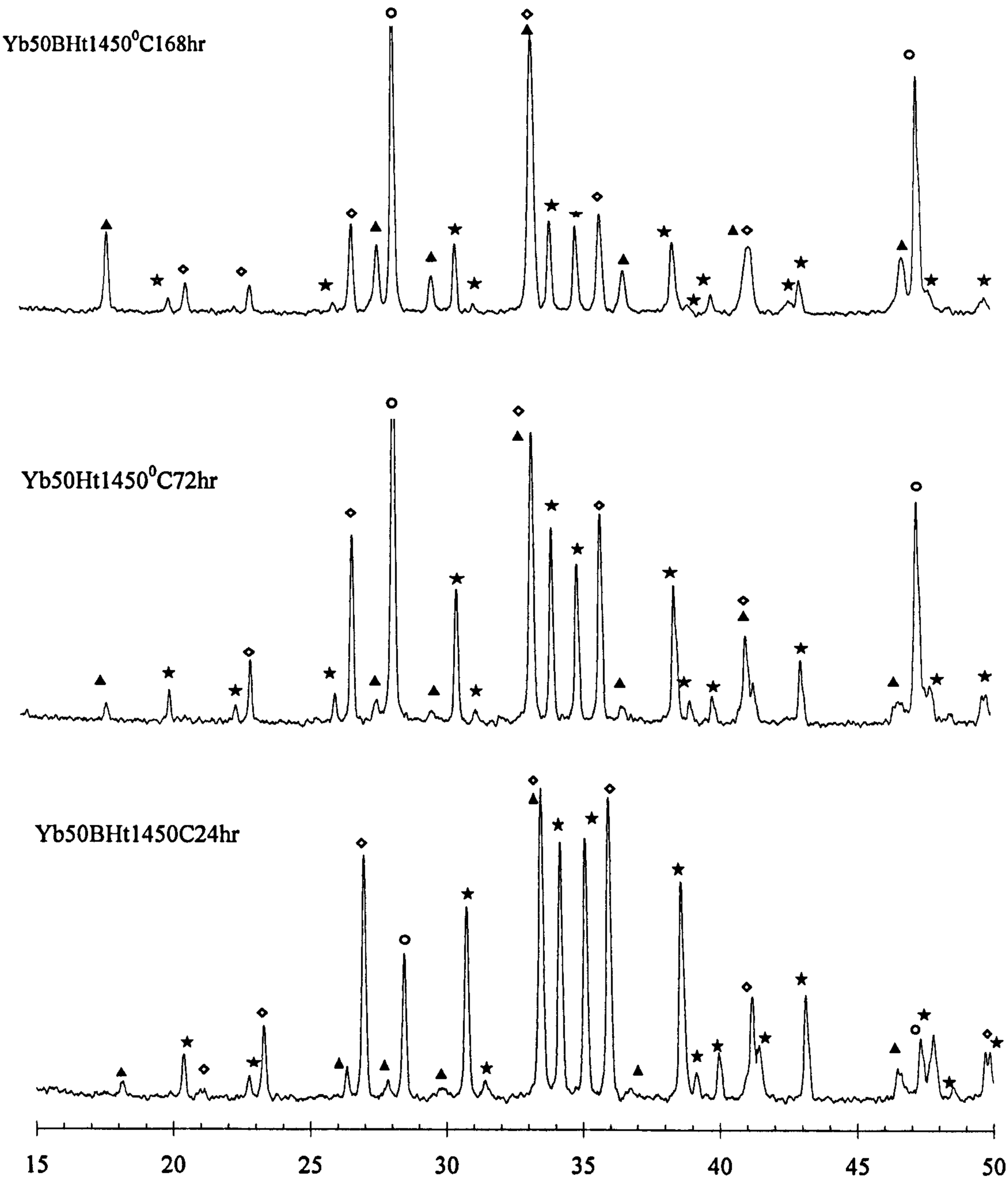

Figure 5.10 The XRD traces of composition Yb50B heat treated at 1450^{0}C for various period of time ◇ β'-sialon, ★ α'-sialon, ▲ YbAG phase and ○ (Si) silicon standard

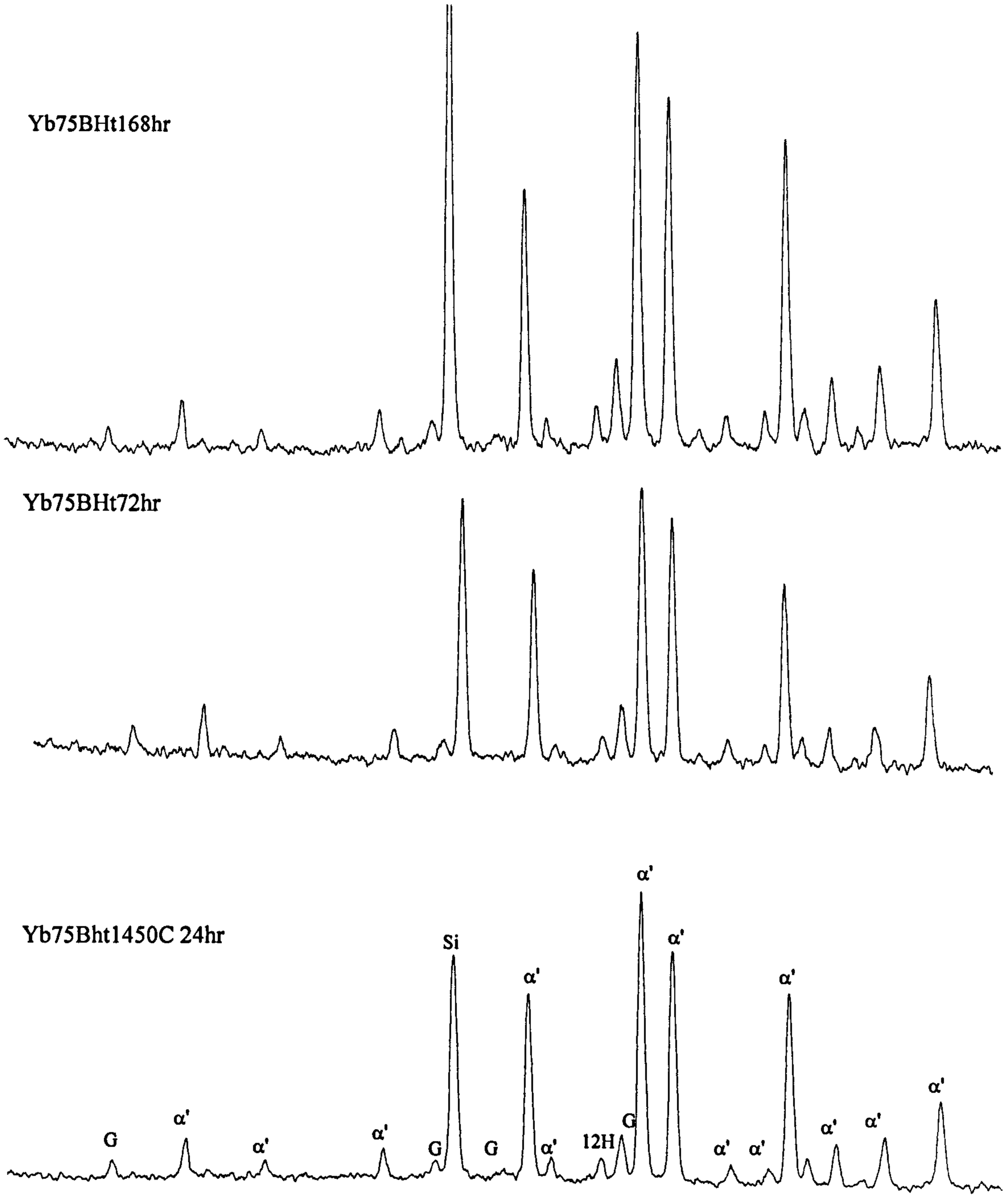

Figure 5.11 The XRD traces of composition Yb75B heat treated at 1450^0C for various period of time, α'= α'-sialon, 12H= AlN polytype and G = garnet phase (YbAG)

high α'/β' ratio of 85/15 and 66/34 see table 5.4 and approximately 12% and 16% residual glass phase respectively. The XRD analysis revealed that after 24 hours at 1450^{0}C, there was a marked decrease in the α' peak intensity and an increase in the β' content, which indicates that the α' to β' phase transformation had taken place at this temperature and the α' phase content decreased from 85% to 72% and from 66% to 49% in composition Yb75B2b and Yb75B5b respectively.

However it was noticed that the prolonged heat treatment of all compositions resulted in surface oxidation. This may affect the overall composition of the materials and therefore increase the fraction of the β' phase.

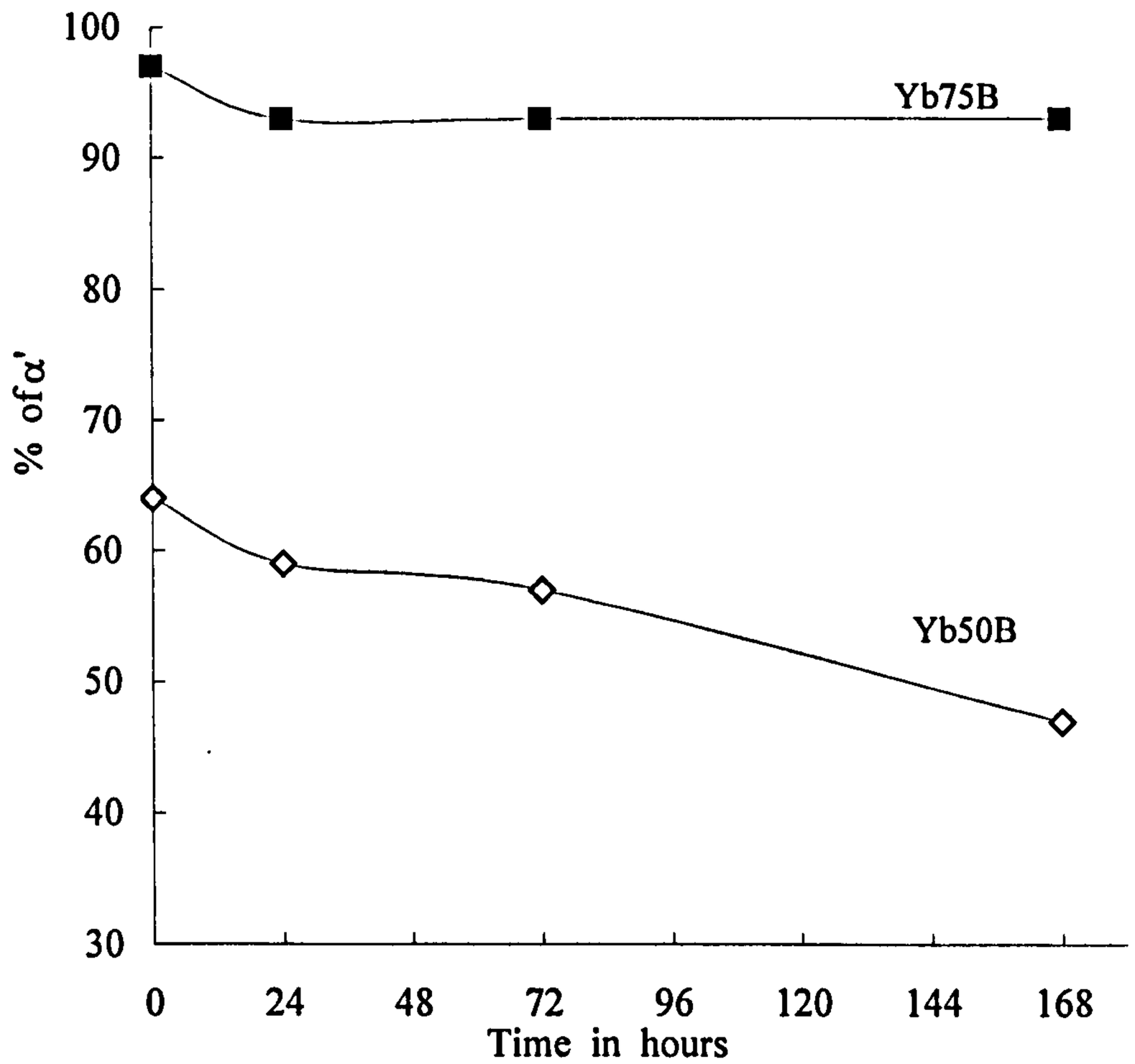

Figure 5.12 The relationship between the α' content and the heat treatment time

5.2.3- Microstructural Observation.

The microstructures of as heat treated compositions were studied by SEM and TEM. Figure (5.13a) illustrates back-scattered electron micrograph of composition Yb75B heat treated for 24 hours at 1450^{0}C. By comparison with Figure 4.10c, it can be seen from the bulk microstructure that the significant change which occurs on post sintering heat treatment was the crystallisation of the residual intergranular glass. There was no distinct change in the α'/β' phase ratio or their grain morphology compared to the as sintered composition. It is also clear from the micrographs that most of the third phase is fine in morphology and is homogeneously distributed at the multi grain junction in the form of nearly spherical shapes and all are of very similar size <1μm with some large ones of around 2μm randomly scattered throughout the structure. An EDAX point analysis in SEM on the residual intergranular phase was not attempted due to the fine structure.

However by increasing the heat treatment up to 1600^{0}C, the microstructure changed very much in the morphology of the α', β' and the grain boundary phase, as shown in Figure (5.14), a back scattered image of composition Yb75B heat treated at 1600^{0}C for 24hrs. The YbAG crystalline phase forms a large white agglomerate larger than the one observed at 1450^{0}C. This was accompanied by a coarsening of the microstructure suggesting that a considerable intergranular migration may have taken place. It is possible that the YbAG at this temperature is partially liquid thus promoting the grain boundary migration.

The effect of prolonged heat treatment of composition Yb75B at temperature 1450^{0}C is shown in Figure 5.13. As can be seen from the micrograph there was no significant change in the α'/β' phase ratio even after 72 hours. It seems that after 72 hour the structure became more coarse and the YbAG forms slightly larger isolated grains (similar microstructure was also obtained from materials heat treated for 168 hours). The porosity level is also increased in some areas.

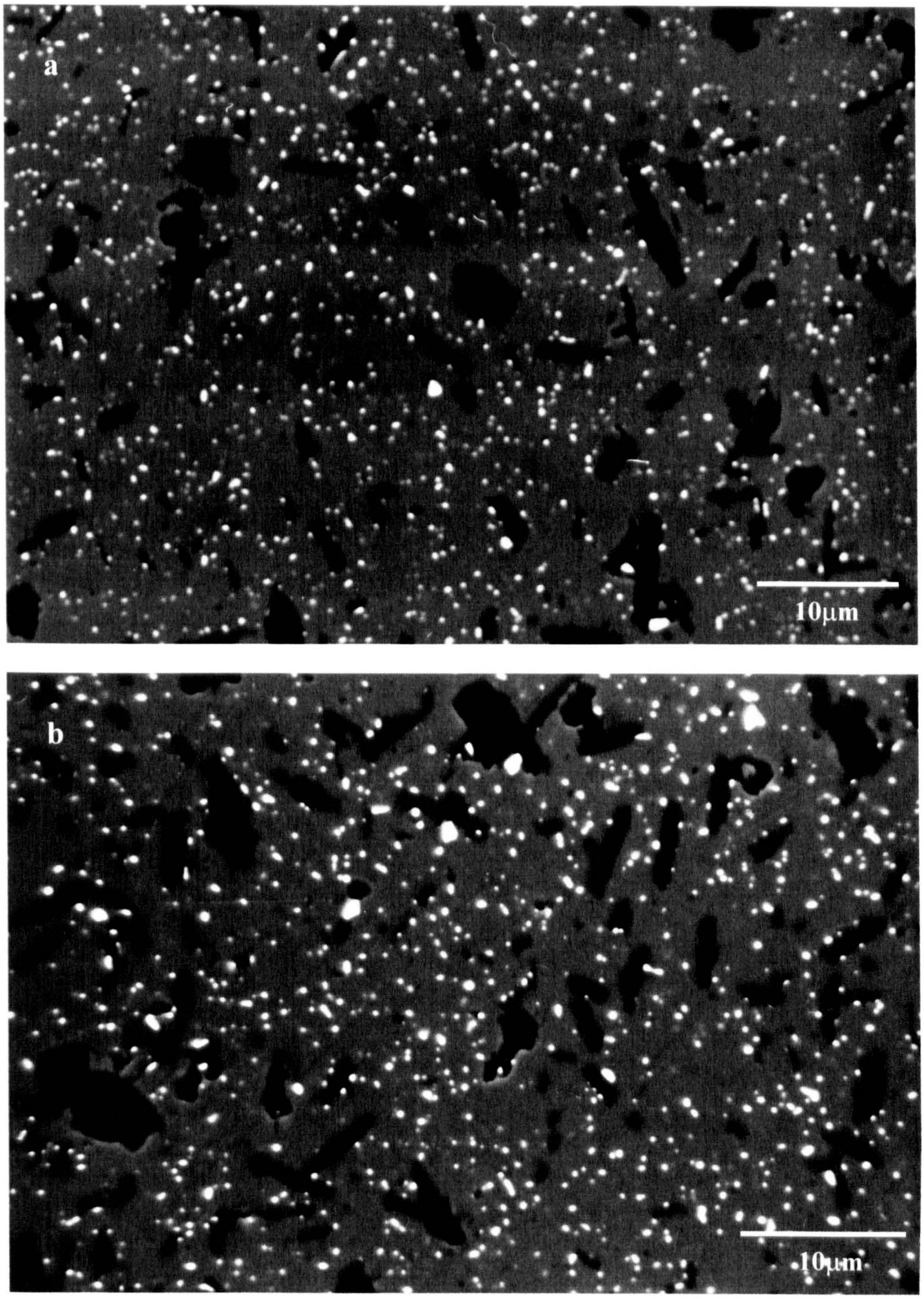

Figure 5.13. The SEM micrographs of composition Yb75B heat treated at 1450^0C for (a) 24hrs and (b) 72hr

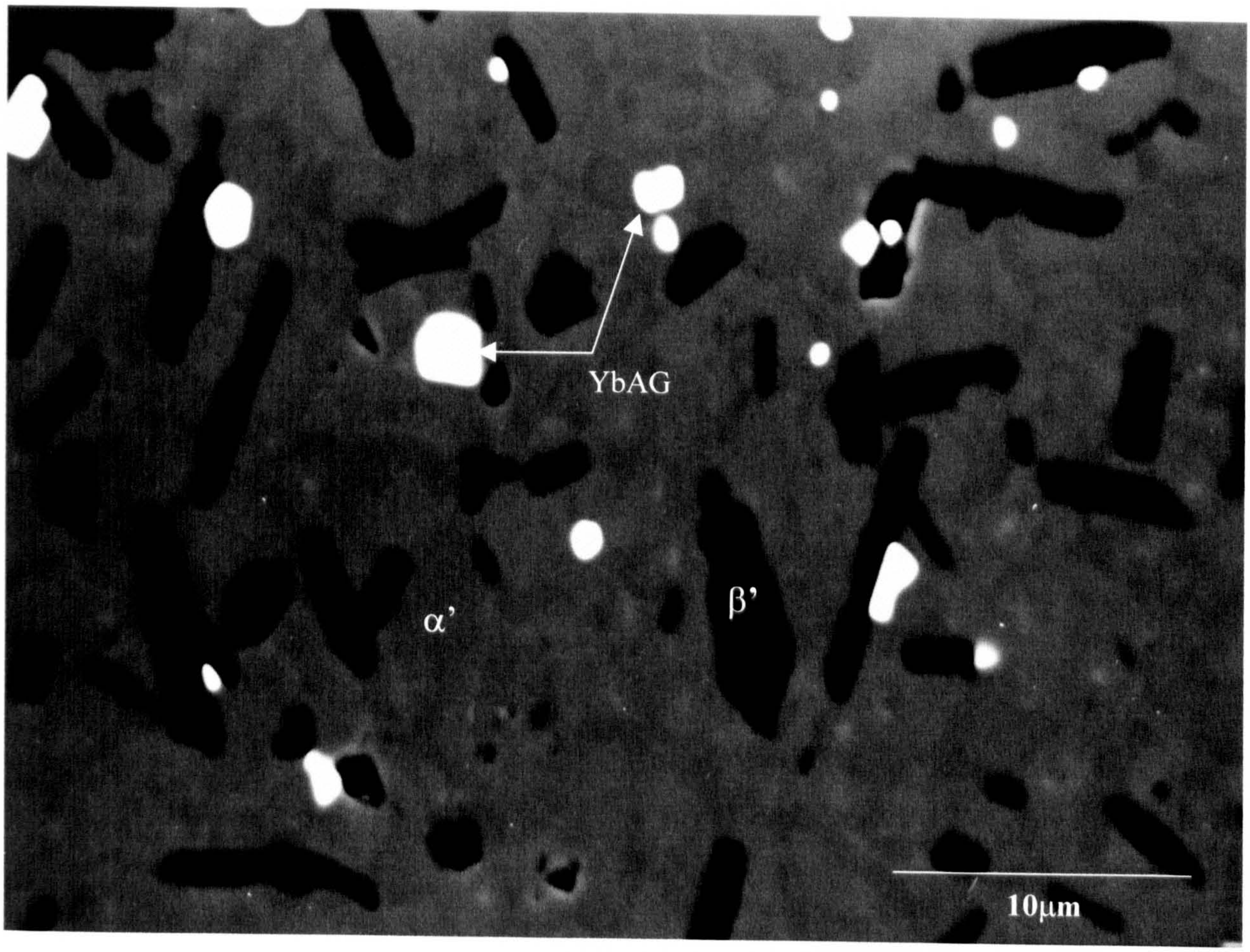

Figure 5.14. SEM image of composition Yb75B after heat treatment at 1600^0C for 24hr

A more detailed microstructure study was carried out using TEM. The observations made on all compositions revealed that the glass phase at the multiple grain junctions of the as sintered samples was crystallised after heat treatment at 1450^{0}C for 24 hours. A typical bright field image of composition Yb75B is shown in Figure (5.15 a). An EDAX analysis Figure (5.15 b) and an electron diffraction Figure (5.15 c) confirmed $Yb_3Al_5O_{12}$ as the intergranular crystalline phase, which is consistent with the XRD. As shown in section 4.4.2.2, the EDAX analysis indicated that the glass phase in the as sintered state contains the elements Yb, Si, Al, O and N with a significant content of both Al and Yb. However when the materials are heat treated at 1450^{0}C the $Yb_3A_{l5}O_{12}$ phase formed as a result of crystallisation process. This phase consumed most of the Ytterbium, aluminium and Oxygen in the glass leaving a phase rich in Si and N. Extensive TEM analysis cannot detect any glassy phase after crystallisation, and there is no new crystalline phase formed other than YbAG, as confirmed from XRD results. Therefore the anticipated Si and N rich phase formed as a result of crystallisation of the glass must be α' and/ or β'. It is known that Si and N in a glassy phase can partition in the existing sialon grains during grain boundary crystallisation (Lewis 1993).

The YbAG phase has an isolated particulate morphology (Figure 5.15a), in contrast to the semi continuous grain boundary glass network associated principally with the major α'-sialon phase. The particulate morphology is promoted by the ability to achieve almost complete crystallisation by the substitution of non-stoichiometric elements with α' and β'-sialons, as discussed in earlier research on α'/β'/YAG sialon (Jasper and Lewis 1992). The resulting interphase boundaries may approach nearly pure solid/solid contacts with little anisotropy in boundary energy (unlike the initial crystal/ liquid interfaces).

An EDAX compositional analysis of the three compositions Yb75B, Yb50B and Yb75B5b, heat treated at 1450^{0}C for 24 hours revealed no significant changes in m values and therefore the substitution levels (x) observed are all comparable with the as sintered values see table 5.5. However an EDAX of extended heat treatment of composition Yb75B up to 72hr showed a further

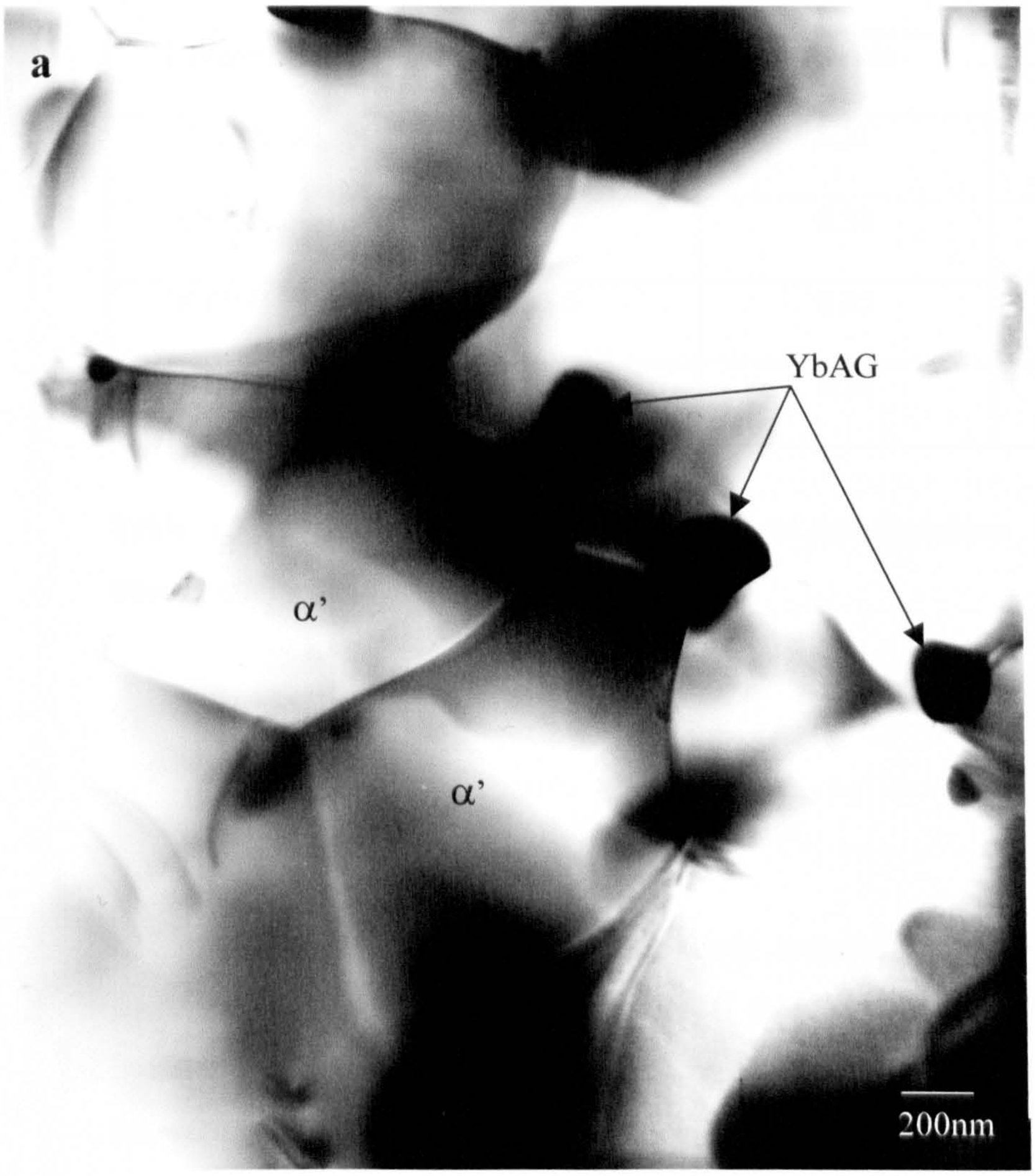

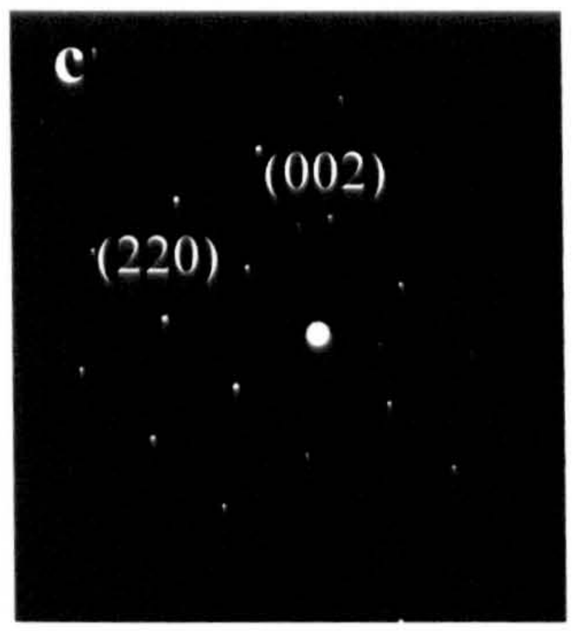

< 110 >

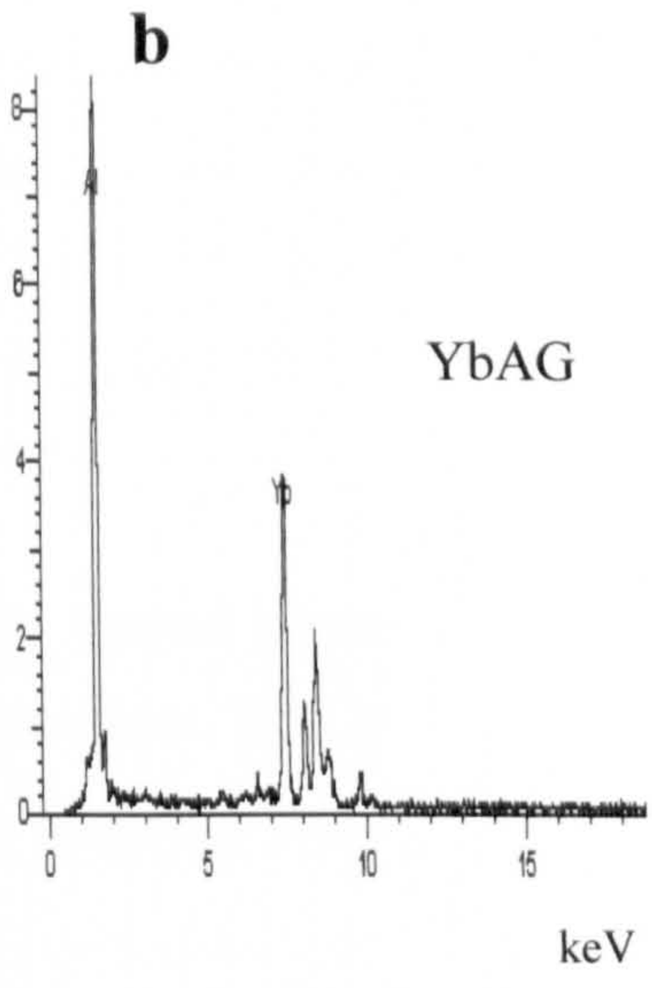

Figure 5.15. TEM micrograph of composition Yb75B after 24hr at 1450^0C (a), (b) EDAX of the intergranular crystalline phase and (c) electron diffraction pattern of YbAG.

reduction in the substitution level of Yb in α' structure and the m-value decreased to approximately 1.05.

Composition	m-value	x-value	z-value
Yb50B/24hr	0.92	0.31	0.87
Yb75B/24hr	1.13	0.38	-
Yb75B/72hr	1.05	0.35	-
Yb75B5b/24hr	1.17	0.38	1.20

Table 5.5 TEM compositional analysis of α' and β'-sialons in selected heat treated compositions.

5.2.4- The Thermal Stability of Yb α'-Sialon

The results obtained from this study revealed only a very limited phase transformation had taken place in most of the heat treated compositions. This is indicative of the good thermal stability of Yb α'-sialon, when compared with other rare-earth α'-sialon systems.

Composition Yb75B contained the highest α'/β' ratio of approximately 98% α'-sialon and its composition may be located near to the boundary between the α'-sialon single phase region and the α'/β' region. As observed in section 5.2.1 composition Yb75B shows no significant change in the α'/β' phase ratio over a range of temperatures below and above 1450^0C. However heat treatment at 1450^0C shows a slight change in the α'/β' phase ratio (Figure 5.12). After the initial 24 hours only a small decrease in the α' phase content (approximately 4%) was detected from the XRD analysis and this was accompanied by a very

small decrease in the m-value and the calculated substitution level remained the same as in the sintered material (x~0.38). By increasing the heat treatment to 72 hours, a further decrease in the α'/β' phase ratio was seen but at a lower rate and the α' -sialon content decreased by only 5% as detected by the XRD. The EDAX analysis of the α'-sialon phase after 72 hours heat treatment revealed that the m value, and therefore the solubility level (x value), were further reduced to 1.05 and 0.35 respectively. This suggested that the diffusion of Yb^{3+} and Al^{3+} occurred within the α' structure during the prolonged heat treatment.

This is similar to the previous work by Shen et al (1996) who have suggested that upon heat treatment, the α'-sialon phase undergoes compositional adjustment over time with compositions moving towards the boundary between the α' and α'+ β' regions. The α'-sialon compositional adjustment is manifested by the reduction in α' lattice dimensions and the m value (Al-N substitution). This indicates the diffusion of the stabilising cations as well as Al^{3+} and N^{3+} from the α' structure during the heat treatment process. Once at this boundary the α' sialon is unstable and α'–>β' transformation may take place.

The results observed from section 5.2.1, revealed that the heat treatments of this composition resulted in a crystallisation of the grain boundary phase in the form of a Yb-garnet phase and its content did not change with prolonged heat treatment time. Hence, it is possible to suggest that the small change in the α'/β' phase ratio observed in composition Yb75B, and after 24 hours heat treatment, may occur as a result of the crystallisation of the residual glass phase in the form of YbAG phase. The formation of $Yb_3Al_5O_{12}$ will consume the Yb^{3+} as well as the Al^{3+} and O^{2-} from the residual liquid phase, leaving the remaining liquid depleted in these elements. However in order to compensate for the difference between the YbAG phase and the glass phase the remaining liquid may precipitate as α' or β'-sialon phase with low substitution level.

The crystallisation of the residual liquid may also require some additional Yb and Al which would be provided by the sialon phases. Therefore a reaction between this liquid and α'-sialon phase may also take place, resulting in a compositional adjustment of the α'- sialon phase as suggested by Shen et al (1996c).

$$\alpha'_1 + \text{liquid} \rightarrow \alpha'_2 + \text{YbAG}$$

However extending the heat treatment up to 168 hours did not show any significant change in the α'/β' ratio despite the presence of 7% β' grains which indicates no transformation had taken place and the system had approached equilibrium. Therefore it is possible to suggest that the α' to β' transformation during the initial duration of heat treatment may be attributed to a combined effect of two different mechanisms: the glass crystallisation, and this possibly plays the major role during the first 24 hours, (since a higher transformation rate was absorved after 24 hours); and also the α' compositional adjustment which is implied by the small reduction in the m-value after prolonged time.

The small shift in the α'/β' phase ratio is not believed to reflect any instability of the α'-sialon phase in this composition, but rather a slow process of approaching an equilibrium between the phases present. This is further supported by the microstructural observation of Figure 5.13, for heat treated materials at different durations of time. As can be seen from the micrographs no significant changes in the α'/β' phase ratio or morphology were observed after prolonged heat treatment, apart from slight change in grain boundary morphology.

The observed result is in contrast to some other rare- earth sialon systems. For example in Nd and Sm sialon systems a continuous decomposition of α'-sialon was observed during prolonged heat treatment (Shen et al 1996b, Zhao 1995 and

Ekstrom 1997). Therefore the stability of present materials further demonstrates the excellent thermal stability of the single phase Yb α'-sialon system.

5.2.5- Thermal Stability of the α'/β' Yb-Sialon

The initial composition of the Yb50B material contained a mixture of the α'/β' sialon phases with the α' composition located at the boundary of the single phase and the α'/β' regions. The XRD analysis of composition Yb50B, heat treated at 1450^{0}C for different periods of time (Figures 5.10 and 5.12), shows a reduction in the α'/β' phase ratio with heat treatment time, which indicates some α'-β' transformation had taken place. After the initial 24 hours a decrease of approximately 5% in the α'-sialon phase was detected by XRD. The small change in phase content was not accompanied by a significant change in the m-value as observed from the XRD and EDAX analysis table 5.5. However extending the heat treatment time results in a continuous α' to β' transformation and around 17% decrease in the α' content was detected by the XRD after 168 hours.

Ekstrom et al (1997) reported that the dominating reaction in stable α'-sialon materials is compositional adjustment and with the presence of a small volume fraction of the residual phase the α'- β' transformation will not take place once the intergranular phase is completely crystallised. Therefore the α'- β' transformation is expected to be lower in Yb50B than Yb75B because of the smaller volume fraction of the residual phase in Yb50B. During the crystallisation process and after the initial period of heat treatment i.e the 24 hours, the volume of the residual grain boundary glass phase will be reduced due to the formation of the YbAG phase. Hence its effect on the transformation would be restricted due to the absence of the liquid as a medium for ionic transport. The observations made on the TEM sample revealed that the 24 hours heat treatment results in an almost complete crystallisation of the intergranular phase at the multi grain junctions, but possibly a thin layer remains between the adjusted grains. However, despite this,

the α'–> β' transformation continued with a prolonged heat treatment duration but at a constant rate (lower than the 24hr) which suggests that other mechanisms may also affect the transformation of this material.

The XRD results are in agreement with EDAX and shows that the as sintered composition Yb50B exhibited a lower cation level x~0.31 (relatively small lattice dimensions) and a lower m value ~0.93 compared to composition Yb75B. This value is near to the reported minium m-value (m~1) required to form a stable α' sialon (Sun 1991 and Ekstrom 1997). It has been suggested that the concentration of the stabilising cation in the α'-structure may have an effect on its stability. An α'-sialon material containing a smaller cation level (near to the solubility limit) is relatively unstable and transforms more easily than materials with a higher cation level (Shen 1996, Ekstrom 1997).

The 24 hour heat treatment shows the higher transformation rate and the EDAX of the α' phase shows only a slight decrease in the m-value from ~0.98 to ~ 0.92 and also a small decrease in the z-value of the β'-sialon. This suggests that the α'–>β' transformation during the initial 24 hours heat treatment possibly occurs as a result of the crystallisation of the residual glass and a small compositional adjustment of the α' sialon. However with prolonged heat treatments the cation level probably continues to decrease and therefore at a critical value below the lowest solubility limit the α'-sialon becomes highly unstable and transforms more easily to β' via decomposition reaction. Hence the presence of even a thin layer of the intergranular phase may be enough to aid transformation as suggested by Shen et al (1996b) and Cheng (1994). Zhao and Cheng (1995) reported that in the unstable α' phase the α'–> β' transformation proceeds without the involvement of a large amount of grain boundary liquid and the liquid formed from the transformed α' may facilitate the transformation.

Furthermore the presence of ~ 33% β' grain in this composition may also be responsible for the α'-β' transformation. Zhao et al (1995), Zhao and Cheng

(1995) have reported that the presence of β' grains within α'-sialon materials may facilitate the progress of the α' to β' transformation. Therefore in the α'/β' materials the transformation may proceed through a heterogeneous nucleation on the existing β', in contrast to the single α'-sialon materials in which a nucleation of a new β' is required for transformation to occur.

The amount of the crystallised YbAG phase in this composition was observed to increase with the duration of the heat treatment (increased from ~2% to ~ 10% after 168hr). It has been suggested that during the α'–>β' transformation because of the compositional difference between the α' and β' phases the decomposition of α' must produce other phases in addition to the β' phase. In the present case an increase in the YbAG phase is in agreement with Shen et al (1996c) who suggest that the α'-sialon may decompose as

$$\alpha' \longrightarrow \beta' + Yb_3Al_5O_{12}$$

From the above results it is possible to suggest that the α'-sialon with smaller lattice dimensions (lower m-value) and containing high β' grains, present in composition Yb50B, was less stable than materials containing a high α' with larger lattice parameters and with no β' grains i.e composition Yb75B in which α'-β' transformation stopped once the intergranular residual phase had completely crystallised in the form of YbAG and α' remained in the stability range.

5.2.6- Effect of Glass on α'→ β' Transformation

It has been suggested in many studies that the addition of glass to an initially α'-sialon composition may result in the formation of α'/β'-sialon materials and during subsequent heat treatment the α'→ β' transformation may be facilitated. Mandal et al (1995) reported that the presence of a large amount of low viscosity intergranular glass/liquid phase surrounding the α' and β'

grains in α'-sialon materials may influence the formation of the α' and encourage the α' to β' transformation in stable systems. Therefore the composition and the amount of the glassy phase in the α' sialon system are seen to be critical to the stability of the α'-sialon phase. In the present work (section 5.1.1.2), the addition of SiO_2 to composition Yb75B was observed to significantly decrease the α'/β' ratio and simultaneously increase the β' content and the volume of glass phase after sintering. Therefore the combined effect of residual glass phase and the pre-existing β' on the α' to β' transformation can be represented by materials with silica addition Yb75B2b and Yb75B5b.

After heat treatment the XRD results obtained from composition Yb75B2b and Yb75B5b presented in table 5.4, revealed that a significant decrease in the α'/ β' phase ratio was observed in both compositions after 24 hours at 1450^0C. As can be seen from the table the α'/β' phase ratio decreased to 72/28 in composition Yb75B2b compared to 85/15 in the as sintered material and decreased in composition Yb75B5b to 49/51 relative to 66/34 in the as sintered materials. It is clear that the transformation of α'→ β' occurred at a higher rate in composition Yb75B5b compared to Yb75B2b, which suggests that the difference of the phase contents and the amount of the residual glass between the two compositions may be the reason.

The prolonged heat treatment of composition Yb75B5b up to 168 hours shows no marked change in the α'/ β' phase ratio indicating no α'–>β' transformation had taken place after the 24 hours heat treatment.

Despite the presence of a higher β' content, which would possibly provide the nuclei for the α'–> β' transformation, the increase in the β'-content in both compositions after 24 hours heat treatment is believed to result from the crystallisation of the larger volume of the intergranular phase. As mentioned in section 5.2.4, the crystallisation of YbAG as a grain boundary phase may result in the precipitation of more β' phase with a lower substitution level and in order to establish an equilibrium a reaction between the α'-sialon and the

remaining liquid may take place, which results in compositional adjustment. Therefore, based on this mechanism, the crystallisation of a larger volume of the intergranular phase increases the competition between the α'-sialon and the crystalline phase for the Yb and Al.

The above suggestions may be supported by a comparison between compositions Yb75B5b and Yb50B. The initial α'/β' phase ratio is similar in both compositions but the amount of the intergranular phase and the composition of the α' sialon are different. Despite the higher m value (~1.16) of the α' phase in composition Yb75B5b, it transforms at a higher rate than Yb50B which indicates that during the crystallisation of < 5% intergranular glass phase (in Yb50B) only a small change in the composition of the liquid may be needed. This can be achieved by a small compositional adjustment of the phases present in the system. Crystallisation of a larger glass/liquid phase in composition Yb75B5b results in formation of more β' and increases the competition for the Yb and Al within the α' phase which may result in instability of α' sialon and thus increase the α'–>β' transformation. This is demonstrated further by the higher transformation rate observed in composition Yb75B2b which contains a lower β' (~15%) content but higher volume of glass (12%) than composition Yb50B. This suggests that the crystallisation of the intergranular glass has a greater effect on the α'/β' phase ratio during the heat treatment than the presence of β'.

The EDAX analysis on α' and β'-sialons of composition Yb75B5b after 24 hours, shows no decrease in the m-value and therefore the solubility level was the same as the sintered value table 5.3. The z-value was lower than the as sintered value. This suggests that during the crystallisation of the YbAG the precipitation of new β' with lower substitution level, similar to the earlier observation on β'/YAG (Lewis 1983), shifts the z to lower values. The EDAX analysis of the glass phase shows that it is rich in Al and Yb which indicates that during the crystallisation of the YbAG only a small amount of Al and Yb may be needed to compensate for the compositional difference between the crystalline phase and the remaining residual glass. The EDAX of the α'

composition revealed that there was a variation in the substitution level within the α'-sialon grains with some grains having m-value below the solubility limit. Hence it is possible that only the α' with the lowest substitution level will be involved in the reaction in order to provide the Al and Yb required for crystallisation. This may be achieved by the decomposition of α'-sialon with the lower Yb^{3+} concentration instead of a change in its composition, therefore it may result in an increase in m-values rather than decrease.

Therefore from the present results it is possible to suggest that the amount of the glass/liquid phase plays an important role in the $\alpha' \rightarrow \beta'$ transformation during the initial heat treatment. The substitution level of Al-N, and therefore the fraction of the cation incorporated in the α'-structure, is also an important factor in the thermal stability of the α'-sialon. When the α' phase is at the position of its lowest stability limit i.e the fraction of Yb^{3+} is low (composition Yb50B), α'–> β' transformation may proceed with the prolonged heat treatment. The more stable α' phase contained a high fraction of Yb^{3+} (composition Yb75B, Yb75B2b and Yb75B5b), so in order for the α'–> β' transformation to occur a crystallisation of large amount of glass/liquid is required. However unless the α'-sialon composition shifts below the solubility limit, no α'–> β' transformation will take place once the glass has completely crystallised.

In most of the α' sialon systems the choice of a potential, appropriate grain boundary phase is limited. Thus the cation chosen to stabilise the α' lattice must also provide the system with a refractory grain boundary phase, after appropriate heat treatment. The investigation of the crystallisation product is therefore an important aspect in the examination of the α'- sialon field.

The nature of the phases that result from the crystallisation of the residual intergranular glass phase during the post sintering heat treatment may also affect the thermal stability of the α' phase. The formation of a cation rich crystalline grain boundary phase, which arises during the crystallisation process will consume a significant amount of the cation from the residual glass. Therefore

the crystallised phase may compete for the remaining cation with the α'-sialon. From previous studies on rare-earth sialon materials, the melilite solid solution formed in less stable α'-sialon systems, such as Nd and Sm, was found to consume a large amount of the cation and nitrogen from the α'- sialon and this is suggested to be one of the factors for the destabilisation of α'-sialon (Shen et al 1996a;1996b and Ekstrom et al 1997).

The more stable α'-sialon system, Yb α' sialon does not form a nitrogen rich phase but an oxide-rich phase (garnet is the most stable phase). The crystallisation of the grain boundary glass in the Yb α' sialon system, during post sintering heat treatment at a range of temperature up to 1600^0C while α'/β' ratio remains constant (composition Yb75B), suggests that the YbAG phase in equilibrium with α' and β' and does not destabilise the α' to compete for Yb^{3+} and Al. Therefore the Yb α' sialon is more stable than the α' sialon in other rare-earth systems. By comparison, the single phase α' Nd -sialon material was reported to begin the α'→ β' transformation within the 24 hours at 1450^0C and α' was continuously decomposed over time. The Gd α' sialon was observed to exhibit similar thermal stability behaviour to Yb α' sialon and this was attributed to the crystallisation of the intergranular phase in the form of $GdAlO_3$ (Jumali 1999). In the Ca α' sialon system, Hewitt (1998) reported that although the single phase α' sialon in this system exhibits excellent thermal stability under extended heat treatments, the pre-existence of β' in the materials was found to facilitate the transformation.

5.3- Summary

The addition of SiO_2 to the high α'-sialon in the Yb system significantly improves the densification and promotes the formation of β' in the final materials. This is encouraging since it exemplifies the ability to exercise some control over the α'/β' ratio via compositional change.

The addition of a small amount of β-Si_3N_4 seeds to Yb α'-sialon had little effect on the α'/ β' phase ratio and slightly improves the β'-sialon morphology, whereas addition of larger amount of seeds had no effect on α'/β' ratio or morphology. The addition of β-Si_3N_4 seeds to Yb α'/β' sialon leads to a grain growth of β' sialon phase.

The Yb α'-sialon investigated in this work exhibited good thermal stability compared to the other rare-earth (Nd and Sm) α'-sialon phases. The β' grains may provide a nucleation site for the secondary β' formation in the materials with unstable α' phase but it is not a necessary requirement for transformation to occur in the stable α' phase. The presence of a large volume fraction of the glassy phase in the α'-sialon material had a more pronounced effect on the initial rate of the α' –> β' transformation.

The crystallisation of the intergranular phase in the form of oxygen rich YbAG phase does not destabilise the Yb α'-sialon to compete for increased fractions of Yb and nitrogen. Thus the influence of the crystallisation phase on the thermal stability in the Yb α' based systems is small.

CHAPTER 6
SIALONS WITH MIXED CATIONS

6.1- Introduction

This chapter involves the use of dual cations as stabilizers for α sialon. The effects of mixed cations on the microstructure and their distribution in the final product have been investigated. The stability of α'-sialon phase in these systems was also studied.

6.2- Material Compositions

Two compositions with mixed Yb/Nd and Gd/Nd as α'-sialon stabilising cations were prepared in this experiment. The composition of α'-sialon was set as $R_{0.5}\ Si_{9.75}\ Al_{2.25}\ O_{0.75}\ N_{15.25}$ where R is the rare earth cation (Nd, Gd and Yb) and m= 1.5 and n=0.75. The rare-earth cations were added in the form of presynthesised glass powder the α'/β' phase ratio was fixed to be 75/25 (in wt%). The compositions of the starting powders are listed in table 6.1 and the compositions were prepared in the same way as in the single cation sialons described in section 3.2. Approximately 50wt% of Nd single cation composition was added to 50wt% of each Yb and Gd sialon to form compositions Yb/Nd and Gd/Nd respectively. The prepared powders were then cold iso-statically pressed (150 MPa for 15 sec) into green body pellets and then pressureless sintered at temperature 1750^{0}C for 4 hours.

Composition	Si_3N_4	AlN	R_2O_3 glass	Predicted z
Nd	61.91	21.50	16.59	3.50
Gd	59.41	21.94	18.65	3.78
Yb	61.12	21.017	17.862	3.46

Table 6.1 The starting Composition (in Wt %) of the sialon materials

6.3- The Density Measurements and Phase Content.

The bulk density measurements of the mixed cation compositions are given in table 6.2, together with the density of the single cation materials for comparison. The density of the mixed cation α'/β'-sialons is higher than their corresponding single cation sialon materials Nd, Yb and Gd with the same composition. This implies that for the mixed cation sialon, the use of a mixture of light and heavy rare earth oxides to form α'-sialons lowers the eutectic temperature of the system and thus promotes the densification of the material.

Composition	Density g/cm^{-3}	α'/β' wt%	m (value) SEM	n (value)	z-value
Nd*	3.34	72/28	1.0 #	1.5 #	0.6
Yb	3.36	98/2	1.2		1.27
Gd*	3.34	95/5	1.32	1.27	
Yb/Nd	3.42	92/8	1.1 0.98 #	1.7 1.9 #	0.81
Gd/Nd	3.37	89/11	1.19	0.69	0.71

Table (6.2). The bulk density, phase contents and EDAX analysis of as sintered materials # TEM * (Jumali 1999)

The X-ray diffraction traces obtained from compositions sintered with mixed rare-earth cations are shown in Figure 6.1. It is evident from the figure that α'-sialon is formed as the major crystalline phase, with small amounts of a β'-sialon phase and an aluminium nitride polytypoid, which is identified as 12H. No other crystalline phase was detected in the compositions suggesting that the cooling rate was fast enough to prevent crystallisation of the liquid phase.

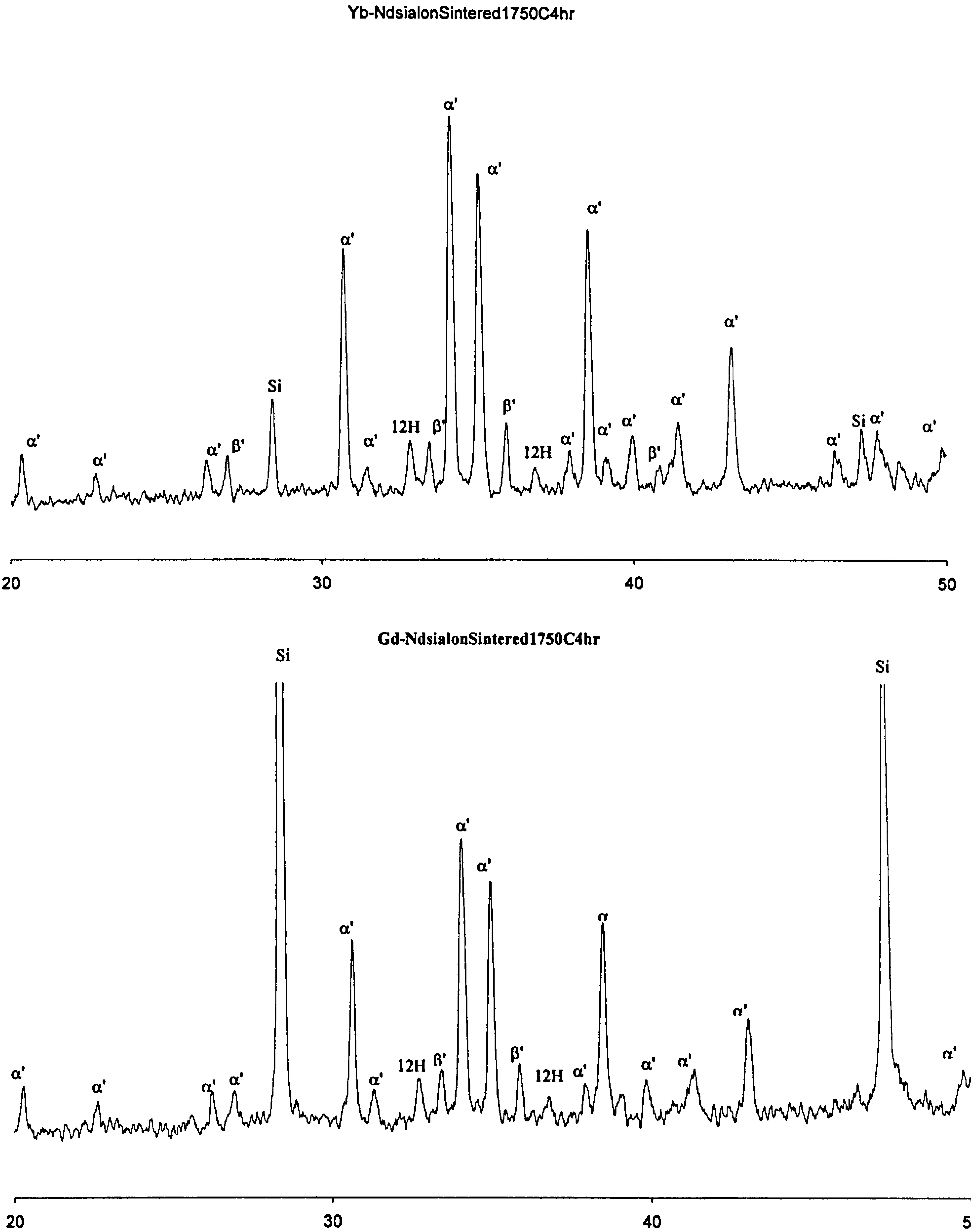

Figure 6.1. The XRD traces of as sintered compositions Yb/Nd and Gd/Nd α'= α'sialon, β'= β'sialon, 12H = AlN polytype and G = YbAG phase

The estimated amount of α' and β'-sialon phases for the as sintered mixed cations compositions are presented in table 6.2. The results from the single cation materials are also incorporated in the table for the purpose of comparison. The data from the single cation Gd and Nd -sialon materials, with compositions similar to those used in this investigation, were obtained from work by Jumali (1999). As can be seen from the table, materials with a high α'-sialon content were obtained from the mixed cations sialon compositions and the ratios observed were significantly higher than the predicted values. Although the starting compositions of the mixed cations Yb/Nd and Gd/Nd were designed to produce materials comprising identical α'/β' phase ratios (i.e 75/25), composition Yb/Nd exhibits a slightly higher α'-sialon content than Gd/Nd. Around 92% α' was detected in composition Yb/Nd and 89% α' in composition Gd/Nd. A similar trend was observed with the single cation sialon materials; see table 6.1. These values are slightly lower than the values observed by their corresponding single Yb and Gd sialon compositions, but significantly higher than that of the Nd sialon composition.

The present results suggest the enhanced size of the single α'-sialon phase field with a decreasing cation size in the rare-earth series. The difference in the ionic radius of Yb (0.086 nm), Gd (0.089 nm) and Nd (~0.099 nm) results in their different ability to form α'-sialon. Yb^{3+} and Gd^{3+} with the smaller cation radius can enter the α'-sialon structure more easily than the larger Nd^{3+} (Mandal 1995).

It has been reported in previous studies that the formation of stable intermediate phases during sintering increases the competition with α' sialon for the stabilising cation and nitrogen. Due to the greater stability of melilite compared with α'-sialon at temperature lower than 1650^0C, the formation of melilite consequently encourages more α' transforming into the β' phase on post sintering cooling. In the present result the XRD analysis of mixed cations-sialon compositions shows no melilite phase. This result is different from that observed in the Nd-sialon system in which the melilite

phase always occurs accompanied by the formation of α' sialon and persists even at 1800^{0}C (Cheng 1994 and Slasor 1986). The absence of the melilite phase in the existing mixed cation compositions suggests that this phase has a lower melting temperature in the mixed cation compositions than the melilite in the Nd- single sialon system and does not significantly retard the formation of α-sialon.

6.4- Microstructure Study of as Sintered Compositions

A microstructure observation of 'as sintered' materials under the scanning electron microscope revealed the difference in the phase content and the morphology of the phases present. Typical back-scattered electron images of the compositions densified with the mixed cations, are shown in Figure (6.2). In general, the microstructures are homogeneous and only a few micropores were observed, which is consistent with the density measurements. Figure (6.2a), shows the microstructure of composition Yb/Nd, a predominately grey α'-sialon phase appears with a wide grain size distribution. Some of the α' grains with high aspect ratio have a mean size of 5μm, and these enclose areas which contain other α' grains which are an order of magnitude smaller. This size distribution was found to be characteristic of most materials investigated in this work. Such an effect relates to the different growth behaviour of sialon grains during the liquid phase sintering. The dark phase, which is homogeneously distributed throughout the α'-matrix, is a mixture of elongated β'-sialon grains (up to 10μm in length) and a 12H AlN polytypoid, mostly with a plate like shape, but sometimes with an irregular shape. The bright intergranular phase is the rare-earth rich glassy phase, which appears semi-continuous. A quantitative imaging technique was used to estimate the amount of this phase from the relative areas of different grey levels in the SEM image and was found to occupy approximately 11%.

The microstructure of as sintered composition Gd/Nd is shown in Figure (6.2b). This material consist of β'-sialon with elongated grains having a high aspect ratio (up to 8μm in length). The matrix α'-sialon exhibited different grain sizes and morphology. Equiaxed, or nearly equiaxed grains with a size ranging from a submicron to larger grains around 2-5μm were found. However some elongated grains with a high aspect ratio (up to 8μm in length) were also observed. Although it has been known that β' grains are easy to develop into an elongated morphology, α' almost always exhibits an equiaxed morphology.

Recent investigations (Shen et al (1997), Nordberg (1997), Chen (1997); Hewitt (1998) and Wang et al (1999)) revealed that α' sialon can develop into an elongated morphology under suitable conditions. Nordberg et al (1997) indicated that in the Ln-Si-Al-O-N system, the liquid phase promotes the formation of elongated α'. Chen et al (1997) reported that the elongated R-α-sialon grains are more likely to occur when using β-Si_3N_4 as starting materials. The compositions used all had a high x-value which is beneficial to form more liquid phase during sintering and to develop α'-grain into an elongated morphology. Wang in his study (1999) found that with composition shifting to low x-value the α' grain became smaller and less elongated.

By comparing the microstructure of the two mixed cation compositions, it is clear that the Gd/Nd contained a slightly higher β' content than Yb/Nd, with α'/β' ratio determined from the quantitative image analysis in agreement with the value obtained from XRD. The small increase in the β' content results in a slight increase in the amount of the rare-earth cation rich-glassy phase in composition Gd/Nd and is estimated to be around 12%. In comparison with the single cation sialon the use of mixed cations (light and heavy) had a significant effect on the α' and β' sialon morphology. It is clear from the micrographs in Figure (6.2) and Figure (4.10c), that the β'-grains in the mixed cations materials had a more elongated morphology compared with those of less elongated with an irregular morphology in the

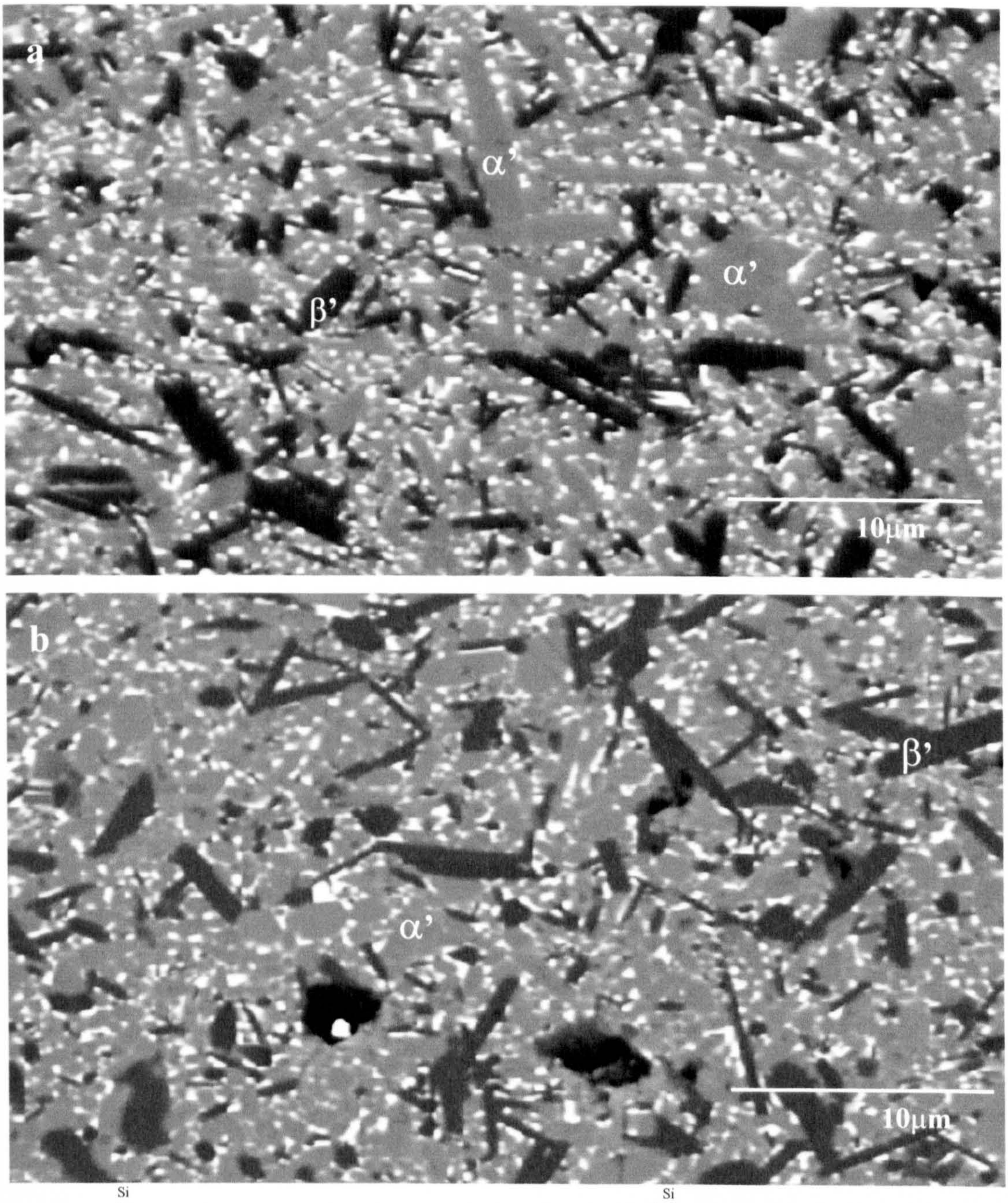

Figure 6.2. Back-scattered electron images of mixed-cation compositions sintered at 1750^0C for 4hrs (a) Gd/Nd, (b) Yb/Nd and EDAX analysis (c) Gd/Nd and (d)Yb/Nd

heavy rare-earth single cation Yb composition. The β' grain in Nd single cation composition shows similar morphology to that of mixed cation compositions. This is possibly due to the difference in the amount of the liquid phase formed during sintering. The higher content of liquid phase present during sintering in the mixed cations Yb/Nd composition allowing unconstrained growth of β'-sialon grains prior to impingement. The prismatic morphology of β'-sialon results from the anisotropy in solid/liquid surface energy and growth kinetics of hexagonal β' crystals. With the lower liquid present during sintering the growth of β'-sialon in materials Yb75B is more restricted. This is reflected in the amount of residual glassy phase in the final microstructures, for example 5% in single cation (Yb75B) composition and 11% in the mixed cations Yb/Nd composition.

The compositional analysis of the phases present was determined from the EDAX point analysis carried out in the SEM on the as sintered compositions Yb/Nd and Gd/Nd. An average of a ten-measurement point analysis was used to measure the distribution of the elements in the α' grains. The analysis of the α'-phase indicates that the Nd^{3+} cation has been incorporated into the α'-sialon structure together with either Yb^{3+} or Gd^{3+} (Figures (6.2c) and (6.2d). Furthermore the atomic concentration of Nd^{3+} in the α'-sialon is lower than the Yb^{3+} and Gd^{3} with a ratio of approximately 1.6 in Gd/Nd and 1.4 in Yb/Nd, suggesting that there is possibly more excess Nd^{3+} than Yb^{3+} and Gd^{3+} remaining in the grain boundary glass.

The substitution levels were calculated for both compositions Yb/Nd and Gd/Nd. The Al-N substitution (m-value) showed an average value of 1.1 and 1.2 respectively whereas the Al-O substitution (n-value) obtained from both compositions is 1.7 for Yb/Nd and 0.69 for Gd/Nd. The solubility of (Yb+Nd) and (Gd+Nd) in the α' structure was calculated and the values were closely similar approximately x=0.37 and x=0.38 for Yb/Nd and Gd/Nd respectively. These values are significantly different from the targeted values set in the starting composition similar to that observed in the single cation compositions. The low solubility of the stabilising cations in the α'-

sialon is possibly due to the formation of a glass phase which contained an appreciable fraction of the stabilising cations. The residual glass phase together with the formation of Al polytypoid may also affect the Al-O substitution in the β'-sialon. The compositional analysis of the β' sialon phase revealed that the z-values were 0.83 and 0.71 in compositions Yb/Nd and Gd/Nd respectively. These values are significantly lower than predicted for the single cation compositions.

A more careful study on composition Yb/Nd was made using the TEM. A micrograph of the Yb/Nd composition is shown in Figure (6.3a). In agreement with the SEM, the structure consists of α' grains with mostly equiaxed morphology and a small amount of elongated β' sialon grains and 12H, as confirmed by the EDAX. A detailed compositional analysis was performed on both α'-grains and the grain boundary glassy phase, using an EDAX point analysis. The EDAX patterns of the α' phase and the glassy pockets are also given in Figure (6.3b) and Figure (6.3.c) respectively. There is a small difference between the values obtained from the SEM and that from the TEM, which is possibly due to the fluorescence effect in the SEM. An approximation of the 10 point analysis on the α' grains indicates that more of the added Yb^{3+} cations have been incorporated into the structure than the Nd^{3+}, which reveals that the rare earth ion with a smaller ionic radius can enter more easily into the α' structure. The measurements gave an average m value of 0.99 and therefore a cation solubility level of approximately x= 0.33 similar to previous reports on the lowest solubility limit (Sun et al 1991).

On the other hand the EDAX analysis of the residual intergranular phase showed that the glassy pocket in composition Yb/Nd contained Si and Al in addition to the two stabilising metal cations (Yb+Nd). The analysis indicates that there exists a larger amount of rare earth cations in the grain boundary than in the α' grains, and the concentration of Nd^{3+} is higher than Yb^{3+}. The Si : Al : Nd : Yb ratio in the residual glass was estimated to be approximately 4:3:2:1. This observation indicates that in the mixed cation

Figure 6.3. TEM micrograph of as sintered composition Yb/Nd (a); EDAX pattern of the equiaxed-sialon grains (b) and EDAX pattern of intergranular phase (c)

doped α' sialon, the smaller rare-earth ions Yb^{3+} and Gd^{3+} enter more easily into the α' structure than the larger Nd^{3+} which remained in higher concentration in the residual intergranular glass phase.

6.5- Post Sintering Heat Treatment and the Grain Boundary Devitrification

In order to investigate the effects of heat treatment on the α'–> β' sialon phase transformation and also on the grain boundary crystallisation behaviour in compositions which contained a double cation as a stabiliser for α'-sialon, the as sintered compositions were subsequently heat treated in a nitrogen atmosphere at two different temperatures 1300^0C and 1450^0C for 24 hours. To study the effects of time on the thermal stability of the α'-sialon in more detail a more prolonged heat treatment was carried out at 1450^0C on both compositions for a duration of up to 168 hours. The crystallisation products and the α'/β' phase ratio after heat treatment are presented in table 6.3.

6.5.1- The α'–>β' Transformation

The crystallisation products and the α'/β' ratio after a 24 hour heat treatment at temperatures of 1300^0C and 1450^0C are given in table (6.3). As can be seen from the table the XRD analysis of both compositions shows no significant change in the α'/β' phase ratio after 24 hours heat treatment at 1300^0C and the α' phase content was almost the same as the sintered materials, approximately 90% in composition Yb/Nd and 88% in composition Gd/Nd. This suggests that the α'-sialon is a stable phase at 1300^0C and no significant α'–>β' phase transformation has taken place. It is possible that the temperature of 1300^0C is below the eutectic temperature of these systems, which implies that the transformation in the solid state is very slow and the presence of a liquid phase is an aid in the

transformation by providing an effective diffusion path. The slight increase in the β' content possibly occurs as a result of the residual glass crystallisation process which may proceed as

$$\text{Glass} \rightarrow \text{crystalline phases} + \beta'$$

Further post sintering heat treatments on both materials were conducted at a higher temperature of 1450^0C. The 24 hour heat treatment results in a small shift in the α'/β' phase ratio. The XRD patterns obtained from the compositions Yb/Nd and Gd/Nd heat treated at 1450^0C are shown in Figure (6.4a) and Figure (6.5a) respectively. The traces show a slight increase in the peak intensity of the β' phase as well as the grain boundary crystallisation product. For example, the value of the β' phase in composition Yb/Nd, which originally contained 8%, increased to 15%, and a similar tendency also occurred for composition Gd/Nd, where the β' phase content increased from 11% in the as sintered to 17% after a 24 hour heat treatment. This indicates that some α'–>β' transformation had taken place at this temperature.

Although the amount of α' and β'-sialon phases has only changed slightly after 24 hours of heat treatment, the amount of these phases was significantly different after extending the heat treatment duration to 168 hours and a continuous α'→β' transformation was observed. This is clearly evident by comparing the peaks intensity of α' and β' in the XRD traces in Figure 6.4b and Figure 6.5b. As can be seen both compositions Yb/Nd and Gd/Nd resulted in a considerable decrease in α'-sialon peaks, which consequently resulted in an increase in β'. The α'/β' phase ratio decreased significantly to 72/28 in composition Yb/Nd and to 57/43 in composition Gd/Nd.

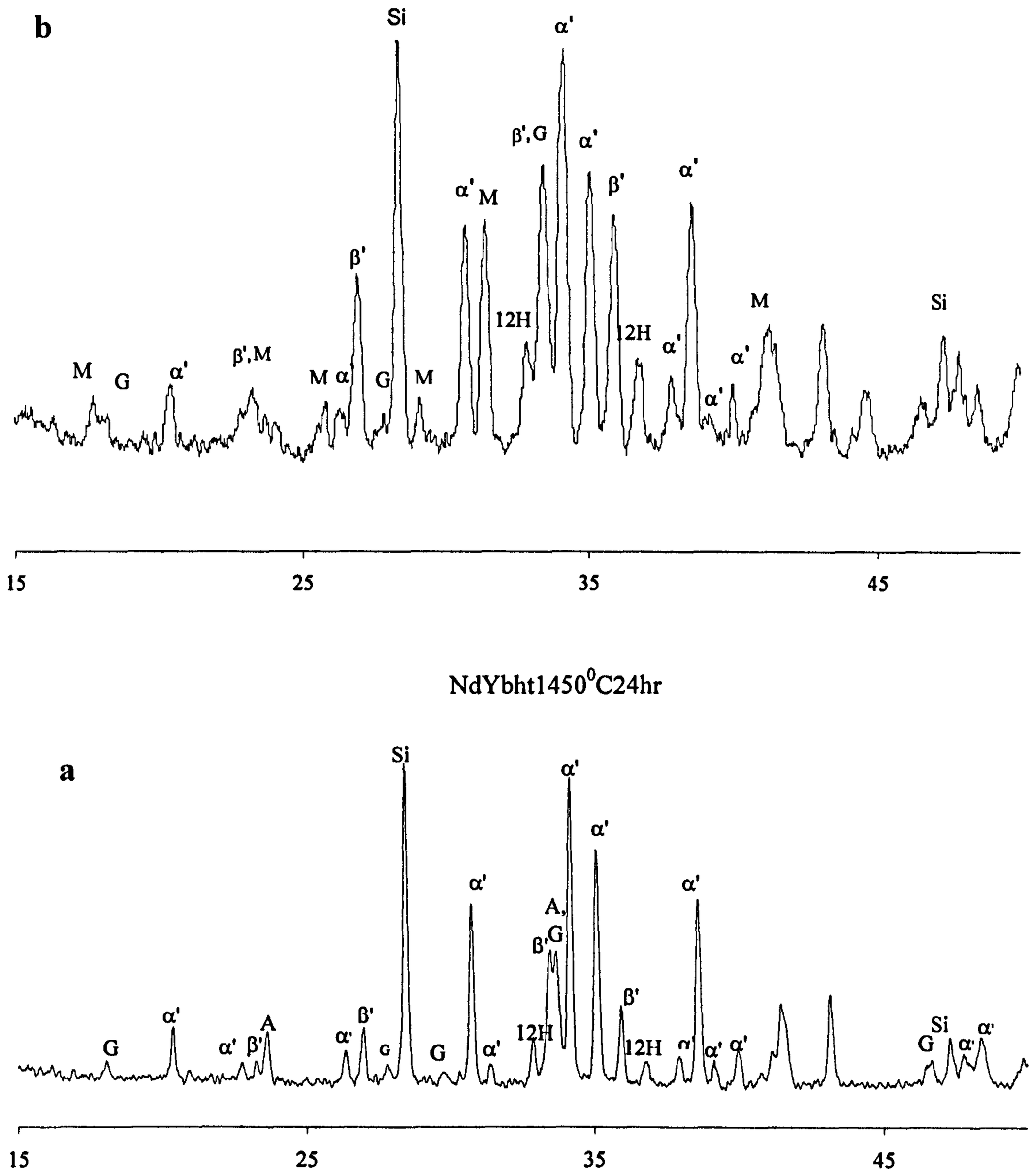

Figure 6.4 The XRD traces of composition Yb/Nd heat treated at 1450^0C for a period of time (a) 24hrs and (b) 168hrs .

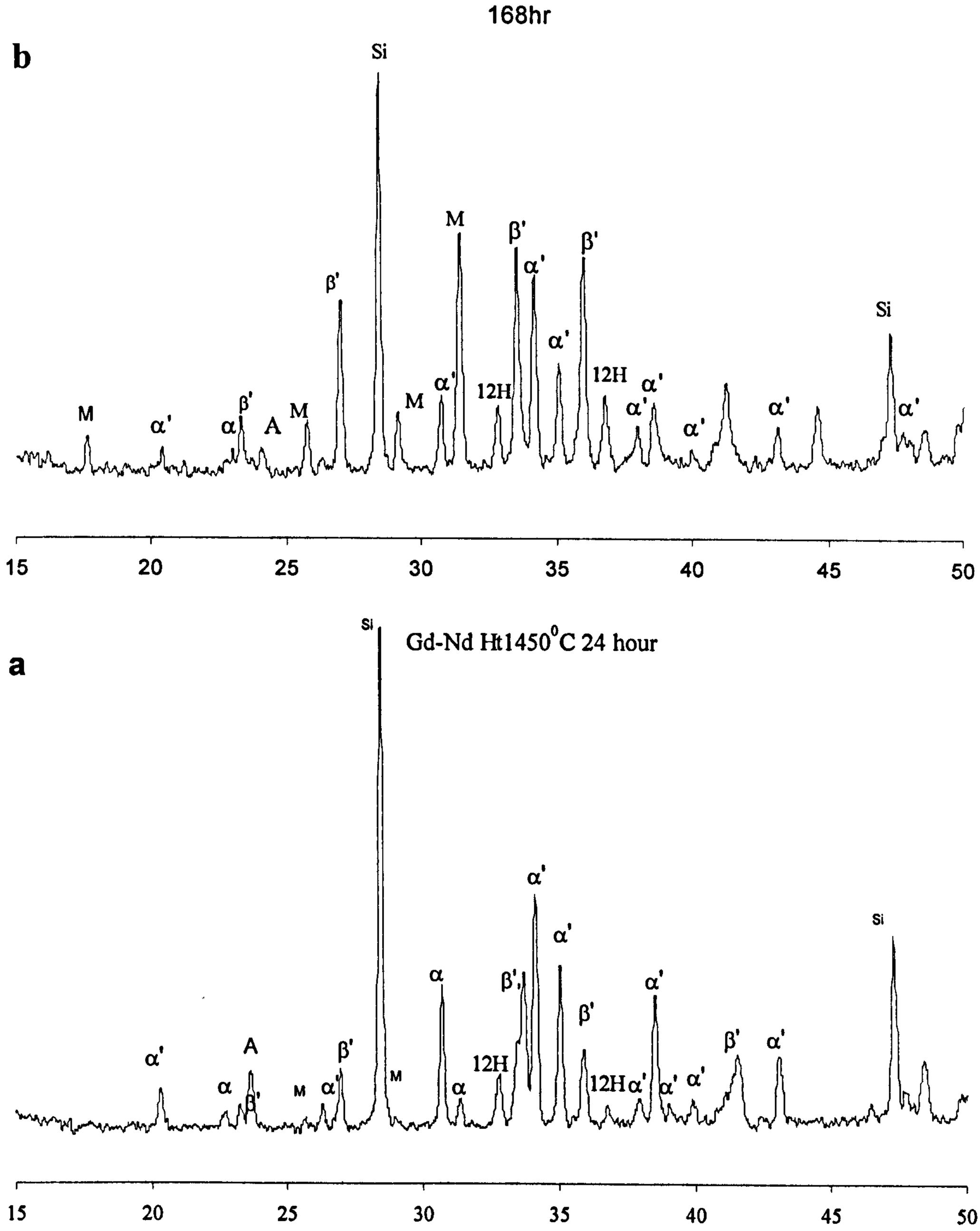

Figure 6.5 The XRD traces of composition Gd/Nd heat treated at 1450^0C (a) 24hr and (b) 168hr .

As observed in section 6.5.2 extending the heat treatment to 168 hours results in the crystallisation of the more nitrogen rich phase (R-melilite) instead of the oxygen rich crystalline phase (R-aluminate). Because of the high stability of melilite phase compared to the α'-sialon at low temperatures (<1650^{0}C), the formation of the stable melilite in these compositions increased the competition with the α'-sialon for the stabilizing cations and the nitrogen, which consequently encourage more α' to transform into the β' phase during heat treatment.

Composition	Yb/Nd			Gd/Nd		
Temperature/time	α'/β'	Crystalline product	m-value	α'/β'	Crystalline product	m-value
Before H.T.	92/8	-	1.1	89/11	-	1.12
1300^{0}C	90/10	A, YbAG	-	88/12	W , M (t)	-
1450^{0}C/24hr	85/15	A, YbAG	1.08	83/17	A	1.08
1450^{0}C/168hr	72/28	YbAG, M'	0.95	57/43	M'	1.02

Table 6.3. The α'/β' phase ratio, the crystalline products and the EDAX of α' sialon in the heat treated materials. W=wollastonite, M=melilite, A=aluminate, YbAG=Ytterbium garnet phase, (t) trace

6.5.2- The Grain Boundary Crystallisation Products

In the present investigation, as shown in table 6.3, the main consequence of the heat treatments was the crystallisation of the grain boundary glassy phase. The heat treatments at different temperatures and durations of time were accompanied by the crystallisation of the residual glassy phase into various phases. The X-ray diffraction analysis revealed that in composition Yb/Nd the heat treatment for 24 hours at a temperature of 1300^{0}C resulted mainly in the crystallisation of the intergranular glass phase into Nd-aluminate ($NdAlO_3$) and a small amount of the Yb-garnet phase ($Yb_3Al_5O_{12}$)

whereas in composition Gd/Nd the grain boundary crystallised in the form of R-wollastonite.

The post sintering heat treatment at a temperature of 1450^{0}C for a duration of 24 hours and 168 hours was observed to induce a change in the type of the crystalline product. Although the initial 24 hour heat treatment did not change the crystalline product in composition Yb/Nd and the $NdAlO_3$ and YbAG phases were observed again as the main crystalline products, but with increasing amounts, in composition Gd/Nd after 24 hours at 1450^{0}C the wollastonite (formed at 1300^{0}C) disappeared and the R-aluminate phases (Gd/Nd AlO_3) were formed as the main crystalline products. The wollastonite phase was observed to be a stable phase up to 1400^{0}C in the single cation Nd-sialon system (Jumali 1999). By extending the heat treatment up to 168 hours the continuous $\alpha' \rightarrow \beta'$ transformation results in a change in the grain boundary phase. The R-aluminate phases completely disappeared in both compositions, and a nitrogen-rich crystalline Nd- melilite (or its solid solution M') and YbAG phases were formed in composition Yb/Nd, whereas in composition Gd/Nd only R-melilite solid solution phases were observed.

Wang et al (1995a) reported that the formation of a rare-earth aluminate as the crystalline grain boundary phase is dependent on the concentration of Al in the liquid phase. More Al-rich liquids tend to devitrify into aluminate whereas liquids with a low Al concentration devitrifys into melilite, with the exception of the Yb sialon system in which YbAG forms instead of an aluminate or melilite phase. Cheng and Thompson (1994)) reported that the aluminate phase forms at temperatures between 1250^{0}C and 1400^{0}C whereas the melilite (M') phase was the only stable intergranular crystalline phase at temperature above 1400^{0}C.

Previous studies on rare-earth α'-sialon materials (Falk et al 1996) have shown that in the light rare-earth systems a nitrogen-rich R-melilite phase (or its solid solution) forms as a grain boundary phase, whereas the oxygen rich garnet phase forms in the heavy rare-earth (Yb^{3+}) systems.

6.5.3- Microstructural Changes After Heat Treatment.

The microstructure changes in the heat treated compositions were investigated by the SEM and the TEM. Figure 6.6, shows the back-scattered electron micrographs of composition Yb/Nd after heat treatment at 1450^0C. The significant transformation from α' to β' and intergranular crystalline phase is clearly seen from the micrographs. After 24 hours (see Figure 6.6a), a small change in the α' and β' grain morphology was observed. In addition to the elongated β' -grains formed in the as sintered composition some grains with an irregular shape were also seen. The α' grain size was slightly coarser. The crystallised residual phase, which is homogeneously distributed, forms an isolated grain morphology similar to that observed in the heat treated single cation sialons. The high heat treatment temperature encourages the liquid phase to diffuse along grain boundaries, breaking the interconnected glassy grain boundary network into isolated pockets. This implies the possibility of completion of crystallisation, developing glass-free interfaces, with reduced energy-anisotropy in the materials, which could be beneficial in improving the high temperature creep resistance. These crystals appear with an average size of approximately 0.5μm, although some large agglomerates of a bigger size (~ 2μm) were also observed scattered throughout. Similar trends were observed in composition Gd/Nd.

The prolonged heat treatment of 168 hours at 1450^0C resulted in significant changes in the phase ratio and the grain morphology as observed from the microstructure of composition Yb/Nd Figure (6.6b). A further increase in the β' sialon and consequent decrease in α'-sialon content is clearly seen from the microstructure, suggesting that more α' –> β' phase transformation has taken place. A significant difference in the microstructure of the grain boundary phase was also observed, although areas with limited amounts of residual glass phase were observed in the as sintered materials and after 24 hours heat treatment. The distribution of the intergranular phase is more agglomerative and inhomogeneous, indicating that grain boundary diffusion

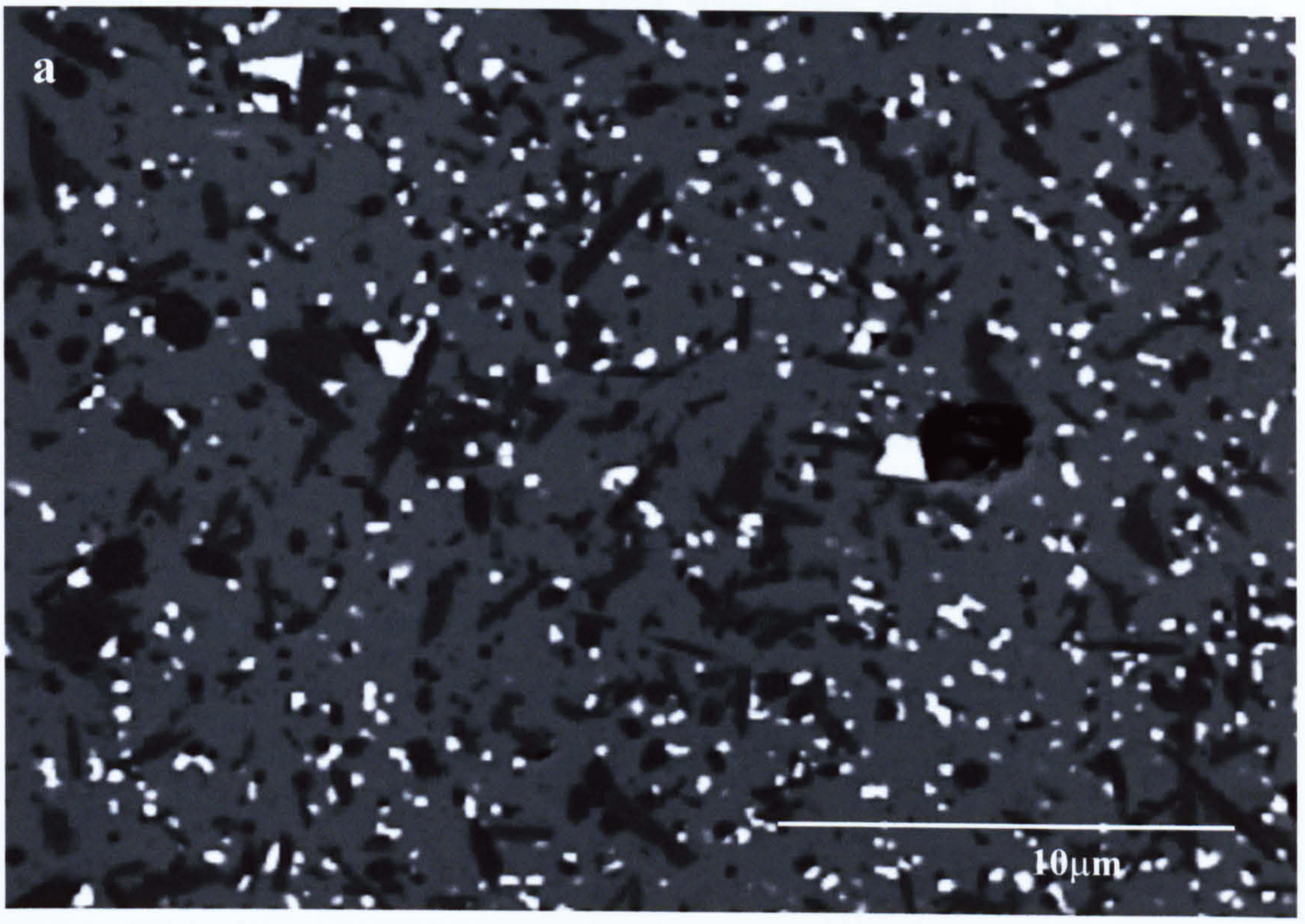

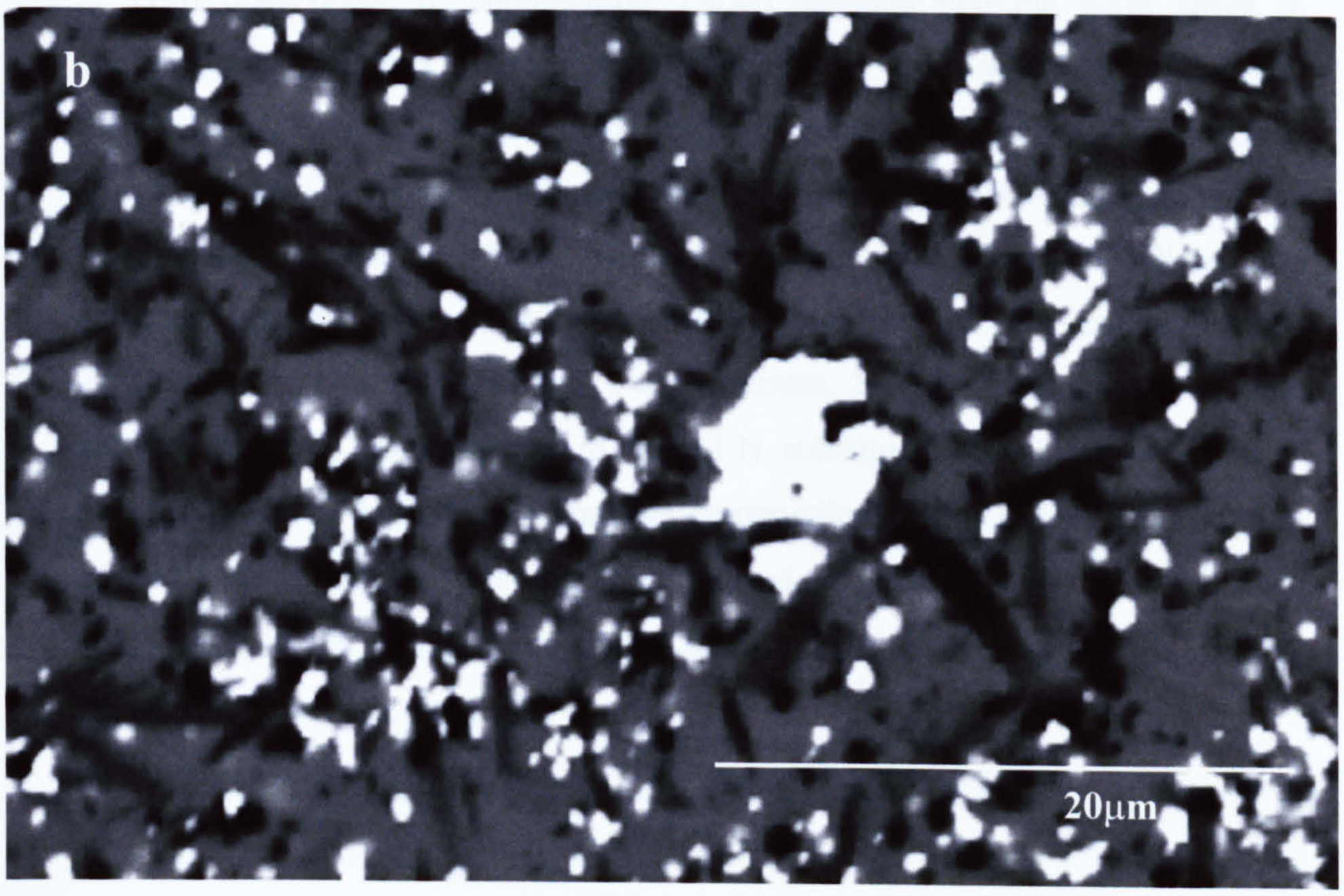

Figure 6.6 The SEM of composition Yb/Nd heat treated at 1450^0C (a) 24 hr (b) 168 hr

from one area to the other may have taken place during the heat treatment at this temperature.

A compositional analysis of the as heat treated compositions revealed that with time the α'-sialon exhibited a slight decrease in m-values. After 24 hours the Al-N substitution (m-value) decreased only slightly in composition Yb/Nd from 1.1 to 1.08 and this value decreased further to 0.98 after 168 hours. Similar behaviour was observed in composition Gd/Nd and m-value was decreased from 1.16 to 1.08 after 24 hours and further to 1.02 after 168 hours. This indicates that a diffusion of the stabilising cation, as well as Al and N, occurs from the α' sialon structure to the intergranular phase during the heat treatment process. The Al-substitution level in β'-sialon phase decreased to 0.79 in Yb/Nd after 24 hours and then increased to 0.82 after 168 hours.

A TEM observation of composition Yb/Nd revealed that the glass phase in the multiple junctions was crystallised after the heat treatment at 1450^0C for 24 hours. A typical bright field image is shown in Figure 6.7. An EDAX analysis Figure (6.7b&c) confirmed the YbAG and the Nd-aluminate as the intergranular crystalline phases. These crystalline phases were localised into separate isolated pockets with a limited solubility of Nd cation in the YbAG and Yb cation in the Nd aluminate. EDAX results showed that although there is no reduction in the Al-N substitution level (m-value) in α' phase compared with the as sintered composition, however, the concentration of Nd^{3+} in α' phase was slightly reduced. A small change in the Al-O substitution level (z-value) of the β'-sialon phase was observed, the z-value decreased from 1.12 to 1.07.

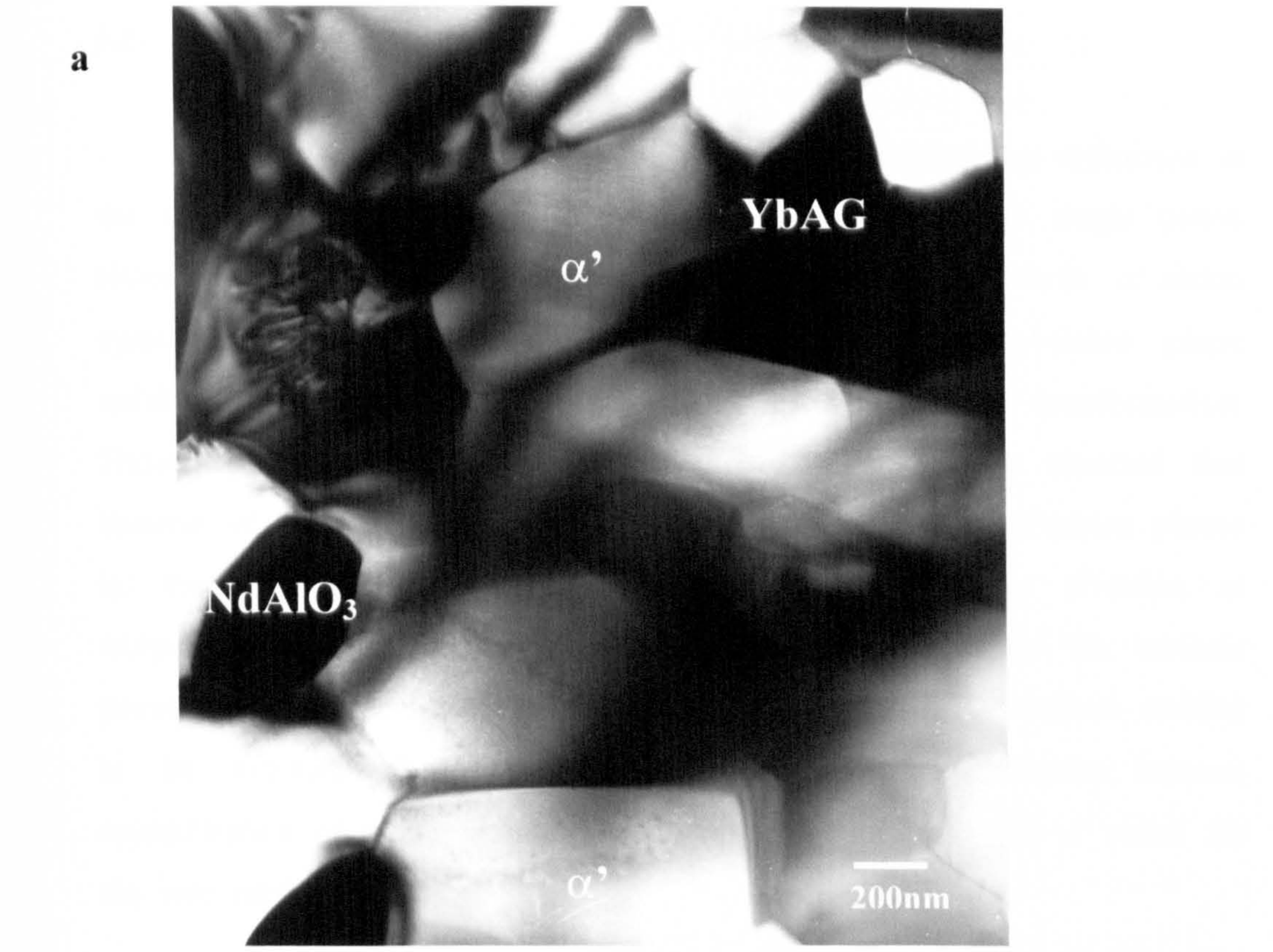

Figure 6.7 TEM micrograph of composition Yb/Nd heat treated at 1450^0C 24 hr (a) bight field image and (b & c) EDAX pattern of the crystalline intergranular phases and (d) the EDAX pattern of α' phase

6.6- Discussion

The results obtained from this experiment revealed the difference in the thermal stability of the mixed cation and that of the single cation sialon materials. Previous studies on single cation rare-earth α' sialon systems showed that at intermediate temperature the α'-sialon phase stabilised with light cation is unstable and undergoes α'–>β' transformation. Thompson and Mandal (1997) and Ekstrom (1997) have reported that because of the fairly large ion size of Nd and Sm cations, α'-sialon phases in these systems exhibits a continuous transformation to β'-sialon at temperature 1450^{0}C. In light rare-earth sialon systems, besides the intrinsic properties of α', the kinetic priority of the formation of intermediate melilite is an extrinsic factor promoting α'-β' phase transformation, because crystallisation of melilite during heat treatment competes with α' sialon for the rare earth cation.

As shown in section 6.5.2 the 24 hours heat treatment at 1450^{0}C resulted in the formation of rare earth oxygen-rich crystalline phases which is in agreement with the results obtained from the single cation sialon systems. In single cation Yb-sialon system the YbAG ($Yb_3Al_5O_{12}$) was formed as the crystallisation products (chapter 5), whereas aluminate $NdAlO_3$ and $GdAlO_3$ phases were formed respectively in the Nd and Gd sialon systems (Jumali 1999). Recent observations (Ekstrom 1997 and Shen 1996) reported that in the single cation Nd-sialon phase the melilite phase (or its solid solution) was formed as a grain boundary phase after 24 hours heat treatment. Previous study by Mandal (1993) showed that R-melilite formation takes place above 1400^{0}C, whereas at lower temperature an aluminate ($RAlO_3$) or garnet may form. With the present results and during the crystallisation process at 1450^{0}C, it is possible that the glass/liquid phase formed contained a high Al content and therefore favoured the nucleation of the oxide-rich phases (Gd/Nd-AlO_3 and YbAG) as detected from the XRD results (see table 6.3). These phases were found to be stable up to 24 hours at 1450^{0}C. With further heat treatment, up to 168 hours, at the same temperature, the R-

AlO_3 phases disappeared and R-melilite solid solution phases were formed instead. Similar trend was observed in the single cation Nd-sialon composition where Nd-M' phase started to form with the extending the heat treatment and Nd-M'+ Nd-AlO_3 phases were detected after 72 hours (Jumali 1999).

The formation of R-aluminate phases during the 24 hours was accompanied by a small decrease in α' and a simultaneous increase in β' phase approximately 7% decrease in α' sialon phase was detected in both compositions. This value is significantly lower than the ~17% decrease detected in the single cation Nd-sialon composition after 24 hours at the same temperature. This suggests that α' sialon in the mixed cations systems transformed at lower rate than in the single cation Nd-sialon system. As mentioned in chapter 5, one of the reasons which may affect the stability of α'-sialon phase is the solubility of the stabilising cations in the α' structure. EDAX analysis on α' phase in the mixed cations compositions after 24 hours heat treatment showed a slight decrease in the m-values and therefore the substitution levels remain almost unchanged and ~x = 0.36 (see table 6.3). This indicates that no significant diffusion of R^{3+}, Al^{3+} and N^{3+} occurred which may have resulted in the α' compositional adjustment. This is in contrast to the single cation Nd-sialon composition which exhibited a clear reduction in the m value (Jumali 1999).

The observed result suggests that the small increase in β' content during the 24 hours heat treatment possibly occurs as a result of the crystallisation of the intergranular residual phase. During the crystallisation process the aluminate phases form and consume the stabilising cations together with the Al from the oxynitride glass leaving the remaining liquid rich in Si and N. To maintain an equilibrium the excess of Si and N may either diffuse into the sialon phases α' and β', therefore reducing the substitution levels similar to early work by (Lewis 1983) or precipitate as a new β' sialon with lower z-value as detected from the EDAX analysis of β' phase section 6.5.3.

Upon extending the duration of heat treatment to 168 hours, a continuous decrease in α' sialon content and therefore an increase in β' content was observed. The proportion of the α' phase reached around 28% in Yb/Nd and 43% in Gd/Nd which is clear evidence of the α' → β' transformation during the isothermal heat treatment. As observed from the microstructure study section 6.5.3, after 24 hours heat treatment at 1450^{0}C, the residual glass phase was almost completely crystallised with the resulting interphase boundaries approaching nearly solid/solid contacts. Therefore in the absence of a liquid phase at the grain boundaries, the transformation from α' –>β' is expected to be very slow. Zhao et al (1995) reported that in the Sm α' sialon system, in the presence of a very small glass phase possibly as a thin layer, the α'→ β' transformation proceeds at constant rate after 24 hours heat treatment at 1450^{0}C. This indicates that in the light rare earth systems the presence of a large volume of glass phase may act as a diffusion path, but it is not the only requirement for α'→ β' transformation, other factors may also affect the transformation. In the single cation Yb system (chapter 5) and the Gd sialon system (Jumali 1999), the amount of the intergranular glass phase was found to significantly affect the α'/β' phase ratio during post sintering heat treatment.

As mentioned before in chapter5, one of factors which may affect the thermal stability of the α'-sialon phase is the nature of the crystalline products that result from the crystallisation of the glassy grain boundary phase during post sintering heat treatment. Figure 6.8 shows the Janecke prism showing the relation between the major SiAlON phases. The relative stability of the phases formed was found to vary with ionic size of the stabilising cation present in α' and the crystalline structure. For example the formation of a stable cation-rich crystalline grain boundary phase such as M' melilite phase was thought to be a factor in destabilisation of α' sialon in Nd sialon systems. The formation of melilite (M') phase ($R_3Si_2AlO_4N_3$) may compete for the stabilising cation within the α'-sialon, and this results in instability of α'. The crystallisation of intergranular phase in the form of garnet phase in the heavy rare-earth sialon systems does not destabilise the

α'sialon to compete for the increased fractions of R^{3+} and nitrogen (chapter 5). The crystallisation of aluminate phase may stabilise the α' at low temperature, however, at high temperature this phase became unstable and therefore destabilises the α'. The critical difference between the garnet phase($R_3Al_5O_{12}$) and the aluminate phase ($RAlO_3$) is the relative stability of YbAG garnet phase which exists up to high temperature (1600^0C) and the cation (R) to Si and Al ratio.

With increasing the duration to 168 hours the Nd and Gd-aluminate completely disappeared and Nd /Gd-melilite formed, except in Yb/Nd where YbAG is still present (figure 6.4b) which indicates that this phase is stable phase at this temperature. The formation of M' phase (containing 55 eq% nitrogen) requires an increase in nitrogen content. The precipitation of M' from an oxynitride glass (contains 20-30 eq % nitrogen) can be achieved by dissolving α'-sialon grains in the grain-boundary liquid with a reaction of α'+ liquid → β'+ M', whereby M' formation is accompanied by α'→ β' transformation (Mandal and Thompson 1993). The significant compositional difference between the two phases ($RAlO_3$) and M' ($R_3Si_2AlO_4N_3$) implies that the phase transformation must require an additional Si and N which may be taken up from the nitrogen rich phase such as α' phase. Slasor et al (1986) reported that in Nd- sialon system both the α' and β' phases are not compatible with the $NdAlO_3$. Cheng and Thompson (1994) reported that the aluminate phase may be formed as a stable phase up to 1400^0C if no β' is present. This suggests that upon further 1450^0C heat treatment the Nd and Gd-aluminate phases possibly became unstable and may form a eutectic liquid through a reaction with other phases present in the systems such as α' and β'. As the heat treatment proceeds more α' and β' will be involved in the reaction. This results in a change in composition of liquid phase to become more nitrogen rich which consequently encourages the precipitation of melilite phase. The existence of this transient liquid is supported by the observation that considerable grain boundary migration occurs when the M' phase forms (see Figure (6.3b)).

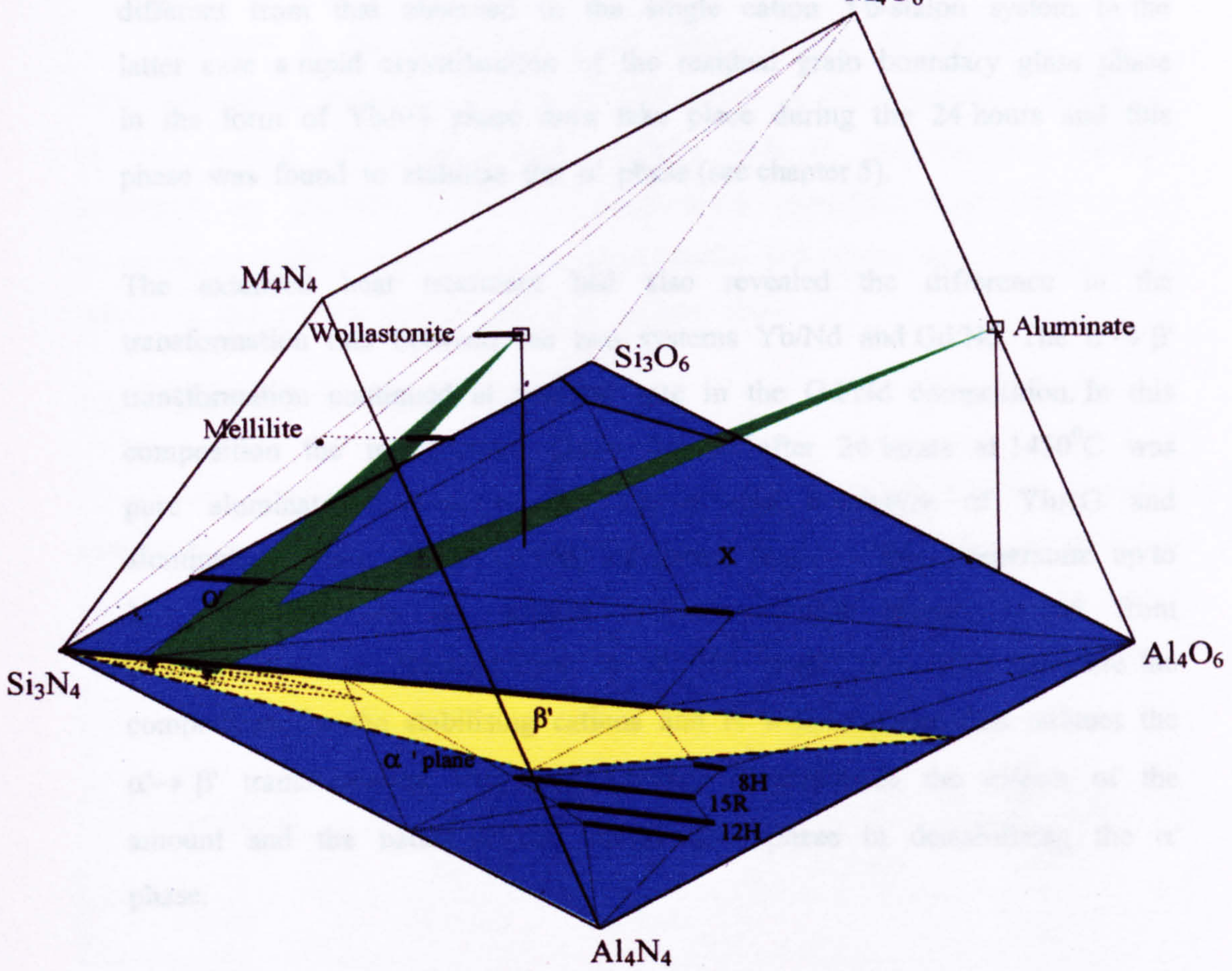

Figure 6.8. The Janecke prism showing the relation between the major SiAlON phases

The melilite phase (M') formed is more stable than the α' phase, therefore as the heat treatment continues, more α'–>β' transformation occurs. This was accompanied by a small compositional adjustment and after 168 hours, the α' phase has m-value of 0.95 for Yb/Nd and 1.02 for Gd/Nd compositions respectively. This behaviour is similar to the single cation Nd-sialon system where α' transformed continuously into β' phase, but on the other hand is different from that observed in the single cation Yb-sialon system. In the latter case a rapid crystallisation of the residual grain boundary glass phase in the form of YbAG phase does take place during the 24 hours and this phase was found to stabilise the α' phase (see chapter 5).

The extended heat treatment had also revealed the difference in the transformation rate between the two systems Yb/Nd and Gd/Nd. The α'→ β' transformation continued at a higher rate in the Gd/Nd composition. In this composition the intergranular phase formed after 24 hours at 1450^{0}C was pure aluminate whereas in the Yb/Nd was a mixture of YbAG and aluminate. Because of the stability of garnet phase at this temperature up to 168 hours, therefore the amount of the melilite phase formed from decomposition of Nd-aluminate in Yb/Nd must be smaller, therefore the competition for the stabilising cations and N with α' phase thus reduces the α'→ β' transformation. This result further demonstrates the effects of the amount and the nature of the intergranular phase in destabilising the α' phase.

CHAPTER 7

MECHANICAL PROPERTIES AND OXIDATION BEHAVIOUR

7.1- Introduction

Changes in the microstructure of materials play an important role in their mechanical properties. In this chapter some of the mechanical properties of the sintered and heat treated ceramics, such as hardness and fracture toughness, are described. The high temperature oxidation behaviour of the materials was also investigated. The experimental procedures used to obtain the results in this chapter are described in chapter three.

7.2- Hardness Measurements.

The hardness of the polished bulk sections of selected sintered compositions was determined at room temperature by a Vickers diamond pyramid indenter with a 50N load. The measurements were carried out using optical and scanning electron microscopes and the results are listed in table (7.1).

Compositions	As sintered materials (GPa)		As heat treated (GPa)	
	SEM	Optical	SEM	Optical
Yb50B	16.8±0.5	13.4±0.3	-	13.5±0.2
Yb65B	15.4 ±0.4	14.4±0.4	16.6±0.5	15.0±0.5
Yb75B	18.4±0.2	16.2±0.5	19.4±0.1	16.4±0.3
20D2S	17.9±1.0	-	-	-
Yb75B5b	17.5±0.8	-	18.1±0.6	-
Yb/Nd	17.7±0.3	-	19.0±0.5	-
Gd/Nd	16.4±0.7	-	17.4±0.3	-

Table 7.1. The hardness values of the as sintered and heat treated materials

It is clear from the table that although the values measured by the optical microscope are lower than the values measured by SEM both techniques showed similar trends. The hardness is determined by the volume of plastic deformation caused by the indenter. Plastic deformation in crystalline ceramics is normally determined by the resistance to dislocation motion in the direction of the resolved stress, hence the greater the resistance to the plastic deformation the higher the hardness value.

It has been generally accepted that α-Si_3N_4 and α-sialon are harder than β-Si_3N_4 or β-sialon as a result of crystallographic differences. The hardness is related to the magnitude of the Burgers vector associated with dislocations which determines the lattice friction stress. Since the c-axis vector in β-Si_3N_4 is smaller than the a-axis vector (see table 2.1) the corresponding Burgers vector is smaller and dislocation motion in this direction is more likely. In the α–Si_3N_4 (α'-sialon)-structure the rearrangement of the hexagonal [0001] layer stacking is such that the c-axis dimension is almost double that of β phase (0.562 nm and 0.29 nm respectively), hence the resistance to dislocation motion in this direction is increased because of the larger Burgers vector. Therefore materials containing a high α'-content are expected to have a higher hardness value. As mentioned in the previous chapters the changes in the starting composition result in changes in the phase contents.

As can be seen from table 7.1 and Figure 7.1, composition Yb75B, which contained the greatest α' content, exhibits the highest hardness value compared to the other compositions. Besides the α'-sialon content, the hardness of α'-β' ceramics is also influenced by the amount and composition of the grain boundary phases and other factors, such as residual porosity. The increase in the residual glass phase resulted in a lower hardness and this is shown by the compositions prepared with the addition of SiO_2. The decrease in the hardness value of composition Yb75B5b can be attributed to two reasons; an increased amount of a 'soft' intergranular glass phase (with HV_{10} varying between 900-1000 depending on the nitrogen level in the glass) and a decreased amount of a hard α'-sialon phase.

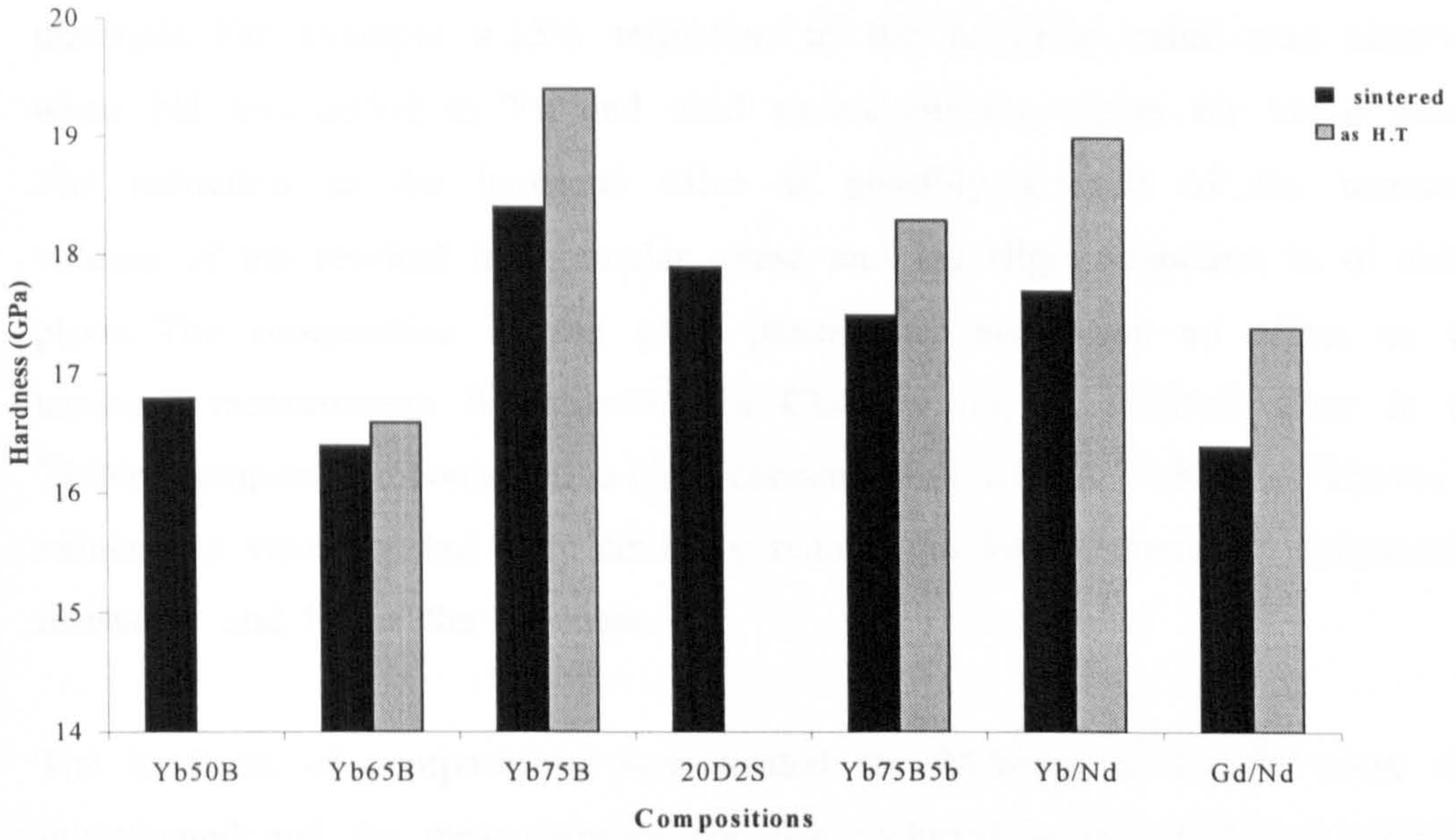

Figure 7.1.The values of the Vickers hardness of Yb α'/β' sialon materials and the mixed cation sialons, as-sintered and as-heat-treated

In the present investigation the effect of porosity on the hardness is evidenced by the lower measured hardness observed for composition Yb65B, even though there is a 95% α'-sialon content and a very small amount of glass present in this composition. The presence of approximately 5% porosity resulted in a lower hardness value compared with Yb75B which contained an almost similar α'/β' ratio. The effect of porosity on the hardness value is also clear by comparing compositions Yb50B and Yb75B5b (both compositions contained an almost similar α' content). Despite the presence of a higher volume fraction of the glass phase in the latter composition the improved density enhanced the hardness. The pores decrease the cross sectional area on which a load is applied and hence reduce the average stress that can be supported by the materials. These results show that the elimination of the residual small percent of porosity from the microstructure should yield a very hard material.

The hardness measurements of the mixed cation α'-sialon in the present investigation are slightly lower than those observed in the single cation materials. For example a 13% reduction in the hardness value was observed when Nd was added to Yb and used as a stabilising cation for the α' phase. The reduction in the hardness value is possibly a result of the increased volume of the residual intergranular phase and the slight reduction in α' sialon phase. The composition of the glass phase may also have an effect on the hardness measurement. As observed in Chapter Six, the residual glass in the Yb/Nd composition contained a high concentration of Nd^{3+}, which is known to reduce the viscosity and may similarly reduce the low temperature deformation resistance and hence the hardness.

The hardness of compositions heat treated for 24 hours at 1450^0C were also investigated and the measurements are also included in table (7.1). As observed in chapter five, the 24 hour heat treatment results in a slight decrease in the α'/β' phase ratio. Despite this increase in the β' content the hardness values were found to increase in the as heat treated materials. For example in composition Yb75B the value increased from 18.4 GPa to 19.4 GPa. The observed increase in hardness is believed to be due to the crystallisation of the grain boundary glass in the form of the YbAG phase, which has a higher hardness (typical value for YAG H_v (2N load)~ 18GPa has been reported by (With and Parren 1985)).

The investigated materials in this study all exhibited high hardness values which have a potential for further improvement if the materials can be produced with a smaller residual porosity and a smaller volume fraction of the intergranular phase. For example the values of hardness determined here for Yb α'/β' are comparable with that reported for other sialon systems; single α' phase in the Ca-sialon system exhibited a hardness value (Hv_{10}) of 17.9 GPa (Hewitt 1998) and in Y α'/β' sialon materials a value around 19 GPa was obtained using gas pressure sintering (Wang et al 1995b). In rare earth sialon systems, typical hardness values ranging between 20 to 22 GPa have been reported for

α' sialon materials (Shen et al 1997, Ekstrom et al 1997, Chen and Roesenflanz 1997, and Ekstrom et al 1995). However it should be noted that most of the reported data were from hot pressed materials and that the pressureless sintered materials are expected to be less hard than the hot pressed.

7.3- Fracture Toughness

The fracture toughness was measured by indentation because of the limited size of sintered billets from which notched beam test specimens could be machined. The fracture toughness of selected compositions was measured using Vickers indents, which exhibited significant cracking at the corners of the indent. After tests had taken place measurements of the surface crack lengths c Figure (3.3) were carried out using a scanning electron microscope. Each measurement is the average of 8~10 indents and in order to be comparable with the majority of other research the K_{IC} was calculated using the method of Anstis et al (1981). The Young's modulus was assumed to be 310 GPa. The measured fracture toughness values of as sintered and as heat treated compositions are given in table (7.2) and presented in Figure (7.2).

compositions	Yb50	Yb75	20D2S	Yb75B2b	Yb/Nd	Gd/Nd
K_{Ic} sintered	4.6±0.02	4.0±0.04	5.2±0.03	4.7±0.03	4.2±0.02	4.6±0.02
K_{Ic} Heat treated	-	3.4±0.03	-	3.9±0.02	3.7±0.03	3.8±0.05

Table (7.2). Fracture toughness by indentation for as sintered and heat treated materials (in **MPam$^{1/2}$**).

The Vickers indentation crack technique is known to give a lower K_{IC} value compared with other methods. It has been reported that different results were obtained for similar material using different techniques (Srinivasan 1981) and that the results obtained from the indentation technique were approximately

30% lower than those from the SENB method. Choi and Salem (1994) measured the K_{IC} of in-situ reinforced Si_3N_4 using different techniques and found that the indentation crack size yielded the lowest results by 46% (indentation measurements; K_{IC}=5.8 MPa $m^{1/2}$, indentation + fracture =8.5 MPa $m^{1/2}$; and chevron notched beam; K_{IC}=10.7 MPa $m^{1/2}$). Jones (1994) found that the Vickers indentation crack method carried out on sialon 101 showed a substantially lower (K_{IC} ~ 4.4 MPa.$m^{1/2}$) value than the accepted value measured by notched beam techniques (K_{IC} ~7.7MPa.$m^{1/2}$). Therefore compared with other values reported in literature care should be taken to allow for compensation in the techniques.

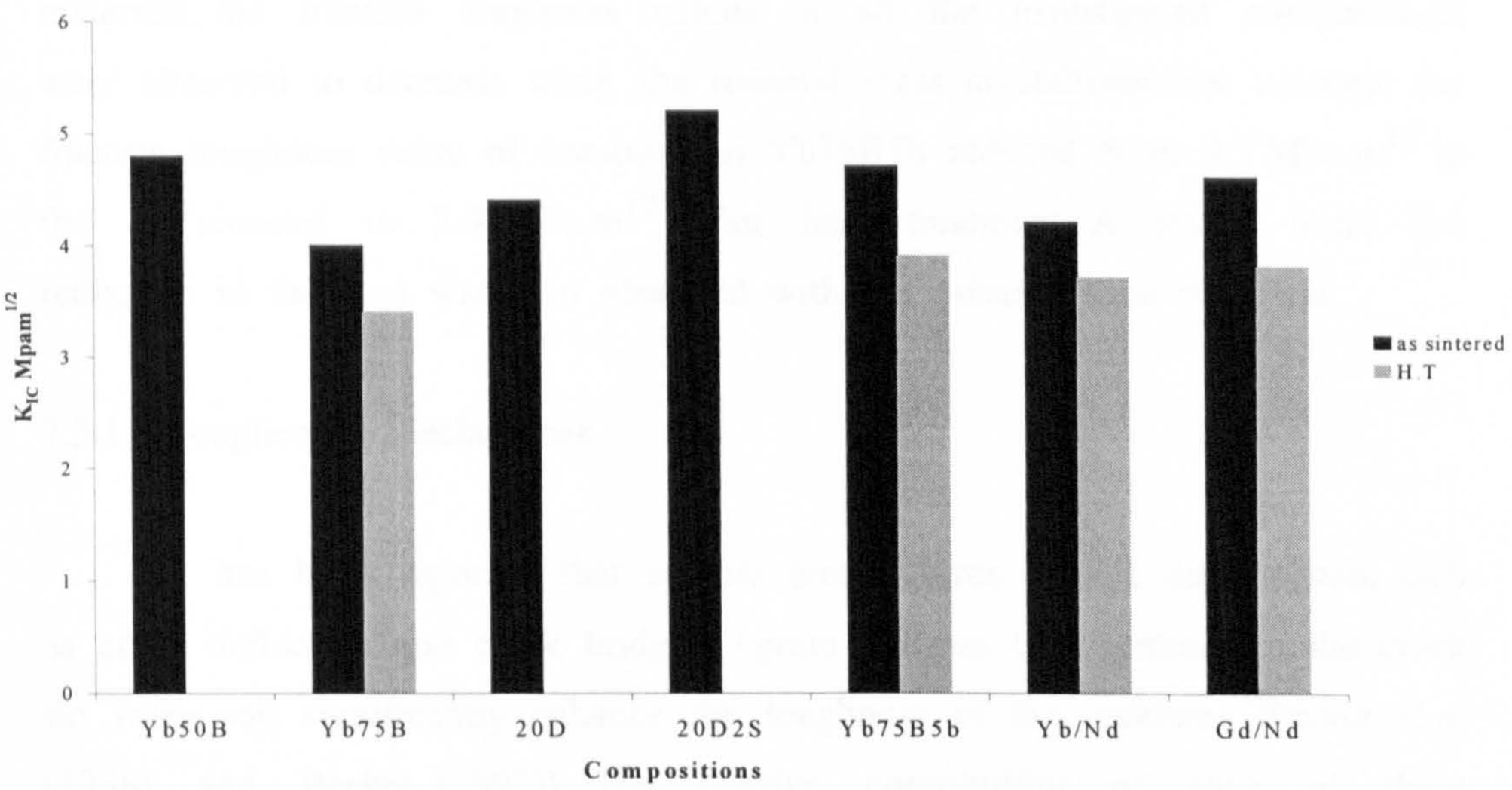

Figure 7.2 The Fracture toughness of Yb α'/β' sialon materials and the mixed cation sialons, as sintered and as heat treated

It is clear from Figure 7.2 that compositions containing a higher β' content exhibited a higher fracture toughness value. For example, higher fracture toughness values were observed in compositions Yb50B and Yb75B5b which contained a higher β'-sialon (of 36% and 33% respectively) compared with composition Yb75B (~2%). Moreover, the fracture resistance was observed to

increase with increases in both the diameter and amount of the elongated large β'-sialon grains. This is evidenced by a comparison with the β-Si_3N_4 seeded materials. Composition 20D2S, which contained an SiO_2 addition, exhibited the highest fracture toughness value (5.2 MPa.$m^{1/2}$). This is a similar effect to that reported for toughening in whisker reinforced ceramics, in which K_{IC} increases with an increase in both the diameter and the volume fraction of whiskers (Becher 1991).

Fracture toughness values obtained from materials heat treated at 1450^{0}C for 24 hours are also included in table (7.2) and Figure (7.2). Despite the small increase in the β'-sialon content in the microstructure of the heat treated materials, the fracture toughness values of all the investigated compositions were observed to decrease when the residual glass crystallised. For example the fracture toughness value of composition Yb75B5b reduced from 4.7 MPa.$m^{1/2}$ in the as sintered to 3.9 MPa.$m^{1/2}$ after heat treatment. A similar trend (i.e reduction in the K_{IC}) was also observed with the mixed cation materials

7.3.1. Toughening Mechanisms

It has been reported that at low temperatures, several mechanisms, such as crack deflection and crack bridging / grain pull-out that operates in the crack tip wake, can significantly enhance the toughness of the ceramics (Becher et al (1988) and Becher (1991)). The relative contribution of each of these mechanisms is dependent upon the interface properties, the amount, size and morphology of the reinforcing phase.

Crack deflection can take place when there are local areas in a ceramic that have a lower resistance to crack propagation. The deviation in the crack path from the plane normal to the axis of the applied stress results in a reduced stress intensity at the crack tip. The initial crack can be deflected by sufficiently weakened reinforcing matrix interface which is preferred crack path Faber and Evans (1983) proposed that crack deflection toughening is highly dependent on the shape and volume fraction of the reinforcing phase. The

toughening by crack bridging results from the interlocking of the two surfaces of the crack by a strong reinforcing phase (Figure 1.1). This induces a closure force on the crack surface, leading to a reduction in the stress intensity.

Debonding of the interface between the matrix and the reinforcing phase is a necessary condition to achieve the toughening effects. A weak interface bonding (needs interface fracture energy ~ 1/4 that of the reinforcing phase (He and Hutchinson 1989)) is a prerequisite for the debonding effect, which in turn promotes the two main toughening mechanisms in the Si_3N_4 ceramics mentioned above, crack deflection and crack bridging, whereas a strong interface bond will result in a fracture travelling directly through the grain and no crack bridging and pull-out occurring. Debonding is also determined by the orientation of the reinforcing particle (or grain boundary) to the crack.

In silicon nitride-based ceramics, the presence of large, prismatic β' grains is desirable to obtain high toughness materials. Tajima et al (1988) observed that the presence of large elongated grains is not sufficient to ensure a toughening effect. This points out the importance of the interface debonding in the crack tip wake process. The properties of the intergranular phase (thermal expansion, fracture resistance or chemical bonding with silicon nitride) would alter the stress state at the interface and the condition for interface debonding. In addition a large volume of a residual intergranular phase may also result in a more tortuous crack path and therefore a higher toughness as shown for α'-sialon (Bartek et al (1992) and Ekstrom (1992)).

In the present investigation the microstructural resistance to crack propagation was examined from indentation induced surface cracking. Figure (7.3a) shows an image of the crack path in composition Yb75B. The crack has propagated via a transgranular fracture of the β'-grains, but there is also evidence of some crack deflection along the grain-boundaries. Figure (7.3b), shows an image of crack propagation in the indented composition Yb75B5b. The crack deflection by the large prismatic β'-sialon grains was most frequently observed and this

was most pronounced when the advancing crack encountered elongated β' grains at a lower angle, indicating that the grain-matrix interfacial bonding was sufficiently weak to allow absorption of the fracture energy by debonding. The occurrence of debonding rather than grain fracture is determined by the ratio of the fracture energies of the interface to the fracture energy of the sialon phase. As mentioned before the pre-condition needed to allow the debonding is that the interfacial fracture energy is ~1/4 of the fracture energy of the reinforcing phase. The presence of a large, prismatic β' with a relatively weak interface at the grain boundary in the microstructure, caused the crack to move along a more tortuous path and thus more energy was required to cause propagation, associated with grain bridging and pull-out. Propagating cracks were also observed to have travelled straight through the β' grains without deviation, most often when the approaching cracks were incident normal to the surface of β' grains i.e parallel to the hexagonal basal plane.

The observed difference in fracture toughness between the as sintered and heat treated materials may be partially related to the difference in the β' grain morphology. Although the amount of β' increased after heat treatment, the aspect ratio of elongated grains did not increase. Grain growth, associated with coalescence of β' grains, was observed, but the main influence on K_{IC} was the almost complete crystallisation of the residual glassy phase resulting in formation of a particulate morphology. The resulting interphase boundaries may approach a nearly solid/solid contact with little anisotropy in boundary energy and an absence of glass which previously initiated intergranular fracture. This results in the development of strong interfacial bonding between both α'/β' and α'/α' grains which would limit the extent of the crack deflection, debonding and grain pull-out toughening mechanisms Figure (7.3c). There is a minor volume expansion as the residual glass is devitrified to a Yb-garnet phase. The crystalline garnet phase has a thermal expansion coefficient ~ $8x\ 10^{-6}$, which is higher than that of silicon nitride. This generates an internal residual stress within the materials which may influence the crack path and further modify the toughness.

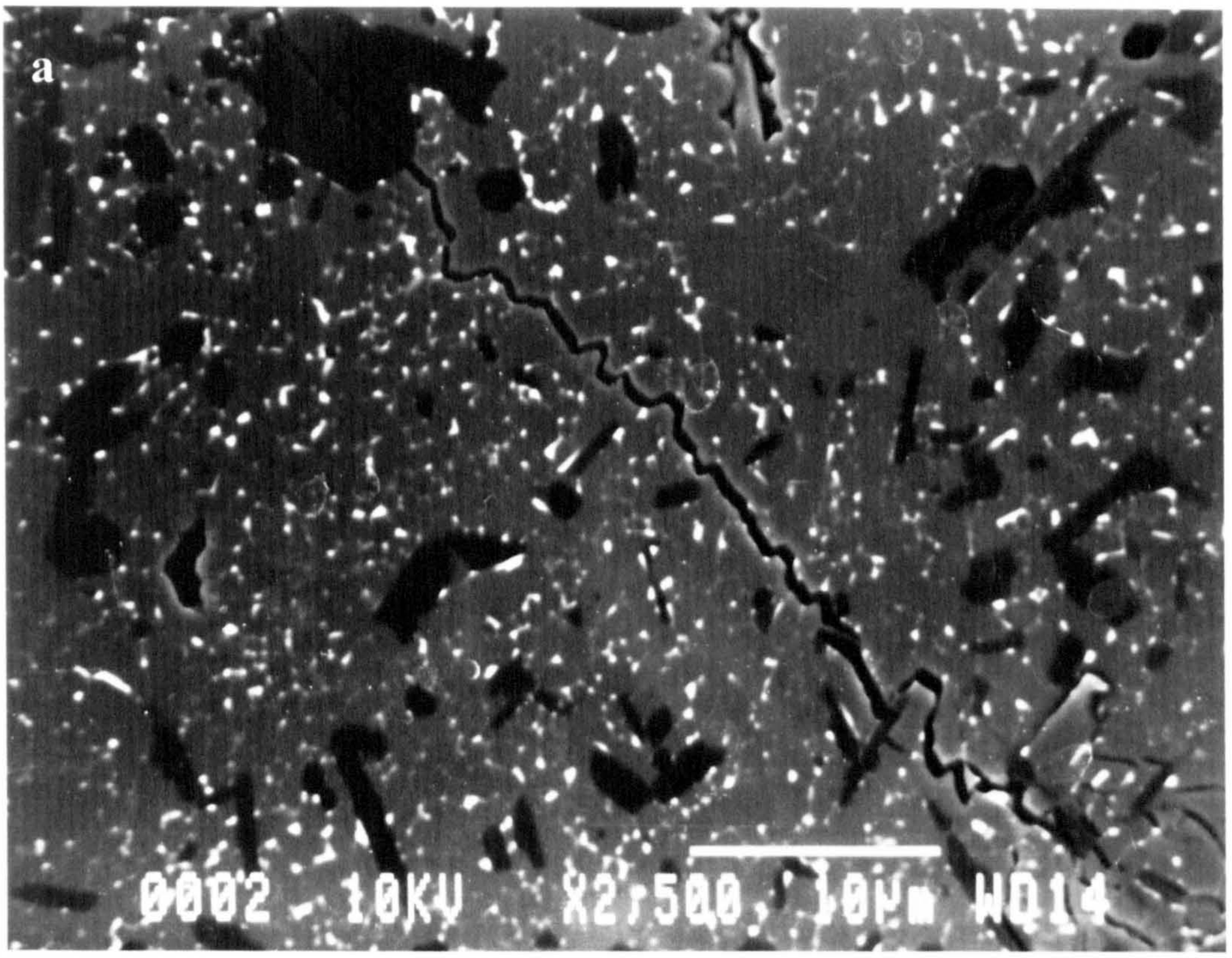

Figure 7.3. The crack propagation in compositions (a) as sintered Yb75B, (b) as sintered Yb75B5b (a) and (c) Yb75B5b as heat treated at 1450^0C

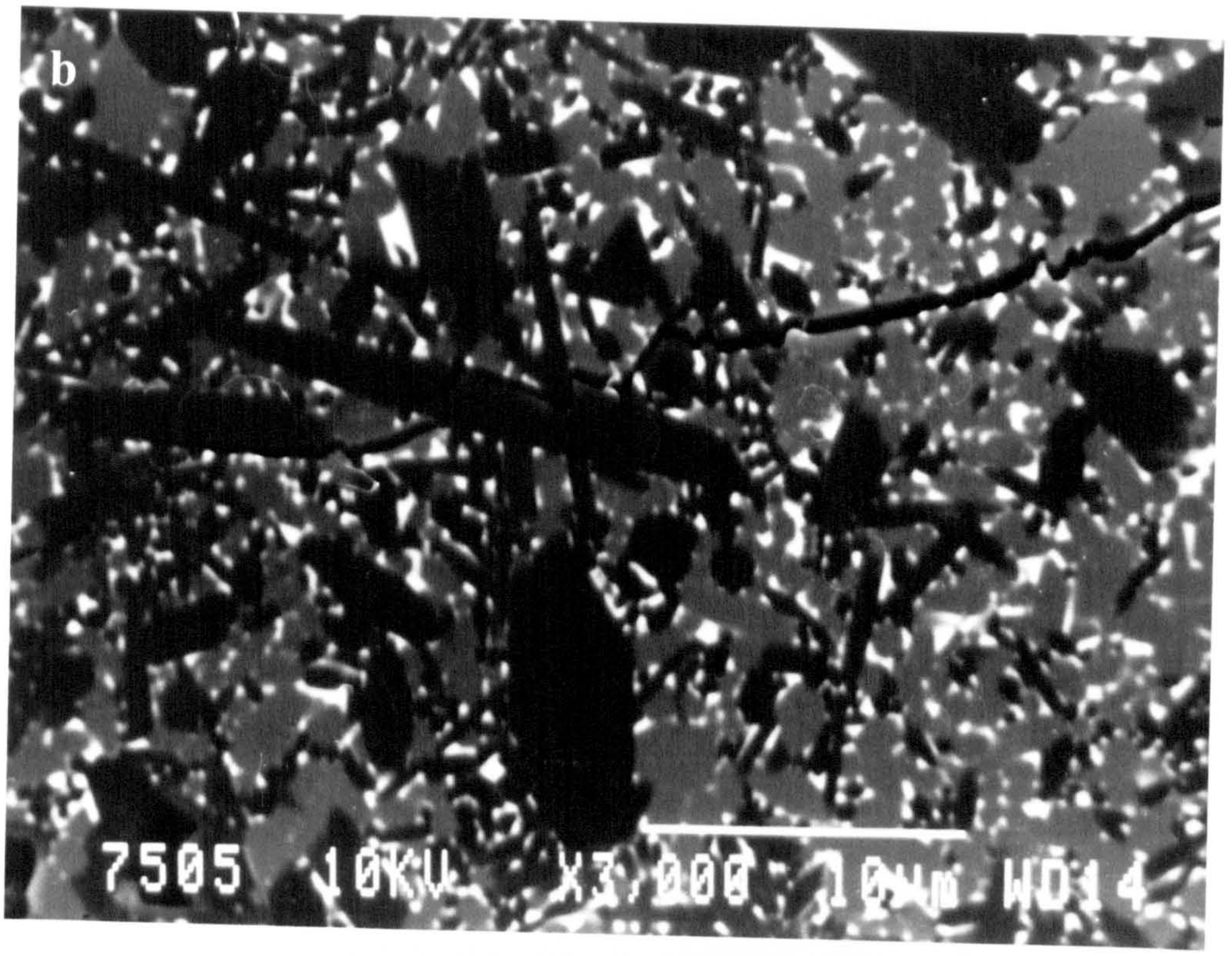
b
7505 10KV X3,000 10μm WD14

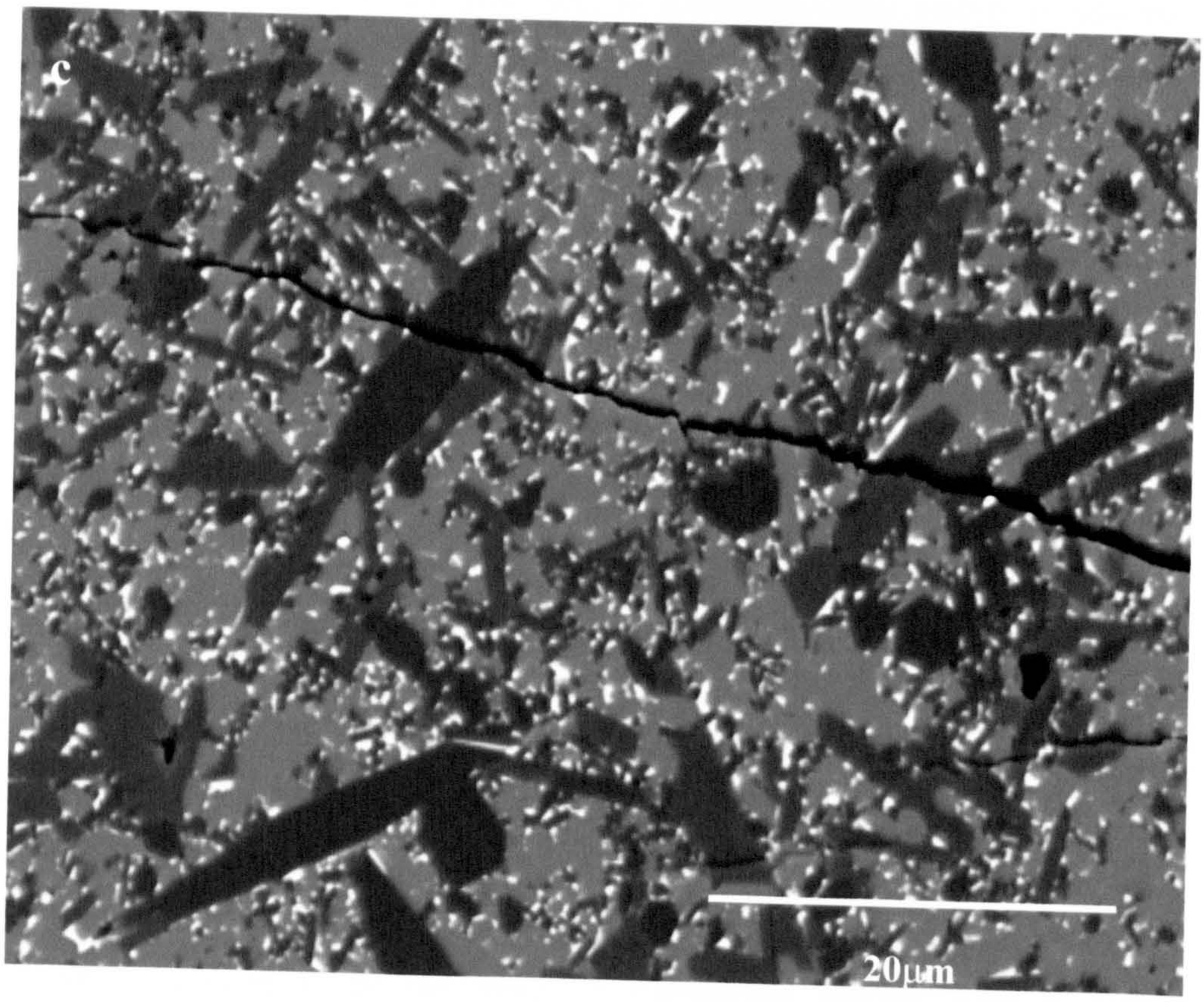
c
20μm

The values of fracture toughness obtained for the single cation and the mixed cation sialon were all found to be comparable with those reported for Ca and rare-earth sialon systems (Hewitt 1998, Shen et al 1996c, Shen et al 1997, Ekstrom et al 1997 and Falk et al 1997). The values however are lower than the accepted value of syalon 101 measured by notched edge beam technique (~7.7 $MPa.m^{1/2}$). If the results of Choi are assumed to be valid for the present materials then composition 20D2S (~5.2) could have K_{IC} value ~ 7MPa using SENB.

7.4- Oxidation Behaviour

7.4.1- Introduction:

The pressureless sintering of dense Si_3N_4 - based ceramics requires the use of sintering additives which give rise to a residual glass and/or crystalline intergranular phase which will have a detrimental effect on the high temperature properties. For example the resistance to oxidation will be reduced.

7.4.2- The Oxidation Results

Selected sintered compositions were oxidised in air at temperatures of 1350^0C and 1450^0C for periods of time of up to 96 hours and 120 hours, respectively. Oxidation was measured by weight change and the surface appearance of the tested samples.

It has been reported that the oxidation behaviour of Si_3N_4 follows a parabolic rate law of the type $(\Delta w/A_0)^2 = kt$ where Δw is the weight gain per unit surface area, k is the rate constant of parabolic oxidation and t is the exposure time. The parabolic oxidation behaviour exhibited by sintered Si_3N_4 ceramics was originally assumed to be the result of a protective surface layer of SiO_2 formed on the surface of the pure Si_3N_4, and the rate determining step is

oxygen diffusing through the SiO_2 layer. Singhal (1976) and Cubicciotti and Lau (1978) reported that the rate of oxidation is indirectly determining by cations out diffusing to the (initially) nearly pure SiO_2 layer, influencing the O_2 transport rate of this layer.

After 96 hours oxidation at 1350^0C, the optical surface appearance of the oxidised compositions within single cation Yb sialon materials remained almost unchanged whereas compositions containing mixed cations were coated with a thin white layer.

After oxidation at 1350^0C, the weight gain per unit surface area of the investigated compositions as a function of time is shown in Figure (7.4). It is evident that the oxidation weight gain of Ytterbium (single cation) sialon materials is very low and that no significant weight change was observed even for the composition containing a larger volume of a residual grain boundary glass (i.e Yb75B5un). The weight gain after 96 hours was recorded as 0.54 mg/cm^2 for composition Yb75B and 0.34 mg/cm^2 for composition Yb75B5un. The higher oxidation rate of Yb50B during the initial stage of oxidation (12 hours) may be due to the open porosity of the samples which showed relatively low density. In comparison with the mixed cation materials, the single cation sialons show better oxidation resistance. For example the Yb/Nd material shows a significant increase in weight with time, especially during the first 12 hours, with approximately a 2.7 mg/cm^2 weight gain observed after 96 hours exposure at 1350^0C.

Composition	Yb50B	Yb75B	Yb75B5b	Yb/Nd	Gd/Nd
$Kp[(mg^2/cm^4s^1)\times10^{-6}]$	1.1	0.6	0.1	20	12

Table 7.3 The parabolic rate constant after 96 hours oxidation at 1350^0C

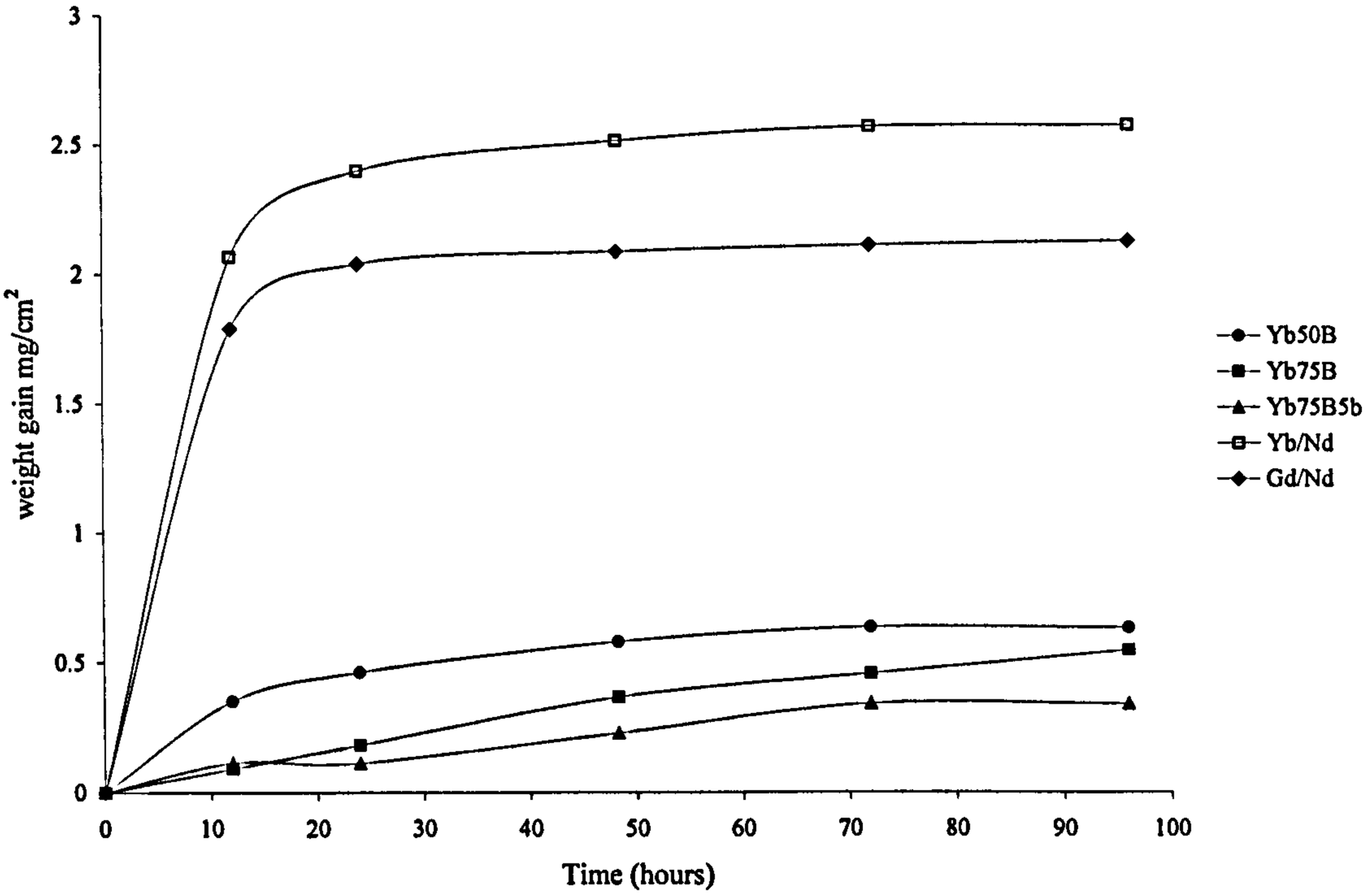

Figure 7.4. The oxidation curves of different α'/β' sialons obtained up to 96 hours at 1350^{0}C.

The squared weight gains recorded over time during oxidation at 1350^{0}C are shown in Figure (7.5). Almost all of the oxidation curves follow a parabolic rate law with rate constant values recorded after 96 hours as shown in table 7.3. A large deviation from the parabolic rate law was observed in the early part of the oxidation curves of the mixed cation compositions. A divergence from the parabolic rate law has, however, been observed in many investigations (Cinibulk and Thomas 1992, Gogotsi et al 1993 and Persson et al 1993). The rate of weight gain of the mixed cations materials was very high at the early stage (during the first 24 hours) and then continued with a rate nearly similar to that of the single cation materials. This can be attributed to the presence of a larger volume of low viscous intergranular glassy phase in these composition in the very early stage of oxidation treatment which results in a higher cations out-diffusion rate. After the 24 hours the oxidation rate in these composition is

reduced possibly due to the crystallisation of the grain boundary phase as well as the formation of a wider depleted zone as shown in section 7.4.3

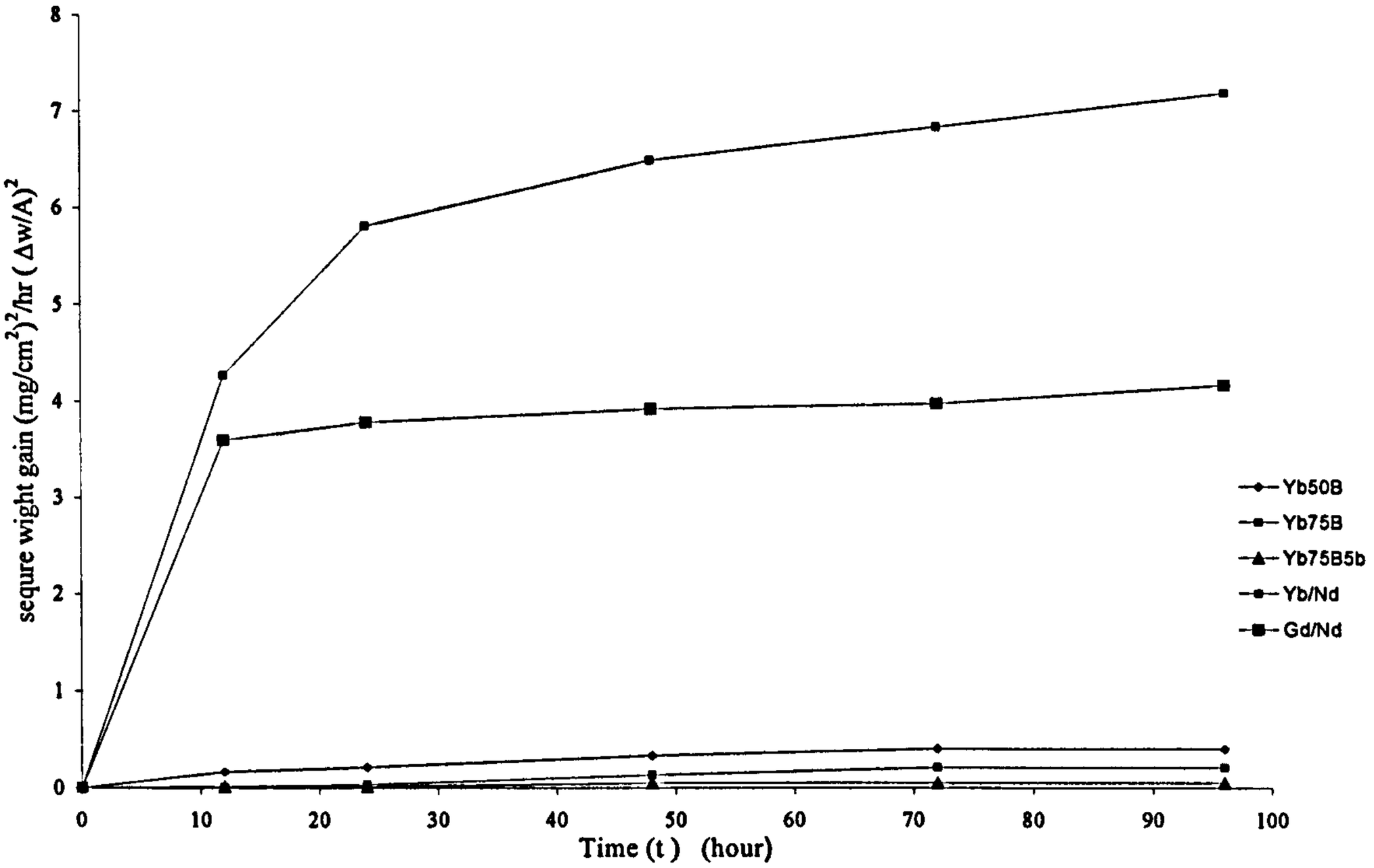

Figure 7.5 The relationship between weight gain per unit area and time during oxidation at 1350^0C.

As mentioned above a parabolic oxidation behaviour indicates the rate-determining step is a diffusional process associated with the migration of additive cations along the grain boundary phases to the SiO_2 layer (as well as the O_2 inward diffusion). Figure 7.6 Shows a schematic diagram for the oxidation process in sialon materials involving the outward diffusion of the cations from different intergranular phases. The presence of a continuous large volume of glass intergranular phase (region A in Figure 7.6a) provides the large reservoir from which the cations diffuse-out, thus resulting in higher oxidation rate.

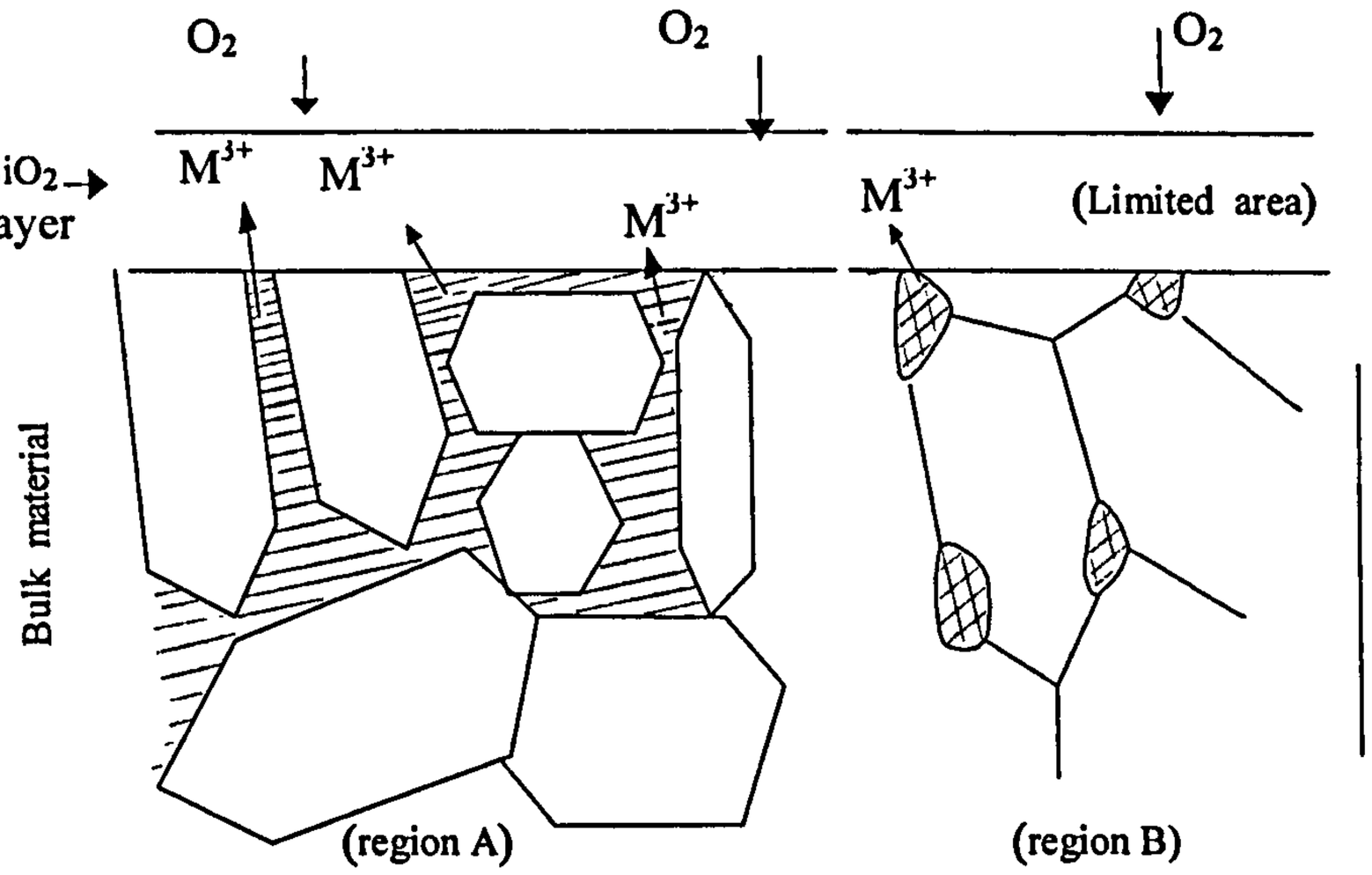

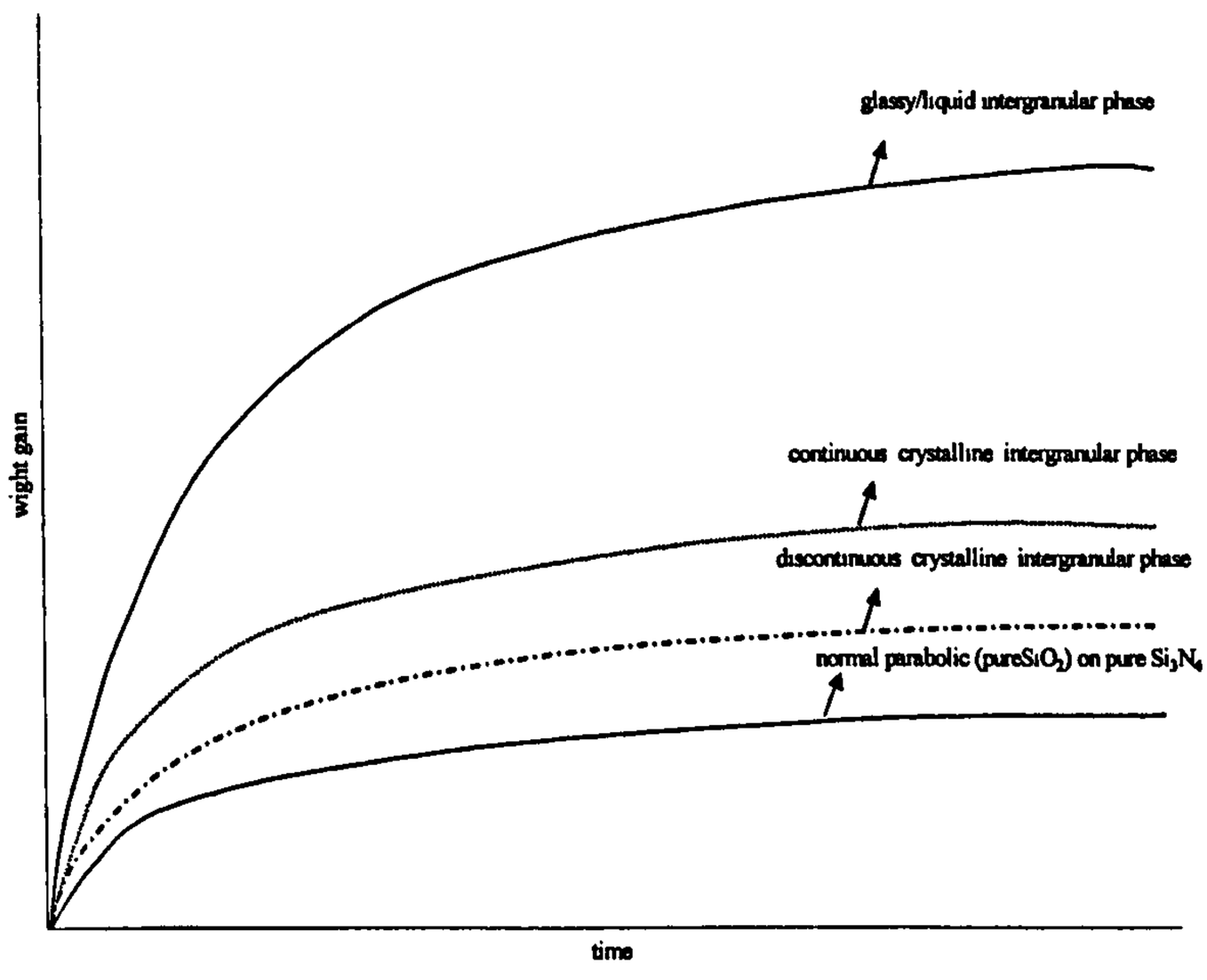

Figure 7.6. A schematic diagram for oxidation process of sialon materials

The continuous outward diffusion of cations causes a compositional gradient beneath the oxide layer; as observed from the long term oxidation (see next section); the extent of this zone, through which the diffusion of O_2 and cations is slow, is governed by the parabolic rate law. A deviation from the parabolic rate law is expected when the composition of SiO_2-rich layer is time dependent (i.e due to a depletion of cations in the near-surface intergranular phase as well as the crystallisation of this phase). This will be accentuated in the pre-heated materials with 'isolated' residual phase where the cation additives become effectively locked in position as shown in Figure 7.6a (region B).

The oxidation rate when carried out at a higher temperature of 1450^0C was more rapid compared with that at 1350^0C, due to the reduced viscosity and higher diffusion rates for both O_2 and cations in the oxide scale. After 120 hours of oxidation, the samples were highly oxidised and the surface was covered with a white layer containing gas bubbles, especially composition Yb50B and the mixed cation sialons. Attempts to measure the weight gain were made at this temperature but during the oxidation experiment a significant continuous decrease in weight was observed. This was due to partial loss of the more fluid glass layer during oxidation and fragmentation of the solidified layer on removal from the furnace.

The good oxidation resistance observed for the compositions prepared with Ytterbium doped sialon materials, may be related to the comparatively high eutectic temperature in the Yb_2O_3-Al_2O_3-SiO_2 system at about 1500^0C (Murakami 1993), which is 150^0C higher than the oxidation temperature (1350^0C). This implies that no liquid phase should be formed in the oxide scale or in the intergranular phase of the single ytterbium doped sialon system. The presence of liquid is assumed to facilitate the inward diffusion of oxygen and outward diffusion of the metal cations to the oxide layer. Apart from the eutectic temperature the crystallisation of the grain boundary glassy phase is expected to occur during the initial stage of the oxidation process and because of the slow rate of diffusion through the crystalline grain boundary phase this will result in better oxidation resistance. It might also be due to the reason

that in Yb-sialon system the Yb^{3+} stabilise the α' phase and that the oxidation does not extract the Yb^{3+} cation from α', furthermore α' in this system does not decompose into the β'-sialon and melilite phases. As observed in chapter 5 the crystallisation product formed in the Yb –sialon system was YbAG phase which is a stable phase compared with the oxynitride melilite. The latter phase is known to be easily oxidised even at temperatures as low as 900^0C (Patel 1988). The rate of oxidation is expected to increase in the sialon system where the melilite phase is formed. However Mandal (1994) reported that aluminium-substituted melilite phase (M') produced in the Ln-sialon system showed a good oxidation resistance at temperatures between 1000 and 1500^0C.

7.4.3- Microstructure of the Oxidised Materials.

The microstructures of the oxide scales formed after oxidation at different temperatures were investigated using a SEM. The back-scattered electron images of the cross section of compositions Yb75B and Yb75B5un after 24 hours and Yb75B after 96 hours of oxidation at 1350^0C, are shown in Figure (7.7) and Figure (7.8) respectively. It is clear from the micrographs that after 24 hours of oxidation no significant change was observed in the bulk microstructure apart from the crystallisation of the grain boundary phase and a very thin oxide scale formed in both compositions (Figure 7.7a and 7.7b). The scale covers a small zone of the near surface microstructure depleted in the cations from the grain boundary region. According to the X-ray phase analysis of the oxidised sample Yb75B, the surface of the scale contained $Yb_2Si_2O_7$ (this appears as a white phase in the oxide scale) and the cristobalite (SiO_2) phase with a dark contrast.

After a long period of exposure of ~ 96 hours at the same oxidation temperature of 1350^0C, the scale and the depleted zone are much thicker. The micrograph in Figure (7.8a) shows the cross-section of composition Yb75B as an example. It is obvious from the micrograph that the structure consists of three distinct

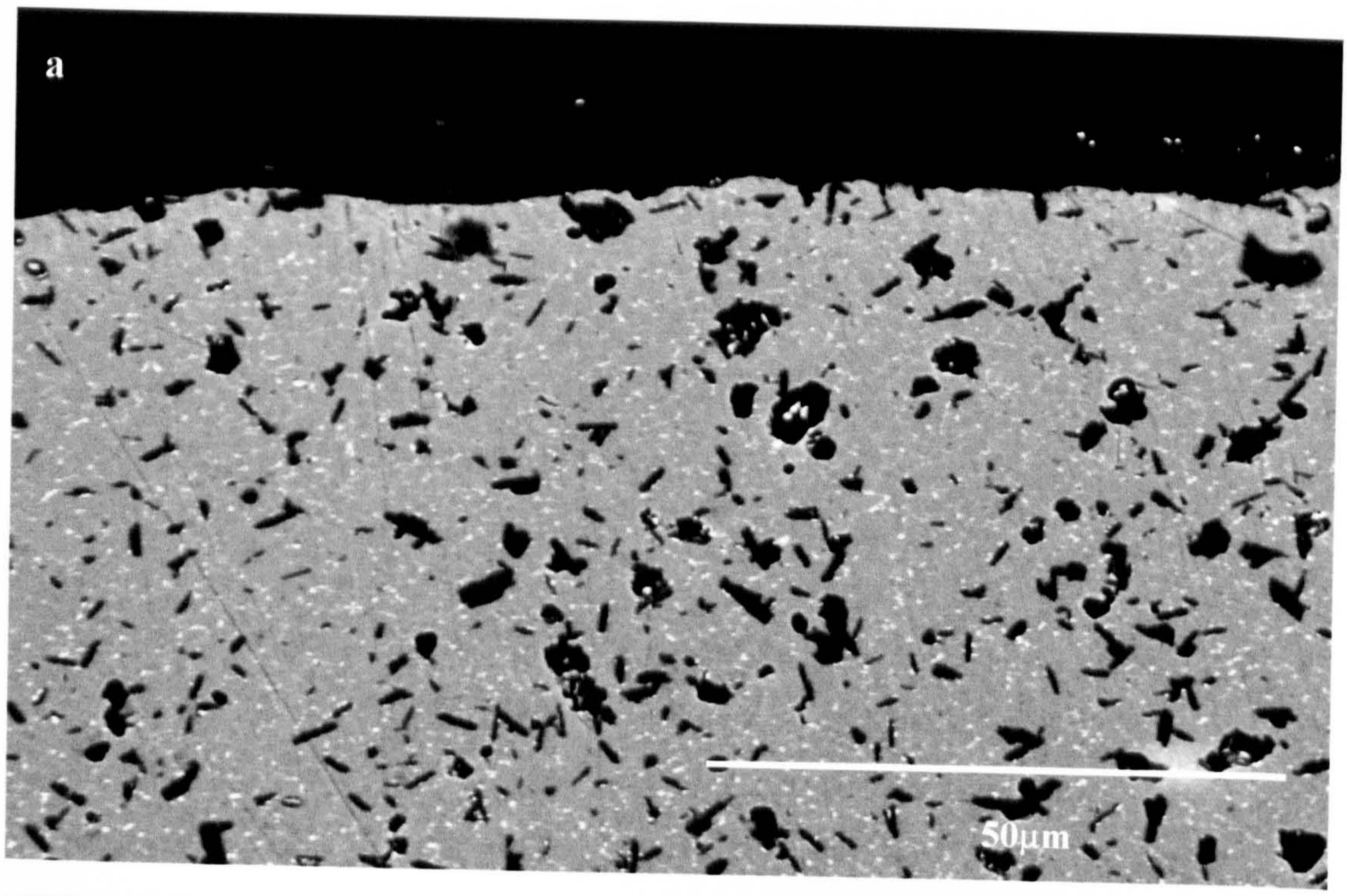

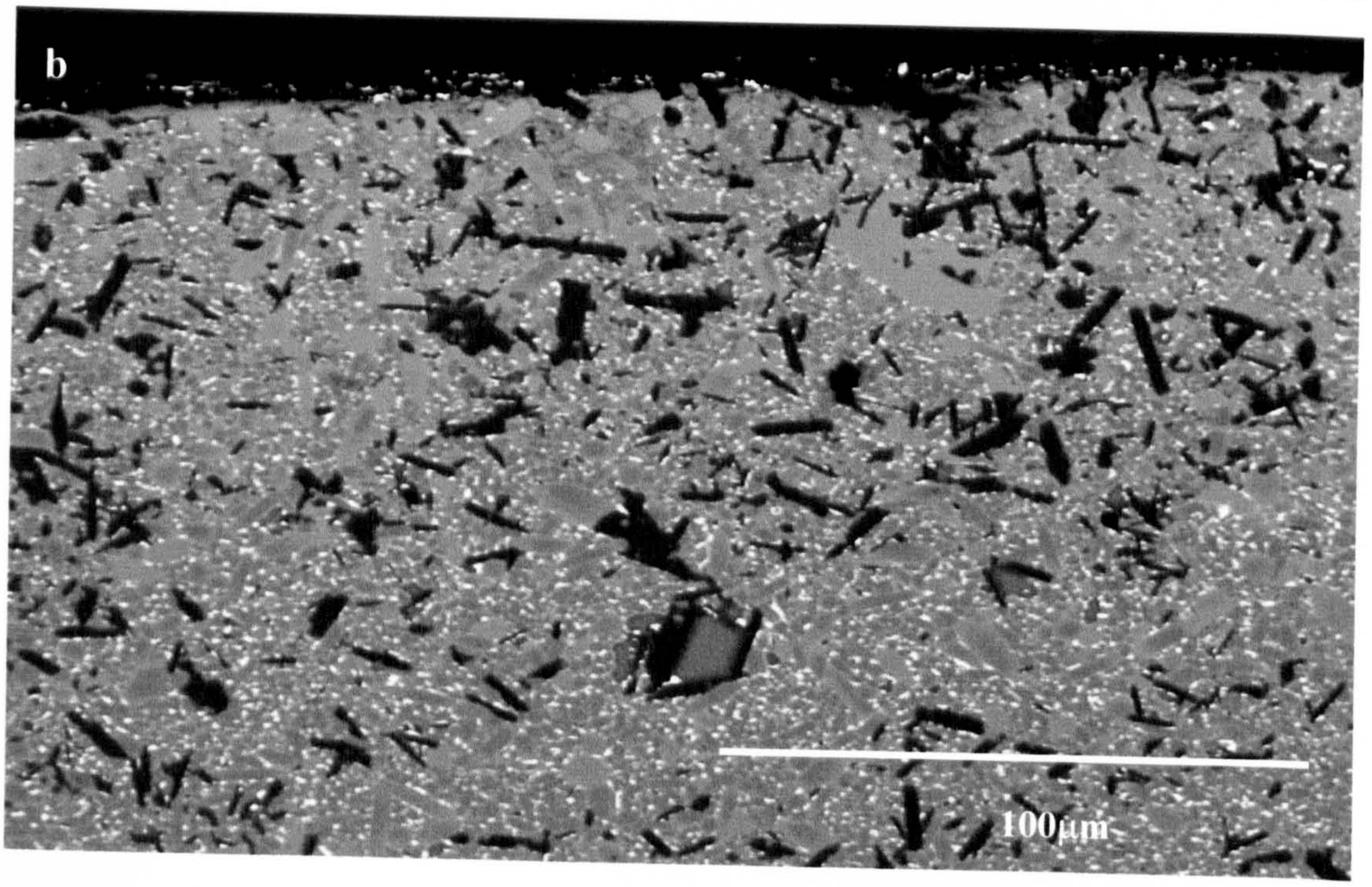

Figure 7.7. SEM micrograph of compositions (a) Yb75B and (b) Yb75B5un after oxidation at 1350^0C for 24hr

zones from the centre to the surface. The bulk ceramic zone exhibited no significant change compared with the unoxidised materials. An approximately 10μm wide zone developed beneath the oxide scale which was depleted in the heavy element Ytterbium. This region can be divided into two different zones. An approximately 4μm thick zone contains no intergranular phase, but only α' and β'-sialon phases present in approximately the same proportion as in the bulk region, which suggests that no decomposition of the α' phase has occurred. As can be seen from micrograph (7.8 b), a more detailed view of the oxide area, the depletion of the heavy metal ions from the grain boundary is clearly seen as channels found between the α'-grains. This implies that the residual glass phase does not fill the space between the grains and indicates a diffusion of the metal elements from the intergranular phase. The second zone, approximately 6 μm thick which is adjacent to the oxide scale does not contain any α'-sialon but only β'-sialon. This indicates the out diffusion of Yb^{3+} cation from α'-sialon to the oxide layer as well as from the grain boundary results in the formation of a β' rich zone due to α' de-stabilisation. A continuous thin layer of cristobalite is present between these two regions. The outer scale has a white contrast due to partial crystallisation, because of the high initial concentration of the cations depleted from the grain boundary, as well as from the α' sialon near to the surface.

The microstructure of the cross sections of compositions Yb/Nd after long term oxidation of ~96 hour at 1350^0C was also investigated Figure 7.9. This Yb/Nd shows that the oxide layer formed and the depleted zone were much thicker than that of single cation compositions. The oxide scale is porous and contained large cavities which is a result of the formation of nitrogen gas bubbles from Si_3N_4 oxidation. A continuously cracked region develops through the interface between the oxide layer and the cation depleted zone beneath.

The oxidation rate in all compositions at 1450^0C was more rapid and this is clearly observed by a comparison of the microstructures of the cross sections

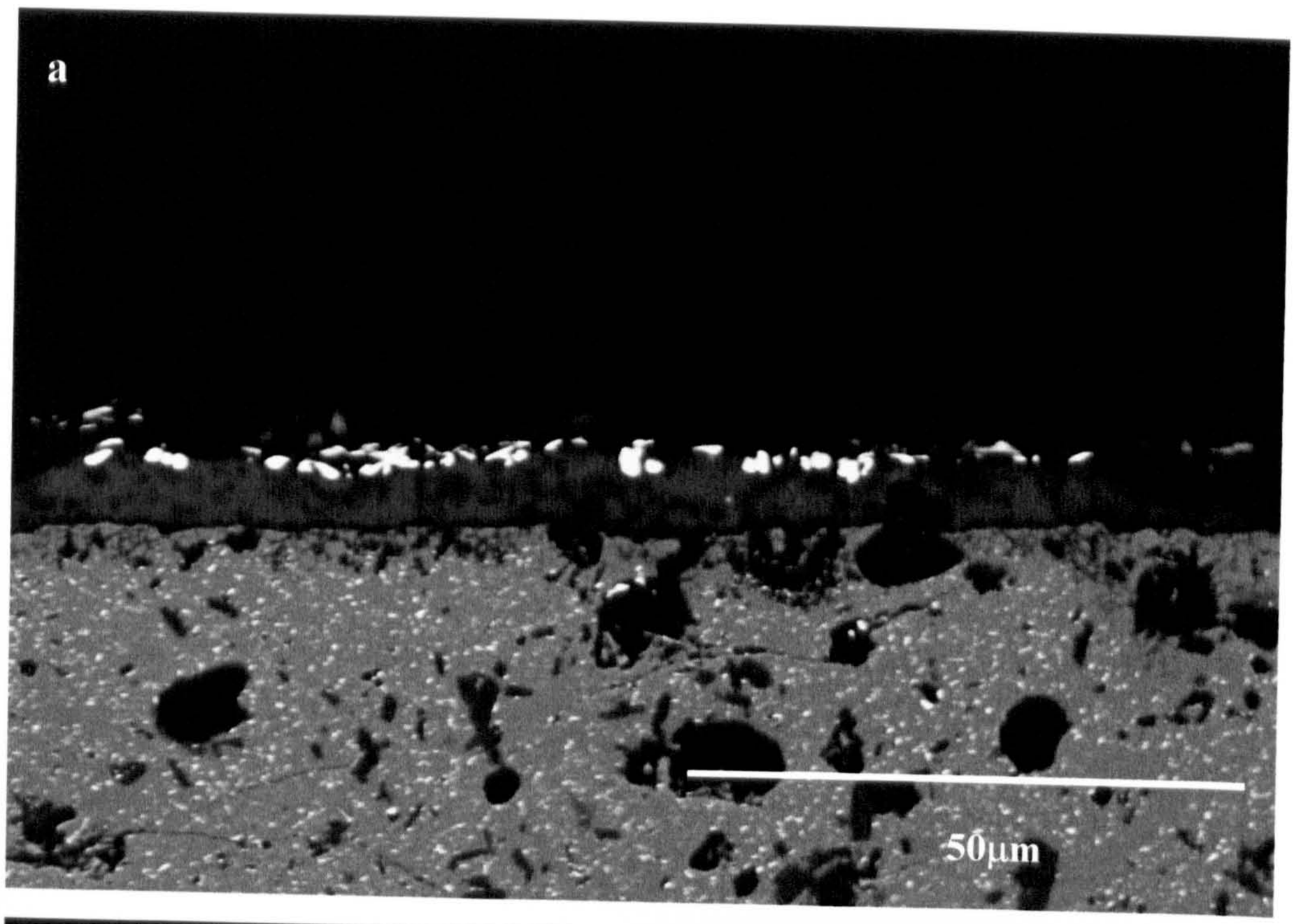

Figure 7.8. The micrographs of composition Yb75B after 96hr oxidation at 1350^0C

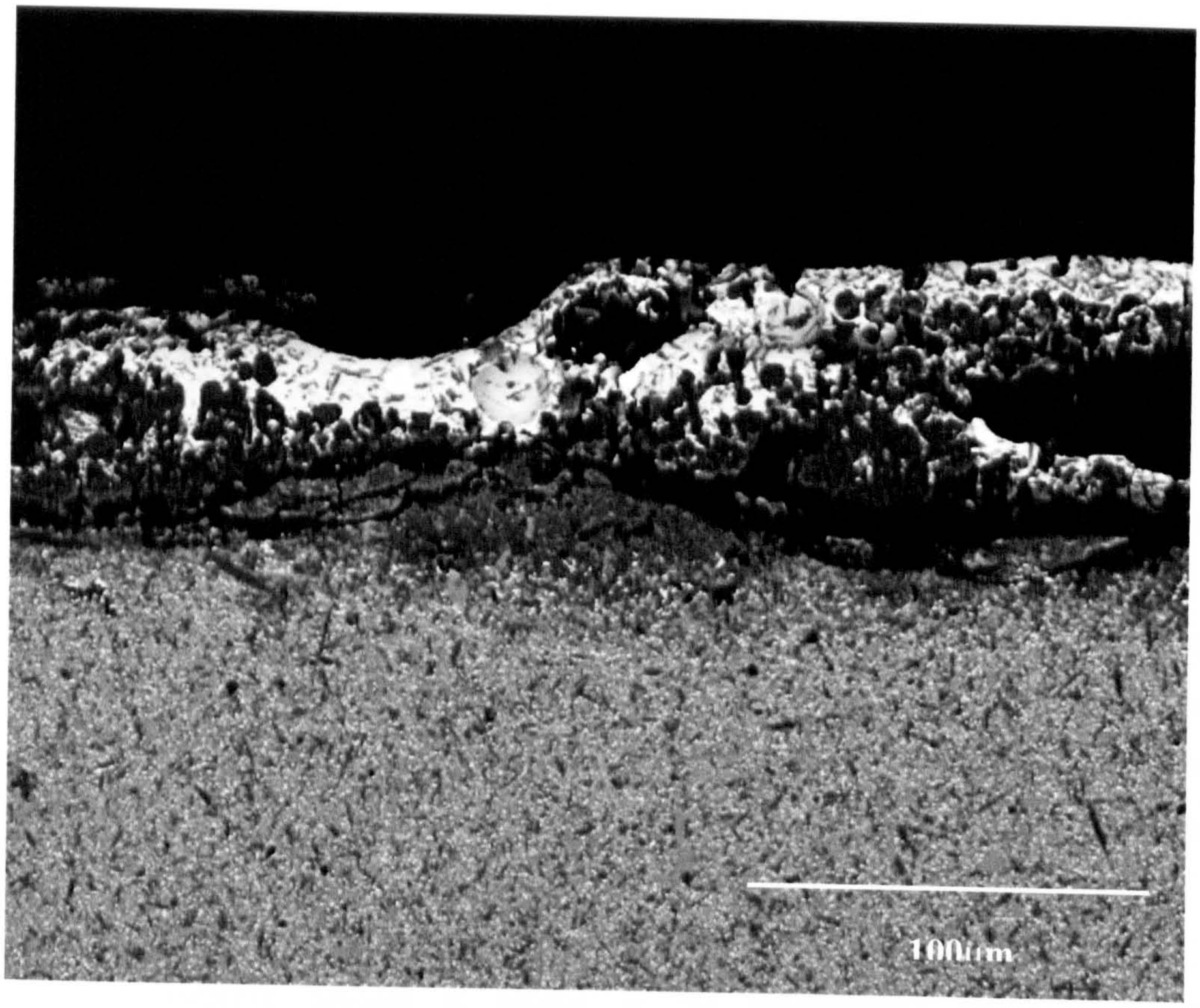

Figure 7.9 The SEM image of composition Yb/Nd oxidized at 1350^{0}C for 96hr

obtained from compositions oxidised for 120 hours at 1450^{0}C with those at 1350^{0}C. The oxide scale and the depleted zone are much thicker and a catastrophic oxidation was observed for composition Yb50B and the mixed cation compositions. Figure (7.10), shows micrographs of the cross section of compositions Yb75B and Yb/Nd. In figure 7.10a, a micrograph of composition Yb75B, a coherent silicate layer is formed with a thickness ranging from approximately 6μm to 20μm. An EDAX analysis of this layer revealed that it contains $Yb_2Si_2O_7$ as well as dark needles of the mullite ($3Al_2O_3.2SiO_2$) phase, possibly formed as a result of increasing the Al concentration in the glass phase due to the enhanced cristobalite formation. This cristobalite formed as a layer on the boundary between the oxide scale and the porous depleted zone which contained only the β' sialon. The oxide layer contained many large bubbles due to a higher rate of nitrogen evolution and reduced viscosity of the silicate liquid at the higher temperature.

Figure (7.10b) is a micrograph of composition Yb/Nd which severely oxidised. The oxide layer formed is much thicker but due to the surface being badly ruptured, thickness measurements were not possible. Excessive crystallisation of cristobalite and rare-earth silica within the oxide layer was generally observed. The depleted zone is wider and contained a high level of porosity. No clear border existed between the depleted zone, bulk material and regions where α' transformed into β'.

The oxidation process is similar to the mechanisms discussed by Singhal (1976), Lewis and Barnard (1980) and Babini et al (1984). Initial oxidation occurs by the reaction of sialon phases with atmospheric oxygen. This forms a silica (SiO_2) layer on the surface which creates a chemical difference between the oxide layer and the bulk. To equilibrate the compositional differences, cations such as M, Al (and impurities) will diffuse out from the grain boundary and the α' phase to the oxide layer. This process causes the crystallisation of the metallic silicate crystal and with reduced viscosity, the mechanisms proceed more rapidly. The oxide scales were severely disrupted due to the evolution of large nitrogen bubbles on the scales causing the oxide layer to fall off.

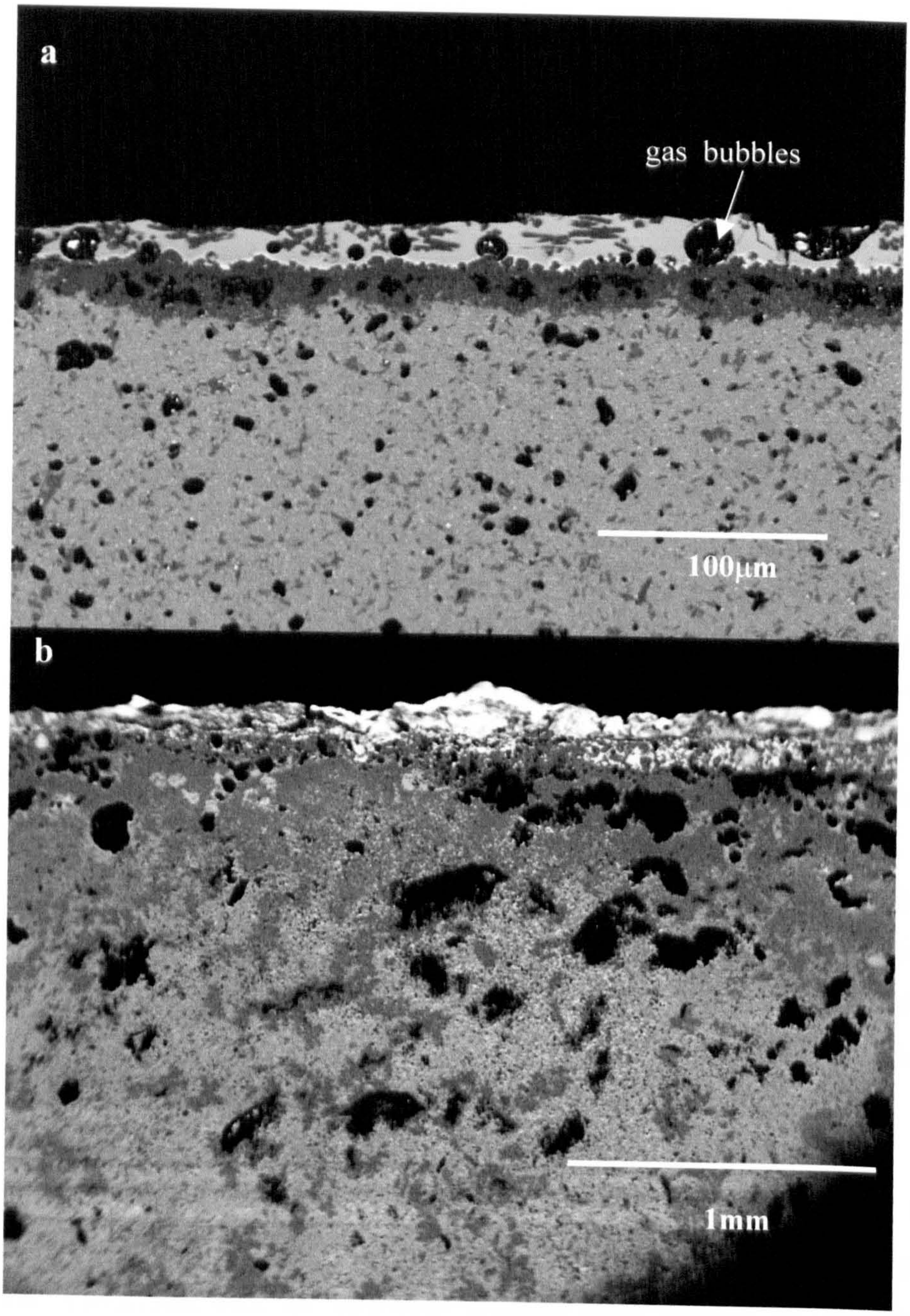

Figure 7.10 The SEM images of compositions Yb75B and Yb/Nd oxidized at 1450^0C for 120hr (a) Yb75B and (b)Yb/Nd

The results obtained from the long term oxidation at 1350^{0}C and 1450^{0}C demonstrate the remarkably good oxidation resistance of the single cation compositions compared with the mixed cation compositions. For example composition Yb75B exhibited a high oxidation resistance compared with mixed Yb/Nd. This may be due partially to the presence of a minimal amount of the grain boundary phase in Yb75B. As already shown in the previous chapter the volume fraction of the intergranular phase increased when Yb/Nd was used as a stabiliser for α'-sialon. The presence of a larger amount of the residual glass phase provides a larger volume within which diffusion can occur and a larger reservoir of cations, so that the oxidation rate is higher. It is unlikely, however, that the smaller volume of the intergranular phase alone can account for the much better oxidation behaviour of the single cation composition Yb75B. The composition of the intergranular phase is also expected to influence the oxidation resistance. The refractory nature of the grain boundary phase mainly determines the initial diffusion rate of cations and anions along the boundary and therefore the oxidation resistance of the materials. Shelby (1990) reported that the rare-earth aluminosilicate glasses show both increasing glass transition and softening temperature with a decreasing radius of the rare-earth ion. Therefore a greater refractory nature of grain boundary glassy phases is expected for materials sintered with rare-earth oxide having a smaller cation radius. Considering the small volume and a higher viscosity of Yb glass compared with the Nd-containing glass, one would also expect that compositions containing mixed cations will exhibit a higher oxidation rate than the pure single cation Yb sialon materials.

The importance of the intergranular phase composition is also obvious by comparing composition Yb75B5un with the other compositions. For example composition Yb75B5un, with an estimated residual glass content of 15% and α' content of approximately 64%, showed better oxidation behaviour than Yb50B (63% α') and Yb75B (2% α'), both of which appeared to have a significantly smaller volume of the intergranular glass phase (approximately 5%). Yb/Nd also has a slightly lower volume of the intergranular phase ~11% and a much higher α' content. The EDAX analysis in section 5.1.1.3,

indicated an increased silica content in the residual glass of Yb75B5un, which suggests that the viscosity of the intergranular glass may be expected to influence resistance to oxidation. It should be noted that the above discussion is mainly relevant to initial oxidation where the largest non-parabolic oxidation occurs (see Figure 7.4). As discussed in chapter 5, the continuous heat treatment results in complete crystallisation of the intergranular phase, thus other factors may affect the oxidation such as the phase stability (i.e the crystalline intergranular phase and the α').

CHAPTER 8

CONCLUSIONS

8.1- Introduction

The main objectives of this research were to investigate the possibility of controlling the microstructure of α'/β' sialon ceramics by compositional change. The research also compared and developed an understanding of the thermal stability of the α' sialon phase using single cation Yb or mixed cation Yb-Nd and Gd-Nd as the stabilising elements for α'. A brief investigation was also carried out into the room temperature mechanical properties of the range of materials in relation to the observed microstructural features together with a study of the high temperature oxidation behaviour.

The initial compositions of the starting materials were calculated using a computer program taking into consideration the oxide layer present on the starting nitride materials. The compositions were tailored with the assumption that all the rare-earth stabilising cations will incorporate within the α' structure, to form composite α'/β' materials with negligible residual cation-containing glass.

It has been demonstrated in the previous chapters that an investigation of phase contents, and microstructural and mechanical properties leads to the following conclusions.

8.2- Yb-Sialon Materials

A range of sialon materials containing Yb as a stabilising cation were prepared using pressureless sintering techniques and were then characterised in terms of densification behaviour, the change in phase content, the microstructure resulting from a variation of Yb level (resulting from variation of Yb alumino-silicate glass) and mechanical properties. In pressureless sintering the amount of the

liquid phase at the sintering temperature must be high enough in order to enhance the densification. After sintering the compositions prepared with a low Yb cation level (represented by compositions prepared in series A) have resulted in poor densification and therefore a high level of porosity. Increasing the Yb content by increasing the ytterbium alumino-silicate glass in the starting composition (series B) has resulted in a greater fraction of the liquid phase at the sintering temperature. This consequently increases densification but at the same time results in more residual glass in the final ceramics.

The as sintered α'/β' phase ratio is dependent upon the stabilising cation content. An increase in the amount of Yb alumino-silicate glass to the starting composition was found to increase the α' phase content. The amount of α' phase in the as-sintered Yb single cation sialon material is always higher than that predicted from the over-simplistic computer program. This is due to the α' composition limit (near m=1) being closer to the average initial composition than predicted.

Microstructural studies (in agreement with XRD) showed that the major crystalline phases formed in all the as-sintered materials were an equiaxed α' sialon phase and a small amount of β' (and/or 12H polytypoid). The volume fraction of the residual intergranular glassy phase formed after sintering was also small and increased slightly as the glass content increases in the starting compositions.

The compositional analysis of α' and β' sialon phases revealed that the substitution level in the β' phase (z-value) and in the α' phase (m-value) significantly deviated from the predicted value. The α sialon compositions show a good consistency in the m-value, with a linear range near m=1, parallel to the β' composition line in the Janecke prism. The larger α'-sialon region in the Yb system has moved the maximum oxygen content to a higher value which is in good agreement with the overall composition. An EDAX analysis of the glassy phase showed the presence of a large fraction of Al and Yb in addition to Si.

The addition of silica (SiO_2) to the high α'-sialon in the Yb system significantly improves the densification and promotes the formation of more β' phase in the as sintered materials. This occurs as a result of the increased liquid phase content at the sintering temperature and a shift in O/N ratio towards the β' composition line.

The microstructure investigation by SEM revealed that significant variations in the phase content and grain morphology have been observed as a result of SiO_2 addition. More elongated β'-sialon grains occur in compositions with SiO_2. This implies that the microstructure is dependent on the amount and composition of the liquid phase formed at the sintering temperature, allowing less-constrained growth of prismatic β' crystals. The volume fraction of the residual Yb-rich intergranular glassy phase was also observed to increase with SiO_2, as predicted from α'/β'/liquid phase relations in the behaviour diagram.

The addition of β-Si_3N_4 as a seeding agent was made in order to encourage β'-sialon formation. An addition of up to 50 wt% β seeds to the starting composition had a very small effect on the α'/β' phase ratio and on the phase morphology (unlike that observed in systems with less-stable α', such as Nd-sialon). Although the addition of β Si_3N_4 seeds to compositions containing added-SiO_2 did not change the α'/β' phase ratio, the seed crystals significantly enhanced the grain size of the β' and α' sialon phases due to heterogeneous nucleation and selective grain coarsening.

8.3- Post Sintering Heat Treatments

Post sintering heat treatments of single cation Yb α'/β'-sialon compositions, at various temperatures in the range between 1200-1600^{0}C and for different duration of time, showed that the Yb sialon materials exhibit excellent thermal stability compared with other rare-earth α'/β' sialon ceramics. The significant effect of the heat treatments was the crystallisation of the

intergranular glassy phase in the form of Yb garnet phase. This phase crystallised at a temperature as low as 1200^{0}C and was found to be stable up to 1600^{0}C in the single cation Yb α'sialon, even after 168 hours. In compositions containing a high α' content and a small amount of intergranular glass phase, the α'/β' grain morphology and phase content remain essentially unchanged even after 168hr.

The amount of the residual glassy phase had the most significant influence on the thermal stability of the Yb α'/β'-sialon. The initial rate of the α' → β' transformation was more pronounced in materials containing a larger volume fraction of the residual glass. The crystallisation of a larger volume of residual glass increases the competition for the α' stabilising cations. However the influence of heat-treatment/ glass crystallisation is much smaller than in other rare-earth sialon systems such as Nd and Sm α'. It may be concluded that the main de-stabilising influences in these systems results from thermodynamic rather than kinetics, factors and is dictated by the relative stability of α' and crystallising grain boundary phases (i.e their competition for the rare-earth cations).

8.4- Mixed-Cation Sialons.

In order to improve sinterability and , microstructure, with the possibility of stabilisation of larger cations in the α'-structure, compositions containing a combination of light and heavy rare earths (Yb-Nd and Gd-Nd) have been prepared using pressureless sintering. It was found that the type of stabilising cations used influence the density and phase morphology of the as sintered material. The X-ray diffraction analysis revealed α' sialon to be the dominant phase in both compositions, with minor contributions from β' and an AlN polytype. The energy dispersive X-ray spectroscopy (EDAX) analysis confirmed the presence of both cations together within the α' crystals. The smaller cation Yb^{3+} and Gd^{3+} enter more easily into α' structure than the larger Nd^{3+}

therefore Yb^{3+} and Gd^{3+} content is higher than that of Nd^{3+} in α' grain and on the other hand, more Nd^{3+} is present in the grain boundary phase.

After the initial 24 hours post sintering heat treatment at 1450^0C both compositions revealed a small α'→ β' transformation. Extended heat treatment up to 168hr resulted in further α'→ β' transformation. The transformation was accompanied by dissolution of $RAlO_3$ and crystallisation of Melilite in both compositions. This result is in contrast to that observed for the single cation Yb-sialon (chapter 5) where α' showed a greater stability over extending the heat treatment up to 1600^0C. The critical difference between the garnet ($R_3Al_5O_{12}$) and the aluminate ($RAlO_3$) phases is R/ Si/Al ratio and the relative stability of YbAG phase which exists up to high temperature, compared with the $RAlO_3$ which dissociates at lower temperature. The transformation in the mixed cation materials proceeds at lower rate than single cation Nd-sialon system where a continuous α'→ β' transformation was observed and melilite formed as the crystallisation product.

8.5- Mechanical Properties and Oxidation Resistance

The room temperature mechanical properties of the selected α'/β' Sialons were related to the microstructural characteristics. Hardness and fracture toughness were found to depend not only on the α'/β' phase content in the microstructure but also to the volume fraction of the residual glass phase, the porosity level, the morphology of β' phase and the crystalline grain boundary phase.

In the as sintered compositions, the hardness value was observed to increase with increasing α' phase content, dense single cation Yb sialon composition shows the highest hardness with an average value of 18 GPa. The mixed cation compositions possessed a slightly lower value, this was attributed to the increased amount of the intergranular glass phase in those compositions. The variation in the cation size has negligible effect on the hardness value. The fracture toughness was found to depend mainly on the amount of β' and its

morphology. The highest K_{IC} ~5.2 Mpa.$m^{1/2}$ was measured for compositions containing a combined SiO_2 and β Si_3N_4 addition, which results in larger prismatic β' grains which enhance grain bridging and 'pull-out' contributions to the toughness.

In the as-heat-treated compositions the hardness was found to increase slightly whereas the fracture toughness decreased. The reduction of the fracture toughness was partially related to the difference in the β' grain morphology. Although the amount of β' increased after heat treatment, the aspect ratio of elongated grains did not increase. Grain growth was associated with coalescence of β' grains. In addition to the development of stronger interfacial bonding between both α'/β' and α'/α' grains which would limit the extent of the crack deflection, debonding and grain pull-out toughening mechanisms.

The oxidation process in the rare earth α'/β' sialon systems is determined by the outward diffusion of cations mainly from the grain boundary phase. The Yb single cation materials exhibited good resistance to oxidation at 1350^{0}C and 1450^{0}C compared with the mixed cation materials. This was attributed to the lower volume and composition of the intergranular phase, stability of α' phase and the crystallisation product (YbAG) formed during the oxidation process.

Thus it can be concluded from the present work that a series of α'/β' sialon materials have been successfully densified without application of pressure during sintering using either single cation (Yb) or mixed cations (Yb/Nd and Gd/Nd) as a stabiliser for α'-phase. The single cation Yb α'/β'-sialon system appears to have a potential for high temperature application, judging by the excellent stability of α' phase in this system and the ease of crystallisation of the intergranular glassy phase in the form of garnet phase, which has been shown to be a stable up to 1600^{0}C.

Composition Yb75B may be chosen as the best composition which combined good mechanical properties and good oxidation resistance in addition to the high stability of α'-sialon in this system. This composition, however, did not

reach the theoretical density. In the mixed cation compositions, despite the improved sinterability, the α' sialon phase was relatively unstable compared with the single cation Yb-sialon compositions. Thus it is possible to suggest that a composition with mixed cation Yb/Nd containing less than 50% Nd may be the optimum composition to develop a fully dense microstructure which is stable at high temperatures.

REFERENCES

Anstis, G. R., Chantikul, Lawn, B.R. and Marshall, D.B (1981), J. Am. Ceram. Soc., 64, P. 539

Babini, G.N, Bellosi, A. and Vincenzini, P. (1984), J. Mater. Sci., 19, P. 3487

Bandyopadhyay, S. and Mukerji, J. (1987), J. Am. Ceram. Soc., 70, P. C273.

Bartek, A., Ekstrom, T., Herbertsson, H. and Johnsson, (1992), J. Am. Ceram. Soc. 75, P. 432

Becher, P.F., Hsueh, C.H., Angelini, P. and Tiegs, T.N (1988), J. Am. Cerm. Soc.,71, P. 1050

Becher, P.F. (1991), J. Am. Ceram. Soc., 74, P. 255

Bown L.J., Carruthers T.G. and Brook L.J. (1978), J Am. Ceram. Soc. ,61, P. 335

Cao, G.Z. and Metselar, R. (1991), Chem. Mater., 3(2), P. 242

Chatfield, C., Ekstrom,T. and Mikus, M. (1986), J. Mater. Sci. ,21, P. 2297

Choi, S.R. and Salem, J.A., (1994), J. Am. Ceram. Soc.,77, P. 1042

Chen, I, W and Roesenflanz, A., (1997), Nature,Vol. 389, P. 701

Cheng, Y.B. and Thompson, D. (1994 a) J. Euro. Ceram, Soc, 14, P. 13

Cheng, Y.B. and Thompson D.P. (1994 b), J. Am. Ceram. Soc., P.343

Cinibulk, M.K. and Thomas, G., (1992) J. Am. Ceram. Soc. P. 2044

Cubicciotti, D and Lau, K.H. (1978), J. Am. Cerm. Soc. 61, P. 512

Drew, P. and Lewis, M.H. (1974), J. Mater. Sci., 9, P. 261

Drew R. A. L., Hampshire S and Jack, K. H. (1983), Progress in Nitrogen Ceramics. The Hague, The Netherlands. Martinus Nijhoff, P. 323

Edwards, A.J., Elias, D.P., Lindley, M.W., Atkinson, A. and Moulson, A.J., (1974), J. Mater. Sci., 9 P.516

Ekstrom, T., Falk, L.K.L. and Shen, Z. (1997), J. Am. Ceram. Soc., 80, P. 301

Ekstrom T., Jansson K., Olsson P.O. and Persson J (1991), J. Euro. Ceram. Soc.,8, P. 3

Ekstrom, T., Kall, P. O., Nygren, M. and Olsson, P. O. (1989), J. Mater. Sci. 24, P1853

Ekstrom, T. and Nygren, M. (1992), J. Am. Ceram. Soc., 75, P. 259

Ekstrom, T., and Persson, J. (1990), J. Am. Ceram. Soc., 73, 2834

Ekstrom, T. and Shen, Z.-J (1995), 5th international Symposium on Ceramic Materials and Components for Engines, Eds. D. S. Yan, X. R. Fu and S. X. Shi, World Scientific, Singapore, P. 206

Ekstrom, T. (1992), J. Hard Mater. Soc.,3(2), P. 109.

Faber K. T. and Evans A. G. (1983), Acta. Metal., 34, P. 565

Falk, L.K.L., Shen, Z. and Ekstrom, T. (1997), J. Euro. Ceram. Soc., 17 P. 1099

Fernie, J.A., Lewis, M.H. and Leng-Ward, G. (1989), Materials Letters, 9, P. 29

Gauckler L. J., Lucas H. L. and Petzow G. (1975), J. Am. Soc. 58(7-8), P. 346

Gogotsi, Y.G., Grathwohl, G., Thummler, F., Yasoshenko, V.P.,Herrmann, M. and Tout, Ch. (1993), J. Am. Ceram. Soc., 11, P. 375

Greil, P. and Weiss, J. (1992), J. Mater. Sci. 17, P. 1571

Hampshire, S., Jack, K.H., (1981) Special Ceramics 7, Proc. Brit. Ceram. Soc.,Vol. 31, Ed. D. W., Taylor & P. Popper, P. 37

Hampshire, S., Park, H.K., Thompson, D.P. and Jack, K.H. (1978), Nature, 274, P. 880

Hardie, D. and Jack. K.H (1957), Nature, 180. P. 392

He, M.Y. and Hutchinson, J.W., (1989), J.Appl. Mech., 56, P> 270

Hewitt C.L. (1998) PhD Thesis, Monash University

Huang, Z.K., Greil, P and Petzow, G. (1983), J. Am. Ceram. Soc.., 66, C96

Huang, Z.K., Tien, T.Y. and Yen, T.S. (1986), J. Am. Ceram. Soc., 69(10), C241

Huang, Z.K. and Yan, D. S. (1992), J. Mater. Sci., 27, P. 5640

Hwang, S. -L. and Chen, I. -W. (1994), J. Am. Ceram. Soc. 77(1), P. 165

Hwang, C.J., Susnitzky, D.W. and Beaman, D.R., (1995), J. Am. Ceram. Soc., 78, P. 588

Jack, K.H. (1976), J. Mater. Sci, 11, P. 1135

Jack, K.H. (1983), Progress in Nitrogen Ceramics, (Ed. F. L. Riley), The Hague, Netherlands, Martinus Nghoff, P. 45

Jack K. H. (1986), Non-Oxide Technical and Engineering Ceramics, Ed. S. Hampshire, New York, USA, Elsevier Appl. Sci. ,P. 1

Jack K. H. and Wilson W. I. (1972), Nature, 238, P. 28

Jasper, C. A. (1990), Ph.D. Thesis, University of Warwick

Jasper, C. A. and Lewis, M. H. (1992), Proc. 4th int. Symp. on ceramic materials and component for engines, (Eds. R. Carlsson et al), Elsevier Science publisher, London, P. 424

Jennings H. M. (1983), J. Mater. Sci. 18, P. 951

Jones, A.H. (1997), Ph.D. Thesis, Warwick university

Jumali, M. H. H. (1999), Ph. D. Thesis, Warwick university

Kall, P.O. and Ekstrom, T. (1990), J. Euro. Ceram. Soc., 6, P. 119

Karunaratne, B. S. B., Lumby, R..J. and Lewis, M. H. (1996), J. Mater. Res., 11(11), P. 2790.

Kato, K., Inoue, Z., Kijimaya, K., Kawada, I., Tanaka, H., and Yamane, T. (1975), J. Am. Ceram. Soc., 58, P. 90

Kingery, W. D., (1959), J. Appl. Phys. 30(3), P. 301

Kuang, S.F., Huang, Z. K., Sun, W.Y. and Yen, T. S. (1990), J. Mater. Sci. Lett., 9, P. 72

Lamkin, M. A., Riley, F.L. and Fordham, R.J. (1992), J. Eur. Ceram. Soc.,10, P. 347

Lewis M. H. and Barnard P. (1980), J. Mat. Sci., 15, P. 443

Lewis, M.H., Powell, B. D., Drew, P., Lumby, R.J., North, B. and Taylor, A.J. (1977), J. Material Science, 12, P. 61

Lewis, M.H., Bhatti, A.R., Lumby, R.J. and North, B. (1980), J. Mater. Sci., 15, P., 103

Lewis, M.H. and Lumby, R.J. (1983), J. Powder Metall., 26, No 2, P. 73

Lewis, M. H., Leng-Ward, G. and Jasper, C.A. (1988), Ceramics Transactions; Ceramic Powder Science II, (Ed. G.L. Messing et al), American Ceramic Society, P. 1019

Lewis, M. H. (1993), Key Engineering Materials, vol. 89-91, eds. M. J. Hoffmann,

Lewis, M. H., Karunaratne, B.S.B. and Lumby, R. J. (1996) presented at: PACRIM2: 2nd International Meeting of Pacific Rim Ceramic Societies Cairns, Australia.

Lumby, R. J., B. North and A.J. Taylor (1974), Special ceramic 6 ed. Popper, (Brit. Ceram. Res. Assoc.)

Lumby, R. J. (1998), Private communication

Mandal H.,Thompson D.P. and Ekstrom T. (1992), Key Eng. Mater., 72-74, P. 187

Mandal, H. and Thompson, D. P. (1995), 4th Euro-ceramics, Ed. G. Galus Gruppo Editoriale. Faenza Editrice S. P. A. Italy, P. 273

Mandal, H., Camuscu, N. and Thompson, D.P. (1995), J. Mater. Sci.,30,5901

Mandal, H., Cheng, Y.B. and Thompson, D.P. (1995), 5th International. Symposium On Ceramic Materials and Components For Engines, Shanghai China, P. 202

Mandal, H., Thompson, D.P and Ekstrom, T. (1993), J. Euro. Ceram. Soc., 12, P. 421

Mandal, H., Thompson, D.P., Sun W. Y. and Ekstrom, T. (1995) 5th International. Symposium On Ceramic Materials and Components For Engines, Shanghai, China, P. 441

Marchand, R., Laurent, Y. and Lang, J. (1969), Acta Crystallogr., B25, P. 2157

Menon, M. and Chen, I.W. (1995a), J. Am. Ceram. Soc., 78, P. 545

Menon, M. and Chen, I.W. (1995b), J. Am. Ceram. Soc., 78, P. 553

Messier, D.R., Riley, F.L. and Brook, R.J. (1978), J. Mater. Sci.,13, P.1199

Mitomo, M. and Ishida, Akira (1999), J.Euro. Ceram. Soc, 19, P.7

Murakami, Y., Yamamoto, H., (1993), J. Ceram. Soc. Of Japan, Int. Edition, P. 1071

Nordberg L. -O., Shen Z., Nygren M. and Ekstrom T. (1997), J. Euro. Ceram. Soc., 17, P.575

Oyama, Y. (1972), J. Appl. Phys, Japn, 11, 760

Oyama, Y. and Kamigaito, O. (1971), J. Appl. Phys, Japn, 10, 1637
Proceeding 287, P. 387

Patel, J.K. and Thompson, D.P. (1988) , J. Br. Ceram. Trans. . , P. 70

Persson, J., Kall, P.O. and Nygren, M. (1993), J. Euro Ceram. Soc. , 12, P. 177

Priest, H.F., Burns, F.C., Priest, G.L. and Skaar, E.C. (1973), J. Am. Ceram. Soc., 56, P. 395

Roesenflanz, A. and Chen, I.W. (1999a), J. Euro. Ceram. Soc. 19, P. 2325

Roesenflanz, A. and Chen, I.W. (1999b), J. Euro. Ceram. Soc. 19,P. 2337

Sarin, V.K. (1988), Mater. Sci. Eng., A105/106, P. 151

Slasor, S., Liddell, K. and Thompson D.P. (1986), Special Ceramic 8, ed. S. P. Howlett & Taylor P. 51

Slasor, S. and Thompson, D.P. (1987), J. Materi Sci. Lett. 6, P. 315

Shelpy, J.E. and Kohli, j. T. (1990), J. Am. Ceram. Soc., 73, P. 39

Shen, Z., Ekstrom, T. and Nygren, M. (1996a), J. Am. Ceram. Soc., 79, P. 721

Shen, Z., Ekstrom, T. and Nygren, M. (1996b), J. Euro. Ceram. Soc., 16, P43

Shen, Z., Ekstrom, T. and Nygren, M. (1996c), J. Phys. D: Appl. Phys, 29, P.893

Shen, Z., Ekstrom, T. and Nygren, M. (1997), J. Mate. Sci., 32, P. 1325

Shen, Z. and Nygren, M. (1997), J. Euro. Ceram. Soc., 17, P. 1639

Shen, Z. and Nygren, M. (1997), 9th International. Symposium On Ceramic Materials and Component for Engines, P. 627

Single, S.C. (1976), J. Mater. Sci., 11, P. 500

Srinivasan M. and Seshadri S. G. (1981), Fracture Mechanics of Ceramics Rocks and Concrete, ASTM STP, 745, S. W. Freiman and E. R. Fuller Eds. American Society for testing and Materials, P. 46

Sun, W. Y. Wu, F.Y. and Yan,D.S. (1987), Mater. Lett., 6, P. 11

Sun, W.Y., Tien, T.Y. and Yen, T.S. (1991), J. Am. Ceram. Soc, 74, P. 2547

Sun, W.Y., Yan, D.S., Gao, L., Mandal, H., Liddle, K. and Thompson, D.P. (1995), J. Euro. Ceram. Soc., 15, P. 349

Sun ,W.Y., Wang, P.L. and Yan, D.S. (1996), Mater. Lett., 26, P. 9

Tajima, Y., Urashima, K., Watanabe, M. and Matsuo, Y. (1988), Ceramic Transaction vol. 1 Ceramic Powder Science II B, G.L. Messing, E.R. Fuller, Jr, and H. Hausner (editors), Am. Ceram. Soc., Westerville, OH

Thompson, D.P. (1977), Nitrogen Ceramics Ed. F. L. Riley, Leyden, Noordhoff, P. 129

Thompson, D.P. and Mandal H. (1997), Bri. Ceram. Trans., 5, P. 199

Wang, P. L., Sun, W. Y. and Yen, T.S. (1993) Materials. Research Society Symposium proceeding 287, P. 387

Wang P. L., Tu H. Y., Sun W. Y., Yan D. S., Nygren M. and Ekstrom (1995a), J. Euro. Ceram. Soc., 15, P. 689

Wang, H., Wang, P.L., Sun, W.Y., Zhuang, H.R. and Yan D.S. (1995bb), 5th Int. Symposium On Ceramic Materials and Components for Engines, P. 215

Wang, P.L., Zhang, C., Sun, W.Y. and Yan, D.S (1999) J. Euro. Ceram. Soc. 19, P. 553

Watari, K., Nagaoka, T. and Kanzaki, S. (1994) J. Mat. Sci.., 29 P. 5801

With G. DE and Parren J. ED (1985), Solid State Ionics, 16, P. 87.

Van den Heeuvel, Hintzen H.T. and Metselarar, (1996), Key Engineering Materials 113, P. 33

Van Tendeloo, Faber K. T. and Thomas G. (1983), J. Mater. Sci, 18, P. 525

Zhao, R.P. and Cheng, Y.B. (1995), J.Euro. Ceram. Soc., 15, P. 1221

Zhao, R. P. and Cheng Y. B. (1996), J. Euro. Cerm. Soc., 15, P. 1001

Zhao, R.P. and Cheng, Y.B. and Drennan, J. (1995), J. Euro. Ceram. Soc., 16, P. 529